NWC TP 6992 ②

Nitramine Composite Solid Propellant Modelling

by
F. S. Blomshield
Research Department

JULY 1989

NAVAL WEAPONS CENTER
CHINA LAKE, CA 93555-6001

Approved for public release; distribution is unlimited.

Naval Weapons Center

FOREWORD

This report summarizes work performed at the Naval Weapons Center to develop a theoretical model for the combustion of nitramine composite solid propellants.

The work described in this report was conducted by the Naval Weapons Center (NWC), China Lake, CA, between December 1984 and December 1988. The work was performed under the Independent Research (IR) Program.

This report has been reviewed for technical accuracy by Professor John Osborn at Purdue University.

Approved by	Under authority of
R. L. DERR, *Head*	J. A. BURT
Research Department	Capt., U.S. Navy
31 July 1988	*Commander*

Released for publication by
G. R. SCHIEFER
Technical Director

NWC Technical Publication 6992

Published by .... Research Department
Collation .... Cover, 93 leaves
First printing .... 150 copies

UNCLASSIFIED
SECURITY CLASSIFICATION OF THIS PAGE

REPORT DOCUMENTATION PAGE

1a REPORT SECURITY CLASSIFICATION
UNCLASSIFIED

1b RESTRICTIVE MARKINGS

2a SECURITY CLASSIFICATION AUTHORITY

2b DECLASSIFICATION / DOWNGRADING SCHEDULE

3 DISTRIBUTION / AVAILABILITY OF REPORT
Approved for public release;
distribution is unlimited.

4 PERFORMING ORGANIZATION REPORT NUMBER(S)
NWC TP 6992

5 MONITORING ORGANIZATION REPORT NUMBER(S)

6a NAME OF PERFORMING ORGANIZATION
Naval Weapons Center

6b OFFICE SYMBOL *(If applicable)*
Code 3895

7a NAME OF MONITORING ORGANIZATION

6c. ADDRESS *(City, State, and ZIP Code)*
China Lake, CA 93555-6001

7b. ADDRESS *(City, State, and ZIP Code)*

8a NAME OF FUNDING / SPONSORING ORGANIZATION

8b OFFICE SYMBOL *(If applicable)*

9. PROCUREMENT INSTRUMENT IDENTIFICATION NUMBER

8c. ADDRESS *(City, State, and ZIP Code)*

10. SOURCE OF FUNDING NUMBERS

PROGRAM ELEMENT NO.	PROJECT NO.	TASK NO	WORK UNIT ACCESSION NO
	1601		

11 TITLE *(Include Security Classification)*
(U) Nitramine Composite Solid Propellant Modelling

12 PERSONAL AUTHOR(S)
F. S. Blomshield

13a. TYPE OF REPORT
Final

13b TIME COVERED
FROM Dec 1984 TO Dec 1988

14. DATE OF REPORT *(Year, Month, Day)*
1989, July 31

15 PAGE COUNT
181

16 SUPPLEMENTARY NOTATION

17 COSATI CODES

FIELD	GROUP	SUB-GROUP

18 SUBJECT TERMS *(Continue on reverse if necessary and identify by block number)*
Nitramine solid propellant modelling, HMX, AP, HTPB, HYPEM, PEM, BDP, Time averaged

19 ABSTRACT *(Continue on reverse if necessary and identify by block number)*

This report summarizes work performed at the Naval Weapons Center to develop a theoretical model for the combustion of nitramine composite solid propellants. A nitramine composite propellant typically consists of several distributions of cyclotetramethylenetetranitramine crystals (HMX) and ammonium perchlorate crystals (AP) mixed in a hydrocarbon fuel binder such as polybutadiene (HTPB). The model, called the High Energy Petite Ensemble Model (HYPEM), is based upon a statistical treatment of the propellant's oxidizer crystals. It is a physio-chemical combustion model with multiple flames situated over HMX and/or AP crystals. The HMX section of the model averages the propellant combustion in time while the AP portion averages the propellant combustion over the surface area of the propellant. Results from the HYPEM combustion model are compared with experimental burning rate, pressure exponent, and temperature sensitivity for a wide variety of propellants containing multiple distributions of HMX and/or AP crystals. Composite propellant combustion properties are examined by parametrically varying particle size, pressure, oxidizer solids loading, and formulation.

20 DISTRIBUTION / AVAILABILITY OF ABSTRACT
☒ UNCLASSIFIED/UNLIMITED ☐ SAME AS RPT ☐ DTIC USERS

21 ABSTRACT SECURITY CLASSIFICATION
UNCLASSIFIED

22a NAME OF RESPONSIBLE INDIVIDUAL
F. S. Blomshield

22b TELEPHONE *(Include Area Code)*
(619) 939-3650

22c OFFICE SYMBOL
Code 3895

DD FORM 1473, 84 MAR

83 APR edition may be used until exhausted
All other editions are obsolete

SECURITY CLASSIFICATION OF THIS PAGE

☆ U.S. Government Printing Office: 1986—607-044

UNCLASSIFIED

TABLE OF CONTENTS

LIST OF TABLES

LIST OF FIGURES

NOMENCLATURE

A - Arrhenius frequency factor or prefactor
AP - Ammonium perchlorate
a - Distance from center of flame to edge of oxidizer crystal
BDP - Beckstead, Derr, Price combustion model
b - Distance from center of the flame to outer edge of burner
C_p - Specific heat of the gas
C_s - Specific heat of the solid
C - Constant (also c)
D - Oxidizer crystal diameter
D_o - Actual oxidizer crystal diameter
D' - Statistically average intersection diameter
$\mathcal{D}$ - Diffusivity
E - Activation Energy
F - Distribution function
fr_a - *Fraction of binder reacting*
GDF - Granular diffusion flame model
HMX - Cyclotetramethylenetetranitramine, $C_4H_8N_8O_8$
HTPB - Polybutadiene
ΔH - Heat of reaction
h - See Figure 6, measure of non-planarity of oxidizer crystal
J_i - Bessel function of the ith kind
K - Kelvin
K - Reaction rate constant (also k)
L - See Figure 6, Oxidizer projection distance
$\dot{m}$ - Mass flow rate
n - Mass interaction parameter
P - Pressure (also p)
PEM - Petite Ensemble Model
Q - Energy released and/or absorbed
R - Gas constant
R - See Figure 8, oxidizer burning surface radius
r - Burn rate
$\bar{r}$ - Mean burn rate
r - Radial coordinate
S - Surface area
T - Temperature
t - Time
t_{ba} - Constant in binder burnthrough time equation
u - Gas velocity
V - Volume
v - Gas velocity
W - Molecular Weight
w - Reaction rate

x - Vertical coordinate
x^* - Flame standoff distance
$\bar{x}^*$ - Mean flame standoff distance
XN - Diameter exponent in volume of fuel equation

GREEK SYMBOLS

α - Oxidizer mass fraction
β - Concentration
β_f - Fraction of reactants that react in primary flame
β_p - Fraction of heat from primary flame to oxidizer
β_{pa} - Constant in β_p calculation
ϵ - Calculated average flame height factor
ϵ - Non-dimensional distance in GDF model
ϵ - Fissure depth in HR model
δ - Geometric constant equal to $2\Delta/D'$
δ_{ign} - Diameter exponent in ignition delay time equation
Δ - Distance from HMX crystal edge to edge of assumed binder annulus
η - Non-dimensional distance
Φ - Fuel to oxidizer ratio
ϕ - Roots of the first order Bessel function
λ - Thermal conductivity
ν - Stoichiometric fuel ratio
ρ - Density
σ_p - Temperature sensitivity of burn rate at constant pressure
σ_{ox} - Oxidizer mode width parameter
τ - Reaction time
μ - Mass of reaction pocket in GDF model
ξ - Non-dimensional radial distance
ξ^* - Non-dimensional flame standoff distance
ψ - Constant in Burke-Schumann flame analysis, $D/(vb)$
ζ - Volume fraction of oxidizer

SUPERSCRIPTS

δ - Reaction order
P - Planar
T - Total
° - Degrees

SUBSCRIPTS

AP - AP or AP flame
b - Binder or fuel
D - Diffusion
DAP - Surface decomposition energy for AP
Db - Surface decomposition energy for binder
DX - Surface decomposition energy for HMX
d - Property of pseudo propellant
f - Fuel or binder
FD - Final diffusion flame

FF - Final flame
ign - Ignition
K - Kinetic
melt - Melting
o - Total
ox - Oxidizer
PD - Primary diffusion flame
PF - Primary flame
p - Propellant
ref - Reference value
s - Solid
s,b - Surface of binder
s,f - Surface of fuel
s,ox - Surface of oxidizer
stoich - Stoichiometric
T - Total
X - HMX or HMX flame
XPD - HMX primary diffusion flame
XPF - HMX primary flame
o - Initial

CHAPTER I

INTRODUCTION

A composite solid propellant typically consists of oxidizer particles, solid metal additives, burning rate modifiers, catalysts and acoustic suppressants all well mixed within a hydrocarbon liquid fuel binder which, after mixing, is polymerized to a solid. Composite solid propellants are used in rocket motors ranging in size from shoulder launched tactical weapons to large space vehicle solid boosters. Efforts to increase solid motor performance has lead to the use of nitramine high energy ingredients. The introduction of these ingredients, often explosive in pure form, into composite propellants offers improved specific impulse, I_{sp}, which translates into greater range and/or payload for a solid rocket system.

Combustion modeling can be used to tailor propellant ingredients in such a fashion as to achieve desired, or optimum, steady and non-steady burning characteristics. In addition, propellant temperature sensitivity and erosive burning effects can be studied. Without a theoretical combustion model; experimental correlations, costly experimental results, past experience, and trial and error methods are all the propellant designer has to accomplish his task.

Early composite solid propellant models focused on predicting burning characteristics of propellants consisting of just binder and a single oxidizer. Later, effects of aluminum in composite propellants were accounted for in combustion models. More recently, models have been developed which describe high energy mono-propellants and/or explosive burning characteristics. The goal of this research is to develop a composite solid propellant combustion model which includes ammonium perchlorate (AP) crystals and high energy cyclotetramethylene-tetranitramine (HMX) crystals in a polybutadiene (HTPB) binder. The model will be used to predict the burning rate, pressure exponent, and temperature sensitivity for a variety of propellants consisting of various combinations of HMX and/or AP crystals.

CHAPTER II

BACKGROUND

Theoretical modeling of solid propellant combustion serves a number of useful purposes in propellant development. It represents the physics and chemistry of the combustion processes in mathematical terms so that the combustion characteristics of formulations can be predicted. It strives to explain the combustion properties which are observed, providing a diagnostic tool to help address anomalous or undesirable combustion behavior. Composite propellants, in their simplest form, consist of a dispersion of particulate oxidizers within a matrix of fuel. Even if all the particles were the same size and shape (ie. spherical) and even if the dispersion of the oxidizer in the fuel was uniform, the combustion of the propellant would involve a multitude of subprocesses. Some of these processes are heating of the condensed phase, decomposition of the oxidizer and the fuel, melting, vaporization, mixing in the vapor phase, and gas-phase combustion. Thus, any attempt at understanding the combustion behavior must identify the key processes that control the burning. Combustion modeling seeks to distinguish governing mechanisms from those of secondary of little importance, so that chemists and engineers may be guided more productively in the means to overcome combustion limitations and achieve propellant tailoring goals. A comprehensive model which describes the combustion of a solid propellant should be based on the key physical and chemical processes involved in the combustion zone. This review of composite propellant modeling will review past modeling efforts. In addition, the observed physics and chemistry of nitramine combustion will be discussed.

2.1 Non-Nitramine Combustion Models

2.1.1 Granular Diffusion Model

The granular diffusion flame (GDF) model was formulated to describe the burning characteristics of ammonium perchlorate (AP) based composite propellants. The granular diffusion flame model was formulated in 1958 and revised in 1960.[1,2] Based on enlarged pictures of the burning zone of simple composite propellants, the authors of the model attempted to theoretically predict the effects of pressure, oxidizer particle size, and fuel-to-oxidizer ratio upon the mean burning rate. The pictures clearly indicated heterogeneity both near the surface and in the vapor phase. Instead of the popular procedures of attempting to "average" the heterogeneity in the vapor phase, the model considered the heterogeneity as a principal feature. The model assumed that vapors of fuel or oxidizer or both are released in the form of pockets of a certain mass content. The average mass content of a pocket was assumed to be much smaller than that of an average oxidizer crystal and to be independent of the temperature and pressure. However, the size of the pockets was assumed to be related to the average oxidizer particle size. The rate at which the pockets are consumed in a chemical reaction as they pass through the flame zone was assumed to be controlled by diffusional mixing and the chemical kinetics. The model assumes mixing of the oxidizer and the fuel occurs only in the gas phase, no sub-surface reactions, the heat of combustion is released in a thin reaction zone in the gas phase and a linear temperature profile from the propellant surface temperature to the temperature of the product combustion gases. The GDF model is the only model to assume a gas phase temperature profile.

2.1.1.1 Equation Development

The following energy equation for the GDF model is based on the quasi-one-dimensional model depicted by Figure 1.

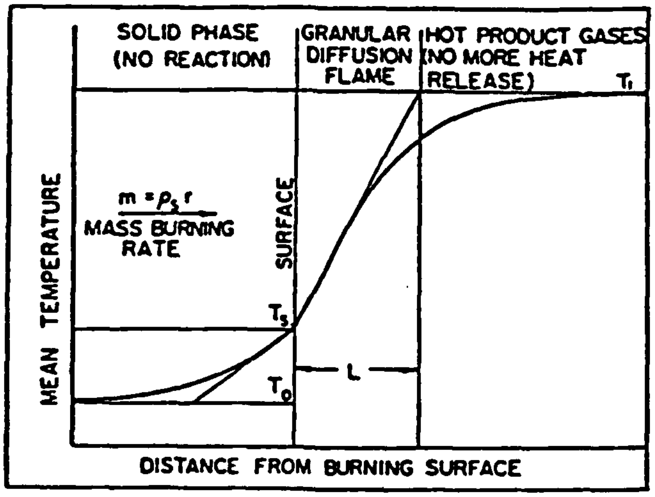

Figure 1
Theoretical Model of Steady State Flame for
Granular Diffusion Flame Model

$$\dot{m}C_s(T_s-T_o) - \lambda_g(\frac{dT}{dx})_g + \dot{m}(Q_r-Q_s) = \dot{m}Q_r \tag{1}$$

where:

$\dot{m}$ = Mass burning rate, $\dot{m} = r\rho_s$, ρ_s is propellant density
C_s = Specific heat of solid (average of fuel and oxidizer)
T_s = Temperature at surface of solid (average)
T_o = Initial temperature of the propellant
λ_g = Average thermal conductivity of flame gas at surface
$(\frac{dT}{dx})_g$ = Temperature gradient in flame gas at surface
Q_r = Heat of combustion of the propellant
Q_s = Net heat release (positive) for gasification of the propellant

Using Figure 1 and approximating the temperature gradient, equation (1) becomes:

$$\dot{m}[C_s(T_s-T_o)-Q_s] = \lambda_g\frac{T_f-T_s}{L} \tag{2}$$

where L is the granular diffusion flame height. The model assumes that L can be written as follows:

$$L = L_D + L_K \tag{3}$$

where L_D is the diffusional mixing distance and L_K is the kinetic reaction distance. Since the mass diffusion coefficient of the reaction species is inversely proportional to pressure while the chemical reaction rate is directly proportional to pressure, the molecular diffusion rate is much faster than the chemical reaction rate at low pressure. Thus, the kinetic reaction distance will be greater than the diffusional mixing distance at low pressure, $L_K >> L_D$. At high pressures the diffusional processes are slower than the kinetic reactions and the combustion process is controlled by the diffusional mixing, $L_D >> L_K$.

In the determination of L_K for the low pressure premixed flame, the model treated the flame as a stream of velocity u in which a second order reaction was taking place. The mean gas velocity in the flame zone is given by:

$$u = \dot{m}/\rho_g \tag{4}$$

where ρ_g is the density of the gas in the flame zone. The flame zone thickness for the premixed flame is given by:

$$L = u\tau \tag{5}$$

where τ is the time it takes the chemical reaction to occur. Assuming a global second order reaction for the premixed gases, the reaction time is given by:

$$\tau = [(1 - \epsilon)^2\rho_g A exp(-E/RT_g)] \tag{6}$$

where an Arrhenius expression is assumed for the rate of reaction, T_g is the average gas phase reaction zone temperature and ϵ is a function of the products of reaction, i.e., ϵ is equal to zero at the propellant surface and ϵ is equal to unity at the completion of the reaction. For simplicity, the model assumed that the average value for $(1-\epsilon)^2$ over the flame zone is unity. Physically this means that most of the overall reaction takes place near the propellant surface.

Combining equation (4), (5) and (6), yields the following for the flame zone thickness for the low pressure premixed flame:

$$L_K = \dot{m}/[\rho_g^2 A exp(-E/RT_g)] \tag{7}$$

when equation (2) is solved for the total mass flux and the result substituted into equation (7), the following thickness is obtained:

$$L_K = \left[\frac{\lambda_g(T_f - T_S)}{[C_s(T_S - T_o) - Q_S]}\right]^{1/2} \frac{1}{\rho_g[A exp(-E/RT_g)]^{1/2}} \tag{8}$$

For the high pressure diffusion flame, the model assumed that the mass of a pocket could be expressed as:

$$\mu = \rho_g D^3 \tag{9}$$

where D is the oxidizer particle diameter. The lifetime of a pocket is determined by the rate of gas diffusion to the surrounding flame. The molecular diffusivities of the fuel and the oxidizer are assumed to be the same and are averaged over the gaseous reaction zone. Under these conditions the lifetime of a fuel pocket is:

$$\tau = \frac{D^2}{\mathcal{D}_g} \tag{10}$$

where $\mathcal{D}_g$ is the average diffusivity of the oxidizer and fuel vapors. The thickness of the flame zone is the product of the velocity of the gas stream and the lifetime of the fuel pocket. Thus:

$$L_D = \mu\tau = \frac{\dot{m}}{\rho_g}\frac{D^2}{\mathcal{D}_g} \tag{11}$$

Combining equation (9) and (11) yields the diffusion flame zone thickness:

$$L_D = \frac{\mu^{2/3}\dot{m}}{\rho_g^{5/3}\mathcal{D}_g} \tag{12}$$

Solving equation (3) for the total mass flux and substituting this into equation (12) yields:

$$L_D = \left[\frac{\lambda_g(T_f - T_S)}{[C_s(T_S - T_o) - Q_S]}\right]^{1/2} \frac{\mu^{1/3}}{\rho_g^{5/6}\mathcal{D}_g^{1/2}} \tag{13}$$

Expressions for the flame zone thickness in the two extreme cases can now be written. For the general intermediate case, the model assumed that the flame zone thickness varies with pressure partly as if it were reaction rate controlled, L_K, and partly as if it were diffusion controlled, L_D, and that the flame zone thickness could be expressed as the sum of the above two. Thus, the general expression for the flame zone thickness, from equation (3), becomes:

$$L = \left[\frac{\lambda_g(T_f - T_S)}{[C_s(T_S - T_o) - Q_S]}\right]^{1/2} \left\{\frac{1}{\rho_g[A exp(-E/RT_g)]^{1/2}} + \frac{\mu^{1/3}}{\rho_g^{5/6} D_g^{1/2}}\right\} \tag{14}$$

Using the ideal gas law, the expression $D_g = K_1 T_g^{3/2}/P$ for the diffusivity, an average gas phase temperature and letting $\dot{m} = r\rho_s$ where ρ_s is the density of the solid propellant, an expression for the burning rate can be obtained by substituting equation (14) for L into the energy equation, equation (3):

$$\frac{1}{r} = \frac{a}{p} + \frac{b}{p^{1/3}} \tag{15}$$

where the constants a and b are given by:

$$a = \left[\frac{\lambda_g(T_f - T_S)}{[C_s(T_S - T_o) - Q_S]}\right]^{1/2} \frac{\rho_s R T_g}{[A exp(-E/RT_g)]^{1/2}} \tag{16}$$

$$b = \left[\frac{\lambda_g(T_f - T_S)}{[C_s(T_S - T_o) - Q_S]}\right]^{1/2} \frac{\rho_s R^{5/6} T_g{}^{1/12} \mu^{1/3}}{K_1^{1/2}} \tag{17}$$

The constants a and b are independent of pressure, p, and are related to L_K and L_D. If $L_K >> L_D$ (reaction rate controlled) a >> b and the burning rate exponent, n, in the burning rate expression that follows:

$$r = cp^n \tag{18}$$

approaches 1. If $L_D >> L_K$ (diffusional mixing controlled) b >> a and the burning rate exponent, n, approaches 1/3. If L_D is of the same order as L_K, then n is between 1 and 1/3. Experimentally, with AP/inert binder propellants, these results are obtained.

2.1.1.2 Discussion

The granular diffusion flame model used equation (15) to correlate experimental burning rate data for a range of ammonium perchlorate propellant formulations. The equations provided good agreement between theory and experiment in predicting the effect of oxidizer crystal size, fuel to oxidizer ratio, and pressure on burning rate. The GDF model developed a burning rate expression that provided, in a closed form, a means of estimating the effects of varying the important propellant combustion parameters on burning rate.

The model was later modified to take into account a distended AP monopropellant flame. This was done to make the model applicable to low pressure combustion.[3] The model was also modified to model polydisperse oxidizer distributions by applying a statistical technique to the differing particle sizes.[4]

2.1.2 Hermance Heterogeneous Reaction Model

The Hermance heterogeneous reaction (HR) model was based on a detailed combination of the steady state decomposition processes of the fuel and oxidizer. The model was first formulated in 1966 and later revised in 1967.[2,5,6] The model postulates an exothermic, heterogeneous reaction between the solid fuel and oxidizer decomposition products and assumes that the gas phase flame position is the sum of the lengths associated with diffusional mixing and chemical reaction. The heterogeneous reaction model was a significant advance in the state of the art of combustion modeling since it was the first model to deal directly with the heterogeneity of the solid phase by taking into consideration arbitrary particle sizes.

The model assumes that the steady state combustion of a composite propellant occurs in three regions; the propellant surface, the gas phase flame zone and the region between the surface and the flame. The surface chemical processes are endothermic fuel pyrolysis, exothermic oxidizer decomposition and an exothermic heterogeneous chemical reaction between the fuel binder and decomposed oxidizer in small regions surrounding individual oxidizer crystals. Each of these reactions produces a mass flux from the propellant surface.

In the gas phase flame zone, an exothermic chemical reaction occurs between the oxygen rich products from the decomposed oxidizer and the paralyzed fuel. Heat from the flame zone is fed back to the propellant surface by conduction. In the region between the surface and the flame zone, the surface decomposition products mix by diffusion and undergo a chemical kinetic delay before ignition at the flame. In the original model only the ignition delay was considered.[5] The processes depend on the pressure level and/or the temperature at the location of the process and are linked together by the temperature distribution in the gas and solid phases.

2.1.2.1 Equation Development

One of the more important aspects of the model is the calculation of the intersection diameter of an oxidizer crystal with the burning surface. If the propellant burning surface is visualized as a plane passing through a randomly packed bed of spherical oxidizer crystals, it can be shown that the statistical average intersection diameter is:

$$D' = \sqrt{2/3}\, D_o \tag{19}$$

where D_o is the actual crystal diameter and D' is the statistical intersection diameter.[7]

The propellant burning rate can be determined from the total mass flux issuing from the propellant surface. It is the sum of the mass fluxes of gaseous species produced by each of the surface decomposition processes multiplied by the fraction of the total propellant surface area associated with each of the processes. Thus:

$$r = \frac{1}{\rho_p}[\dot{m}_f(S_f/S_o) + \dot{m}_{ox}(S_{ox}/S_o) + \dot{m}_{sr}(S_{sr}/S_o)] \tag{20}$$

where ρ_p is the density of the propellant, $\dot{m}$ is the mass flux and S is surface area. The subscripts f, ox, o and sr designate fuel, oxidizer, total propellant and surface reaction respectively. Assuming a planar surface, the ratio of fuel and oxidizer surface area to the total propellant surface area can be expressed as a function of the volume fraction of oxidizer, ζ, in the propellant:

$$\frac{S_f}{S_o} = (1 - \zeta) \quad \text{and} \quad \frac{S_{ox}}{S_o} = \zeta \qquad \text{(21) and (22)}$$

The area on which the surface reaction occurs is calculated by postulating that an oxidizer crystal decreases in size during decomposition as shown in the top of Figure 2. This size reduction produces a fissure of depth ϵ between the oxidizer crystal and the fuel binder which is the region where the heterogeneous reaction takes place. Arrhenius type functions are used to describe the surface regression of both fuel and oxidizer.

The model divides the steady state combustion process of composite propellants into three regions as shown in the bottom of Figure 2. The differential form of the energy equation is solved for each region simultaneously. The required boundary conditions result by matching temperature and heat flux at the interface of each section. The analysis results in three equations with three unknowns. They are the burning rate equation, the surface temperature equation and the flame temperature equation. These equations in condensed form are:

$$r = a_1 exp(-E_f/E\theta_s) + \frac{b_1 P^\delta}{\theta_s^{1/2}}\left[\frac{c_3}{r} - \frac{d_1}{P^m}\right] exp\left[\frac{-(E_{ox} + E_{sr})}{E\theta_s}\right] \tag{23}$$

$$\theta_s = b_2 + \frac{b_1 P^\delta}{\theta_s^{1/2}}\left[\frac{c_3}{r} - \frac{d_1}{P^m}\right] exp\left[\frac{-(E_{ox} + E_{sr})}{E\theta_s}\right] - \frac{a_2}{r} exp(-E_f/E\theta) + a_3 exp(-\xi^*) \tag{24}$$

$$\theta_f = \theta_s + a_3[1 - exp(-\xi^*) \tag{25}$$

where a_1, a_2, a_3, b_1, b_2, b_3 and d_1 are constants containing the physical and chemical properties of the propellants; E is the activation energy, ξ^* is the non-dimensional flame standoff distance and P is the ambient pressure. The burning rate, surface temperature and flame temperature are calculated by numerical iteration using the above three equations.

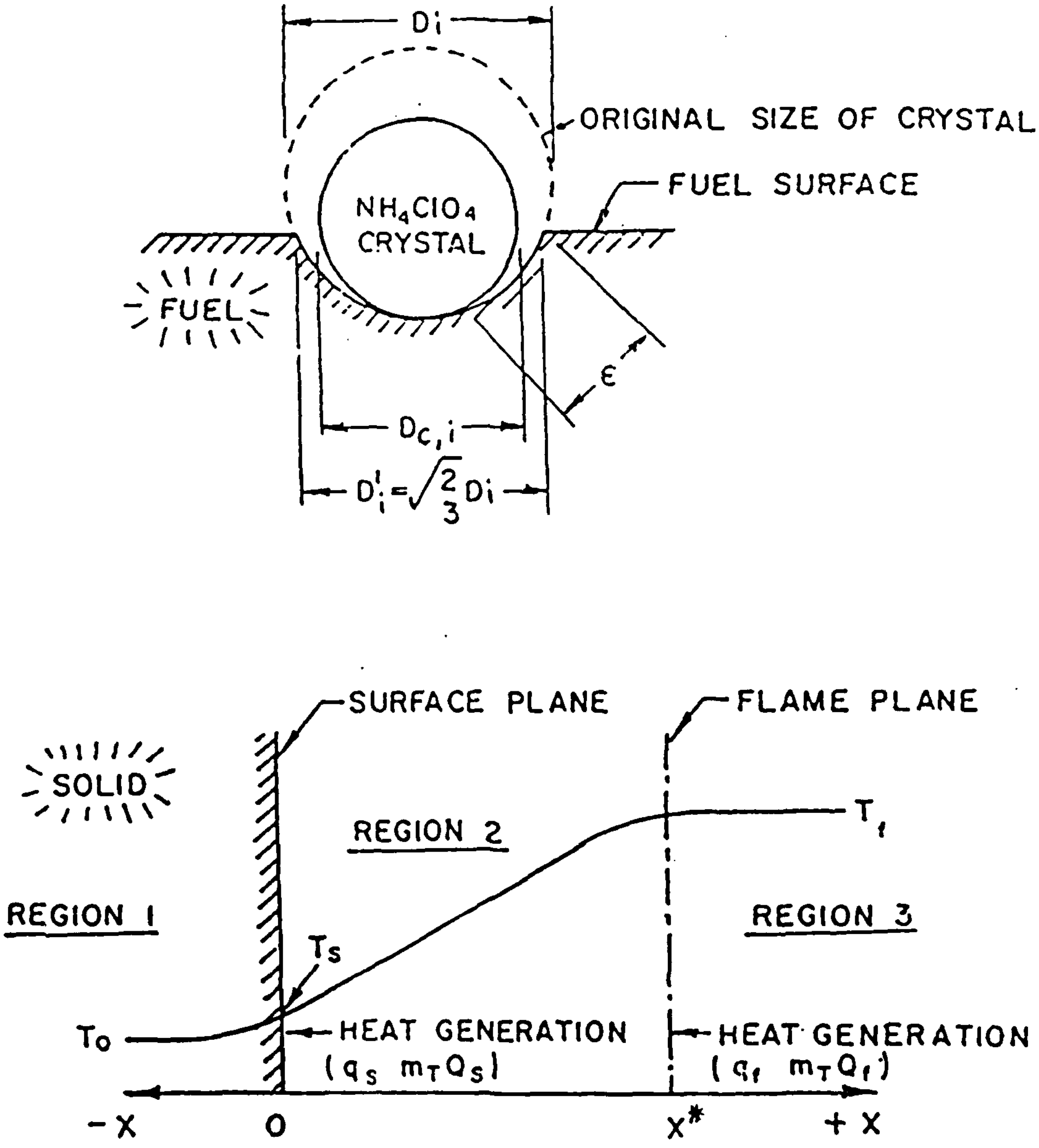

Figure 2
Physical Description of the Hermance Heterogeneous Reaction Model

2.1.2.2 Discussion

The Hermance heterogeneous reaction model solved the above three simultaneous equations with a set of input data which represented the combustion properties of a polysulfide AP composite propellant. The model obtained a reasonable fit to experimental burning rate data taken over the pressure range from 1 to 400 atmospheres. The model qualitatively predicts the effect of oxidizer particle size on the propellant burning rate at pressures above 200 atmospheres.

At low pressure the model predicts very little heterogeneous reaction while at high pressure the crevice becomes huge and the heterogeneous reaction dominates, as depicted in Figure 3. Moreover, the calculated surface temperature is almost constant with increasing pressure indicating that the temperature dependent Arrhenius type function will be essentially constant. Thus, the burning rate characteristics predicted by the HR model are determined almost completely by the crevice and its formation. Yet there is no physical evidence to support the formation of a crevice as postulated by the model.[5]

2.1.3 Beckstead, Derr, Price (BDP) Model

The goal of the Beckstead, Derr, Price model was to develop a new analytical model of composite propellant combustion based on a realistic physical model, utilizing information derived both from experimental studies concerning the surface structure of extinguished propellants and previous analytical modeling efforts.[1-6,8-12] The goal was not to predict exact burning rates, but of predicting changes in burning rate for a given change in propellant formulation.

After extensive experimental observation of the surface structure of a burning composite solid propellant, Beckstead, Derr and Price formulated a multiple flame composite propellant combustion model based on the postulated existence of three flames in the region of each exposed oxidizer particle.[13,14] The three flames are the AP flame, the primary flame and the final diffusion flame.

The AP flame occurs between the decomposition products of the AP forming O_2 and inert products. Thus:

$$NH_3 + HCLO_4 \longrightarrow \text{Inert Products} + O_2 \qquad (26)$$

Since the AP decomposition products are premixed, the AP flame standoff distance is dependent only upon chemical kinetics.

The primary flame occurs between fuel pyrolysis products and the AP decomposition products. Thus:

$$\text{Fuel Products} + HClO_4 \text{ (decomposition products)} \longrightarrow \text{Primary Flame Combustion Products} \qquad (27)$$

The primary flame height is dependent on diffusional mixing as well as kinetics.

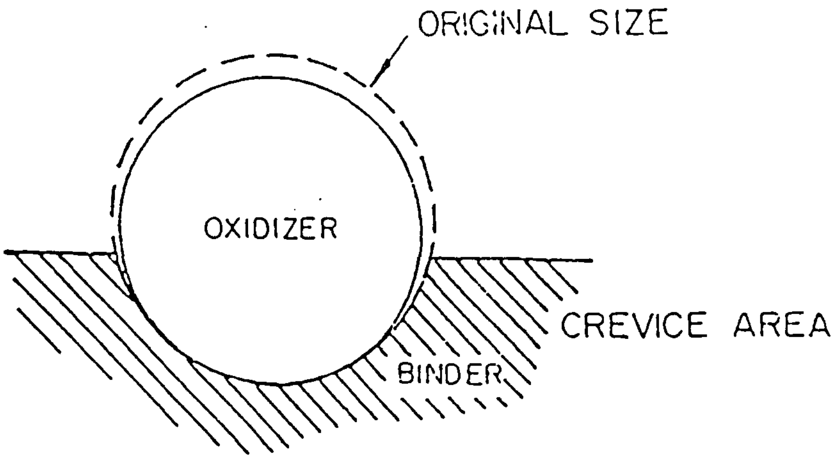

LOW PRESSURE-VERY SMALL CREVICE AREA

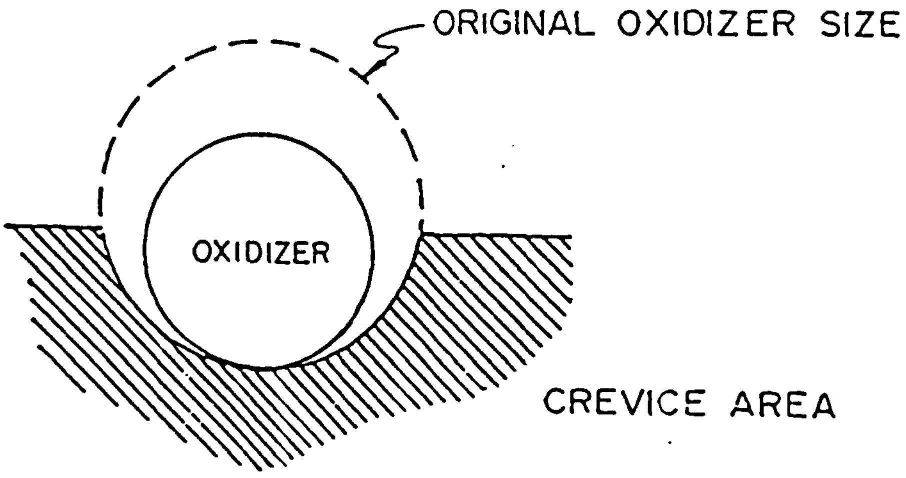

HIGH PRESSURE-VERY LARGE CREVICE AREA

Figure 3
The Pressure Dependence of the Hermance Crevice

The final diffusion flame occurs between the binder decomposition products and the oxidizing products from the AP flame. Since the reactants of the final diffusion flame are preheated, the kinetics are very fast, thus, the final flame height is dependent only on diffusional mixing. The geometric relationship of the assumed flame structure is shown in Figure 4.

The flame standoff distances are a function of the combustion pressure. At low pressures (<100 atm) the propellant is considered to burn as a premixed flame with the oxidizer and binder decomposition products mixing completely before a reaction occurs. As the pressure increases, the mixing path length increases, and the reaction path length decreases so that the two reaction paths (ammonia + oxidizing products and binder products + oxidizing products) become competitive. At higher pressures (>100 atm) the ammonia reacts with the oxidizing products before the binder products can diffuse into the oxidizer stream and react. Due to the fuel rich nature of composite solid propellants, a final diffusion flame always occurs above the AP flame. The flame structure variation with pressure is depicted in Figure 5.

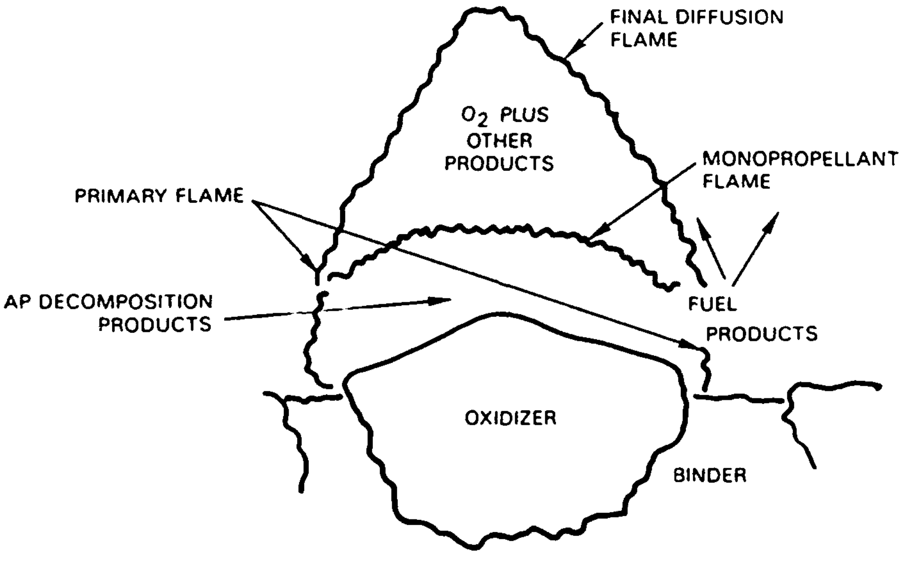

Figure 4
BDP Multiple Flame Structure

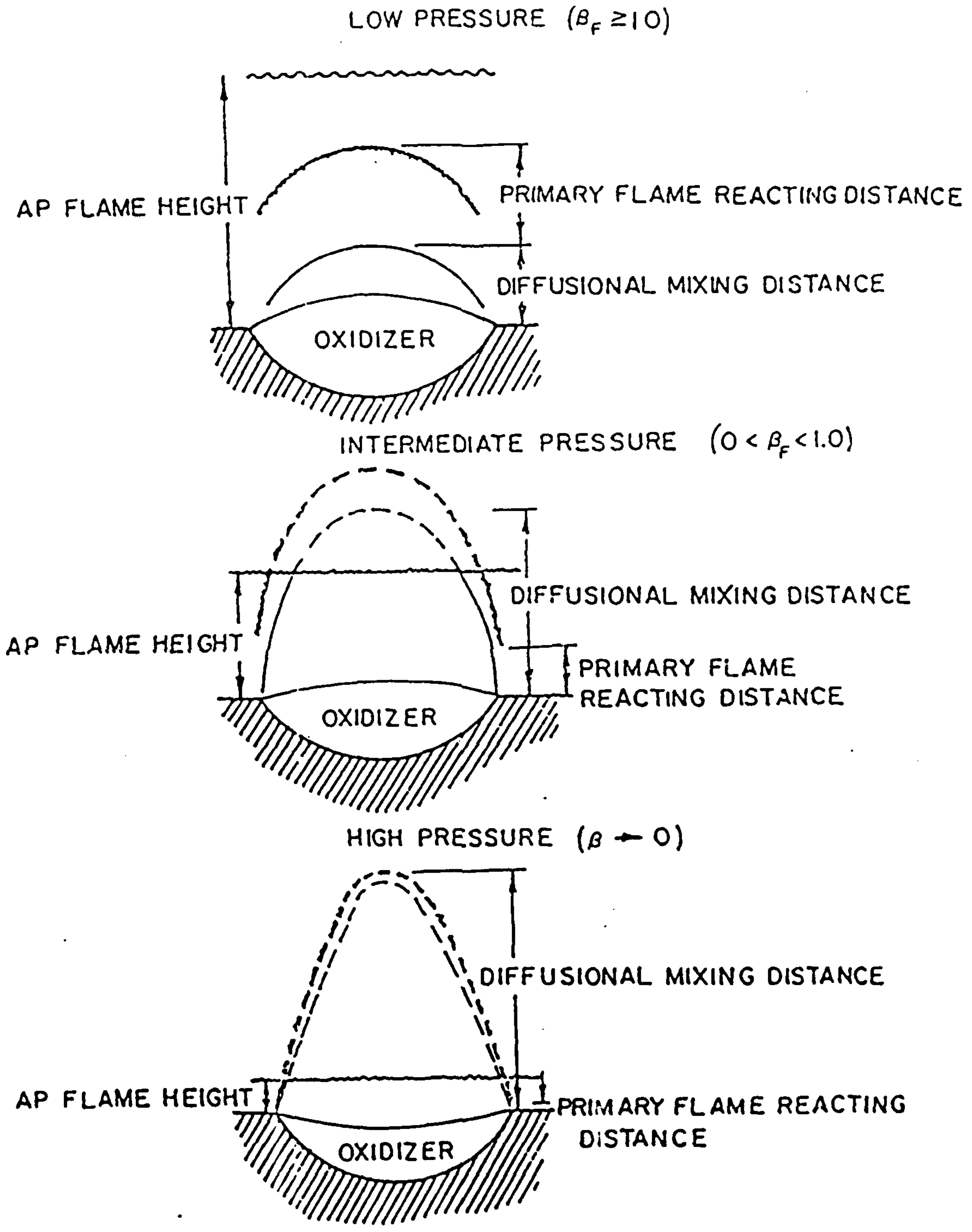

Figure 5
Multiple Flame Structure Variation with Pressure

At the propellant surface the initial decomposition step of both the binder and the oxidizer is endothermic. However, while still adsorbed on the surface, either set of products can undergo a condensed phase reaction before passing into the gas phase. Products from the surface decompositions then pass into the gas phase and begin mixing and reacting.

The burning surface of the exposed oxidizer particle is assumed to be spherical in shape. Due to an ignition delay, the burning oxidizer surface protrudes above the planar fuel surface at low pressure but is recessed below the planar fuel surface at high pressure. The oxidizer regression is assumed to be the overall rate controlling mechanism, and an overall average temperature is defined for the entire burning surface.

In addition to the above assumptions, radiation heat transfer is neglected, an average value for the solid and the gas phase specific heat is assumed, and the mass diffusion coefficient and thermal conductivity of the reacting gases is averaged over the gas phase reaction zone.

2.1.3.1 Conservation of Mass

In the model's original form, the oxidizer was assumed to be monomodal, monodisperse and spherical. However, the model has since been extended to bimodal and trimodal monodisperse propellants.[15-18] In the original BDP model the propellant surface temperatures of the AP and binder were assumed equal. Later versions of the model accounted for differing surface temperatures.[19-20] The case of monomodal monodisperse particle distribution and an uniform surface temperature will be discussed here.

It is assumed that global kinetics adequately describe the decomposition of the oxidizer and binder. Once a surface temperature is assumed, the mass flux rates of both the binder and AP or oxidizer are calculated from the following Arrhenius expressions:

$$\dot{m}_{ox} = r_{ox}\rho_{ox} = A_{ox}exp(-E_{ox}/RT_s) \qquad (28)$$

$$\dot{m}_f = r_f\rho_f = A_f exp(-E_f/RT_s) \qquad (29)$$

where A is the Arrhenius frequency factor, E is the activation energy, R is the gas constant and T_s is the average surface temperature. The subscripts ox and f represent the oxidizer and fuel, respectively.

The conservation of mass equation can be written as follows:

$$\dot{m}_T = r\rho_p = \dot{m}_f\left(\frac{S_f}{S_o}\right) + \dot{m}_{ox}\left(\frac{S_{ox}}{S_o}\right) \qquad (30)$$

This represents the total mass flux of the burning propellant. S_o is the total propellant area and r is the total burn rate. The propellant density is ρ_p. The oxidizer mass fraction is defined as:

$$\frac{\dot{m}_{ox}\left(\frac{S_{ox}}{S_o}\right)}{\dot{m}_f\left(\frac{S_f}{S_o}\right)} = \frac{\alpha}{1-\alpha} \tag{31}$$

where α is the oxidizer mass fraction. Rearranging Equations (30) and (31) a new expression for the total mass flux can be derived:

$$\dot{m}_T = \frac{\dot{m}_{ox}}{\alpha}\frac{S_{ox}}{S_o} = \frac{\dot{m}_f}{1-\alpha}\frac{S_f}{S_o} \tag{32}$$

In these expressions everything is known except the area ratios. The propellant surface geometry will be discussed next.

2.1.3.2 Surface Geometry

The goal of this section is to find an expression for the area ratio:

$$\frac{S_{ox}}{S_o} \quad .$$

This ratio is the oxidizer particle surface area ratio to the area of the total propellant. Because of the random nature of the oxidizer particles a statistical description of the propellant surface must be used. This was first used in the fore mentioned heterogeneous reaction model.[5] If the propellant burning surface is visualized as a plane passing through a randomly packed bed of spherical oxidizer crystals, it can be shown that the statistical average intersection diameter is:[7]

$$D' = \sqrt{2/3}\, D_o \tag{19}$$

where D_o is the actual oxidizer crystal diameter.

Referring to Figure 6, the exposed oxidizer surface area to the total propellant area ratio can be determined solely on geometrical principles. This ratio can be expressed as:

$$\frac{S_{ox}}{S_o} = \frac{\varsigma\left[6\left(\frac{h}{D_o}\right)^2 + 1\right]}{\left[6\varsigma\left(\frac{h}{D_o}\right)^2 + 1\right]} \tag{33}$$

where the term h/D_o is given by:

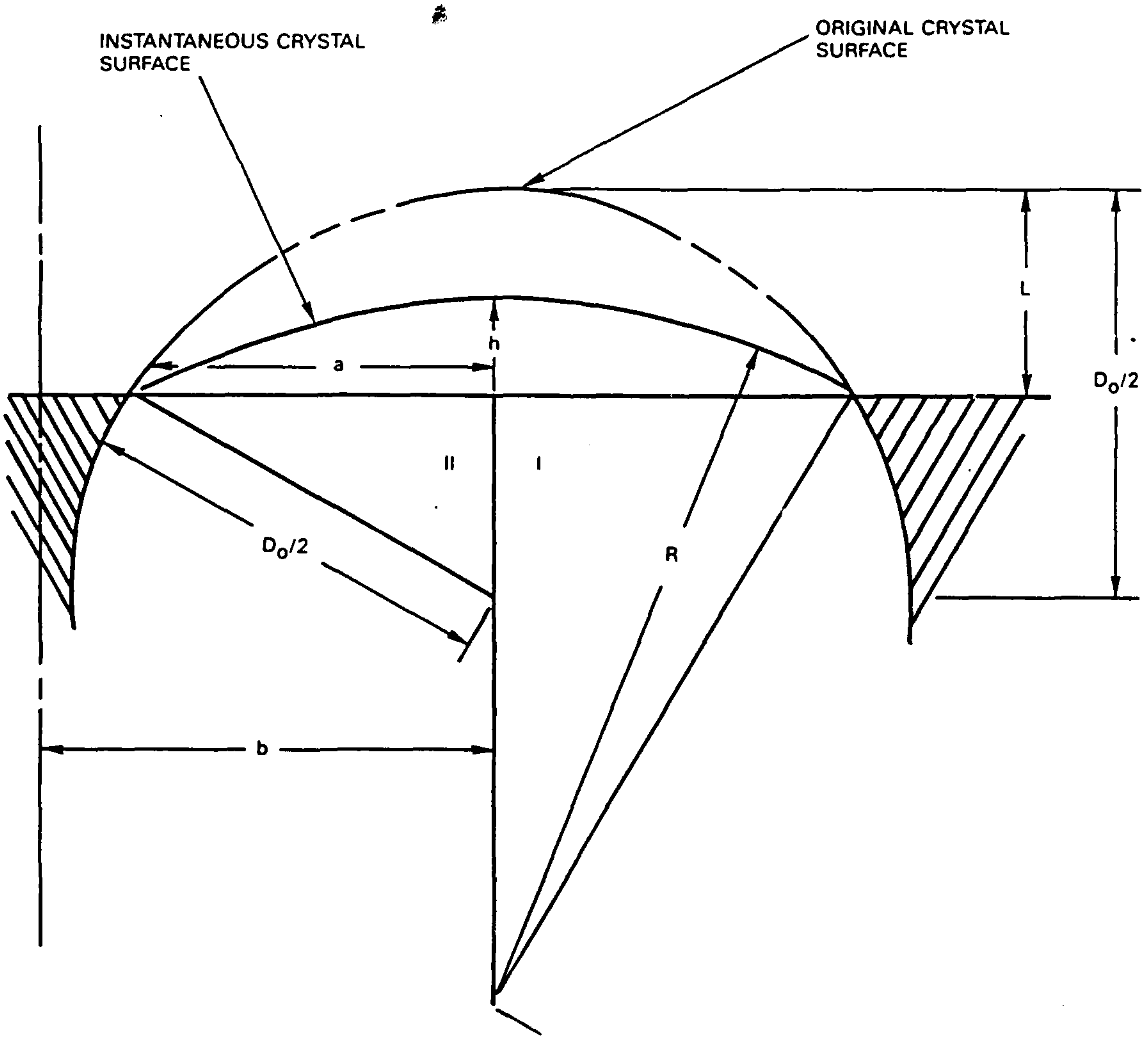

Figure 6
Geometrical Relationship of the Oxidizer Crystal to the Burning Area

$$\frac{h}{D_o} = \frac{1}{2}(1 \pm \sqrt{1/3})\left(1 - \frac{r_{ox}}{r_f}\right) + r_{ox}\frac{t_{ign}}{D_o} \qquad (34)$$

In the above expressions ζ is the volume fraction of oxidizer, h is the distance a oxidizer crystal either protrudes above or is depressed below the surface of the propellant, t_{ign} is the ignition delay time of the oxidizer crystal and D_o is the oxidizer crystal diameter. r_{ox} and r_f are the burning rates of the oxidizer and fuel respectively, given by equations (28) and (29). The + or - in equation (34) refers to the positive or negative particles, ie. whether the lower hemisphere or the upper hemisphere is cut by the planar surface. It is assumed that there are an equal number of positive and negative crystals.

2.1.3.3 Energy Balance

Figure 7 shows the heat transfer from the three flames above the propellant's surface, the surface decomposition energies and the state values of enthalpy at the propellant surface and deep into the propellant. From Figure 7, the one-dimensional energy balance at the burning surface is:

$$\dot{m}_T C_p(T_s - T_o) = -\dot{m}_{ox}(S_{ox}/S_o)Q_L - \dot{m}_T(S_f/S_o)Q_f +$$
$$\beta_f Q_{PF}\dot{m}_T exp(-\xi^*_{PF} + (1-\beta_f)\dot{m}_{ox}(S_{ox}/S_o)[Q_{AP}exp(-\xi^*_{AP}) + Q_{FF}exp(-\xi^*_{FF})] \qquad (35)$$

where C_p is the average specific heat of the gases and the solid and T_o is the initial propellant temperature, Q_L and Q_f represent the energy required to vaporize the oxidizer and fuel respectively, Q_{PF}, Q_{AP}, and Q_{FF} represent the energy released in the final flame, and AP flame and the primary flame respectively, β_f is the fraction of reactants that react in the primary flame, and ξ^*_{PF}, ξ^*_{AP}, and ξ^*_{FF} are the non-dimensional flame standoff distances for the final flame, the AP flame and the primary flame, respectively.

After rearranging equation (35) and combining with equation (31), the equation for the average surface temperature can be written:

$$T_s = T_o - \alpha Q_L/C_p - (1-\alpha)Q_F/C_p + \beta_f(Q_{PF}/C_p)exp(-\xi^*_{PF})$$
$$+ (1-\beta_f)[(Q_{AP})/C_p)exp(-\xi^*_{AP})$$
$$+ (Q_{FF}/C_p)exp(-\xi^*_{FF})] \qquad (36)$$

The heat release terms can be expressed by:

$$Q_{PF} = C_p(T_f - T_o) + \alpha Q_L + (1-\alpha)Q_f \qquad (37)$$

$$Q_{AP} = C_p(T_{AP} - T_o) + Q_L \qquad (38)$$

$$Q_{FF} = (C_p/\alpha)[(T_f - T_o) - \alpha(T_{AP} - T_o) + (1-\alpha)Q_f/C_p] \qquad (39)$$

where T_f and T_{AP} are the final flame temperature and the AP monopropellant flame temperature respectively.

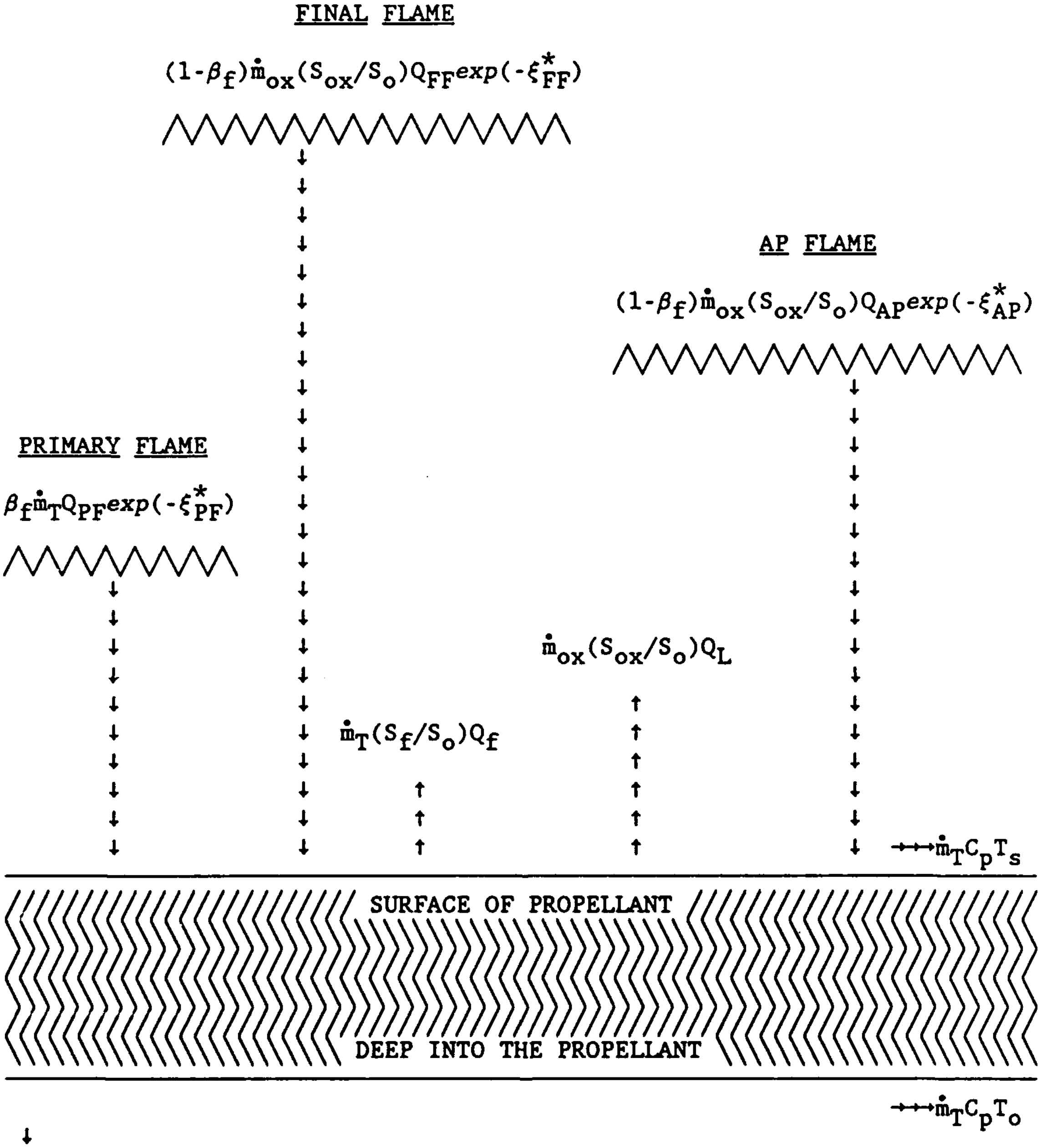

↓
↓ - Heat Transfer from Flames to Propellant Surface
↓

↑
↑ - Heat Transfer from Surface Decomposition Reactions
↑

→→ - The Enthalpy Terms at the Surface and Deep into the Propellant

Figure 7
The BDP Surface Energy Balance

2.1.3.4 Flame Standoff Distances

The non-dimensional primary flame standoff distance is the sum of the diffusional mixing distance plus the kinetic reaction distance and is given by:

$$\xi^*_{PF} = \frac{c_p\dot{m}_T}{\lambda}(\bar{x}^*_{PD} + x^*_{PF}) = \frac{c_p\dot{m}_T}{\lambda}\bar{x}^*_{PD} + \frac{c_p\dot{m}_T{}^2}{\lambda k_{PF}P^\delta} \tag{40}$$

In this expression $\bar{x}^*_{PD}$ is the effective diffusional standoff distance, x^*_{PF} is the kinetic reaction distance, λ is the thermal conductivity, k_{PF} is the reaction rate constant for the primary flame and δ is the reaction order. The non-dimensional AP monopropellant flame standoff distance consists of a kinetic reaction distance only and is:

$$\xi^*_{AP} = \frac{c_p m_{ox}}{\lambda}x^*_{AP} = \frac{c_p\dot{m}_{ox}{}^2}{\lambda k_{AP}P^\delta} \tag{41}$$

The final flame standoff distance is assumed purely a diffusional flame but is assumed to occur above the AP monopropellant flame. Hence, is the sum of the AP kinetic flame standoff distance plus the diffusional mixing distance of the final flame and is given by:

$$\xi^*_{FF} = \frac{c_p\dot{m}_{ox}}{\lambda}(x^*_{AP} + \bar{x}^*_{FD}) = \frac{c_p\dot{m}_{ox}{}^2}{\lambda k_{AP}P^\delta} + \frac{c_p\dot{m}_{ox}}{\lambda}\bar{x}^*_{FD} \tag{42}$$

Using global kinetics the generic form of the kinetic reaction distance can be expressed as:

$$\xi^* = \frac{c_p\dot{m}}{\lambda}x^* \tag{43}$$

To determine the diffusional flame standoff distance the authors assumed that the burning oxidizer crystal surrounded by fuel could be represented by Bunsen burner type of flame. An analysis reported by Burke and Schumann on this type of flame and later modified by Williams, was used to arrive at the following equation for the average diffusional flame standoff distance.[13,21,22]

$$\bar{x}^*_D = \frac{2c_2h'A_{fh}}{\dot{m}\left\{\left[1+\left(\frac{2c_2\phi_1}{\dot{m}_b}\right)^2\right]^{1/2}-1\right\}} \tag{44}$$

In this equation c_2 is a constant related to the propellant properties, η is a constant relating to the stoichiometry of the flame, ϕ_1 is the first non zero root of the first order Bessel function and b is a characteristic dimension at the surface. The term A_{fh} is a constant that determines the effective planar flame height. The Burke-Schumann flame height analysis determines the maximum height of the diffusion flame. The diffusional heights used in equation (40) and (42) are effective planar flame heights. In the equations (43) and (44) the appropriate mass flux, reaction order, rate constant, and physical constants are used to arrive at correct flame standoff distances used in equations (40), (41) and (42).

2.1.3.5 The Competing Flames

There is one final term needed in the energy equation which has not been defined. This term, β_f, is the fraction of the total reactants issuing from the propellant surface that react in the primary flame. This term is required since there is competition for the oxidizer decomposition products between the primary flame and the AP monopropellant flame. Based solely on geometry, and assuming that the primary diffusion flame is parabolic in shape, this term can be calculated with the following expression:

$$\beta_f = \frac{x_{AP}^* - x_{PF}^*}{x_{PD}^*} \qquad (45)$$

In this expression the numerator is the difference between the primary flame and AP monopropellant flame kinetic reaction distance. The denominator is the actual primary diffusion flame height given by equation (44) with A_{fh} equal to one.

2.1.3.6 Discussion

Comparisons were made with a series of unimodal AP polysulfide propellants.[13] The predicted dependence of burning rate on oxidizer concentration was nearly the same as observed experimentally, where the dependence of the burning rate on the oxidizer particle size was greater than observed experimentally. The dependence of the burning rate on the initial temperature was found to be in qualitative agreement with the available experimental data.

The Beckstead, Derr, Price multiple flame composite propellant combustion model laid the foundation for the subsequent Petite Ensemble Model which will be described next.

2.1.4 Petite Ensemble Model (PEM)

In both the Beckstead, Derr, Price multiple flame model and the Hermance heterogeneous reaction models, it was assumed that the macroscopic behavior of an ensemble of different flames surrounding several sized oxidizer particles can be replaced by a multiple flame structure centered about a single, characteristically sized oxidizer particle. In actuality, the burning propellant surface is much more complicated with many different sized oxidizer crystals all burning simultaneously and reacting with a binder medium. A statistical approach to deal with a more complicated burning surface structure was first presented in 1974.[23] The combination of a statistical formalism within a Beckstead, Derr, Price multiple flame model was called the Petite Ensemble Model (PEM).[24-28]

In the PEM, the burning surface of a composite propellant is assumed to consist of a random arrangement of polydisperse, or multi-sized, oxidizer particle/fuel binder surface pairs. It is further assumed that each oxidizer particle at the propellant surface has associated with it a portion of the total available fuel binder that is assumed to surround every oxidizer crystal. Therefore, each oxidizer particle/fuel binder pair will produce a unit flame structure centered about the oxidizer particle. If it is assumed that all of the oxidizer/fuel pairs burn independently of each other, then the burning propellant surface can be mathematically rearranged into imaginary families of monodisperse, or all one size oxidizer particles, propellants. These monodisperse propellants are subsequently referred to as pseudo propellants.

The statistically-based PEM calculates the overall burning rate of a polydisperse propellant with a summation scheme incorporating the calculated pseudo propellant burning rates. That is, if the available combustion model can determine the burning rate of each of the monodisperse pseudo propellants, or more precisely, of each of the oxidizer/fuel pairs, then with a knowledge of the oxidizer particle size distribution, the overall propellant burning rate can be determined.

2.1.4.1 Statistical Formulation

Before presenting the expression describing the overall propellant burning rate as a function of the pseudo propellant burning rates, a description of the oxidizer size and size distribution will be presented. A composite propellant is a heterogeneous mixture of finely ground oxidizer particles all mixed in with a liquid fuel binder which is polymerized into the solid propellant. The oxidizer particles used in composite propellants range in size from less than a micron to several hundred microns in diameter.

The number density of oxidizer particles in a composite propellant usually varies in a log normal distribution fashion with the size of the particle. This variation of particle number density with particle diameter is termed a particle size distribution. Figure 8 depicts a typical particle size distribution for a nominal diameter of 10 microns. Composite propellants usually contain several distribution modes in order to achieve high solids loading to obtain high oxidizer to fuel ratios. A log normal distribution function can be expressed by the following equation:

$$F_d = \frac{1}{\sqrt{2\pi}\, ln\sigma_{ox}} \, exp\left[-\frac{1}{2}\left(\frac{lnD_{ox} - ln\bar{D}_{ox}}{ln\sigma_{ox}}\right)^2\right] \tag{46}$$

The mean diameter, $\bar{D}_{ox}$ is the fifty percent weight mean diameter, since half of the oxidizer's mass is composed of diameters less than $\bar{D}_{ox}$. The term σ_{ox} represents the actual width of the distribution about this mean oxidizer diameter. A mode width parameter, σ_{ox}, equal to unity corresponds to a monodisperse oxidizer mode; that is all oxidizer particles in that mode are of one diameter, $\bar{D}_{ox}$. A mode width parameter exceeding unity represents a polydisperse oxidizer mode distribution. In a polydisperse mode, the oxidizer mass is distributed about the mean particle size; the larger the value of σ_{ox}, the wider the distribution of oxidizer mass about $\bar{D}_{ox}$.

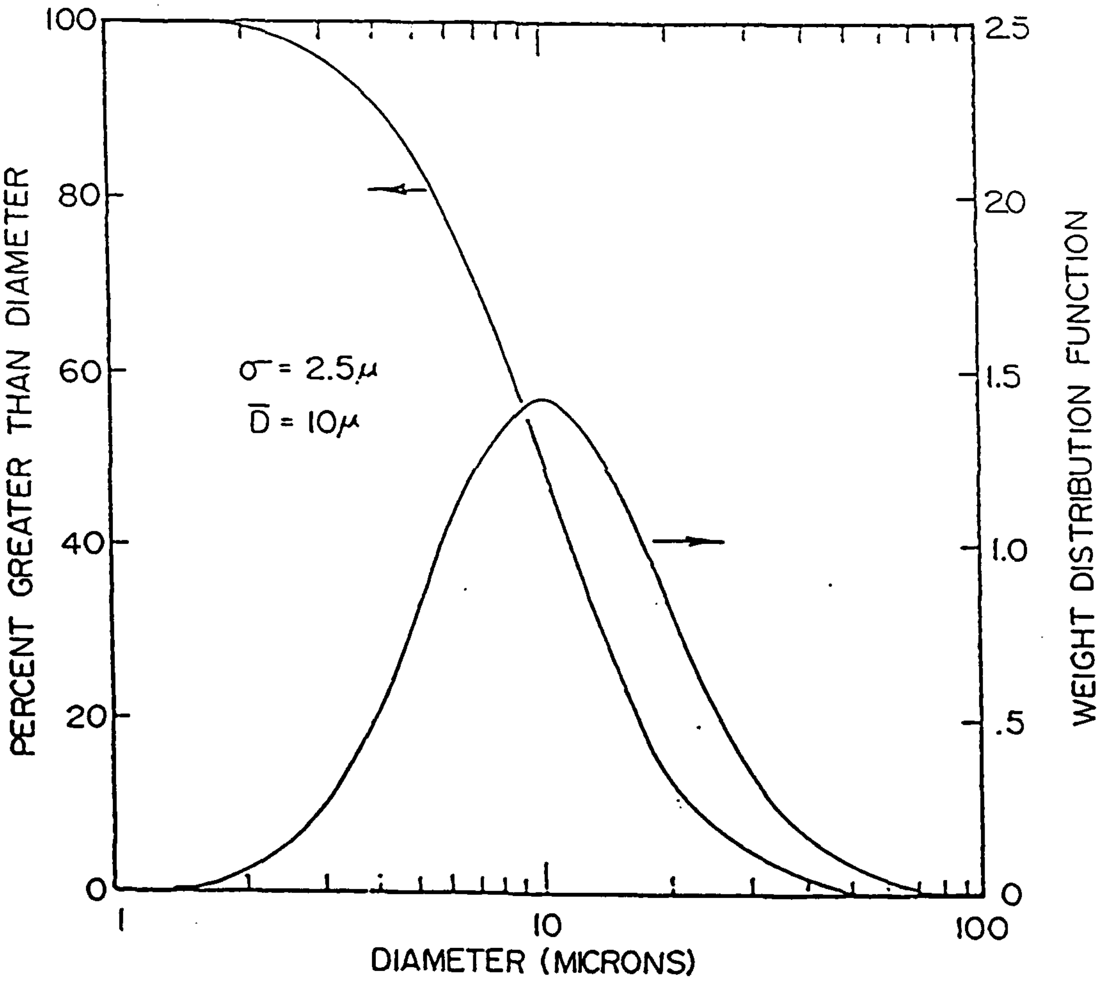

Figure 8
A Typical Particle Size Distribution

By utilizing the log normal distribution function given in equation (46), each oxidizer mode within a composite propellant can be represented by the two independent parameters, $\bar{D}_{ox}$ and σ_{ox}, and the oxidizer particle size distribution can easily be characterized by a simple log normal expression of the form given by equation (46). An expression for the overall polydisperse propellant burning rate, $\bar{r}$, can now be presented:

$$\bar{r} = \oint_{D_{ox}} (r_d F_d)\, d\,ln D_{ox} \tag{47}$$

In this expression, r_d and F_d are the burning rate and distribution function, respectively, of each of the monodisperse pseudo propellants of a given oxidizer diameter (as designated by the subscript d).

2.1.4.2 Separate Surface Temperatures

In the development of the basic equations comprising the Petite Ensemble Model (PEM), many of the assumptions evoked in the Beckstead, Derr, and Price (BDP) model discussed previously are retained. This is especially true in the description of the surface geometry of the oxidizer crystal embedded in the fuel binder. In the subsequent analysis, it will be assumed that the propellant is composed of spherical oxidizer crystals and a fuel binder.

In describing the propellant surface, it is assumed that the oxidizer crystals are randomly mixed within a fuel binder. Like the Beckstead, Derr, Price multiple flame model the statistical average intersection diameter, D', is:

$$D' = \sqrt{2/3}\, D_o \tag{19}$$

As in the BDP model the oxidizer mass burning rate and the fuel binder burning rate are assumed to be represented adequately by an Arrhenius expression based on the surface temperature. Unlike the original BDP model, the surface temperatures of the oxidizer and binder are different. The Arrhenius expressions are as follows:

$$\dot{m}_{ox} = r_{ox}\rho_{ox} = A_{ox} exp(-E_{ox}/RT_{s,ox}) \tag{48}$$

$$\dot{m}_f = r_f \rho_f = A_f exp(-E_f/RT_{s,f}) \tag{49}$$

In these expressions $T_{s,ox}$ and $T_{s,f}$ are the surface temperature of the oxidizer and fuel, respectively.

2.1.4.3 Surface Energy Balance

Like the BDP multiple flame model the entire PEM analysis of the burning behavior of a solid propellant rests upon the solution of the energy balance equation written at the propellant surface. The energy transmitted back to the surface from the individual flames situated above the surface must be equal to the heat required to bring the propellant from an initial propellant temperature, T_o, up to a given temperature at the surface and to supply heat, if required, for constituent gasification at that surface. It has already been shown that the rate of gasification of each of the reactants is tied directly to its respective surface temperature. The surface energy equation couples the solid phase and gas phase processes occurring simultaneously during the burning of solid propellant.

Assuming the oxidizer has a surface temperature, $T_{s,ox}$, and the fuel binder has a possible different surface temperature, $T_{s,b}$, the surface energy balance takes the following form:

$$\alpha C_{p,ox}(T_{s,ox}-T_o) + (1-\alpha)C_{p,f}(T_{s,b}-T_o) = \alpha Q_L + (1-\alpha)Q_f$$

$$+ \beta_f Q_{PF} exp(-\xi^*_{PF}) + (1-\beta_f)\alpha Q_{AP} exp(-\xi^*_{AP}) + (1-\beta_f)Q_{FF} exp(-\xi^*_{FF}) \qquad (50)$$

The terms on the left-hand side of equation (50) are simply the sensible heat terms associated with bringing the oxidizer and fuel binder, in their respective relative proportions, up to their surface temperatures. It is assumed throughout this analysis that the oxidizer and fuel binder have different values of solid phase specific heat, $C_{p,ox}$ and $C_{p,f}$, respectively. The next two terms represent net energy either absorbed or released at the surface, Q_L is the latent heat of oxidizer surface decomposition and Q_f is the heat of pyrolysis for the fuel binder. The convention adopted for this analyses is that the terms Q_L and Q_f are positive if the phase change reaction is endothermic and negative if the phase change reaction is exothermic.

Finally, one has three terms associated with the heat released by the three flames. The energy actually released by each of the individual flames per unit mass of reactants is given the designation Q_{PF} for the primary flame, Q_{AP} for the oxidizer monopropellant flame and Q_{FF} for the final flame. The actual quantity of energy transferred back to the propellant surface can be shown to be equal to the quantity of energy released in the flame times the $exp(-\xi^*)$, where ξ^* is a non-dimensional flame standoff distance. Separate energy balances can be utilized to evaluate each of the three flame heat release terms:

$$Q_{AP} = C_{p,ox}(T_{s,ox}-T_o) + C_{p,g}(T_{AP}-T_{s,ox}) + Q_L \qquad (51)$$

$$Q_{PF} = \alpha C_{p,ox}(T_{s,ox}-T_o) + (1-\alpha)C_{p,f}(T_{s,b}-T_o)$$

$$+ (1-\alpha)Q_f + \alpha C_{p,g}(T_F-T_{s,ox}) + (1-\alpha)C_{p,g}(T_F-T_{s,b}) \qquad (52)$$

$$Q_{FF} = (1-\alpha)C_{p,f}(T_{s,b}-T_o) + (1-\alpha)C_{p,g}(T_F-T_{s,b})$$

$$+ \alpha C_{p,g}(T_F-T_{AP}) + (1-\alpha)Q_f \qquad (53)$$

In these expressions, T_F and T_{AP} are adiabatic flame temperatures for the overall propellant mixture and for pure AP, respectively.

2.1.4.4 Flame Standoff Distances

The flame standoff distances are computed performing a modified Burke-Schumann flame analysis like in the Beckstead, Derr, Price model described earlier. However, there are several important improvements. The modified Burke-Schumann solution for the shape of a Bunsen burner type flame surface is:[21,22]

$$\frac{\nu-(1+\nu)c^2}{2(1+\nu)c} = \sum_{n=1}^{\infty} \frac{1}{\phi_n}\frac{J_1(c\phi_n)}{[J_o(\phi_n)]^2} J_o(\phi_n\xi)\; exp\left[\frac{-\left([1+(2\psi\phi_n)^2]^{1/2}-1\right)\eta}{2\psi^2}\right] \tag{54}$$

In the equation ν is the stoichiometric ratio given by:

$$\nu = \frac{\Phi_{actual}}{\Phi_{stoich}} \tag{55}$$

where the actual stoichiometric ratio is:

$$\Phi_{actual} = \frac{1-\alpha-\beta}{\alpha} \tag{56}$$

and Φ_{stoich} is related to the type of fuel and oxidizer considered and can be readily found within the literature. The variable c is the ratio of the inner oxidizer radius, a, to the outer fuel binder radius, b. ϕ_n represents roots of the first order Bessel function, J_1. J_o is a Bessel function of the zeroth kind. ψ is a function of diffusivity, gas stream velocity, and the outer radius b; $\psi = D/(vb)$. ξ is the non-dimensional radial distance and η is the non-dimensional axial distance.

In the BDP model and early versions of the PEM only the first term of the Bessel function series is computed in equation (54).[13,24] This is called the short flame approximation. In later versions of the Petite Ensemble model, terms are computed in the series until the terms become very small yielding a more exact solution to the diffusional height, x^*_D.[25-28] Equation (54) is solved by setting the non-dimensional radial distance, ξ, to zero and solving for the non-dimension axial distance, η.

The second difference is that the averaged effective flame height is exactly computed instead of using the assumed constant, A_{fh}, of equation (44). If is assumed that the flame shape over a oxidizer surrounded by a fuel binder is parabolic, it can be shown that a distributed heat release all along the parabolic flame front surface can be represented by a planar flame sheet at some fraction of the diffusion flame height. This parameter, ϵ, is calculated from the non-dimensional flame height, ξ^*, by the relation:

$$\epsilon = \frac{[ln(\xi^* exp(\xi^*)) - ln(exp(\xi^*)-1)]}{\xi^*} \tag{57}$$

so the effective planar flame heights are given by:

$$\bar{x}^*_{PD} = \epsilon_{PD}x^*_{PD} \quad \text{and} \quad \bar{x}^*_{FD} = \epsilon_{FD}x^*_{FD} \tag{58}$$

In this expression, $\bar{x}^*_{PD}$ and $\bar{x}^*_{FD}$ are the primary and final diffusional flame effective planar flame standoff distances and x^*_{PD} and x^*_{FD} are the actual diffusion flame heights determined at the center of the two flames.

The final expressions for the net flame standoff distances are the same is seen previously and are given by:

$$\xi_{PF}^{*} = \frac{c_p \dot{m}_T}{\lambda}(\bar{x}_{PD}^{*} + x_{PF}^{*}) = \frac{c_p \dot{m}_T}{\lambda}\bar{x}_{PD}^{*} + \frac{c_p \dot{m}_T^{\,2}}{\lambda k_{PF} P^{\delta}} \tag{40}$$

$$\xi_{AP}^{*} = \frac{c_p m_{ox}}{\lambda} x_{AP}^{*} = \frac{c_p \dot{m}_{ox}^{\,2}}{\lambda k_{AP} P^{\delta}} \tag{41}$$

$$\xi_{FF}^{*} = \frac{c_p \dot{m}_{ox}}{\lambda}(x_{AP}^{*} + \bar{x}_{FD}^{*}) = \frac{c_p \dot{m}_{ox}^{\,2}}{\lambda k_{AP} P^{\delta}} + \frac{c_p \dot{m}_{ox}}{\lambda}\bar{x}_{FD}^{*} \tag{42}$$

The final term needed for equation (50) is β_f which represents the fraction of reactants that react in the primary flame. This term is based solely on geometry and is computed in the same manner as in the BDP model:

$$\beta_f = \frac{x_{AP}^{*} - x_{PF}^{*}}{x_{PD}^{*}} \tag{45}$$

2.1.4.5 Discussion

The Petite Ensemble Model was compared against AP polybutadiene (HTPB) propellants which contained up to 4 distributions of AP particles ranging in size from 0.7 to 400 microns.[29,30] The model successfully predicted the burning rate and exponent of these formulations with over seventy-five percent of the data being within ten percent of the predicted values.[25] The model successfully predicted the effects of particle size on propellant burning rate as well as the dependence of particle size distribution on burning rate.[26] The model has also been used to predict temperature sensitivity, and more importantly, predict the effects of particle size and propellant parameters on temperature sensitivity of composite propellants.[27]

2.2 The Physics and Chemistry of HMX Combustion

2.2.1 Physical Description of HMX

The cyclic nitramine cyclotetramethylenetetranitramine, commonly called HMX, is an important ingredient in propellants used in gun and solid rocket propulsion systems. HMX has also been called 1,3,5,7-tetranitro-octahydro 1,3,5,7-tetrazocine; 1,3,5,7-tetra-nitro 1,3,5,7-tetrazacyclo-octane; octahydro-1,3,5,7 tetranitro-1,3,5,7-tetrazocine; and, in the Soviet literature, octogen.[31]

HMX was first discovered in the 1920's simultaneously in the United States and Germany where it was found in small amounts during the production of the explosive RDX, a compound similar to HMX.[32] Because HMX melted 64°C higher than RDX, it was called the "high melting explosive" and, hence, the name HMX. It wasn't until the early 1940's when large quantities of explosives were required by the war effort that HMX was produced in any appreciable quantities.[32] The first important use of HMX was the detonating explosive for the first atomic weapons due to its thermal stability and high energy.

HMX is a cyclic molecule consisting of four methylene groups and four nitramine groups as shown in Figure 9. The chemical formula of HMX is $C_4H_8N_8O_8$. HMX in its pure form is an explosive and can be very hazardous due its sensitivity to shock. There are several advantages in using HMX as a propellant ingredient. Due to the high energy content of HMX, its high density and the low molecular weight of gas produced during its combustion, high values of specific impulse for rocket propellants and impetus for gun propellants can be achieved. In contrast to propellants based on ammonium perchlorate (AP), nitramine propellants do not produce hydrochloric acid (HCl) unless, AP is incorporated into the propellant to serve as a ballistic modifier. Besides being corrosive, HCl in the exhaust provides nucleation sites for moisture droplets to condense upon, thereby producing a visible contrail or secondary smoke. The decomposition, ignition and deflagration of HMX will be described in the following sections.

2.2.1.1 HMX Decomposition

Before the combustion and deflagration behavior of HMX can be modeled, it is necessary to have an understanding of the decomposition chemistry. An understanding of the detailed chemical decomposition might well make it possible to suggest new types of additives for combustion modification. Combustion models require decomposition kinetic parameters as inputs and the product distributions from the decomposition reactions are needed for detailed flame models.

The decomposition of solid HMX has been studied by heating the HMX and observing what evolves from the surface. Techniques used to measure the decomposition products include mass spectrometry, gas chromatography, and various laser diagnostic techniques.[33-51] The major nitrogen species found are N_2, N_2O, NO_2, NO, and NH_3 and the major carbon species found are CH_2O (formaldehyde), CO, CO_2 and HCN. The relative yield of the products is a function of the decomposition temperature and heating rate.[52-60] Figure 10

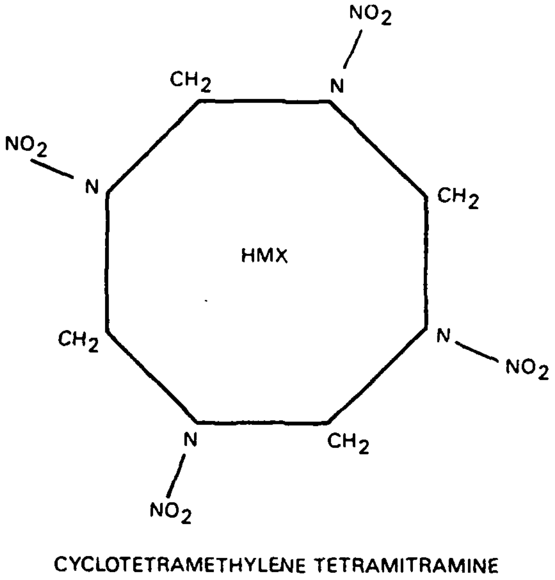

Figure 9
Chemical Structure of the HMX Molecule

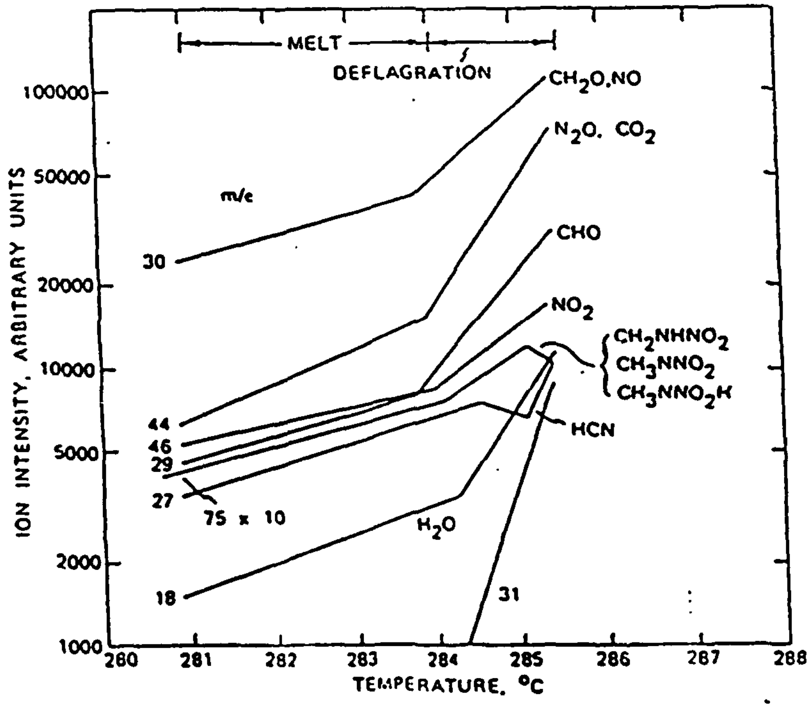

Figure 10
Change in HMX Decomposition Products Produced as a Function of Surface Temperature

shows the change in HMX decomposition products produced as the surface temperature is varied.[33] In studies in which the heating rates are low, ie. less than 100°C per second and, the primary species are CH_2O, NO, N_2O, CO_2 and CHO.[33-43] In studies where the heating rates are greater than 1000°C per second the primary species are NO, CO and HCN.[44-51] In an actual burning propellant the heating rates are extremely high, on the order of 10^5°C per second.

Several reaction mechanisms have been proposed on how HMX decomposes. Referring to Figure 9, one scenario is that C-N bond fission initiates the decomposition, and that in the gas phase the $N\text{-}NO_2$ bond rupture is important.[61] A two step flame is proposed: a near field, only microns off the surface, of exothermic nitramine decomposition to produce H_2CO, NO_2 and N_2O at a flame temperature of about 1100°K; and a far field driven partly by the oxidation of H_2CO by NO_2. This scenario has been extended to include a fizz zone near the surface of the $H_2CO + NO_2$ reaction and a preparation and final flame zone involving reduction of NO and oxidation of CO.[58] These analyses do not include HCN as an active specie.

A second scenario that includes HCN as an important specie, is that the HMX molecule initially eliminates an NO_2 molecule which greatly destabilizes the ring (refer to Figure 9) to produce rapid ring cleavage forming 3 molecules of H_2CNNO_2 and $H_2CN + NO_2$, with the H_2CNNO_2 further decomposing to H_2CO and N_2O or H_2CN and NO_2.[60] The H_2CN rapidly decomposes to H + HCN and the H attacks NO_2 to from NO and OH.

At low heating rates, 1°C/sec, HMX deflagrates at temperatures a few degrees above the liquefaction point of 280°C.[31,62] Since actual heating rates during HMX combustion are considerably higher, HMX surface temperatures during combustion are considerably higher. Little information is available on the actual surface temperature during actual HMX combustion, however, some work has been done with embedded thermocouples in which the surface temperature was measured to be around 500°C.[63-65]

As HMX is slowly heated to between 185°C - 190°C, it undergoes an endothermic crystallographic phase change process from beta to delta HMX.[62] Further heating leads to slightly exothermic decomposition, beginning at about 271°C.[31] This process is interrupted by a sharp endotherm at the liquefaction point, which is then quickly followed by exothermic deflagration at about 280°C.[33] The nature and proximity of the liquefaction and deflagration renders it difficult to define heats of fusion and decomposition for use in combustion models. If the heating rate is slow enough, the sample is observed to melt in bulk and commence vigorous boiling indicative of gas evolution in the melt phase.[31,33] The liquid is brown in color, and quickly disappears in a puff of brown smoke. The reaction from the melt phase is an exothermic process.[66]

The surface decomposition activation energies and frequency factors are important parameters in combustion modeling which are needed in the Arrhenius expressions which determine the surface regression rate as a function of surface temperature (see equations 28, 29, 48 and 49). The measured activation energies associated with decomposition of HMX range from 10 to 256 kcal/mole and frequency factors range from 1.0×10^5 to unrealistically high values of 2.7×10^{25} 1/sec.[67-73] This wide range of values may be attributed to various causes. Sources of error include an insufficient temperature range over which the measurement is made, uneven heating of the sample of HMX, effects of pressure, sublimation and gas phase reactions.[66,70,73] In view of the relatively narrow temperature range over which the principal events occur; ie. crystallographic phase change at around 190°C, solid phase decomposition at 271°C, liquefaction at 284°C and finally deflagrating between 285 and 500°C; it is possible that a reported activation energy reflects an average of several processes which change with temperature and physical state. A statistical analysis of available decomposition data suggests a "global" activation energy of 53 Kcal/mole and a frequency factor of 8.9×10^{19} 1/sec.[67] Where the surface of deflagrating HMX is a mixture of liquid and gas, it may be necessary to treat two processes of decomposition in combustion models.

The solid phase specific heat of pure HMX has been determined using a differential scanning calorimeter. A value of 0.25 cal/gr-°K was determined at 298°K.[74] The results showed that the differences in specific heat values for single crystals, powdered and partially decomposed samples were small.[75] In addition, the solid phase specific heat was found to be a linear function of temperature around 298 to 450°K. The solid phase thermal conductivity is also a linear function of temperature and has a value of 0.022 cal/cm-sec-°K at 298°K.[76,77]

2.2.1.2 HMX Ignition

The ignition of HMX has been studied using a xenon arc-image furnace and CO_2 laser apparatus to apply known heat fluxes to the crystal surface.[78-80] When a sample of HMX is subjected to an energy flux, several processes occur. At first, no reactions occur. This is a period of inert heating of the sample and is shown as Region I of Figure 11.[79] At some time, depending on the level of the flux and the sample itself, the sample will start to gasify, producing pyrolysis products. The occurrence of this gasification is shown by the "first light, first gasification" line of Figure 11. Unlike the behavior of AP propellants which almost immediately ignite upon gasification at the fluxes of most tests, HMX displays significant pre-ignition behavior. The pyrolysis gases flow from the surface but do not immediately ignite. This is the pre-ignition region, shown as Region II of Figure 11. If conditions are favorable, the flame "snaps back" to an equilibrium position, and the sample is said to have ignited. That is, the energy release from the flame is sufficient to further pyrolyze the surface providing more reactants and the process can become self-sustaining. The point at which the combustion can be sustained, upon interruption of the external flux, is said to be full or go/no-go ignition. The "go/no-go" ignition locus is shown in Figure 11 dividing Regions II and III.[79] As is shown in Figure 11, there is a significant delay between gasification of the solid and ignition of HMX.

The experimentally observed behavior shown in Figure 11 has also been analytically modeled using two different approaches. The first approach was to use Bradley's Unified Ignition Theory which includes both mass and thermal diffusion effects.[81] This approach, because of the completeness of the analytical description, is difficult to run so a simpler, modified flame sheet analysis was also used.[82] The results of calculations using both methods are also indicated in Figure 11. These analyses were then used to predict ignition behavior of HMX at other fluxes and pressures.[79] It was concluded that gas-phase reactions and diffusion processes, specifically the reaction of pyrolysis products to final products and the rate at which these reactions occur, control the ignition event. Other HMX ignition studies found that the time to ignite depended on the atmosphere and upon the pressure, further evidence that ignition takes place in the gas phase.[83,84]

A different study which examined the ignition of catalyzed RDX (a compound similar to HMX) concluded that the gas phase reactions were also responsible for controlling the ignition behavior. The ignition was studied using a reflected shock technique by shock-heating N_2 at reflected shock temperatures of 600-1200°K and pressures of 0.1-1.5 MPa.[85] For temperatures greater than 750°K, ignition delays were independent of pressure and almost independent of temperature. For temperatures less than 750°K, temperature dependence increased markedly and the HMX ignition delays showed an inverse pressure dependence. It was concluded that for temperatures less than 750°K the gas phase reactions and diffusional processes control ignition.[85]

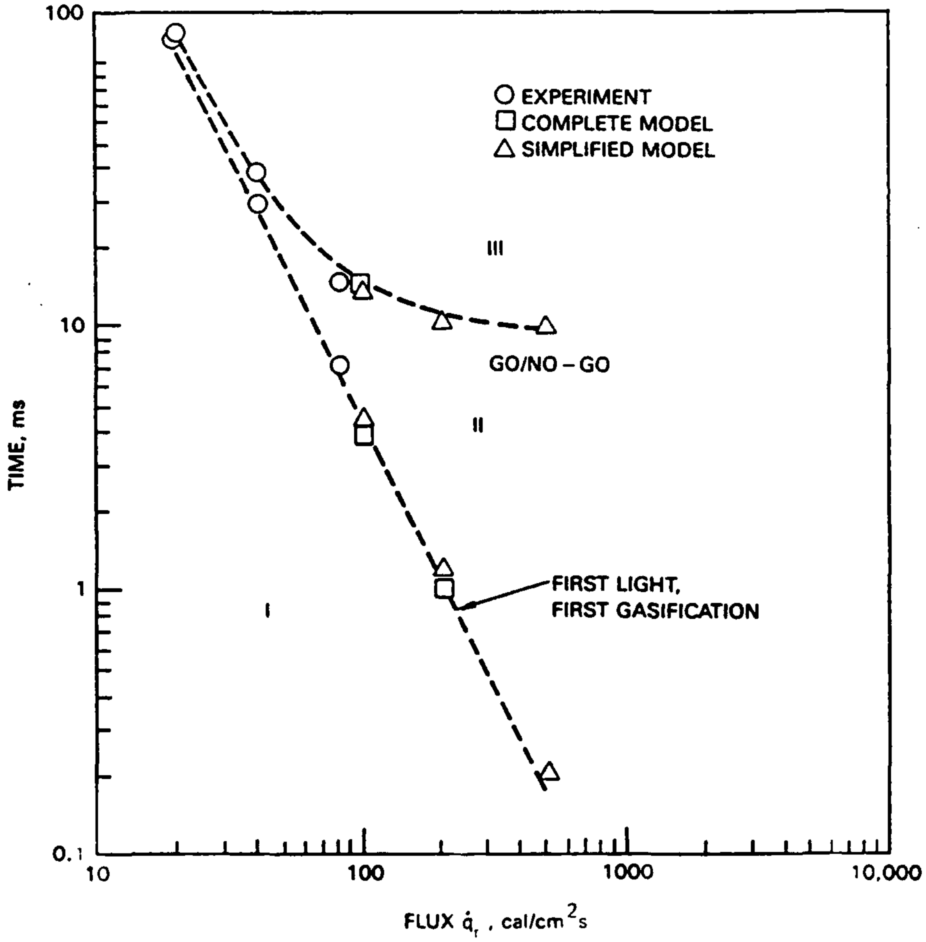

Figure 11
Ignition of HMX Pressed Pellets Using Xenon Arc-image Furnace

2.2.1.3 HMX Deflagration

Motion pictures and quench techniques have been applied to observe the surface characteristics of deflagrating HMX. At one atmosphere, there is a thick bubbling melt layer. The melt layer thins at higher pressure, becoming about 4μm thick at 1000 psia and not discernible above 1700 psi.[38] The presence of gas bubbles in the melt layer of deflagrating HMX is observed in electron microscope photography of extinguished sample surfaces.[86]

At 1700 psi, the characteristic thermal wave thickness in the HMX is about 6μm and the heating rate becomes about 10^6°C per second, so depending upon the surface temperature, a melt layer of less than 1μm would is reasonable.[62] Another interesting surface feature of deflagrating HMX is the presence of dark spots. These dark spots are probably a polymeric residue of decomposition.[62] HMX is slightly fuel-rich and similar spots have been observed on the surfaces of deflagrating nitrocellulose propellants which are slightly fuel-rich.

The gas phase at pressures below 1000 psia consists of a transparent blue flame and white smoke.[62,80] The white smoke was originally believed to be condensed H_2CO, formaldehyde. Recent investigations have shown this to be incorrect. Using Coherent Anti-Stokes Raman (CARS) temperature measurements and planar laser induced fluorescence, NO_2, NO, CN, NH and OH were seen in the product gases but there was no evidence of H_2CO.[48-51]

Flame standoff distances are difficult to determine since the reaction zone is not a simple flame sheet. At pressures above 2000 psia, the gas phase consists of a bright orange flame.[62,79] This orange color may be due to additional soot in the combustion products.[51] This change would seem to be significant, yet the burning rate-pressure curve is not significantly altered at ambient temperature.[31,62]

The burning rates of HMX have been measured using single crystals and pressed pellets of HMX from atmospheric pressure to 50000 psi and over various initial propellant temperatures.[86-91] Data near one atmosphere are considered to be uncertain due to the nature of the bubbling decomposition at low pressure.[62] These burning rate, pressure and temperature dependence data are needed by combustion modelers to check limiting conditions of the model and to deduce values of unknown constants by fitting the model to the data.

One interesting result that has been observed in the combustion of HMX are the discontinuities in the burning rate dependence on pressure.[86,88-91] Figure 12 shows the burning rate of HMX versus pressure from 100 to 50000 psia.[89] As can be seen in Figure 12, there is an abrupt change in the burning rate at around 700 psi where the pressure exponent becomes very large over a narrow pressure range and elevates the burning rate by several orders of magnitude. Very small HMX particles do not show this behavior and have a much smoother burning rate versus pressure curve.[90]

One explanation for this burning rate behavior is attributed to the formation of non-uniform melt layer over the surface of the HMX. Smaller particles are more easily heated and, hence, are covered by a melt layer of molten HMX. The melt layer over the small particles prevents the permeation of hot gases into the HMX solid particle bed. In larger crystals the melt layer is uneven, thinner and more readily broken by protruding HMX crystals. As a consequence, depending on particle size and beyond a given pressure, the liquid layer in larger crystals is non-uniform and allows hot gases to diffuses into the HMX and increase the mass burning rate by increasing the heat transfer to the crystals.[92,93]

A second theory, which is an extension of the first, states that the added heat transfer to the larger crystals causes the crystals to crack due the added thermal stresses.[94-97] The thermal cracking increases the exposed crystal surface area. The greater surface area increases the burning rate by allowing even greater heat transfer into the solid.

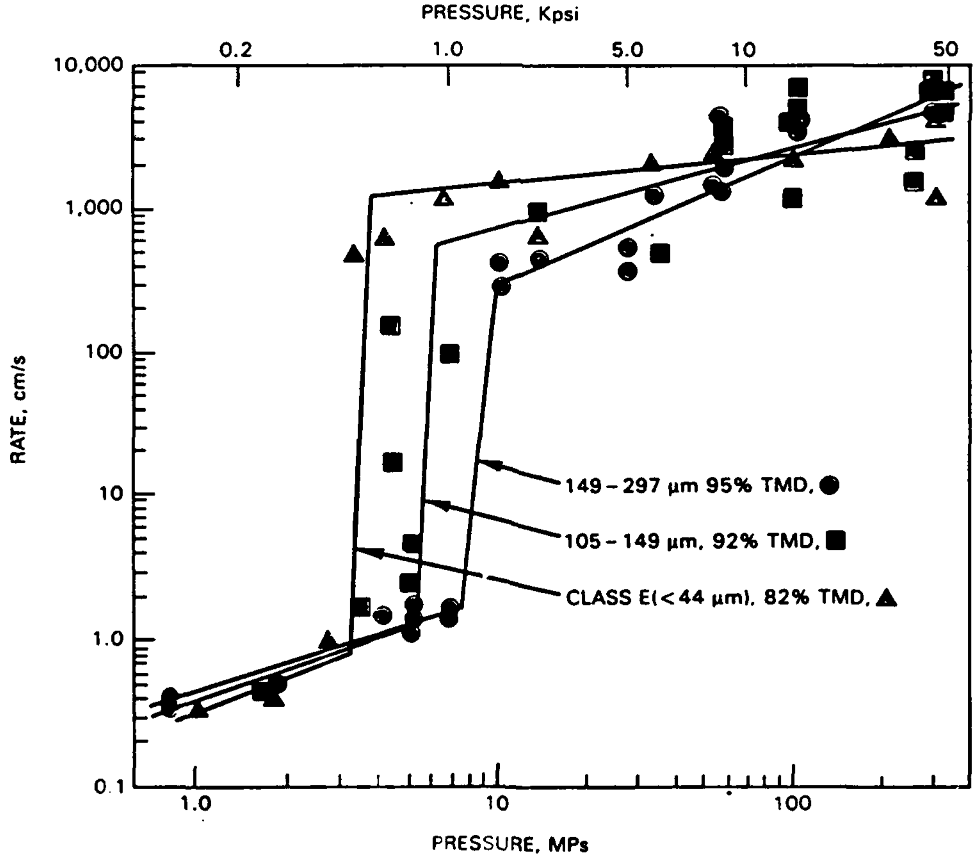

Figure 12
Apparent Burning Rates of HMX

The above explanations indicate that the slope breaks shown in Figure 12 result from structural changes in the HMX crystals, and not changes in the actual burning rate pressure dependence of pure HMX. In an effort to prove that structural phenomenon like crystal cracking is an important aspect in HMX combustion, an attempt was made to make tougher, less fragile crystals by an acetone pressing technique.[96,98] The burning rate of these samples was measured in a closed combustion bomb at pressures from 1 atmosphere to 50,000 psi. The burning rate versus pressure curve is shown in Figure 13. In Figure 13, there are no slope breaks and the pressure exponent is approximately one.

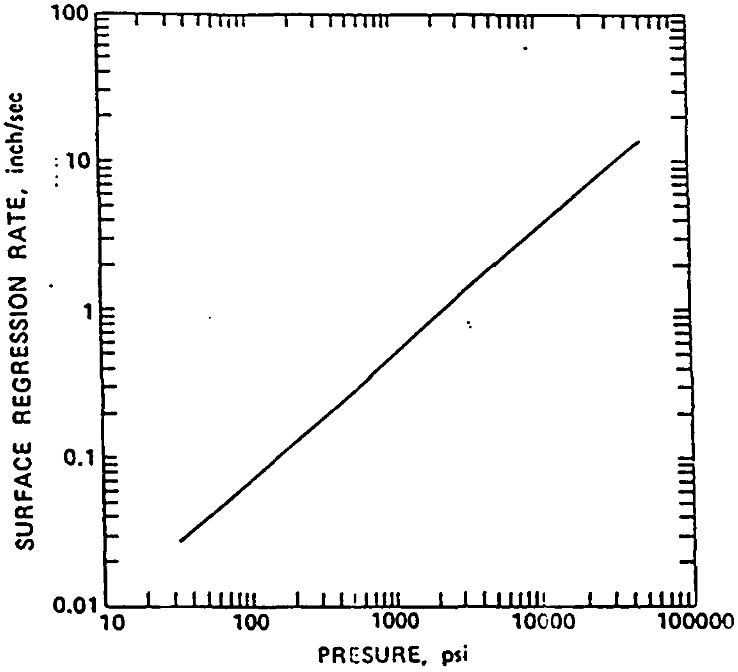

Figure 13
Pure HMX Burning Rate Data with no Crystal Cracking

2.2.2 HMX Composite Propellants

Propellants containing cyclotetramethylenetetranitramine (HMX) are of considerable interest for solid rocket propulsion. The average molecular weight of the combustion products of composite nitramine propellants is lower than that of more conventional AP based composite propellants. Consequently, the propellant performance is greater than AP propellants at equivalent flame temperatures since propellant performance is inversely proportional to the molecular weight of the exhaust products. Furthermore, propellants with HMX crystals tend to have higher densities than AP propellants and, thus, their density impulse is greater. Other advantages gained by using nitramines in propellant formulations include excellent thermal stability, low propellant flame temperature and non-toxic, non-corrosive combustion products. However, numerous problems have been encountered by the substitution of HMX for AP in propellant formulations. These include high burn rate exponents, exponent shifts, low burning rate, and difficulty in tailoring these low burning rates and high pressure exponents. In addition, nitramine composite propellants are much more difficult to ignite when compared to AP-based composite propellants.[99,100]

The pressure exponent of nitramine composite propellants exhibits complex behavior as pressure changes. The pressure exponent for HMX inert binder propellants ranges from 0.6 to 0.7 at pressures below 3000 psi. The value can exceed 1.5 between 3000 and 10000 psi and decreases to a value of approximately 1.0 as pressure is increased beyond 10000 psi.[101-111] For comparison, AP composite propellants exhibit exponents ranging from 0.3 to 0.9 to 3000 psi and are less sensitive to pressure changes.

Figure 14 illustrates the slope break phenomena typically observed for HMX mixed with an inert binder.[103] In Figure 14, the burning rate is a function of the HMX particle size. The two lines represent propellants containing coarse 195μm and fine 5μm HMX particles, respectively. At low pressures the larger particle size propellant exhibits burning rates significantly lower than that of the pure nitramine.[98] At about 3000 psi, a sudden increase in the pressure exponent occurs, and the burning rate rapidly approaches that of the pure nitramine. A second discontinuity then occurs, and thereafter the burning rate appears to follow that expected for the pure HMX (see Figure 13). Fine particle propellant exhibits higher burning rate at low pressure. A milder slope break occurs at a pressures higher than the coarse particle slope break. At very high pressures the burning rate approaches that of the pure nitramine.

One explanation advanced for the slope break phenomenon of HMX propellants is that at high pressures the HMX crystals are burning independently of the propellant binder.[103,104] At low pressures the propellant strand is able to burn as a complete propellant because the inert binder melts and fills the crystal interstices, wetting and encapsulating the crystals. A new composite propellant is formed that did not fully exist in the original cured propellant. At some higher pressure the burning rate of the HMX is fast enough to lead the development of the binder melt such that the the strand is able to burn as an HMX strand depending upon the extent of crystal contact and void interstices in the original propellant.

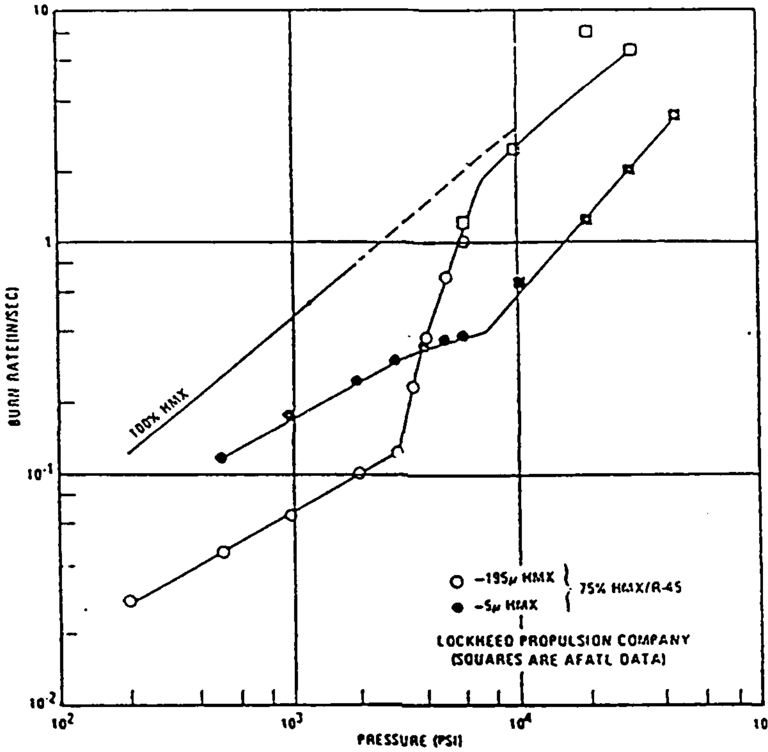

Figure 14
Burning Rate Characteristics of Pure HMX and HMX
Inert Binder Propellant

Other explanations for the slope break behavior of nitramine propellants include crystal fracture, change from condensed phase to gas phase control when the thickness of the thermal wave approaches the crystal dimension, condensed phase reaction at the binder nitramine interface and an ignition delay for the nitramine crystals which becomes unimportant for higher pressures.[110] However, none of these mechanisms explain all of the observed features of nitramine propellant combustion

Increasing the binder energy and, therefore the binder burning rate, to a value close to that of the HMX increases the low pressure burning rate. The use of energetic binders minimizes the magnitude of the large particle slope changes but still results in high pressure exponents.[112,113] Bimodal HMX (ie. a mixture of coarse and fine) propellants behave very much like propellants containing fine HMX only.[114]

An explanation for the small variation in burning rate at pressures less than 3000 psi is that HMX composite propellants, although heterogeneous in physical structure, burn more as a homogeneous propellant.[115-117] During burning, the crystalline HMX melts together with the polymeric binder on the propellant burning surface and forms a chemically energetic liquid mixture. Because of this melting, the combustion waves in the gas phase are homogeneous.

The burning rates of HMX propellants are usually much lower than comparable propellants containing AP. HMX inert binder propellants have burning rates of 0.05 to 0.20 in/sec at 1000 psia versus rates of 0.3 to 1.5 in/sec for similar inert binder propellants containing AP.[30,118] In order to achieve 0.3 to 1.5 in/sec variation in burning rate the AP particle size is adjusted in the propellant. As a general rule fine AP particles will give higher burning rates. However, for HMX propellants, variations in particle size have minimal effect on changing the burning rate as can been seen by comparing the burning rate range above with that of AP propellants. In order to increase the burning rate, propellant formulators have turned to additives such as Ferrocene and metal borohydrides.[119,120] In some cases the burning rates were accelerated by a factor of 2.2 using sodium borohydride but the pressure exponent was high and these rates are still below that of AP based propellants.[120]

2.3 HMX Combustion Models

2.3.1 HMX Monopropellant Models

One approach to the problem of understanding the combustion of HMX propellants has been to study the combustion of HMX itself, as a monopropellant. Two kinetic flame models and a Beckstead, Derr, Price type model will be discussed below which attempt to model the combustion of HMX as a monopropellant.

2.3.1.1 Kinetic Flame Model

Detailed analysis of solid mono-propellant deflagration traditionally incorporate a single overall reaction, with an imposed reaction order. This type of modeling ensures that the calculated burning rate will exhibit the correct pressure dependence, but may often be at odds with observations of the chemical kinetics of the process, and for example, cannot explain a variable pressure exponent. A complex flame structure, such as that indicated for nitramines, cannot be expected to be adequately represented by a single overall reaction model. An HMX monopropellant model based on nitramine flame chemistry was developed to address these considerations.[61,121-124]

The model postulates a high-gradient, relatively thin near field where primary decomposition dominates and an extended far field dominated by secondary reactions where gradients are small in comparison. The kinetic flame model demonstrated that the presence of the considerable weaker secondary reactions can enhance the primary decomposition reaction. This points to a mechanism of indirect coupling between the far field processes and the burning rate, through which the far field effect is amplified. Figure 15 shows the relative importance of the near field and far field reaction at varying distances from the propellant surface.[122]

The kinetic flame model was aimed primarily at testing the combined effects of particular chemical mechanisms, kinetics data and available thermophysical properties rather than calculating the burning rate. In addition, the model allows for distinct, simultaneous gas phase reactions.

The following assumptions were made. First, initial decomposition may occur in both the vapor phase and condensed phase, following unimolecular-overall kinetics. Second, the mechanism in the condensed phase is probably initiated by C-N bond fusion, whereas in the gas phase N-NO_2 bond rupture is the initial step leading consequently to different decomposition mechanisms for the vapor and condensed states. Finally, a large number of secondary reactions can occur, leading to the final combustion product and flame temperatures.

In the vapor phase, two major reaction categories were defined. The first is primary decomposition reactions forming reactive products such as CH_2O, NO_2, and N_2O. Second, these products may undergo further reactions that are somewhat slower and are typically of second order. CH_2 and NO_2 reactions lead to final complete combustion products such as H_2O, CO, CO_2, N_2 and NO. The two reactions are as follows:

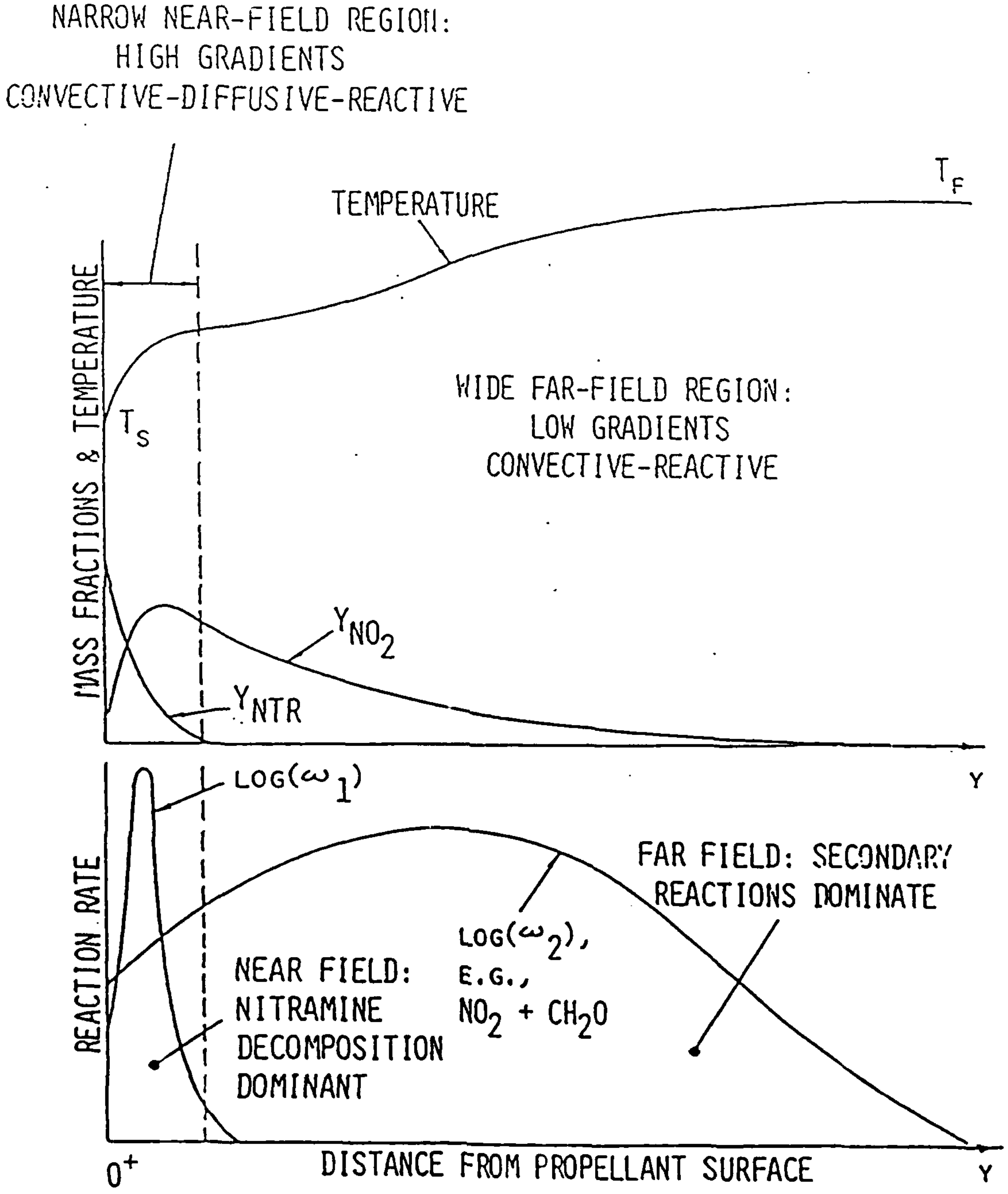

Figure 15
Gas Phase Diagram, Showing the Near Field and Far Field Configuration for the HMX Deflagration Wave (the near field region is magnified for clarity)

$$C_4H_8N_8O_8 \longrightarrow \tfrac{4}{3}NO_2 + \tfrac{4}{3}N_2O + 4CH_2O + 2N_2 \qquad (59)$$

$$NO_2 + \tfrac{5}{7}CH_2O \longrightarrow NO + \tfrac{3}{7}CO + \tfrac{2}{7}CO_2 + \tfrac{5}{7}H_2O \qquad (60)$$

All the reactions occur simultaneously and are thermally and chemically coupled. By introducing suitable approximations for the specific heat and thermal conductivity as a function of temperature, the above reactions containing nine separate species can be represented by a non-linear system of differential equations which are solved numerically. The consideration of two overall chemical reactions has led to the physical picture of the gaseous deflagration region. Figure 16 shows the mass fraction of species participating in the primary and secondary reactions, equation (59), versus distance from the surface at three different pressures.[122]

Later revisions to this model accounted for gas bubbles in the melt layer and the addition of a equilibrium nitramine evaporation law to facilitate independent calculation of the mass burning rate.[124] It was assumed that the bubbles are small relative to the overall melt layer thickness; the thermal relaxation times within the bubbles and between the bubbles and the liquid can be considered instantaneous; constant temperature exists throughout the bubbles; and the mean intrinsic thermophysical properties of specific heat, thermal conductivity and density are constant.

In the model's original form the experimental burning rate was an input into the model.[121] To facilitate independent calculation of the burning rate, an additional physical constraint was required. This physical condition is provided by the equilibrium evaporation law at the melt/gas interface. The process of evaporation, at any instant, involves molecules of the substance leaving the liquid in an outward flux, $\dot{m}_{out}$, and an influx of molecules effectively returning to the surface, $\dot{m}_{in}$. When the net effect is $\dot{m}_{out} = \dot{m}_{in}$, the vaporization is termed at equilibrium. This was assumed to occur at the surface of deflagrating nitramines.

A primary weakness of this type of model is a lack of complete and accurate kinetic reaction rate data. Without such data, experimental burning rates are needed to curve fit the insufficient kinetic data. Because of these problems, the model is largely empirical in nature. As more reaction rate data are available, this type of model will become more important.

A second flaw in the model is the reaction scheme employed for the near field, equation (59). The reaction includes CH_2O, formaldehyde, as a important specie. CH_2O has been shown to not be a dominate specie in the decomposition of HMX at realistic heating rates, and hence, burning rates. Formaldehyde is present at very low heating rates, but these heating rates are not representative of actual HMX combustion.

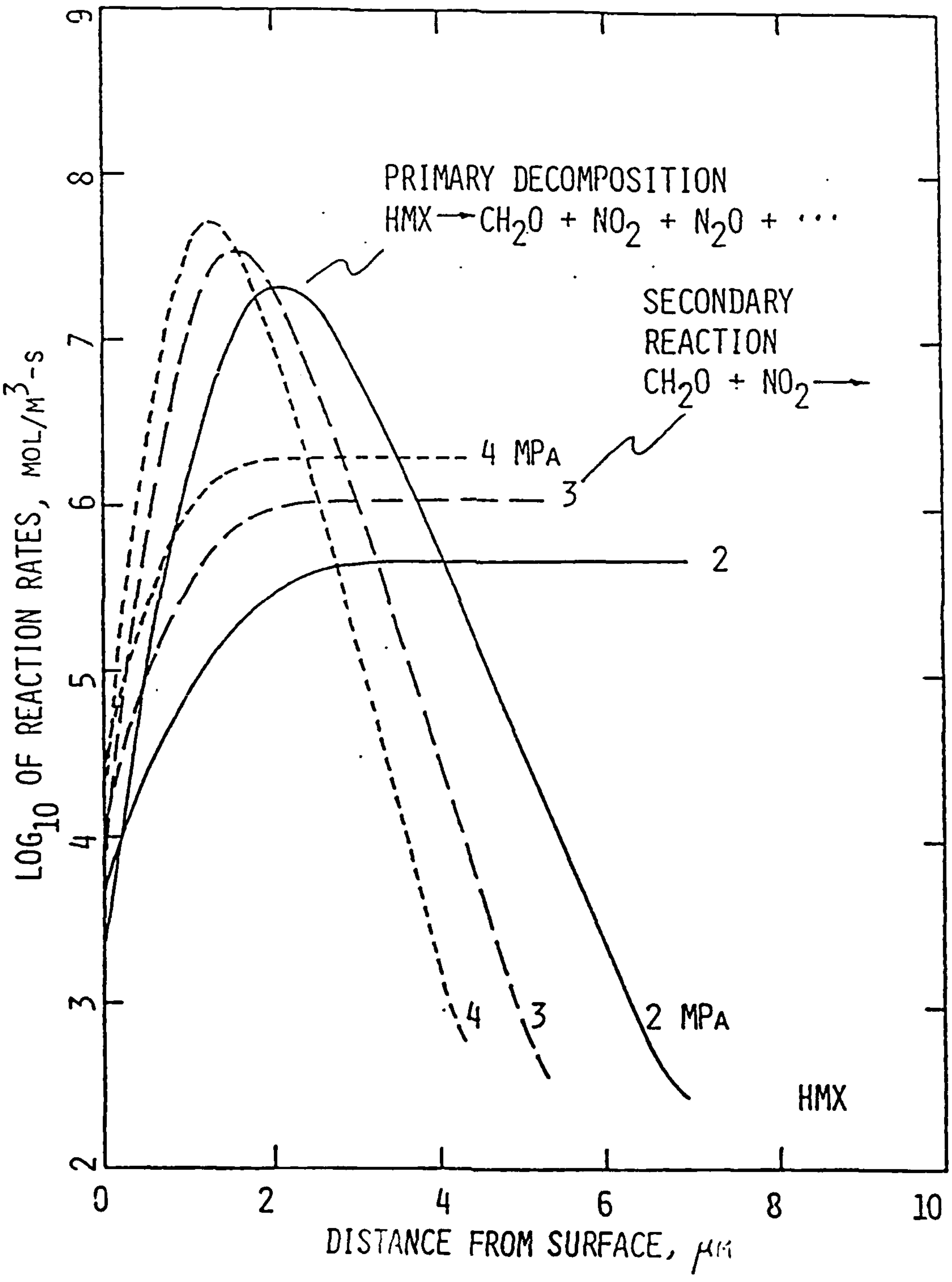

Figure 16
Near Field Distribution for HMX Deflagration at Three Pressures

2.3.1.2 Enhanced Kinetic Flame Model

The enhanced kinetic flame model simulating HMX combustion is an extension of kinetic flame model described above.[125-126] It builds upon the previous work in the following respects. First, it updates the combustion chemistry to include more chemical reactions. Second, it allows for an alternate scheme based upon the formation of H_2CN and NO_2 as well as the more conventional scheme where CH_2O (formaldehyde) and N_2O are formed. Finally, several simplifications were made to reduce the computer cost and numerical convergence problems.

Although the precise nature of the chemistry is not known, the combustion model assumes two possible reaction schemes: one based upon the formation of CH_2O, and one based upon the formation of H_2CN or HCN. In the current model, the two schemes are treated separately for liquid phase and vapor phase decomposition.

The first scheme, which may involve C-N bond rupture in the liquid phase and N-N bond rupture in the vapor phase, is presented in Table 1. The reactions are shown as sequences of global steps, with β being the fraction of HMX that vaporizes. The reactions following liquid phase decomposition follow in a straightforward manner, with the assumption that the water-gas reaction is the mechanism by which final products are achieved at the end of the combustion zone. The final product distribution was established by thermochemical calculations. The sequence following vapor-phase decomposition is based on the premise that the reaction with NO_2 is relatively rapid and that the reaction with NO (high activation energy) occurs at higher temperatures further out in the combustion zone. The formation of CO_2 and H_2 present at thermochemical equilibrium is derived from the water-gas reaction.

The alternative scheme, which may involve a molecular rearrangement, depolymerization or N-N bond rupture, is presented in Table 2. This scheme is more difficult to establish, and is shown to be more complicated. The first step in liquid phase decomposition is a global representation of the initial formation of H_2CN and NO_2, A rapid decomposition to HCN and reaction of the H_2. The subsequent steps follow the same reasoning as above. The first step in vapor phase decomposition is also a global representation of a process that includes H_2CN formation, but the mechanism produces CH_2O as well.

The analysis assumes constant thermal properties. The analysis also neglects the bubbles in the liquid layer that were considered by the previous kinetic flame model.[124] These simplifications help to achieve a closed form solution for the liquid layer.

Calculated burning rates are shown, together with experimental data, in Figure 17.[126] These calculations were based upon Table 1 chemistry. It is observed that the burning rate, pressure exponent and temperature sensitivity are predicted quite well by this model. Values of surface temperature calculated ranged from 569°K at 0.2 MPa to 698°K at 20 MPa. Values of β ranged from 0.92 to 0.98, β decreasing with increasing pressure because of the relatively high activation energy (high sensitivity to temperature) of liquid phase decomposition. Values of β close to 1 indicate that the major portion of HMX decomposition occurs in the vapor phase, and that the combustion is controlled by vapor phase decomposition. The CH_2O-N_2O reaction is not a

Table 1
HMX Combustion Chemistry: CH_2O Scheme

A. From liquid phase decomposition:

1. $(1-\beta)C_4H_8N_8O_8 \longrightarrow 4(1-\beta)CH_2O + 4(1-\beta)N_2O$
2. $4(1-\beta)CH_2O + 4(1-\beta)NO_2 \longrightarrow 4(1-\beta)[CO + H_2O + N_2]$
3. $(1-\beta)CO + (1-\beta)H_2O \longrightarrow (1-\beta)CO_2 + (1-\beta)H_2$

B. From vapor phase decomposition:

1. $\beta C_4H_8N_8O_8 \longrightarrow \frac{4}{3}\beta NO_2 + \frac{4}{3}\beta N_2O + 4\beta CH_2O + 2\beta N_2$
2. $\frac{4}{3}\beta CH_2O + \frac{4}{3}\beta NO_2 \longrightarrow \frac{4}{3}\beta NO + \frac{4}{3}\beta CO + \frac{4}{3}\beta H_2O$
3. $\frac{4}{3}\beta CH_2O + \frac{4}{3}\beta N_2O \longrightarrow \frac{4}{3}\beta CO + \frac{4}{3}\beta H_2O + \frac{4}{3}\beta N_2$
4. $\frac{4}{3}\beta CH_2O + \frac{4}{3}\beta NO \longrightarrow \frac{4}{3}\beta CO + \frac{4}{3}\beta H_2O + \frac{2}{3}\beta N_2$
5. $\beta CO + \beta H_2O \longrightarrow \beta CO_2 + \beta H_2$

Table 2
HMX Combustion Chemistry: HCN Scheme

A. From Liquid phase decomposition:

1. $(1-\beta)C_4H_8N_8O_8 \longrightarrow (1-\beta)[4HCN + 2NO + 2H_2O + 2NO_2]$
2. $2(1-\beta)HCN + 2(1-\beta)NO_2 \longrightarrow (1-\beta)[2CO + H_2O + NO + \frac{3}{2}N_2]$
3. $2(1-\beta)HCN + 3(1-\beta)NO \longrightarrow (1-\beta)[2CO + H_2O + \frac{5}{2}N_2]$
4. $(1-\beta)CO + (1-\beta)H_2O \longrightarrow (1-\beta)CO_2 + (1-\beta)H_2$

B. From vapor phase decomposition:

1. $\beta C_4H_8N_8O_8 \longrightarrow 3\beta CH_2O + 3\beta N_2O + \beta HCN + \frac{1}{2}\beta NO$
   $+ \frac{1}{2}\beta H_2O + \frac{1}{2}\beta NO_2$
2. $\beta CH_2O + \frac{1}{2}\beta NO_2 \longrightarrow \beta CO + \beta H_2O + \frac{1}{4}\beta N_2$
3. $\beta HCN + \frac{3}{2}\beta N_2O \longrightarrow \beta CO + \frac{1}{2}\beta H_2O + 2\beta N_2$
4. $\frac{3}{2}\beta CH_2O + \frac{3}{2}\beta N_2O \longrightarrow \frac{3}{2}\beta CO + \frac{3}{2}\beta H_2O + \frac{3}{2}\beta N_2$
5. $\frac{1}{2}\beta CH_2O + \frac{1}{2}\beta NO \longrightarrow \frac{1}{2}\beta CO + \frac{1}{2}\beta H_2O + \frac{1}{4}\beta N_2$
6. $\beta CO + \beta H_2O \longrightarrow \beta CO_2 + \beta H_2$

factor because too little is formed in the liquid layer and the reaction rates are too slow at the calculated surface temperatures. The good agreement with data was achieved by adjusting the kinetics of vapor phase decomposition.

Calculations incorporating Table 2 chemistry produced the same results. Since the same kinetics were used for liquid phase decomposition, the essential result that β is close to 1 was obtained and the fact that the decomposition is now endothermic rather than exothermic made a negligible difference. However, the heat release of the Table 2 vapor phase decomposition is much less than that of Table 1, so it was necessary to increase Table 2's vapor phase rate constants in order to reproduce the burning rates. Reactions between liquid phase decomposition products at the surface continue to be negligible. Therefore, meaningful differences in the chemistries will not show up until farther out in the gas phase.

The enhanced kinetic flame model was significant since it made use of more accepted chemical reaction schemes, ie. the presence of HCN in the decomposition products. The model was also able to accurately predict HMX monopropellant burning rates. However, Like the kinetic flame model described earlier, this model relies heavily on reaction rate data which is difficult to obtain and often nonexistent.

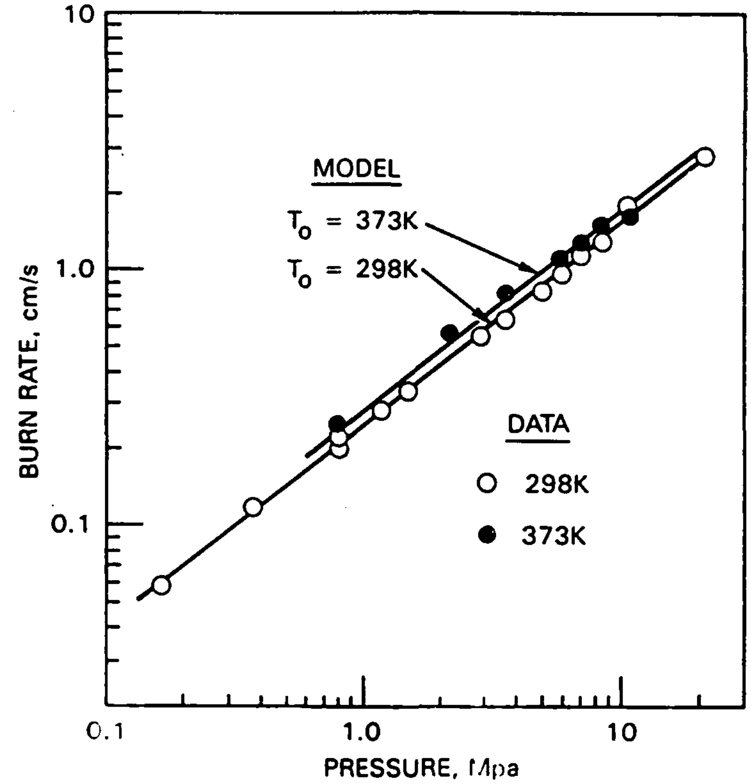

Figure 17
Comparison of Calculated and Experimental
HMX Burning Rates

2.3.1.3 Beckstead, Derr, Price Monopropellant Models

Because of the widespread use of the Beckstead, Derr, Price model with AP composite propellants it was logical to attempt to apply the model methodology to HMX monopropellant combustion.[82,127-134] For the monopropellant case, three basic equations are used. The surface regression rate is described by a one-step Arrhenius expression:

$$r\rho = A\exp(-E/RT_s) \tag{61}$$

where r is the burning rate, ρ is the propellant density, A is the prefactor, E is the activation energy and T_s is the surface temperature. The surface temperature is derived from an energy balance at the surface and is expressed by:

$$T_s = T_o - (Q_L/C_p) + (Q_f/C_p)\exp(-C_p m x^*/\lambda_g) \tag{62}$$

In this expression T_o is the initial propellant temperature, λ_g is the thermal conductivity of the gases, x^* is the kinetic flame standoff distance, Q_L is the energy of decomposition and Q_f is the gas phase energy release given by:

$$Q_f = C_p(T_f - T_o) - Q_L \tag{63}$$

where T_f is the adiabatic flame temperature.

The HMX burning rates determined from these equations were limited to a narrow range of pressures. The simplicity of the equations did not allow for the complex behavior of HMX decomposition and deflagration. This simplified Beckstead, Derr, Price approach did provide a basic starting point to develop more sophisticated models based on the above three equations. A modified Beckstead, Derr, Price model was developed which attempted to accurately define the self deflagration rates of HMX over the range of initial temperatures from 198°K to 423°K and over the pressure range from atmospheric to 8000 psia.[132]

The heat balance utilized in the original BDP model included the surface heat term, Q_L. This was initially envisioned as a latent heat at the surface as in an ablating material. It seen became apparent that condensed phase reactions were of some importance to the process and the term Q_L became the net surface heat release, and could be either exothermic or endothermic. However, this term was considered to have a fixed value for a given material, in the manner of a state property. Because of this, two competing condensed phase reactions were considered, one exothermic, the other exothermic. The first reaction is:

$$C_4H_8O_8N_8 \longrightarrow 4CH_2O + 4N_2O \tag{64}$$

This reaction is exothermic in nature with a heat of reaction of 170 cal/gm. The second reaction is:

$$C_4H_8O_8N_8 \longrightarrow 4CHN + 4NO_2 + 2H_2 \tag{65}$$

This reaction is endothermic and has a heat of reaction of -482 cal/gm.

The net result of these reactions was lumped into a net surface heat release term, but it was no longer a pseudo-state material property. It was determined by the ratio of the two reaction rates, and becomes a rate-variable term.

The mass flows deriving from the endothermic and exothermic reactions in the condensed phase were cast, as done previously, in an Arrhenius form:

$$\mathrm{Mox}_F = A_1 \, exp(-E_1/RT_s) \tag{66}$$

$$\mathrm{Mox}_G = A_2 \, exp(-E_2/RT_s) \tag{67}$$

where Mox is the mass flow rate and the subscripts F and G refer to the exothermic and endothermic reaction products, respectively. Furthermore, the products resulting from these condensed phase reactions were treated as reacting independently in the gas-phase, leading to a two-flame model analogous to the treatment of composite AP/HTPB propellants in the original model. The ratio of the mass flows was determined by the kinetics of the condensed phase reactions, rather than by the composition of the propellant. The parameter β was used to represent the mass flow proceeding from the endothermic process. The net surface heat release can now be defined as:

$$Q_L = \beta \Delta H_{end} + (1-\beta)\Delta H_{exo} \tag{68}$$

In order to retain the simplicity of the original BDP analysis, the condensed phase reactions are lumped at the surface, and the gas-phase reactions are concentrated into a "flame sheet" at a rate-sensitive standoff distance. This leads to an implicit relationship involving a surface energy balance where the solution is reached by iterating on the surface temperature. The energy equation is as follows:

$$\int_{T_o}^{T_s} C_p dT + \beta \Delta H_{end} - (1-\beta)\Delta H_{exo} = \beta(Q_f + \Delta H_{end}) exp(-\xi^*_{end}) + (1-\beta)(Q_f - \Delta H_{exo}) exp(-\xi^*_{exo}) \tag{69}$$

In this expression C_p is the solid phase specific heat, ΔH is the heat of reaction, and ξ^* is the non-dimensional flame standoff distance.

Later versions of this approach included distributed condensed phase reactions.[133,134] The condensed-phase reactions are modeled as first order distributed reactions with dependence on the vertical distance above the propellant surface. The condensed phase heat feed back to the surface is more complicated since heat can be released or absorbed in a distributed region above the surface. A solution was obtained when the heat transfer to the surface equaled the heat required to raise the propellant to the surface temperature. Figure 18 shows burning rate results over a wide range of pressures for the deflagration rate of HMX.[132]

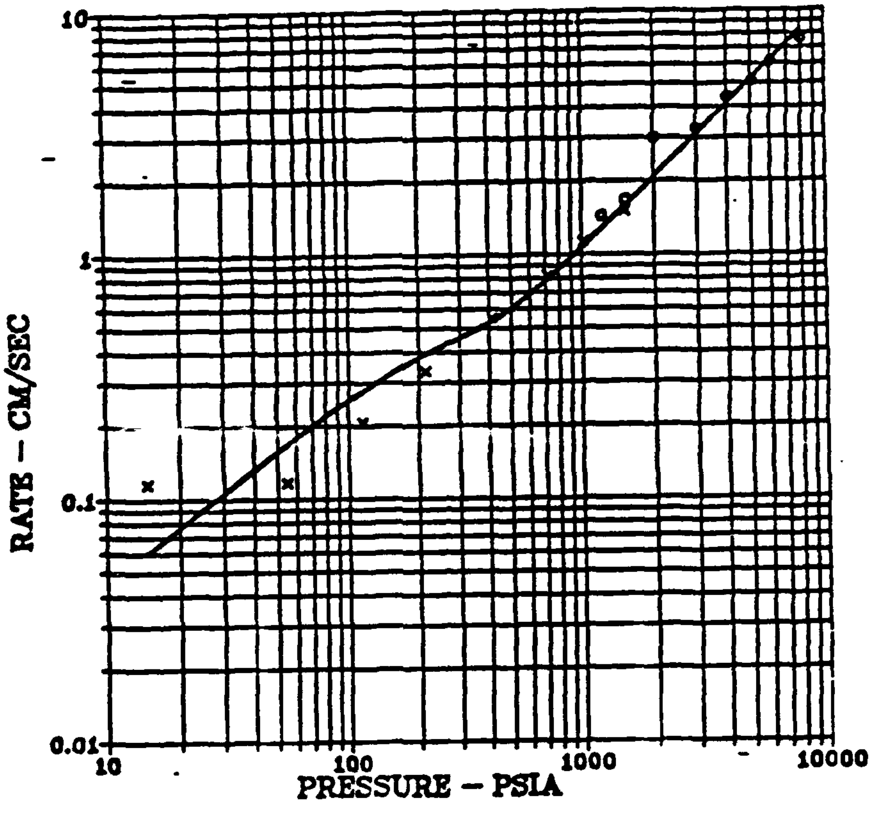

Figure 18
HMX Burning Rate Versus Pressure at 298°K

2.3.2 HMX Composite Combustion Models

2.3.2.1 Multiple Flame Models

The Beckstead, Derr, Price multiple flame model has also used to model composite propellants containing HMX.[103,135-138] Model modifications take account of the different surface and flame structures of nitramine propellants and the different physical and chemical properties of nitramines relative to AP propellants and AP. The assumed flame structure consists of an primary flame and the HMX monopropellant flame, as shown in Figure 19. The primary flame occurs between the decomposing HMX and the binder. There is no assumed final diffusion flame between the HMX monopropellant flame products and unburned binder since HMX burns nearly stoichiometric as a monopropellant so it has no free oxygen in its combustion products.[103,135-138]

New expressions were developed for the area of the exposed HMX crystal to describe both the planar and cratered surface states. For the planer state, the particle volume fraction was corrected by a floating parameter to attempt to account for the peripheral binder interference. For the planar state the exposed oxidizer surface area to total surface area with out this correction is:

$$S_{ox}/S_o = \varsigma \qquad (70)$$

where ς is the volume fraction of oxidizer.[103] This expression is much simpler than the expression for AP propellants, see equation (33). Based on correlations with experimental data there is more interference with coarse particles than with fine particles. Additionally, an change in the surface

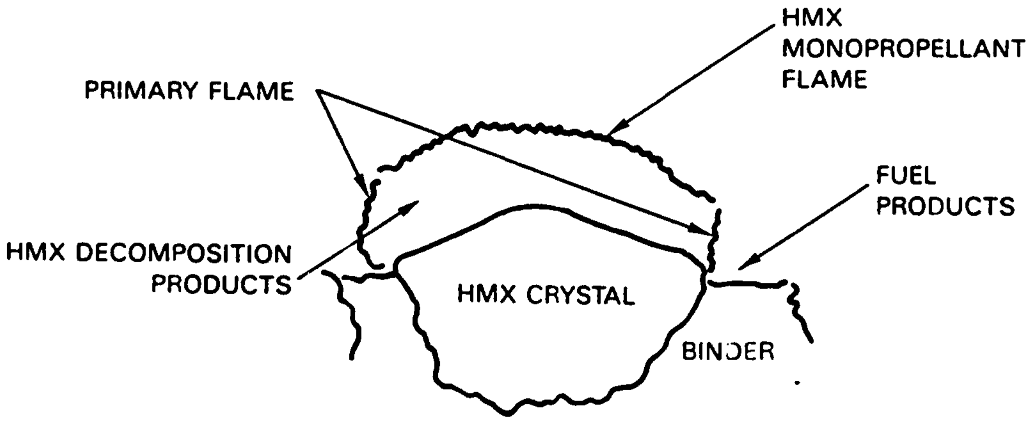

Figure 19
HMX Multiple Flame Structure

structure occurs if the burning rate is such that the thermal wave across a spherical particle is too steep to heat the bulk particle to its melting point. The criterion is derived by a simple transient heating analysis of a spherical particle. The shift in the surface structure is the proposed mechanism for a major shift in pressure exponent observed with nitramine propellants. The equation for the area ratio that is corrected for these effects is:

$$S_{ox}/S_o = \zeta(KD_o^a) \tag{71}$$

where D_o is the particle diameter and K and a are constants.

Because of the experimentally observed differences in surface temperature between HMX and inert binders, separate surface temperatures were used in the energy energy equation:[137,138]

$$\alpha C_{p,HMX}(T_{s,HMX}-T_o) + (1-\alpha)C_{p,b}(T_{s,b}-T_o) = \alpha Q_L + (1-\alpha)Q_f + \beta_f Q_{PF} exp(-\xi^*_{PF}) + (1-\beta_f)\alpha Q_{HMX} exp(-\xi^*_{HMX}) \tag{72}$$

The equation is similar to the energy equations used previously by the Beckstead, Derr, Price multiple flame model and the Petite Ensemble Model, equations (35) and (50), except that there is no heat feedback term from a final diffusion flame.

In other respects the model is identical to the previously mentioned BDP model, ie. the surface temperature is iterated on until the heat transfer from the HMX monopropellant flame and HMX primary flame equals the heat needed to raise the propellant from its initial temperature to the surface temperature. Results from this type of model are shown in the previously discussed Figure 14 by the solid lines.[103] The exponent breaks are successfully modeled and the burning rate agreement is very good.

2.3.2.2 Time Averaged Multiple Flame Model

The time averaged multiple flame combustion model is another derivative of the Beckstead, Derr, Price multiple flame model but has several underlying differences which separate this model from previously discussed multiple flame models.[139-142] The time averaged multiple flame model treats the surface structure of a HMX composite propellant in a completely different fashion than Beckstead, Derr, Price combustion model.

The authors recognized that the combustion characteristics of HMX when compared with those of AP exhibit numerous differences. First, HMX monopropellant burns 30 to 40 percent faster with much higher adiabatic flame temperatures than AP monopropellant at similar pressures and initial temperatures. The monopropellant flame temperature for HMX is approximately 3200°K compared to only 1400°K for AP. Second, the adiabatic flame temperature of AP propellants is between 2500 and 3000°K depending on the AP concentration. In comparison, the adiabatic flame temperature of HMX propellants is between 1800 and 2200°K. Finally, AP composite propellants typically burn at rates higher than the AP monopropellant rate with a very strong dependence on particle size and concentration. HMX propellants burn at rates 3-10 times slower than their respective monopropellant rates with little dependence on particle size or concentration.

Differences in burning rates and flame temperatures are easily explained since HMX burns nearly stoichiometrically as a monopropellant. The introduction of any other substance such as a fuel binder will lower the HMX composite propellant flame temperature and burning rate. The monopropellant AP, on the other hand, burns stoichiometrically with the addition of inert binder with a resulting flame temperature greater than that for pure AP.

The time averaged multiple flame model authors phenomenological interpretations of these observations are outlined in Figure 20.[140] With fine HMX as depicted at the bottom of Figure 20, diffusion mixing distances can be expected to be very short (i.e., less than the monopropellant flame height). The relatively cool HMX/binder primary flame dominates the combustion and suppresses the rate below that of the monopropellant.

However, with coarse HMX seen at the top of the Figure 20, the primary flame should not be able to dominate because of the increased diffusional mixing distances. The authors initially assumed that larger crystals burn at a rate approximating that of the monopropellant, and the propellant rate would also be expected to be close to that of the monopropellant. However, from window bomb movies, coarse crystals appear to ignite very slowly but burn out very rapidly leaving depressions on the propellant surface.[143,144] The

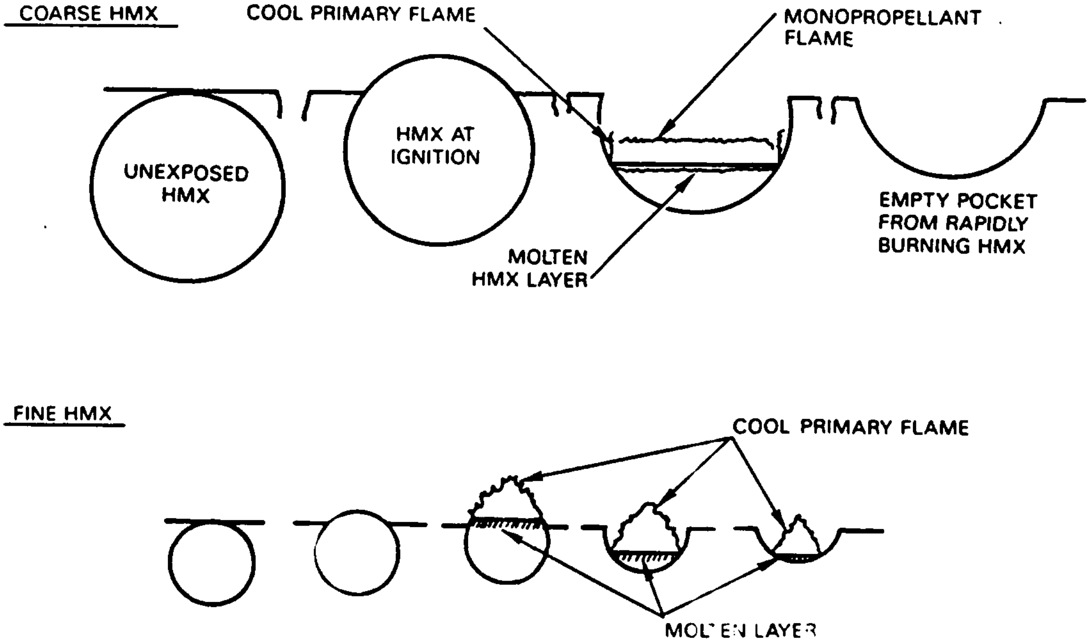

Figure 20
Phenomenological Picture of HMX Combustion

relatively short burn time combined with the long ignition time results in an unstable, erratic burning at the propellant surface. Statistically, very few crystals burn at the same time, with the end result being a much reduced burning rate. Large crystals reside on the surface as the binder burns by and then ignite and disappear rapidly.

In summary, the rate controlling mechanism for fine HMX crystals is the relatively cool primary flame between the HMX and the binder. For large crystals the controlling mechanism is the HMX ignition delay time coupled with the fuel binder pyrolysis and/or combustion that controls the overall burning rate of the propellant.[140]

The time averaged multiple flame model uses a Beckstead, Derr, Price multiple flame approach but instead of space averaging the burning rate, a time averaging approach is used.[139-142] In the original BDP model the burning surface area of the fuel and various oxidizer fractions were used throughout the model. The basic need for the surface areas comes from the space-averaged overall continuity equation:

$$m_T S_o = m_{ox} S_{ox} + m_b S_b \tag{73}$$

Where m_T, m_{ox} and m_b are the mass fluxes of the total propellant, the oxidizer and the binder respectively. S_o, S_{ox} and S_b are their respective burning surface areas. Solving for the average linear burning rate yields:

$$\bar{r} = \frac{1}{\rho_p}\left(m_{ox}(S_{ox}/S_o) + m_b(S_b/S_o)\right) \tag{74}$$

so that the surface areas are normalized with the total burn surface area.

In addition, the oxidizer surface area is assumed to be a spherical sector such as shown in Figure 21.[140] This is probably a reasonable assumption as long as the oxidizer and binder rates are similar and the protrusion or recession relative to the intersection plane is small. However, when the rates differ significantly or when the ignition delay time is too long, unrealistic surface areas result. Furthermore, for such limiting conditions the calculated surface area becomes large, reaching a maximum at the conditions shown in Figure 21. This results in an abrupt discontinuity in the calculation of the oxidizer burning surface area at the limiting conditions. AP propellants with very wide particle size distributions (ie. a propellant containing both coarse and fine AP crystals), double-base propellants (double-base propellants contain nitrocellulose gelled with a nitrate ester such an nitroglycerin), and propellants containing HMX will all result in conditions where either the oxidizer binder rates are significantly different or where widely differing oxidizer distributions will lead to the unrealistic limiting conditions. Also, scanning electron microscope (SEM) examination of quenched samples shows crystals with relatively flat surfaces, although often with a rounded protrusion in the center.[140] Therefore, an assumption of a planar oxidizer surface is more realistic than a spherical sector, considering the limiting conditions shown in Figure 21 or SEM photographs of quenched samples.

Utilizing a planar area derivation, calculations were performed with a conventional space averaged multiple flame model that proved to be numerically unstable. The reason for the instability can best be visualized by examining

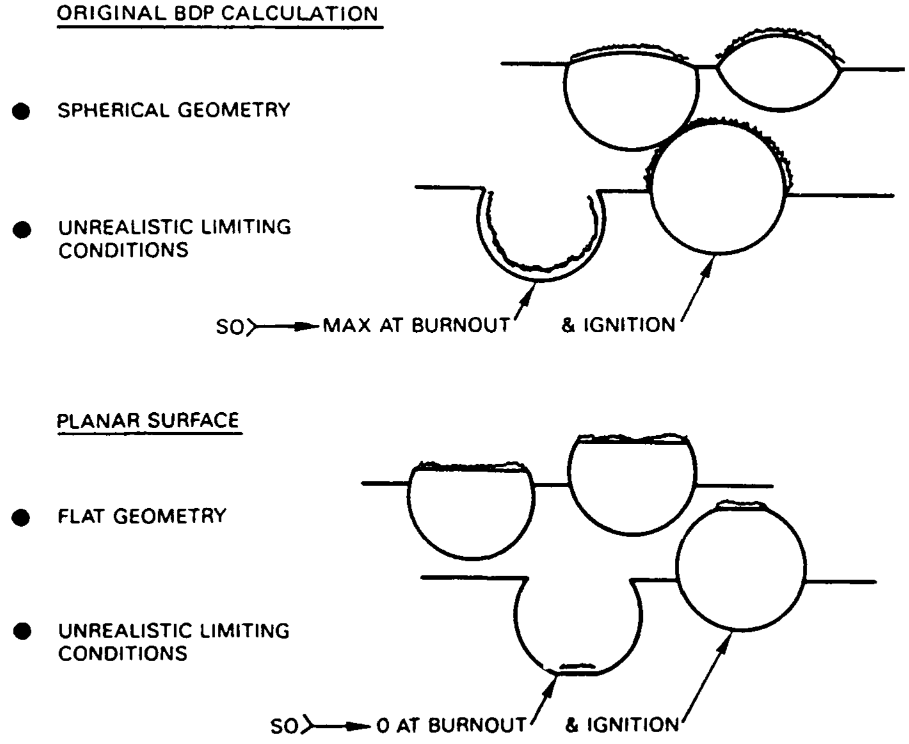

Figure 21
Comparison of Surface Area Calculations for a Spherical Sector Versus Flat Sector

a map of a normalized ignition delay time versus the ratio of oxidizer-to-binder burning rate as shown in Figure 22.[140] In this figure it is assumed that the statistical intersection line drawn parallel to the surface intersects half the particles in the upper half and half the particles in the lower half. The shaded areas are the regimes where finite S_{ox} values are calculated. In the nonshaded areas, S_{ox} values of zero are calculated for the various configurations indicated. The upper shaded area corresponds to one-half of the oxidizer crystals burning and the other half not yet ignited. The lower shaded area corresponds to the other half of the crystal ignited with the first configuration burned out.

From this map, it is apparent that, for large ignition delay times or for oxidizer-to-binder rate ratios greater than 2, both oxidizer configurations will not be burning simultaneously. Either one or the other or neither configuration could result. This is apparently what happens for HMX composite propellants.

Figure 23 is a plot of burning rate versus surface temperature for AP, HMX, HTPB (a typical propellant binder) and double base propellant using typical activation energies and pyrolysis parameters for each ingredient.[140] For the range of burning rates of interest, the differences between HMX and HTPB are extremely large. Their rates are quite different, and one can expect an oxidizer to binder ratio of 5-10 being the norm.

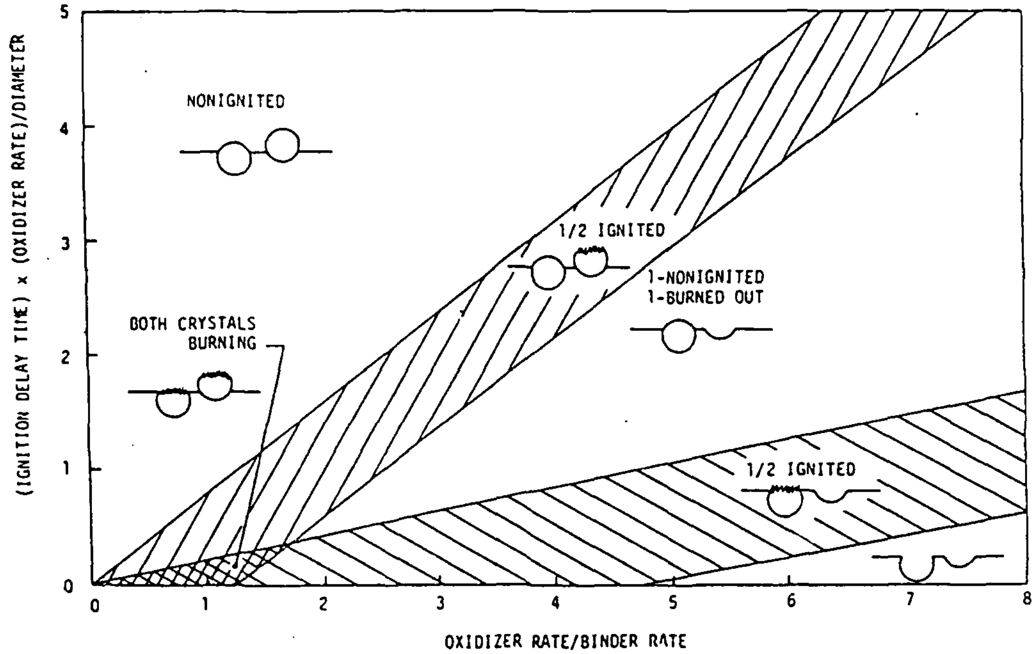

Figure 22
Ignition Delay Time Versus Oxidizer to Binder Burning Rate Ratio

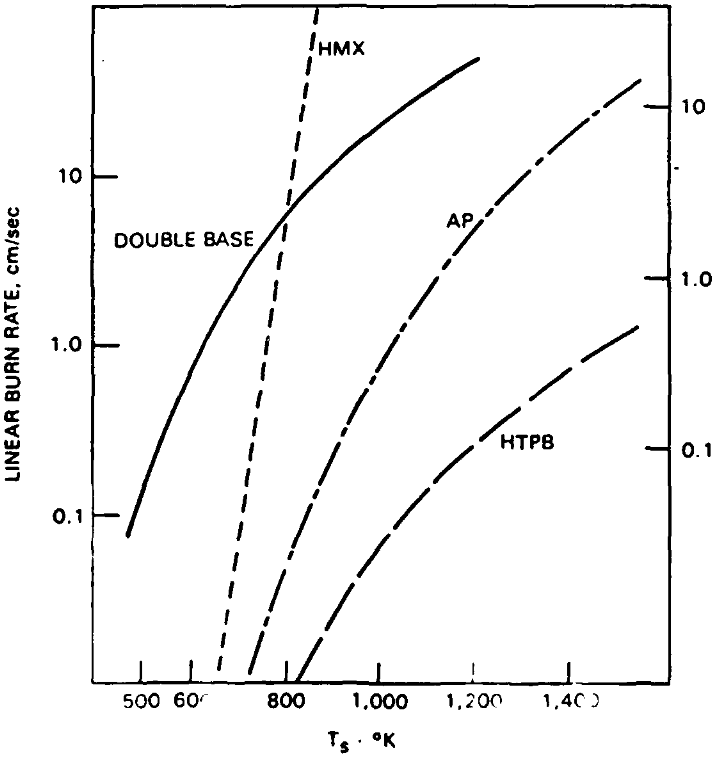

Figure 23
Decomposition Rates of Common Propellant Ingredients

The net result is that, statistically, few oxidizer crystals are burning on the surface at any one time. This can lead to a very unstable surface configuration, which leads to totally unrealistic results. It can also be shown that the original BDP assumption of a spherical sector will lead to very similar unacceptable results. Use of the Petite Ensemble model (PEM) statistics will tend to smear out the discontinuities since PEM the model examines distributions of oxidizer particles not just discrete particle sizes. For large ignition delay times and/or large discrepancies in the oxidizer-binder burning rates, even the PEM statistics will not fully resolve the numerical problems caused by having empty and/or unignited crystals on the surface. Therefore, the conclusion ultimately was reached that the space-averaging BDP model if used consistently will result in numerical instabilities and unrealistic physical limiting conditions.

The approach of assuming a time-averaged propellant surface is realistic on a physical basis because the binder and oxidizer appear to burn in series, rather than in parallel as in the original BDP model. The equation for the average propellant burning rate is of the form:

$$\bar{r} = \frac{\sum \text{distances}}{\sum \text{times}} = \frac{\sum \text{distances}}{\sum (\text{distances/rates} + \text{delay times})} \tag{75}$$

The distances involved are an oxidizer dimension and an associated binder dimension. Figure 24 shows what occurs on a statistical basis.[140] Burning will be somewhat random. However, for a sufficiently large sample it can be assumed that burning occurs approximately in a straight line through a packed bed of oxidizer/binder. The statistical intersection diameter for straight line combustion is the same as used in the previously described BDP and Hermance models:[5,13]

$$D' = \sqrt{2/3}\, D_o \tag{19}$$

The intercrystal thickness of binder associated with a crystal is calculated assuming that the binder is distributed according to the specific surface area of the individual particle sizes and that all of the binder forms an annulus around each particle.[23]

In other respects the time averaged approach is similar to the Beckstead, Derr, Price multiple flame model discussed previously. The two flames assumed in the analysis are the kinetic HMX mono-propellant flame and the primary diffusion flame between the decomposed HMX crystal and the binder (see Figure 19). Unlike the Beckstead, Derr, Price model, separate surface temperatures were assumed for both the HMX and the binder and two energy equations were written, one over the HMX crystal and one over the binder. Each energy equation balances the heat feedback from the flames above the propellant against the energy required to raise the HMX and the binder to their respective surface temperatures. The full details of this model will be discussed later in this report.

The model was very successful in determining the burning rates for a series of HMX/HTPB composite propellants which contained particle sizes from 4μm to 400μm.[140] Parametric calculations were performed varying particle size, solids loading, and initial propellant temperature. These calculations agreed well with expected experimental and observed results.

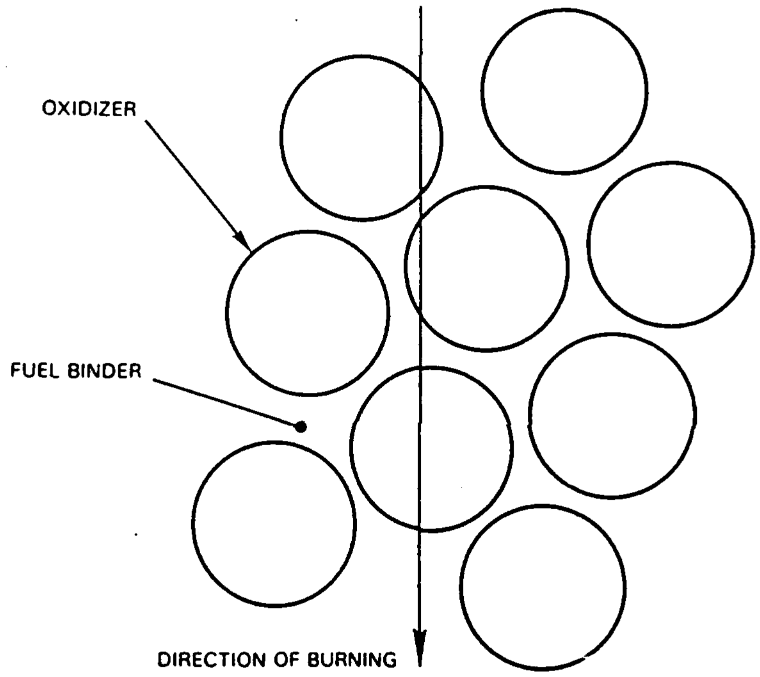

Figure 24
Time Averaged Propellant Burning

CHAPTER III

HIGH ENERGY PETITE ENSEMBLE MODEL (HYPEM)

3.1 Theoretical Procedure

3.1.1 Structure of the Model

3.1.1.1 Statistical Analysis

The structure of the High Energy Petite Ensemble Model, HYPEM, as the name implies is based on the Petite Ensemble Model (PEM) described previously.[29] The PEM framework recognizes the fact that a propellant is made up of a distribution of oxidizer particles. The burning surface of a polydisperse propellant with many oxidizer diameters is statistically rearranged into imaginary families of monodisperse propellants which consist of only one particle size. These monodisperse propellants burn as individual "pseudo" propellants and do not interact physio-chemically with the flames of surrounding oxidizer particles. The total burning rate is computed by statistically adding up all the pseudo monodisperse propellant burning rates. Real propellants are made up of several distributions of oxidizer crystals each with their own oxidizer mass fraction. Equations (46) and (47) presented above describing the PEM model are for propellants with only one distribution of particles. The equation for the distribution function, now called $F_{d,ox}$, for a particular particle distribution is:

$$F_{d,ox} = \frac{\alpha_{ox}}{\sqrt{2\pi}\,ln\sigma_{ox}}\, exp\left[-\frac{1}{2}\left(\frac{lnD_{ox} - ln\bar{D}_{ox}}{ln\sigma_{ox}}\right)^2\right] \tag{76}$$

In this equation α_{ox} is the oxidizer mass fraction of a particular particle distribution. The constants $\bar{D}_{ox}$ which represents the fifty percent weight diameter of a unique oxidizer mode and σ_{ox} which is the mode width parameter are inputs to the model which are determined by the properties of the particular oxidizer grind. The total propellant burning rate is computed by the following expression:

$$\bar{r} = \frac{1}{\alpha_T} \oint_{D_{ox}} (r_d F_d)\, d\,lnD_{ox} \tag{77}$$

Where α_T is the total propellant oxidizer mass fraction, r_d is the pseudo propellant burning rate and F_d is the distribution function given by equation (76). This expression for the total propellant burning rate is an integral over all particle sizes for both AP and HMX particle size distributions.

3.1.1.2 Oxidizer Mass Fraction

A very important parameter in characterizing the pseudo propellant is the amount of binder that forms an annulus around individual oxidizer particles. It is assumed that the volume of the fuel binder associated with each oxidizer crystal can be related to the effective diameter of the assumed spherical oxidizer particle raised to a power. This expression is as follows:

$$V_b = CD^{XN} \tag{78}$$

Where V_b is the volume of binder, D is the oxidizer particle diameter, XN is assumed to be between 2 and 3 and C is a constant that must be solved for by considering the propellants oxidizer distribution along with other overall propellant properties. In order to develop an meaningful expression for the constant C several relationships must be developed. Integrating F_d over $\ln D$ yields:

$$\oint_D F_d \, d\ln D = \alpha_T \tag{79}$$

Where α_T is the overall propellant oxidizer mass fraction. With this knowledge the differential amount of oxidizer mass about some diameter, D, per unit mass of total propellant, dm_d, can be written as:

$$dm_d = F_d \, d\ln D \tag{80}$$

The differential number of oxidizer particles of some diameter, D, per unit mass of total propellant, dN_d, can be written as:

$$dN_d = \frac{dV_{ox,d}}{V_{ox,d}} = \frac{(dm_d/\rho_{ox})}{\frac{\pi}{6}D^3} \tag{81}$$

Where ρ_{ox} is the density of the oxidizer and $V_{ox,d}$ is the volume of one oxidizer particle of diameter, D. $dV_{ox,d}$ is the differential volume of oxidizer of diameter, D, per unit mass of total propellant. From equation (78) and (81) the differential amount of binder associated with oxidizer particles of diameter, D, per unit mass of total propellant, dV_b, can be written as:

$$dV_b = V_b dN_d = CD^{XN} dN_d \tag{82}$$

Integrating this expression over all diameters yields the total binder volume per unit mass of total propellant. By introducing the overall propellant density, ρ_p, and the overall propellant oxidizer volume fraction, ζ_T, the following expression can be written:

$$\rho_p \oint_D dV_b = (1-\zeta_T) \tag{83}$$

Utilizing expressions (80), (81), and (82); equation (83) becomes:

$$\rho_p \oint_D \frac{CD^{XN}F_d d\ln D}{\rho_{ox}(\frac{\pi}{6}D^3)} = (1-\zeta_T) \tag{84}$$

Since C is a constant in the above expression, it can be removed from the integral and solved for:

$$C = \frac{\frac{\pi\rho_{ox}}{6\rho_T}(1-\zeta_T)}{\oint_D D^{XN-3}F_d d\ln D} \tag{85}$$

Now that the constant C is known it will be possible to write expressions for the various pseudo propellant properties in terms of C and known propellant properties. The most important of these is the oxidizer mass fraction for each pseudo propellant.

$$\alpha_d = \frac{m_{ox}}{m_b + m_{ox}} = \left(1 + \frac{m_b}{m_{ox}}\right)^{-1} \tag{86}$$

Where m_{ox} and m_b are the mass of oxidizer and fuel in the pseudo propellant. Defining these variables further yields:

$$m_b = \rho_b \Delta V_b = \rho_b C D^{XN} \tag{87}$$

$$m_{ox} = \rho_{ox}(\tfrac{\pi}{6}D^3) \tag{88}$$

Finally, substituting equation (85), (87), and (88) into equation (86) the pseudo propellant oxidizer mass fraction is:

$$\alpha_d = \left[1 + \frac{6\rho_b}{\pi\rho_{ox}} C D^{XN-3}\right]^{-1} \tag{89}$$

The only value that remains to be defined to characterize the pseudo propellants is the value for XN. If XN is assumed to be equal to two, it is the same as stating that the volume, or mass, of fuel binder associated with a given oxidizer particle is related to the surface area of the oxidizer particle. In a like fashion, if XN is assumed to be three, then the volume of fuel surrounding a particle of oxidizer is proportional to the volume of the oxidizer. When the value of XN is equal to three, the analysis indicates that each of the oxidizer particle/fuel binder pairs, regardless of the size of the oxidizer particle, burn at the same value of oxidizer-to-fuel ratio; this ratio being the overall oxidizer-to-fuel ratio of the propellant formulation. Any value of XN less than three dictates that the small oxidizer particles within the propellant distribution burn rich while the larger oxidizer particles burn fuel lean, all with respect to the overall oxidizer-to-fuel ratio of the propellant. A detailed analysis of this variable oxidizer-to-fuel ratio burning of the individual oxidizer particles showed that the predictive capability of bimodal propellants was enhanced.[145] Since there is no ideal value for this parameter it is an HYPEM model input which can be set to any value between two and three.

3.1.1.3 HYPEM Model Procedure

From the above analysis each pseudo propellant is now completely characterized. The particle size, volume of fuel allocated to each particle, fuel density, particle density, particle type and input parameters such as pressure and initial propellant temperature are the only parameters needed to compute the burning rate of the individual pseudo propellants. These burning rates of the individual pseudo propellants along with their respective distribution functions will be used in equation (77) to compute the total propellant burning rate.

Because of the many differences in the manner in which AP and HMX crystals burn and especially differences in the way the crystals burn in a binder medium, it was decided to determine the burning rates of the two types of pseudo propellants by separate mathematical approaches. The AP propellants are computed by a modified Beckstead, Derr, and Price (BDP) multiple flame surface averaging technique while the HMX propellants are computed using a time averaged approach developed by Beckstead and McCarty.[13,140] Each method, although different in many of the details, is similar in structure.

For both methods, separate surface temperatures must be initially chosen for the binder and respective oxidizer crystal. Then, the mono-propellant mass burning rates are computed by the Arrhenius expression:

$$\dot{m}_{ox} = r_{ox}\rho_{ox} = A_{ox}e^{(-E_{ox}/RT_{s,ox})} \tag{90}$$

$$\dot{m}_{b} = r_{b}\rho_{b} = A_{b}e^{(-E_{b}/RT_{s,b})} \tag{91}$$

where A is the Arrhenius frequency factor, E is the activation energy, R is the gas constant and T_s is the surface temperature. The subscripts ox and b represent the oxidizer and binder, respectively.

Each pseudo propellant is postulated to have certain flames over the oxidizer crystal surrounded by the fuel or binder annulus. For the AP propellants their are three flames; the AP mono-propellant flame, the primary flame where decomposed products of AP and binder react, and the final diffusion flame in which binder pyrolysis products react with AP mono-propellant flame products (see Figure 4). For the HMX propellants their are only two flames; the HMX mono-propellant flame and the primary flame between the HMX and binder (see Figure 19). There is no final flame since the products of the HMX mono-propellant flame are assumed inert. For both types of pseudo propellants, an energy equation is written over the propellant. One side of the equation is the heat transferred from the various flames to the surface. This is compared to the other side of the energy equation which is the amount of heat required to raise the propellant from its initial temperature to the surface temperature. The solution to the energy balance is obtained by iterating on the various surface temperatures until the two heat transfers are equivalent. As mentioned above the details in computing the pseudo propellant burning rates different in many ways. The two methods will be described in detail and their differences and similarities examined.

3.1.2 HMX Portion

3.1.2.1 Time Averaged Burning Rate

As mentioned previously, very few HMX crystals burn at the same time on the propellant surface and the use of surface averaging over the total propellant surface leads in unrealistic results. A more accurate approach is to average the burning surface in time. The HMX/binder burn rate will be computed using a time averaged burning rate approach developed by Beckstead and McCarty.[31] The burning rate can be defined as:

$$r = \frac{\sum \text{distances}}{\sum \text{times}} = \frac{\sum \text{distances}}{\sum (\text{distances/rates} + \text{delay times})} \tag{75}$$

rewritten:

$$r = \frac{D' + 2\Delta}{\left(\dfrac{D'}{r_X} + t_{ign} + \dfrac{2\Delta}{r_b} + t_b \right)} \tag{92}$$

where: D' - statistical intersection diameter of HMX crystal

Δ - distance from HMX crystal edge to edge of assumed binder annulus

t_{ign} - ignition delay time of HMX crystal

t_b - binder burn through time for a given HMX crystal

r_X - burning rate of HMX crystal

r_b - average binder burning rate

Dividing through by D' yields the following:

$$r = \frac{(1 + \delta)}{\left(\dfrac{1}{r_X} + \dfrac{t_{ign}}{D'} + \dfrac{\delta}{r_b} + \dfrac{t_b}{D'} \right)} \tag{93}$$

where: $\delta = 2\Delta/D'$

Incomplete reaction of the binder affects the burn rate, especially in HMX composite propellants. Windowbomb movies show shedding of layers of binder from the burning surface of HMX composite propellants.[143,144] Stoichiometry indicates that HMX composite propellants burn very fuel rich. It is probable that all of the fuel is only partially oxidized or, more likely, that part of the fuel does not even react. The windowbomb movies seem to indicate the latter is more accurate; that sheets of binder lift from the surface unreacted.

To simulate the effect of unreacted binder within the time averaged burning rate equation, two terms will be introduced. The first is a fraction binder reacted (fr_b) term which will be incorporated into the surface energy balances for binder and oxidizer and must be incorporated into the time-averaged equation. The second, the binder burnthrough time (t_b), is incorporated into the time-averaged equation above. The final equation for the time-averaged rate is:

$$r = \frac{(1+\delta)}{\left[\frac{1}{r_X} + \frac{t_{ign}}{D'} + \frac{\delta fr_b}{r_b} + \frac{t_b(1-fr_b)}{D'}\right]} \qquad (94)$$

3.1.2.2 Fraction of Binder Reacting

Quantitative data are not available to allow estimation of the fraction of binder that does react as a function of pertinent variables. Based on the windowbomb movies, binder shedding appears to be much worse at low pressures than at high but did not appear too dependent on particle size or solids loading.[143,144] Logically, it would seem that the amount of binder reacting should depend principally on the energy feedback from the primary flame over the binder. It would appear to be related to the initial temperature and possibly the stoichiometry. Therefore, the following function is assumed:[140]

$$fr_b = fr_a\left(\frac{O/F}{\Phi_{st}}\right)\left(\frac{T_o}{298}\right) exp(-\xi^*_{PF}) \qquad (95)$$

Where fr_a is an arbitrary constant, O/F is the oxidizer to fuel ratio, Φ_{st} is the stoichiometric oxidizer to fuel ratio, T_o is the initial propellant temperature and ξ^*_{PF} is the non-dimensional height of the primary flame associated with HMX. By matching the data with fr_a as an arbitrary constant it was found to require a value of 1.2.[140] The fraction of binder that reacts increases with higher initial propellant temperatures and oxygen rich mixtures and decreases with higher primary flame heights. The assumed form seems reasonable and appears to give the appropriate dependencies.

3.1.2.3 Binder Burnthrough Time

The binder burnthrough time is meant to represent the unsteady nature of binder pyrolysis in a propellant environment, particularly in fuel-rich situations. As an oxidizer burns, the binder adjacent to the oxidizer is heated by the primary flame, with the resultant pyrolysis products participating in the flame. However, as the oxidizer burns out, particularly in cases where the oxidizer rate is much faster than the binder rate, there is no direct heat source to continue heating the binder, except the energy stored in the thermal wave. At this point, the pyrolysis will slow down and possibly stop. For the remaining binder to burn or slough off, energy must be robbed from an adjacent particle. Alternatively, if underlying particle gets ignited from another direction, it could burn under the binder, resulting in the binder sloughing off. This effect has been seen in the windowbomb movies. Strahle proposed a format for the binder burnthrough concept.[146] The equation for the burnthrough time is:

$$t_b = t_{ba} \frac{\delta}{r} exp\left(\frac{\delta r_b}{\alpha}\right) \tag{96}$$

where r is the overall burning rate of the propellant, r_b is the binder burning rate, δ is the non-dimensional ratio of twice the binder annulus thickness around the oxidizer crystal to the statistical intersection diameter of the oxidizer crystal, α is the thermal diffusivity and t_{ba} is a proportionality constant. Thus, the burnthrough time increases with increasing interparticle distance and decreases with increasing average rate. The exponential term approaches unity for most cases that have been considered.

3.1.2.4 Ignition Delay Time

The postulated ignition delay time results from the discontinuous nature of composite propellants (i.e., the crystals are not necessarily in good thermal contact with the binder). The ignition delay time is the time it takes an oxidizer crystal to ignite, assuming that the ignition process starts when a crystal first becomes exposed to the burning surface. As the burning surface sweeps over the crystal, heat is fed to the crystal, which heats up and starts to decompose. The time required for this process to occur is the ignition delay time.

The first attempt to incorporate this concept into a combustion model was made by Hermance using data generated by Shannon for weakly pressed AP strands.[5,147] The Beckstead, Derr, Price multiple flame model and other derivative models have all incorporated the same idea and form of equation, which is:

$$t_{ign} = C_{ign} \frac{D_o^{1.8}}{p^{0.721}} \tag{97}$$

In most of these models, varying the ignition delay time parameters has little effect on the net burning rate. However, the ignition delay of the HMX crystals can be a dominant mechanism in determining the burning rate of the propellant.[140] Furthermore, the previously used equation for ignition delay was developed for AP, and there are no corresponding data for HMX (pressed strands of HMX burn with a relatively thick molten layer on the surface).

To incorporate a diameter dependence, Beckstead and McCarty tried to apply transient two-dimensional heat transfer analysis. A solution to the two-dimensional differential heat conduction equation was obtained from Carslaw and Jaeger.[140,148] However, it was concluded that the Carslaw and Jaeger solution could not be applied directly because of nonuniform boundary conditions, (i.e., heating occurs on only one side of the crystal). Beckstead and McCarty decided to use an empirical data correlation for the ignition delay time. From the derivation and from the data, it was apparent that an ignition delay time should be proportional to the diameter raised to a power and inversely proportional to the rate.[140]

$$t_{ign} = C_{ign} \frac{D_o^{\delta_{ign}}}{r} \qquad (98)$$

A linear regression analysis of Shannon's data for AP gives:

$$t_{ign} = 4.321 \mathrm{sec/cm}^{0.7} \frac{D_o^{1.7}}{r} \qquad (99)$$

The similarity between equations (97) and (99) is readily apparent. The difference is that use of burning rate in place of pressure as a variable is more accurate considering the transient heat-transfer equations. Use of burning rate also permits application of the equation to HMX crystals. For HMX it was determined that a diameter exponent of around 1.0 gave the best results.[140] The ignition delay time should also be proportional to the chemical activity of the oxidizer. In other words, the higher the activation energy of the initial decomposition reaction, the longer the ignition delay time. After the crystal has been heated, there is probable a chemical induction time before ignition is established completely. Therefore, the ignition delay time should be proportional to the chemical activity in some form or another and to the ignition temperature. To simulate these effects, C_{ign} was defined as:[140]

$$C_{ign} = \frac{E_{ox}(T_{melt}-T_o)}{E_{ref}(T_{ref}-T_o)} \qquad (100)$$

where E_{ox} is the surface reaction activation energy, T_{melt} the melting temperature of the oxidizer crystal, and E_{ref} and T_{ref} arbitrary reference values. In actuality, a reference $C_{ign,ref}$ is input instead of a E_{ref} value. E_{ref} is then computed by:

$$E_{ref} = \frac{E_{ox}(T_{melt}-T_o)}{C_{ign,ref}(T_{ref}-T_o)} \qquad (101)$$

and equation (100) is used in to compute C_{ign} which is used in equation (98).

3.1.2.5 Remaining Terms

All the terms in the time averaged burning rate expression have been defined except the non-dimensional primary flame standoff distance, ξ^*_{PF}, and determination of the surface temperatures which are used by the Arrhenius expressions in equation (90) and (91) to determine the burning rates of the mono-propellant oxidizer and binder, respectively. Since the methods to compute these values is very similar to the AP portion of the model they will be described later together with the AP explanation.

3.1.3 AP Portion

3.1.3.1 Surface Averaged Burning Rate

The computation of the AP pseudo propellant burning rate is based on many of the assumptions evoked in the Beckstead, Derr, and Price (BDP) model discussed earlier. This especially true in the description of the surface geometry of the oxidizer crystal embedded in the fuel binder. Unlike the HMX pseudo propellants where the burning rate was computed by averaging in time, the AP pseudo propellant burning rate is averaged in space over the surface of the propellant. In describing the propellant surface, it is assumed that the oxidizer crystals are randomly mixed within the fuel binder. The statistical average intersection diameter, D'_{ox}, is the same as defined previously:

$$D'_{ox} = \sqrt{2/3}\, D_{ox} \tag{19}$$

As in the BDP model and the HMX section described above the AP oxidizer mass burning rate is assumed to be represented adequately by an Arrhenius expression based on the temperature of the oxidizer surface, $T_{s,ox}$:

$$\dot{m}^T_{ox} = A_{ox}\, exp(-E_{ox}/RT_{s,ox}) \tag{102}$$

In this expression, A_{ox} and E_{ox} are the pre-exponential frequency factor and the activation energy, respectively, of the oxidizer surface decomposition reaction. The oxidizer mass flux, $\dot{m}^T_{ox}$, has a superscript, T, denoting that the flux is based on total exposed oxidizer surface area, S^T_{ox}. Since the oxidizer crystal can be either protruding or recessed, the total oxidizer surface area can be greater than the planar oxidizer surface area, S^P_{ox}, calculated from the average intersection oxidizer diameter, D'_{ox}. The linear burning rate of the oxidizer surface, r_{ox} can be determined from this mass flux and the density of the oxidizer, ρ_{ox}, as such:

$$r_{ox} = \frac{\dot{m}^T_{ox}}{\rho_{ox}} \tag{103}$$

In a similar fashion, the fuel surface is assumed to pyrolyze in a fashion also represented by an Arrhenius expression:

$$\dot{m}_b = \dot{m}^T_b = \dot{m}^P_b = A_b\, exp(-E_b/RT_{s,b}) \tag{104}$$

In this expression, A_b and E_b are the pre-exponential frequency factor and the activation energy, respectively, of the fuel pyrolysis reaction. Since the fuel surface is assumed to be planar, then the mass flux based on total fuel surface area, $\dot{m}_b^T$, can be used interchangeable with the fuel mass flux based on planar fuel area, $\dot{m}_b^P$. In this fuel pyrolysis equation, $T_{s,b}$, is the surface temperature of the fuel binder. This temperature can be either equal to or not equal to the oxidizer surface temperature, $T_{s,ox}$, depending upon whether a single or dual surface temperature analysis is employed. As was the case with the oxidizer, the linear burning rate of the fuel, r_b, can be determined from the fuel mass flux and the fuel density, ρ_b:

$$r_b = \frac{\dot{m}_b}{\rho_b} \tag{105}$$

The equation of mass conservation can be written for the burning propellant based on the mass fluxes and surface areas of the oxidizer and binder:

$$\dot{m}_T^P S_T^P = \dot{m}_{ox}^P S_{ox}^P + \dot{m}_b S_b^P \tag{106}$$

Note that all the mass fluxes are based on planar areas. The total planar mass flux, $\dot{m}_T^P$, is desired since it can be directly related to the propellant burning rate, $\bar{r}$, and the total propellant density, ρ_p:

$$r = \frac{\dot{m}_T^P}{\rho_p} \tag{107}$$

where:

$$\rho_p = \left[\frac{\alpha}{\rho_{ox}} + \frac{(1-\alpha)}{\rho_b}\right]^{-1} \tag{108}$$

The mass conservation equation can be written for $\dot{m}_T^P$:

$$\dot{m}_T^P = \dot{m}_{ox}^P \frac{S_{ox}^P}{S_T^P} + \dot{m}_b \frac{S_b^P}{S_T^P} \tag{109}$$

The total planar mass flux is related to the oxidizer and binder planar mass fluxes by:

$$\dot{m}_T^P = \dot{m}_{ox}^P \frac{\rho_p}{\rho_{ox}} = \dot{m}_b \frac{\rho_p}{\rho_b} \tag{110}$$

and the density ratios are related to the oxidizer mass fraction, α, and volume fraction, ζ, by:

$$\zeta_{ox} = \alpha \frac{\rho_p}{\rho_{ox}} \tag{111}$$

Combining equation (110) and (111) the following can be derived:

$$\dot{m}_T^P = \dot{m}_{ox}^P \frac{\zeta_{ox}}{\alpha} = \dot{m}_b \frac{(1-\zeta_{ox})}{(1-\alpha)} \qquad (112)$$

The planar mass flux of the oxidizer, $\dot{m}_{ox}^P$, can be related to the total surface mass flux of oxidizer, $\dot{m}_{ox}^T$, represented by equation (102) by the following:

$$\dot{m}_{ox}^P = \dot{m}_{ox}^T \left[\frac{S_{ox}^T}{S_{ox}^P}\right] \qquad (113)$$

The goal of this section is to find an expression for the area ratio:

$$\frac{S_{ox}^T}{S_{ox}^P}$$

Referring to Figure 25, the surface area of the spherical segment representing the burning AP surface is:

$$S_{ox}^T = 2\pi R\,|h| \qquad (114)$$

From triangle I:

$$R^2 = a^2 + (R - h)^2$$

$$2R\,|h| = a^2 + h^2 \qquad (115)$$

From triangle II:

$$(D_o/2)^2 = a^2 + (D_o/2 - L)^2$$

$$a^2 = D_oL - L^2 = L(D_o - L) \qquad (116)$$

Substituting equations (114) and (115) into equation (116):

$$S_{ox}^T = \pi\left[h^2 + L(D_o - L)\right] \qquad (117)$$

where h is a measure of the non-planarity of an oxidizer crystal and L is the distance from the top of the original crystal surface to the fuel surface. From equation (19) describing the statistical average intersection diameter, D′ or 2a, equation (116) can be rewritten:

$$a^2 = \left[\frac{\sqrt{2/3}\ D_o}{2}\right]^2 = \frac{{D_o}^2}{6} = L(D_o - L) \qquad (118)$$

and:

$$L = \frac{D_o}{2}\left[\ 1 \pm \sqrt{1/3}\ \right] \qquad (119)$$

Combining equation (117) with equation (118) gives:

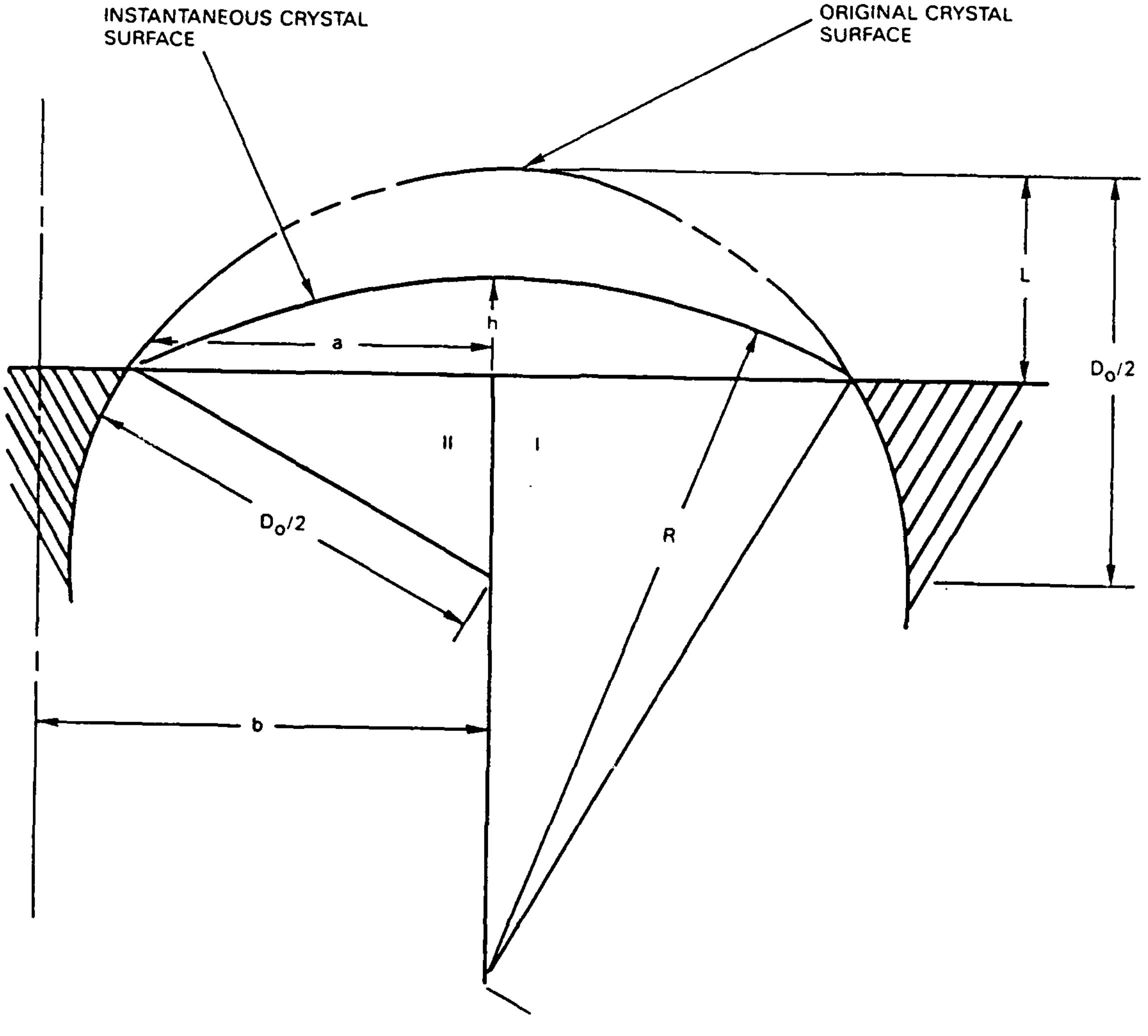

Figure 25
Geometrical Relationship of the Oxidizer Crystal
to the Burning Area (Same as Figure 6)

$$S_{ox}^{T} = \pi D_o^2 \frac{1}{6}\left[6\left(\frac{h}{D_o}\right)^2 + 1\right] \tag{120}$$

The term involving h/D_o can be evaluated using the same ignition delay concept employed by the HMX portion described previously and developed by Beckstead and McCarty.[140] Thus, referring to Figure 25:

$$h = L - y_{ox} \tag{121}$$

where y_{ox} is the linear distance that the AP crystal regresses and is equal to the product of the linear burning rate of AP under the given conditions and the time that the crystal burns. The burning time of the crystal is equal to the total time necessary for the surface to regress the distance L minus the ignition delay time. Thus:

$$h = L - r_{ox}(t_b - t_{ign})$$

$$h = L - r_{ox}\left(\frac{L}{r_f} - t_{ign}\right) \tag{122}$$

where the average regression rate of the fuel binder has been used to evaluate the total burning time. Equation (122) can be divided by D_o and combined with equation (119) to give:

$$\frac{h}{D_o} = \frac{L}{D_o}\left(1 - \frac{r_{ox}}{r_b}\right) + r_{ox}\frac{t_{ign}}{D_o}$$

$$= \frac{1}{2}\left(1 \pm \sqrt{1/3}\right)\left(1 - \frac{r_{ox}}{r_b}\right) + r_{ox}\frac{t_{ign}}{D_o} \tag{123}$$

where the ignition delay time is assumed to have the form derived by Beckstead and McCarty and discussed previously.[140]

$$t_{ign} = C_{ign}\frac{D_o^{\delta_{ign}}}{r} \tag{98}$$

The + or − refers to the positive of negative particles, that is, whether the lower hemisphere of the upper hemisphere is cut by the planar surface. It is assumed that there are an equal number of positive and negative crystals.

The planar surface area of the oxidizer crystal can be written as:

$$S_{ox}^{P} = \frac{\pi}{4}D'^2 = \frac{\pi}{4}(\sqrt{2/3}\, D_o)^2 = \frac{\pi}{6}D_o^2 \tag{124}$$

Dividing equation (120) by (124) yields the final relationship for the total to planar area ratio of the exposed oxidizer crystal:

$$\frac{S_{ox}^{T}}{S_{ox}^{P}} = 3\left(\frac{h}{D_{ox}}\right)_{+}^{2} + 3\left(\frac{h}{D_{ox}}\right)_{-}^{2} + 1 \tag{125}$$

This can now be used to determine the planar mass flux of the oxidizer given by equation (113), and then the total mass flux off the propellant surface can be determined with equation (112). The solution to this set of equations is iterative in nature. Given a surface temperature of the oxidizer, a initial guess of the binder surface temperature is used to compute the binder burning rate used in equation (105). In order for mass continuity to be maintained equation (112) must be satisfied. This equation relates the three planar mass fluxes off the surface; $\dot{m}_T^P$, $\dot{m}_{ox}^P$, and $\dot{m}_b$. The binder mass flux is recomputed and the binder surface temperature computed that would be required to yield this mass flux. The procedure is to iterate on binder surface temperature until all equations are satisfied. If the oxidizer and binder are assumed to have like surface temperatures, mass continuity cannot be maintained.

3.1.3.2 Surface Geometry

In the following analysis, it is assumed that the diffusion flames above the propellant surface are calculated in a manner based upon the original Burke-Schumann diffusion flame analysis.[19] In such an analysis, the two reactant constituents are assumed to issue from the surface in two separate streams. The oxidizer decomposition products flow from the surface in a circular duct centered above the oxidizer crystal. The fuel binder decomposition products flow in a concentric annulus around the oxidizer stream. The physical dimensions of these tubes are important in calculating the diffusion distances and can be related directly to the propellant surface geometry. The inner tube radius, a, is equal to half the intersection diameter, D'_{ox}, whereas the outer fuel radius, b, can be obtained from D'_{ox} and the oxidizer volume fraction, ζ_{ox}. More precisely:

$$a = \frac{D'_{ox}}{2} = \frac{1}{\sqrt{6}}D_{ox} \tag{126}$$

$$b = \frac{D'_{ox}}{2\sqrt{\zeta_{ox}}} = \frac{1}{\sqrt{6\zeta_{ox}}}D_{ox} \tag{127}$$

also:

$$\zeta_{ox} = \frac{S_{ox}^{P}}{S_{T}^{P}} = \frac{\pi a^{2}}{\pi b^{2}} = \left(\frac{a}{b}\right)^{2} \tag{128}$$

There are now three planar mass fluxes which have been calculated; $\dot{m}_{ox}^P$, $\dot{m}_b^P$, and $\dot{m}_T^P$. Since the Burke-Schumann analysis requires that the mass flux from each tube be equal, the analysis holds the outer tube radius, b, constant and permits the inner tube radius, a, to vary, via a flow slipline, so that the following conditions exists:

$$\dot{m}_b^P = \dot{m}_{ox}^P = \dot{m}_T^P \tag{129}$$

The new inner tube radius, a', can be shown to be related to a and propellant formulation variables as such:[140]

$$a' = a\left(\frac{\alpha}{z_{ox}}\right)^{1/2} \tag{130}$$

3.1.4 Energy Balance

3.1.4.1 HMX Energy Balance

The fundamental equation which both the HMX and AP portions of the HYPEM model revolve around is the surface energy balance. The energy transmitted to the surface from the various flames situated above the propellant constituents must equal the amount of energy needed to bring the ingredients from their initial temperature, T_o, to their surface temperature. For the HMX pseudo propellants, two separate energy balances are used, one over the HMX crystal and one over the binder. The energy equation over the HMX crystal is:

$$\begin{aligned} \dot{m}_X C_{s,X}(T_{s,X}-T_o) = & - \dot{m}_X Q_{DX} \\ & + \beta_p(\dot{m}_{X,PF} + \dot{m}_{b,PF})Q_{XPF}e^{-\xi^*_{XPF}} \\ & + (\dot{m}_X - \dot{m}_{X,PF})Q_X e^{-\xi^*_X} \end{aligned} \tag{131}$$

where: ξ^* - non-dimensional flame heights of primary and HMX flames
$\dot{m}_X$ - mass flux rate of HMX leaving the HMX crystal
$\dot{m}_{X,PF}$ - mass flux rate of HMX reacting in primary flame
$\dot{m}_{b,PF}$ - mass flux rate of binder reacting in primary flame
Q_{DX} - decomposition energy of HMX
Q_{XPF} - energy release in HMX primary flame
Q_X - energy release in HMX flame
$C_{s,X}$ - solid phase specific of HMX
$T_{s,X}$ - surface temperature of HMX crystal
T_o - initial propellant temperature
β_p - fraction of heat from primary flame to oxidizer

The left hand side of this equation represents the heat required to raise the HMX crystal from its initial temperature, T_o, to its surface temperature. The first term on the right hand side of equation (131) is the energy either absorbed or released at the surface. The final two terms represent the heat feedback to the propellant from the primary flame and HMX mono-propellant flame. The actual quantity of energy transferred back to the crystal's surface is equal to the energy released in the flame times the *exp*$(-\xi^*)$, where ξ^* is the non-dimensional flame standoff distance.

An assumption is made that the binder and oxidizer decomposition products react in the primary flame in stoichiometric proportions:

$$\dot{m}_{X,PF} = \Phi_{ST} f r_b \dot{m}_b \tag{132}$$

Where Φ_{ST} is the stoichiometric oxidizer to fuel ratio and fr_b is the fraction of binder that reacts in the primary flame. In addition, the following relationships are known:

$$\dot{m}_b fr_b = \dot{m}_{b,PF} \quad \text{and} \quad \dot{m}_X \beta_f = \dot{m}_{X,PF} \tag{133}$$

β_f is the fraction of HMX that reacts in the primary flame. Solving equation (131) for $T_{s,X}$ and utilizing relationships (132) and (133) the follow equation results:

$$T_{s,X} = T_o - \frac{Q_{DX}}{C_{s,X}} + \beta_p \beta_f \left(1 + \frac{1}{\Phi_{ST}}\right) \frac{Q_{XPF}}{C_{s,X}} e^{-\xi^*_{XPF}} + (1-\beta_f) \frac{Q_X}{C_{s,X}} e^{-\xi^*_X} \tag{134}$$

In the above equations, and in the ones that follow, the solid phase specific heat of HMX, AP and binder are computed from measured solid phase specific heat versus temperature data.[77] The temperature used to determine the specific heat from the data is the average of the surface temperature and the initial propellant temperature, T_o. The use of variable solid phase thermal properties have improved the results in similar multiple flame combustion models.[149]

Next, an equation for the binder is developed. The surface temperature equation for the binder fuel is analogous to equation (131) for the HMX crystal and is:

$$\begin{aligned} \dot{m}_b C_{s,b}(T_{s,b} - T_o) = & -fr_b \dot{m}_b Q_{Db} \\ & + (1-\beta_p)(\dot{m}_{X,PF} + \dot{m}_{b,PF}) Q_{XPF} e^{-\xi^*_{XPF}} \end{aligned} \tag{135}$$

Where $\dot{m}_b$ and $C_{s,b}$ are the mass rate of binder leaving the surface and the solid phase specific heat of the binder. The left hand side of this equation represents the heat required to raise the binder from its initial temperature, T_o, to its surface temperature. The first term on the right hand side of equation (135) is the energy either absorbed or released at the surface. The final term represent the heat feedback to the propellant from the primary flame. As before, the use of equations (132) and (133) into (135) will yield a expression for the binder surface temperature, $T_{s,b}$:

$$T_{s,b} = -T_o - \frac{fr_b Q_{Db}}{C_{s,b}} + (1-\beta_p) fr_b (\Phi_{ST}+1) \frac{Q_{PF}}{C_{s,b}} e^{-\xi^*_{XPF}} \tag{136}$$

The energy release terms are defined as follows:

$$\begin{aligned} Q_{XPF} = & \ \alpha[C_{s,X}(T_{s,X} - T_o) + C_p(T_{XPF} - T_{s,X}) + Q_{DX}] \\ & + (1-\alpha)[C_{s,b}(T_{s,b} - T_o) + C_p(T_{XPF} - T_{s,b}) + Q_{Db}] \end{aligned} \tag{137}$$

$$Q_X = \alpha[C_{s,X}(T_{s,X} - T_o) + C_p(T_X - T_{s,X}) + Q_{DX} \tag{138}$$

In these expressions α is the mass fraction of HMX in the pseudo propellant, C_p is the gas phase specific heat, T_{XPF} is the HMX adiabatic primary flame temperature, T_X is the HMX mono-propellant adiabatic flame temperature.

The decomposition energy, Q_{DX}, is computed by assuming that the decomposition involves two steps. First a solid to liquid phase transition and then a liquid to gas phase transition. The solid to liquid phase transition energy is assumed constant. The liquid to gas phase transition energy is a function of pressure which has been empirically computed.[132] The decomposition energy for AP is computed in a similar manner.[18]

Equations (134) and (136) for $T_{s,X}$ and $T_{s,b}$ are non-linear equations and are solved for simultaneously. This adds considerable numerical complexity to the model. The constants β_p and β_f which represent the fraction of heat from the HMX primary flame to the oxidizer and the fraction of HMX entering the primary flame along with the non-dimensional flame heights, ξ^*_{XPF} and ξ^*_X will be discussed in a later section.

3.1.4.2 AP Energy Balance

The energy equation for the AP pseudo propellants consists of only a single expression since the AP portion of the model averages the propellant properties over the entire surface of the pseudo propellant. This equation performs an energy balance over both the AP oxidizer crystal and the binder simultaneously:

$$\begin{aligned}&\alpha C_{s,AP}(T_{s,AP}-T_o) + (1-\alpha)C_{s,b}(T_{s,b}-T_o) \qquad (139)\\ &= -\alpha Q_{DAP} - (1-\alpha)Q_{Db}\\ &+ (1-\beta_f)Q_{AP}e^{-\xi^*_{AP}} + \beta_f Q_{PF}e^{-\xi^*_{PF}} + (1-\beta_f)Q_{FF}e^{-\xi^*_{FF}}\end{aligned}$$

where $C_{s,AP}$ ia the solid phase specific heat of AP; $T_{s,AP}$ is the AP crystal's surface temperature; Q_{DAP}, is the surface decomposition energy of AP; Q_{AP}, Q_{PF}, and Q_{FF} are the heat release terms associated with the AP mono-propellant flame, AP primary flame between decomposed AP and binder pyrolysis products and the final flame between AP mono-propellant flame products and unreacted binder; and, finally, ξ^*_{AP}, ξ^*_{PF}, and ξ^*_{FF} are the non-dimensional flame heights associated with the three flames. Like in the previous energy equations, the left hand side represents the sensible energy required to raise the propellant ingredients to the surface temperature. The first term on the right side represents surface decomposition or pyrolysis energy released of absorbed at the surface. The remaining three terms include the energy transferred back to the propellant surface by the AP mono-propellant flame, primary flame and the final flame. Solving for the AP surface temperature yields

$$T_{s,AP} = T_o - \frac{(1-\alpha)C_{s,b}}{\alpha C_{s,AP}}(T_{s,b}-T_o) - \frac{\alpha Q_{DAP}}{\alpha C_{s,AP}} - \frac{(1-\alpha)Q_{Db}}{\alpha C_{s,AP}} \tag{140}$$

$$+ \frac{(1-\beta_f)Q_{AP}}{\alpha C_{s,AP}} e^{-\xi^*_{AP}} + \frac{\beta_f Q_{PF}}{\alpha C_{s,AP}} e^{-\xi^*_{PF}} + \frac{(1-\beta_f)Q_{FF}}{\alpha C_{s,AP}} e^{-\xi^*_{FF}}$$

The energy release terms are as follows:

$$Q_{PF} = \alpha[C_{s,AP}(T_{s,AP}-T_o) + C_p(T_{PF}-T_{s,AP})] \tag{141}$$

$$+ (1-\alpha)[C_{s,b}(T_{s,b}-T_o) + C_p(T_{PF}-T_{s,b} + Q_{Db})$$

$$Q_{FF} = \alpha C_{p,FF}(T_{FF}-T_{AP}) \tag{142}$$

$$+ (1-\alpha)[C_{s,b}(T_{s,b}-T_o) + C_p(T_{FF}-T_{s,b}) + Q_{Db}]$$

$$Q_{AP} = \alpha[C_{s,AP}(T_{s,AP}-T_o) + C_p(T_{AP}-T_{s,AP}) + Q_{DAP}] \tag{143}$$

In these equations α is the mass fraction of AP in the pseudo propellant, T_{PF} is the adiabatic primary flame temperature, T_{FF} is the adiabatic final flame temperature, band T_{AP} is the AP mono-propellant adiabatic flame temperature. These flame temperatures and those used in the HMX energy equations are calculated by using a aerothermo-chemistry program with the various propellant ingredients. In the model a table look-up routine is used to compute the flame temperature as a function of pressure and oxidizer mass fraction.

Unlike the HMX section where the two temperatures must be solved for by simultaneously solving two energy equations for $T_{s,X}$ and $T_{s,b}$, The two surface temperatures are coupled through the continuity of mass relationships discussed previously.

3.1.5 Flame Standoff Distances

Both the HMX and AP mono-propellant flames are kinetic premixed flames whose flame standoff distance is purely kinetically controlled. Both the AP and HMX primary flames are assumed to be partially kinetic controlled and partially diffusion controlled. The total flame height is assumed to the sum of the kinetic and diffusion heights. The final flame over the AP crystal is assumed to be purely diffusion controlled since the reacting species are preheated by both the AP mono-propellant flame and the primary flame beneath, thus, the reaction kinetics are assumed to be very fast.

3.1.5.1 Kinetic Flames

The general form of the equations describing the kinetics and combustion of a premixed flame can be derived in a simple manner considering global kinetics. For a uniform flow rate, the distance from the propellant surface to the flame can be approximated as the linear gas velocity multiplied by the time it takes the reactants to react:

$$x^* = v\tau \tag{144}$$

where both the velocity and the time are averaged quantities, and it is assumed that the reaction occurs in one simple step. From continuity the gas velocity can be evaluated as:

$$v = \frac{\dot{m}_{solid}}{\rho_g} \tag{145}$$

where ρ_g is the gas density. For an arbitrary reaction order the reaction rate is:

$$w = kP^{\delta} \tag{146}$$

where k is the rate constant, and δ the order. Integration of the reaction rate to give the reaction time results in the proportionality:

$$\tau \approx \frac{1}{kP^{\delta-1}} \tag{147}$$

Combining equations (145) and (147) with (144) and applying the ideal gas law yields the standoff distance as:

$$x^* = \frac{\dot{m}}{kP^{\delta}} \tag{148}$$

where k now represents a pseudo rate constant, i.e., the rate constant combined with the proportionality constant of equation (147).

The flame standoff distance is normally applied in a non-dimensional form as in equation (134), (136) and (140) which define the various surface temperatures. From the heat conduction equation (i.e., the energy equation written as a second order differential equation) the non-dimensional standoff distance is:

$$\xi^* = \frac{c_p\dot{m}}{\lambda}x^* \tag{43}$$

where c_p is the specific heat and λ is the thermal conductivity of the gas. λ is defined as:

$$\lambda = \lambda_{ref}\left[\frac{T}{T_{ref}}\right]^{1/2} \tag{149}$$

where λ_{ref} is the gas phase thermal conductivity at some reference temperature, T_{ref}.

3.1.5.2 Diffusion Flames

Diffusional processes are important in the model because of the physical separation of the binder and oxidizer. As reaction times become short with increasing pressure, the diffusional processes become significant and even dominant. The diffusional mixing distance is the quantity that will be applied in the model, and will be discussed here.

A successful detailed analysis of a diffusion flame was reported by Burke and Schumann in 1928.[19] They solved the mass conservation equation for a Bunsen burner type of flame. Because of the circular symmetry involved in their analysis, it appears to be very appropriate for the present problem of an assumed spherical oxidizer crystal surrounded by a fuel. A complete review of the analysis and assumptions was made by Williams.[25] One of the assumptions involved neglecting one of the derivatives along the axis of the flame, which in effect, limits the assumption to tall flames. Initial calculations indicated that the flame height for the propellant configuration and typical mass burning rates was on the order of the oxidizer dimensions. Therefore, the Burke-Schumann analysis was modified to include short flames.

Utilizing the nomenclature of Williams, the diffusion equation can be written as:[25]

$$\frac{\partial^2 \beta}{\partial x^2} + \frac{1}{r}\frac{\partial}{\partial r}\left(r\frac{\partial \beta}{\partial r}\right) = \frac{v}{D}\frac{\partial \beta}{\partial x} \tag{150}$$

where β is a concentration term and the second derivative with respect to x is the term that is usually neglected. D is the gaseous diffusivity and is defined as:

$$D = D_o\frac{(T/T_{ref})^{1.75}}{(P/P_{ref})} \tag{151}$$

where, T is the gas temperature, P is the pressure, and D_o is a reference value of diffusivity at T_{ref} and P_{ref}.

The Burke-Schumann solution of the equation for the flame surface location neglecting the second derivative in equation (150) is:

$$\frac{\nu-(1+\nu)c^2}{2(1+\nu)c} = \sum_{n=1}^{\infty}\frac{1}{\phi_n}\frac{J_1(c\phi_n)}{[J_o(\phi_n)]^2}J_o(\phi_n\xi)\, exp\left(-\phi_n^2\eta\right) \tag{152}$$

where ν is a stoichiometric ratio, J represents a Bessel function, ϕ represents roots of the first order Bessel function, ξ is the non-dimensional radial distance, and η is the non-dimensional axial distance. The constant c is related to the burner geometry and is equal to a/b where a is the radial distance from the center of the flame to the edge of the oxidizer crystal and b is the radial distance from the center of the flame to the outer edge of the binder annulus around the crystal (See Figure 25). The constants a and b were defined previously in equations (126) and (127). The non-dimensional distances ξ and η are defined as:

$$\xi = \frac{r}{b} \tag{153}$$

$$\eta = \frac{x\psi}{b} \tag{154}$$

where ψ is defined as $D/(vb)$. The stoichiometric ratio, ν, is the stoichiometric oxygen to fuel ratio divided by the actual oxygen to fuel ratio.

Solving this equation at the center of the flame, ξ equal to zero, and only using the first term in the summation, the flame height is:

$$x^* = \frac{vb^2}{D\phi_1{}^2} \, ln \left[\frac{2(1+\nu)cJ_1(c\phi_1)}{\nu-(1+\nu)c^2\phi_1[J_o(\phi_1)]^2} \right] \tag{155}$$

This is the form of the equation used in the original Beckstead, Derr, Price multiple flame model discussed previously.

In the modified solution to equation (150) including the second derivative with respect to the axial direction, the equation for the location of the flame surface becomes:

$$\frac{\nu-(1+\nu)c^2}{2(1+\nu)c} = \sum_{n=1}^{\infty} \frac{J_1(c\phi_n)}{\phi_n[J_o(\phi_n)]^2} \, J_o(\phi_n\xi) \, exp \left[\frac{-\left([1+(2\psi\phi_n)^2]^{1/2}-1\right)\eta}{2\psi^2} \right] \tag{54}$$

which is identical to equation (152) with the exception of the term in the exponent where $\psi = D/(vb)$. This is the equation which is solved in the HYPEM combustion model and is also used in the Petite Ensemble Model.

There are two possible solutions to this equation, one when the flame closes over the oxidizer crystal and one when it closes over the binder. These conditions correspond to the fuel rich and oxygen rich conditions, respectively. The first solution is obtained by setting ξ equal to zero, the center of the flame. The second solution is obtained by setting ξ to 1 which represents the outer edge of the binder annulus. To determine which condition to solve for, the left hand side of the equation (54) is examined:

$$\frac{\nu-(1+\nu)c^2}{2(1+\nu)c} \tag{156}$$

If this expression is positive equation (54) can only be solved when ξ is zero (flame closes over oxidizer) and if it is negative ξ must be set to 1 (flame closes over binder) for a solution to exist. Either way, the solution is iterative in nature and terms in the series are used until they become very small.

If the assumption is made that the flame has a parabolic shape, it can be shown that a distributed heat release all along the parabolic flame front surface can be represented by a planar flame sheet at some fraction of the diffusion flame height, ϵ.[29] This parameter is calculated from the non-dimensional flame height ξ^*, by the relation:

$$\epsilon = \frac{1}{\xi^*}\left[ln(\xi^* exp(\xi^*)) - ln(exp(\xi^*) - 1)\right] \tag{57}$$

The diffusion height, x_D^*, calculated from equation (54) is multiplied by ϵ to determine the effective planar flame height, $\bar{x}_D^*$:

$$\bar{x}_D^* = \epsilon x_D^* \tag{157}$$

3.1.5.3 Flame Standoff Distances

The various flame heights will now be presented in their final form which can be used in the surface temperature equations (134, 136, and 140). Since the final flame sits over the AP crystal its flame height is the sum of two terms, the AP kinetic flame height, x_{AP}^*, given by equation (148) and the final flame effective diffusion height, $\bar{x}_{FD}^*$, given by equations (54) and (157) and normalized by equation (43):

$$\xi_{FF}^* = \frac{c_p\dot{m}_{ox}}{\lambda}(x_{AP}^* + \bar{x}_{FD}^*) = \frac{c_p\dot{m}_{ox}^{\,2}}{\lambda k_{AP}P^{\delta}} + \frac{c_p\dot{m}_{ox}}{\lambda}\bar{x}_{FD}^* \tag{42}$$

Similarly, the primary flame standoff distance is the sum of two terms. In the primary flames, the components must mix together and then react so that there is a diffusion distance, $\bar{x}_{PD}^*$ for the AP primary flame and $\bar{x}_{XPD}^*$ for the HMX primary flame, followed by the kinetic distance required for the ingredients to react, x_{PF}^* for AP and x_{XPF}^* for HMX. Again in the non-dimensional form:

$$\xi_{PF}^* = \frac{c_p\dot{m}_T}{\lambda}(\bar{x}_{PD}^* + x_{PF}^*) = \frac{c_p\dot{m}_T}{\lambda}\bar{x}_{PD}^* + \frac{c_p\dot{m}_T^{\,2}}{\lambda k_{PF}P^{\delta}} \tag{40}$$

$$\xi_{XPF}^* = \frac{c_p\dot{m}_T}{\lambda}(\bar{x}_{XPD}^* + x_{XPF}^*) = \frac{c_p\dot{m}_T}{\lambda}\bar{x}_{XPD}^* + \frac{c_p\dot{m}_T^{\,2}}{\lambda k_{XPF}P^{\delta}} \tag{158}$$

where ξ_{PF}^* and ξ_{XPF}^* are the non-dimensional distances of the AP and HMX primary flames. The final non-dimensional distances needed to evaluate the surface temperature is that of the kinetically controlled oxidizer flames. These kinetic flame heights are from equations (148) and (43):

$$\xi^*_{AP} = \frac{c_p \dot{m}_{ox}}{\lambda} x^*_{AP} = \frac{c_p \dot{m}_{ox}{}^2}{\lambda k_{AP} P^{\delta}} \quad (41)$$

$$\xi^*_{X} = \frac{c_p \dot{m}_{ox}}{\lambda} x^*_{X} = \frac{c_p \dot{m}_{ox}{}^2}{\lambda k_{X} P^{\delta}} \quad (159)$$

for the AP and HMX mono-propellant flames where ξ^*_X is the HMX monopropellant flame height.

The reaction rate constants for each flame can be written in Arrhenius fashion as follows:

$$k_{AP} = A_{AP} exp(-E_{AP}/RT_{AP}) \quad (160)$$

$$k_{PF} = A_{PF} exp(-E_{PF}/RT_{F}) \quad (161)$$

$$k_{X} = A_{X} exp(-E_{X}/RT_{X}) \quad (162)$$

3.1.5.4 The Competing Flames

The fraction of the total oxidizer that reacts with the primary flame, β_f, can be determined from the foregoing flame heights. This term is required since there is competition for the oxidizer decomposition products between the primary flame and the oxidizer monopropellant flame. Based solely on geometry, again assuming that the primary diffusion flame is parabolic in shape, this term can be calculated with the following expression:[29]

$$\beta_f = \frac{(x^*_{AP} - x^*_{PF})}{x^*_{PD}} \quad (45)$$

This is the equation for the AP pseudo propellants, by substituting x^*_X for x^*_{AP}, x^*_{XPF} for x^*_{PF} and x^*_{XPD} for x^*_{PD} this equation will determine β_f for the HMX pseudo propellant.

The final parameter that must be defined is β_p, the fraction of heat from the HMX primary flame to the HMX crystal. This parameter is needed in the energy equations to determine how the heat transfer from the primary flame is distributed between the HMX crystal and the binder. It is to assumed that β_p is proportional to β_f, the fraction of HMX entering the primary flame, the mass fluxes at the surface, the properties of the gas, and inversely proportional to the primary flame height. Therefore, the following function is assumed.[140]

$$\beta_p = \beta_{pa}\sqrt{\beta_f}\,\frac{\dot{m}_b}{\dot{m}_{ox}}\, e^{\left(\frac{-Cp_{av}}{\lambda\beta_f}\bar{x}^{*}_{XPF}\right)} \tag{163}$$

In this equation a high binder to oxidizer flow rate, a high thermal conductivity, λ, and a large value of β_f increases the heat transfer to the oxidizer from the primary flame while a increase in the primary flame height, $\bar{x}^{*}_{XPF}$, and average specific heat, Cp_{av}, decreases β_p. β_{pa} is a constant that has a value of 0.2. In addition, equation (163) is constrained to never be greater than 0.8 and never less than 0.05. Despite the complexity of the expression, β_p is usually about 1/3 the value of β_f.

3.1.6 Pseudo Propellant Interactions

As will be described later in the model validation section, the HYPEM model successfully predicts the burn rate of a wide variety of HMX/HTPB propellants and AP/HTPB propellants. However, when the model was used with propellants containing both HMX and AP crystals the agreement with experimental data was poor when compared with results of propellants containing only one type of oxidizer.[150] Two modifications were made to the model to help correct the problem.

3.1.6.1 Mass Interaction Parameter

First, a change was made in the way the pseudo propellant mass fraction was determined. AP is a true oxidizer and requires binder to burn stoichiometric so that all oxygen is reacted and a high flame temperature can be achieved. HMX, on the other hand, burns stoichiometric as a monopropellant and the introduction of binder reduces the flame temperature. It is reasonable to assume that AP crystals of comparable size will rob binder from corresponding equal sized HMX crystals. It was decided to lower the AP pseudo propellant mass fraction, thereby, enriching the AP pseudo propellants, by introducing the mass interaction parameter. This parameter multiplies the AP mass fraction, α_d, by a constant less than or equal to one. In order for continuity to be maintained the HMX mass fractions would have to be multiplied by a factor greater than one. These two constants are obviously related and depend on the overall mass fractions of both oxidizer types. Given the AP mass fraction multiplier, it can be shown that the factor for the HMX crystals is:

$$n_X = \frac{n_{AP}\alpha_X}{n_{AP}\alpha_T - \alpha_{AP}} \tag{164}$$

where n_{AP} is the AP mass interaction parameter, n_X is the HMX mass interaction parameter, α_T is the total propellant oxidizer mass fraction, α_{AP} is the total AP mass fraction and α_X is the total HMX mass fraction. In order for the modified pseudo propellant mass fractions to remain less than one, limits must be placed on the mass interaction parameter such that no pseudo propellant mass oxidizer mass fraction exceeds one. A value of approximately 0.98

significantly improved the burn rate predictions for propellants containing both AP and HMX crystals.

3.1.6.2 Flame Temperature Modifications

A second source of error in computing the burn rate for propellants containing both AP and HMX crystals is the use of discrete values for the various flame temperatures used in the energy equations. As discussed in section 2.3.2.2 describing the differences between AP and HMX combustion, the flame temperature of the AP/HTPB mixture can be over 1000°K higher that that for the HMX/HTPB mixture. In reality there is a smearing the propellant flame temperatures since the flames are not actually discrete flames but are combined over the propellant surface. To account for this smearing, the actual flame temperatures used in the model are mass weighted by the amount of AP and HMX in the propellant. The mono-propellant flame temperatures for AP and HMX were not modified since these flames sit directly over the crystal and should be less affected by other flames. The primary flames, on the other hand, are assumed to be at the outer edges of pseudo propellant and are more easily influenced by surrounding flames. As with the mass interaction parameter, a noticeable improvement resulted in predicting the burning rate of propellants containing both types of oxidizer crystals.

3.2 Summary of Equations

The basic equations of the HYPEM composite combustion model have all been derived. A summary of the primary equations in the model follows. First is the overall controlling equations that determine the overall burning rate of the propellant and the pseudo propellant properties:

$$F_{d,ox} = \frac{\alpha_{ox}}{\sqrt{2\pi}\, ln\sigma_{ox}} \, exp\left[-\frac{1}{2} \left(\frac{lnD_{ox} - ln\bar{D}_{ox}}{ln\sigma_{ox}} \right)^2 \right] \quad (76)$$

$$\bar{r} = \frac{1}{\alpha_T} \oint_{D_{ox}} (r_d F_d)\, d\,lnD_{ox} \quad (77)$$

$$\alpha_d = \left(1 + \frac{6\rho_b}{\pi\rho_{ox}} CD^{XN-3} \right)^{-1} \quad (89)$$

Next are the Arrhenius equations which determine the burn rate of the individual propellant ingredients:

$$\dot{m}_{ox} = r_{ox}\rho_{ox} = A_{ox}e^{(-E_{ox}/RT_{s,ox})} \quad (90)$$

$$\dot{m}_b = r_b\rho_b = A_b e^{(-E_b/RT_{s,b})} \quad (91)$$

The time averaged burning rate expression for the HMX pseudo propellant:

$$r = \frac{(1 + \delta)}{\left(\frac{1}{r_X} + \frac{t_{ign}}{D'} + \frac{\delta fr_b}{r_b} + \frac{t_b(1 - fr_b)}{D'} \right)} \quad (94)$$

AP pseudo propellant burning rate and surface geometry equations:

$$r = \frac{\dot{m}_T^P}{\rho_p} \quad (107)$$

$$\dot{m}_T^P = \dot{m}_{ox}^P \frac{\zeta_{ox}}{\alpha} = \dot{m}_b \frac{(1 - \zeta_{ox})}{(1 - \alpha)} \quad (112)$$

$$\dot{m}_{ox}^{P} = \dot{m}_{ox}^{T}\left[\frac{S_{ox}^{T}}{S_{ox}^{P}}\right] \tag{113}$$

$$\frac{h}{D_o} = \frac{L}{D_o}\left(1 - \frac{r_{ox}}{r_b}\right) + r_{ox}\frac{t_{ign}}{D_o}$$

$$= \frac{1}{2}\left(1 \pm \sqrt{1/3}\right)\left(1 - \frac{r_{ox}}{r_b}\right) + r_{ox}\frac{t_{ign}}{D_o} \tag{123}$$

$$\frac{S_{ox}^{T}}{S_{ox}^{P}} = 3\left(\frac{h}{D_{ox}}\right)_{+}^{2} + 3\left(\frac{h}{D_{ox}}\right)_{-}^{2} + 1 \tag{125}$$

The three surface temperature relationships:

$$T_{s,X} = T_o - \frac{Q_{DX}}{C_{s,X}} + \beta_p\beta_f\left(1 + \frac{1}{\Phi_{ST}}\right)\frac{Q_{XPF}}{C_{s,X}}e^{-\xi_{XPF}^{*}} + (1-\beta_f)\frac{Q_X}{C_{s,X}}e^{-\xi_{X}^{*}} \tag{134}$$

$$T_{s,b} = -T_o - \frac{fr_bQ_{Db}}{C_{s,b}} + (1-\beta_p)fr_b(\Phi_{ST}+1)\frac{Q_{PF}}{C_{s,b}}e^{-\xi_{XPF}^{*}} \tag{136}$$

$$T_{s,AP} = T_o - \frac{(1-\alpha)C_{s,b}}{\alpha C_{s,AP}}(T_{s,b}-T_o) - \frac{\alpha Q_{DAP}}{\alpha C_{s,AP}} - \frac{(1-\alpha)Q_{Db}}{\alpha C_{s,AP}} \tag{140}$$

$$+ \frac{(1-\beta_f)Q_{AP}}{\alpha C_{s,AP}}e^{-\xi_{AP}^{*}} + \frac{\beta_f Q_{PF}}{\alpha C_{s,AP}}e^{-\xi_{PF}^{*}} + \frac{(1-\beta_f)Q_{FF}}{\alpha C_{s,AP}}e^{-\xi_{FF}^{*}}$$

Equations describing the kinetic flame height, the non-dimensionalization of the flame heights and the diffusional flame height equation:

$$x^{*} = \frac{\dot{m}}{kP^{\delta}} \tag{148}$$

$$\xi^{*} = \frac{c_p\dot{m}}{\lambda}x^{*} \tag{43}$$

$$\frac{\nu-(1+\nu)c^2}{2(1+\nu)c} = \sum_{n=1}^{\infty} \frac{J_1(c\phi_n)}{\phi_n[J_o(\phi_n)]^2} J_o(\phi_n\xi)\exp\left[\frac{-\left\{[1+(2\psi\phi_n)^2]^{1/2}-1\right\}\eta}{2\psi^2}\right] \qquad (54)$$

The five flame standoff distances are:

$$\xi^*_{FF} = \frac{c_p\dot{m}_{ox}}{\lambda}(x^*_{AP} + \bar{x}^*_{FD}) = \frac{c_p\dot{m}_{ox}^{\,2}}{\lambda k_{AP}P^{\delta}} + \frac{c_p\dot{m}_{ox}}{\lambda}\bar{x}^*_{FD} \qquad (42)$$

$$\xi^*_{PF} = \frac{c_p\dot{m}_T}{\lambda}(\bar{x}^*_{PD} + x^*_{PF}) = \frac{c_p\dot{m}_T}{\lambda}\bar{x}^*_{PD} + \frac{c_p\dot{m}_T^{\,2}}{\lambda k_{PF}P^{\delta}} \qquad (40)$$

$$\xi^*_{XPF} = \frac{c_p\dot{m}_T}{\lambda}(\bar{x}^*_{XPD} + x^*_{XPF}) = \frac{c_p\dot{m}_T}{\lambda}\bar{x}^*_{XPD} + \frac{c_p\dot{m}_T^{\,2}}{\lambda k_{XPF}P^{\delta}} \qquad (158)$$

$$\xi^*_{AP} = \frac{c_p\dot{m}_{ox}}{\lambda}x^*_{AP} = \frac{c_p\dot{m}_{ox}^{\,2}}{\lambda k_{AP}P^{\delta}} \qquad (41)$$

$$\xi^*_{X} = \frac{c_p\dot{m}_{ox}}{\lambda}x^*_{X} = \frac{c_p\dot{m}_{ox}^{\,2}}{\lambda k_{X}P^{\delta}} \qquad (159)$$

Finally, the fraction of oxidizer that reacts in the primary flame and the fraction of heat from the HMX primary flame that is feed back to the HMX crystal:

$$\beta_f = \frac{(x^*_{AP} - x^*_{PF})}{x^*_{PD}} \qquad (45)$$

$$\beta_p = \beta_{pa}\sqrt{\beta_f}\,\frac{\dot{m}_b}{\dot{m}_{ox}}\,e^{\left(\frac{-Cp_{av}}{\lambda\beta_f}\bar{x}^*_{XPF}\right)} \qquad (163)$$

3.3 HYPEM Model Options

3.3.1 Model Inputs

The HYPEM composite combustion model is written in standard FORTRAN and will run on most computers supporting FORTRAN. Inputs to the model can be grouped in three categories. The first type of inputs are the many propellant constants such as densities, reaction orders, and specific heats. These constants default to known values and seldom need to be modified. The second type are the propellant characterization variables such as oxidizer particle size, type (either AP and/or HMX), and the overall mass fraction of the various particles. Up to four particle distributions may be specified. The binder is assumed to be HTPB. The final type of inputs are the control variables which specify the propellant conditions to evaluated the burning rate. These include pressure and initial propellant temperature. Up to ten values of both pressure and initial propellant temperature may be input. In addition, the model can determine the burning characteristics of more that one propellant per execution of the computer code. A sample computer output from the HYPEM model is located in the appendix.

3.3.2 Pressure Exponent

If more than one pressure is input the burning rate pressure exponent is calculated by using a least squares fit of the equation:

$$r = cP^n \tag{18}$$

where r is the burning rate of the entire propellant computed by equation (77), c is a calculated constant, P is the pressure and n is the pressure exponent. An important factor in determining if a combustion model is correctly understanding propellant behavior is if the model not only can predict the correct burning rate, but also the burning rate dependence on pressure, hence, predict the pressure exponent.

3.3.3 Temperature Sensitivity

If more than one initial propellant temperature is input the temperature sensitivity of the propellant is calculated. The temperature sensitivity is the sensitivity of the burning rate to changes in initial propellant temperature. This is very important in determining how a solid rocket motor will behave if it is conditioned to a initial temperature. This temperature can range from -40°F in the Arctic to 140°F in desert areas. The temperature sensitivity is defined as:

$$\sigma_P = \left[\frac{\partial \ln r}{\partial T_o}\right]_P \tag{165}$$

where σ_P is the temperature sensitivity, r is the burn rate, T_o is the initial propellant temperature and the subscript P indicates that σ_P is computed at a constant pressure. This parameter is automatically computed and averaged over the initial temperatures that are input to the model.

CHAPTER IV

COMPARISON OF THEORETICAL AND EXPERIMENTAL RESULTS

4.1 Determination of Propellant Constants

Many constants are required to successfully use the HYPEM combustion model. These constants include physical properties of HMX, AP and HTPB binder such as density, solid phase specific heat and, phase transition temperatures. Constants such as these are easily found in chemistry and physics handbooks. The energy equation for both the HMX and AP sections of the model require monopropellant flame temperatures, primary flame temperatures and final flame temperatures and the respective molecular weights of the products. Tables were created for all flames and molecular weights as functions of oxidizer to fuel ratio and pressure from calculations performed with an aerothermochemistry program.[151] These tables are incorporated into the HYPEM combustion model and appropriate values are automatically determined as functions of pressure and air to fuel ratio by the computer program.

Some values of required constants are not as readily known but upper and lower limits can be placed on their values from known values of similar compounds. For example, the gas phase thermal conductivity of the product gases has not been measured but handbooks of physical constants do have conductivity values for the primary species found in the products. For other constants, the range of measured values is considerably large, and specific values cannot be accurately determined. For example, the measured range of the HMX decomposition frequency factor ranges from 1.0×10^{5} to 2.7×10^{25} 1/sec.[67-73] In this case the many different values were averaged and a value of near 1.0×10^{19} 1/sec was used.

As in the case with other steady state burning rate models, the HYPEM combustion model requires the use of several input constants such as activation energies and pre-exponential frequency factors for the gas phase reactions considered, the heats of fuel pyrolysis and oxidizer decomposition, and the gas phase specific heats. Some of these constants are known only to a small degree of precision. Many of these parameters can only be estimated and experimental burning rate and pressure exponent data for known propellant formulations must be used.

An optimization program was utilized to evaluate some of these lessor known constants. In this manner, some of the lesser known numerical input constants can be varied, each within prescribed physical limits, until the best fit to the experimental burning rate and exponent data is obtained. By computing the burning rate and pressure exponent for 61 propellants, the optimization program was able to minimize the errors between experimental and theoretically determined values. (These propellants will be explained in the next section.) This optimization process required hours and sometimes days of computer time to satisfactorily determine a value for a constant. Once a satisfactory value was determined, however, it was fixed and was not allowed to vary between propellants or propellant types to improve the performance of the model. In the following data comparison plots the model's input constants are fixed for all different propellant types and are not allowed to vary. Table 3 presents all the physical constants used in the HYPEM model. Constants with a "yes" in the OPT column are ones that were determined by the optimization process.

Table 3
HYPEM Combustion Model Physical Constants

Constant Name	Value	Opt
HMX crystal density	1.900 g/cm^3	
AP crystal density	1.950 g/cm^3	
HTPB binder density	0.930 g/cm^3	
Mass proportionality exponent	3.0	yes
HMX decomposition frequency factor	1.17E+19 g/cm^2-sec	yes
HMX decomposition activation energy	50000.0 cal/mole	
AP decomposition frequency factor	173359.0 g/cm^2-sec	yes
AP decomposition activation energy	22000.0 cal/mole	
HTPB pyrolysis frequency factor	300.0 g/cm^2-sec	
HTPB pyrolysis activation energy	16900.0 cal/mole	
HMX solid phase specific heat (298°K)	0.246 cal/g-K	
change in HMX specific heat with temp.	.000652 cal/g-K^2	
AP solid phase specific heat-298°K	0.2615 cal/g-K	
change in AP specific heat with temp.	.0005194 cal/g-K^2	
HTPB solid phase specific heat-298°K	0.4549 cal/g-K	
change in HTPB specific heat with temp.	.000593 cal/g-K^2	
HMX gas phase specific heat	0.25333 cal/g-K	yes
AP gas phase specific heat	0.23218 cal/g-K	yes
HMX gas phase thermal conductivity	.0036112 cal/g-sec-K	yes
AP gas phase thermal conductivity	.0003990 cal/g-sec-K	yes
HMX or AP gas phase thermal diffusivity	.16244 cm^2-atm/s-K	
HMX flame frequency factor	13.8 g/cm^3-sec-K	yes
HMX flame activation energy	22021.0 cal/mole	yes
HMX flame reaction order	1.39	yes
AP flame frequency factor	278.5 g/cm^3-sec-K	yes
AP flame activation energy	7929.2 cal/mole	yes
AP flame reaction order	1.64	yes
HMX primary flame frequency factor	77.3 g/cm^3-sec-K	yes
HMX primary flame activation energy	16746.0 cal/mole	yes
HMX primary flame reaction order	1.15	yes
AP primary flame frequency factor	179.0 g/cm^3-sec-K	yes
AP primary flame activation energy	20594.0 cal/mole	yes
AP primary flame reaction order	2.02	yes
HMX total heat of decomposition @1000psi	55.0 cal/g	
AP total heat of decomposition @1000psi	260.0 cal/g	
HTPB total heat of decomposition	500.0 cal/g	
HMX primary flame stoich. oxidizer/fuel	10.143	yes
AP primary flame stoich. oxidizer/fuel	5.211	yes
AF final flame stoich. oxidizer/fuel	12.129	yes
HMX ref. ignition delay constant	0.78	
HMX ref. temperature for ignition delay	675.0 K	
HMX ignition delay diameter exponent	1.10	
HMX melting point	553.0 K	
AP ref. ignition delay constant	4.321	
AP ref. temperature for ignition delay	480.0 K	
AP ignition delay diameter exponent	1.70	
AP melting point	865.0 K	

4.2 Burning Rate, Pressure Exponent and Temperature Sensitivity Prediction

The HYPEM model has been used to predict the burning rate, pressure exponent and temperature sensitivity of four types of HMX/AP/HTPB propellants, a total of 61 different propellants. While all of the following propellant types contain HTPB as a binder, the type and relative amount of oxidizer changes. Type I propellants contain only HMX, Type II propellants contain only AP, Type III propellants contain mostly HMX with 5 to 10 percent AP, and Type IV propellants contain mostly AP with 10 to 15 percent HMX. These propellants contain HMX particles from 4μm to 400μm and AP particles from 0.7μm to 450μm. The solids loading (amount of oxidizer) ranges from 70 to 88 percent. For all of these propellants, the oxidizer particle distribution data are known and will be presented along with the propellant formulation data.

The burning rate was computed for each propellant at three different pressures and at an initial temperature of 298°K. The pressures used were dependent on where the available experimental data was taken for a given type of propellant. The pressure exponent, n, was then determined by performing a least squares fit of equation (18):

$$r = cP^n \tag{18}$$

The pressure exponent was then compared with the experimentally determined value. The burning rate was also computed at initial propellant temperatures of 248, 298 and 348°K and at a chamber pressure of 1000 psi. The temperature sensitivity, σ_p, was then determined by computed σ_p between 248 and 298°K and between 298 and 348°K with equation (165):

$$\sigma_p = \left[\frac{\partial \ln r}{\partial T_o}\right]_P \tag{165}$$

and averaging the two results. The temperature sensitivity was then compared with experimental values.

The HYPEM model results of each class of propellant will now be presented along with comparisons to the actual measured burning rate, pressure exponent and temperature sensitivity.

4.2.1 HMX Composite Propellants: Type I

The first class of propellants to be examined, Type I, contain only HMX crystals dispersed in a HTPB binder medium. These propellants were formulated by Hercules, Inc.[118] For the series of 17 propellants, the solids loading (amount of HMX) ranges from 70 percent to 85.5 percent and the particle size ranges from 4 to 400 microns.

Table 4 presents the formulation data for these HMX/HTPB propellants. Table 5 presents the experimental data and the theoretical prediction for the burning rate at 600, 1000 and 1600 psi, the pressure exponent at an initial temperature of 298°K and the temperature sensitivity at 1000 psia. Figures 26, 27 and 28 plot the theoretical HYPEM values on the vertical axis versus the experimental values on the horizontal axis for the burning rates at 1000 psi, the pressure exponents, and the temperature sensitivities, respectively, shown in Table 5. On each plot there is a number by each data point which corresponds to the propellant identification number in Table 4 and 5. Error bands shown by the dashed lines are included in the Figures 26, 27 and 28. The burning rate and pressure exponent plots have 10 percent error bands while the temperature sensitivity plots have 20 percent error bands. The solid line represents perfect agreement between experiment and model prediction.

As can be seen in Figures 26 and 27, the HYPEM model predicts the burning rates and exponents for the majority of these propellants within ±10 percent. Figure 28 indicates that the HYPEM model's burning rate temperature sensitivity prediction consistently over estimates the experimental prediction by more than 20 percent.

Table 4
HMX/HTPB Propellant Formulations: Type I

			%HMX			
			$400\mu^*$	200μ	58μ	4μ
		$\bar{D}$	400μ	147μ	42.4μ	4.46μ
No	%HTPB	σ	2.00	1.86	2.68	1.99
1	30.00		-	-	70.00	-
2	30.00		70.00	-	-	-
3	30.00		-	-	35.00	35.00
4	30.00		35.00	-	35.00	-
5	30.00		-	23.33	23.33	23.33
6	22.00		-	-	-	78.00
7	22.00		-	-	78.00	-
8	22.00		-	78.00	-	-
9	22.00		78.00	-	-	-
10	22.00		-	39.00	39.00	-
11	22.00		-	26.00	26.00	26.00
12	14.50		-	28.50	28.50	28.50
13	14.50		-	38.50	29.90	17.10
14	14.50		-	42.75	-	42.75
15	14.50		-	64.10	-	21.40
16	14.50		-	42.75	42.75	-
17	30.00		-	-	-	70.00

* Distribution data unavailable, the values shown are assumed.

Table 5
Predicted and Experimental Burning Rates, Exponents and Temperature Sensitivities for HMX/HTPB Propellants: Type I

	Burning Rate* - in/sec						Exponent		Temperature Sensitivity %/°K**	
	600psia		1000psia		1600psia					
No	r_{ex}	r_{th}	r_{ex}	r_{th}	r_{ex}	r_{th}	n_{ex}	n_{th}	$\sigma_{p,ex}$	$\sigma_{p,th}$
1	0.048	0.050	0.066	0.064	0.088	0.086	0.618	0.545	--	--
2	0.030	0.040	0.041	0.056	0.067	0.074	0.816	0.630	0.26	0.32
3	0.070	0.072	0.095	0.095	0.125	0.127	0.591	0.578	--	--
4	0.042	0.045	0.057	0.060	0.077	0.080	0.618	0.584	0.22	0.34
5	0.060	0.060	0.083	0.081	0.113	0.109	0.645	0.603	--	--
6	0.093	0.120	0.128	0.160	0.173	0.214	0.633	0.591	--	--
7	0.074	0.073	0.093	0.095	0.116	0.120	0.458	0.509	--	--
8	0.052	0.053	0.073	0.075	0.099	0.104	0.657	0.690	--	--
9	0.054	0.054	0.073	0.075	0.112	0.100	0.742	0.619	--	--
10	0.070	0.063	0.092	0.085	0.119	0.112	0.541	0.589	--	--
11	0.084	0.082	0.120	0.110	0.166	0.146	0.695	0.590	--	--
12	0.103	0.122	0.143	0.163	0.195	0.213	0.651	0.567	0.18	0.25
13	0.097	0.112	0.134	0.149	0.180	0.195	0.630	0.567	0.13	0.26
14	0.104	0.125	0.144	0.169	0.195	0.225	0.641	0.601	0.12	0.24
15	0.095	0.105	0.129	0.143	0.170	0.191	0.593	0.612	--	--
16	0.092	0.100	0.127	0.133	0.177	0.172	0.667	0.550	--	--
17	0.072	0.094	0.103	0.125	0.140	0.168	0.677	0.595	0.21	0.33

* The subscript ex refers to experimental data
The subscript th refers to theoretical model prediction

** The temperature sensitivity was computed by evaluating the burning rate at initial temperatures of 248, 298, and 348°K

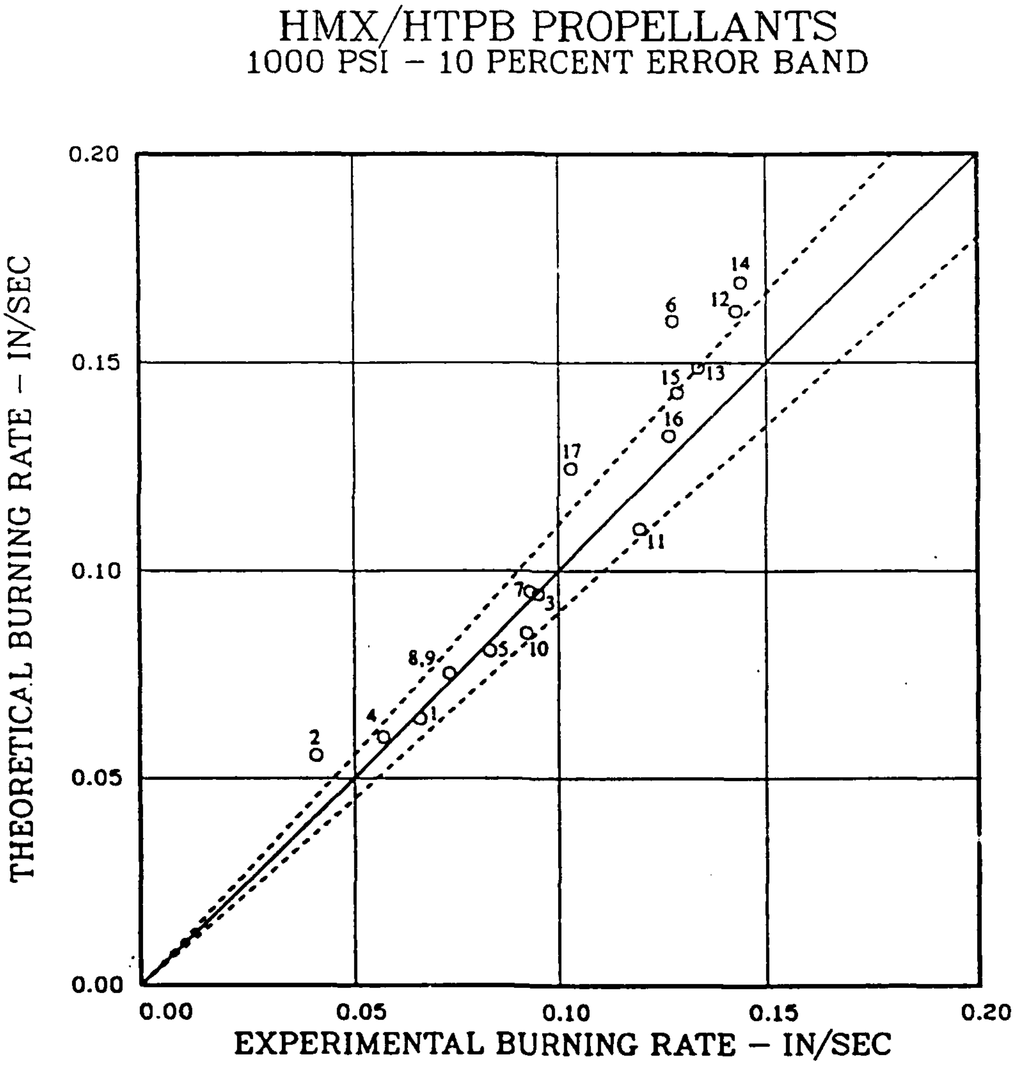

Figure 26
Theoretical Versus Experimental Burning Rate
for HMX/HTPB Propellants: Type I

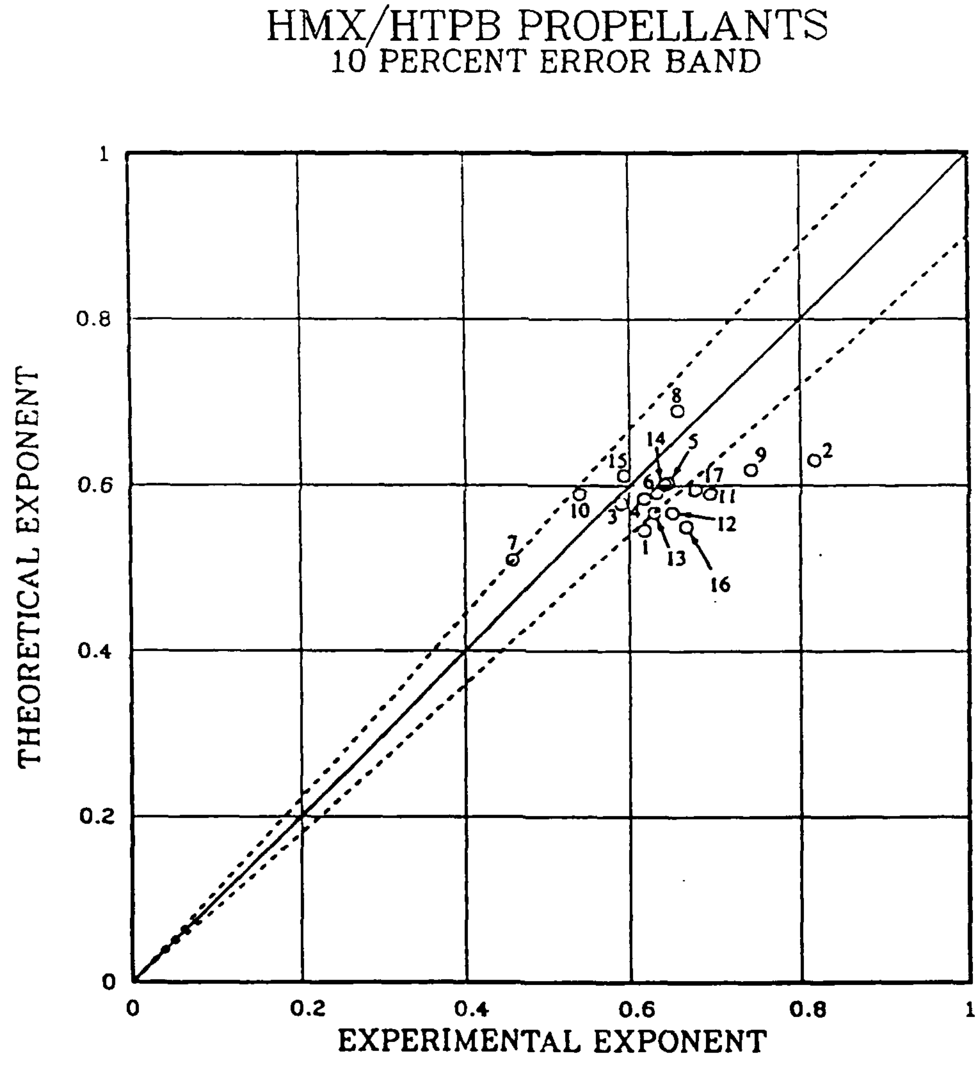

Figure 27
Theoretical Versus Experimental Exponent
for HMX/HTPB Propellants: Type I

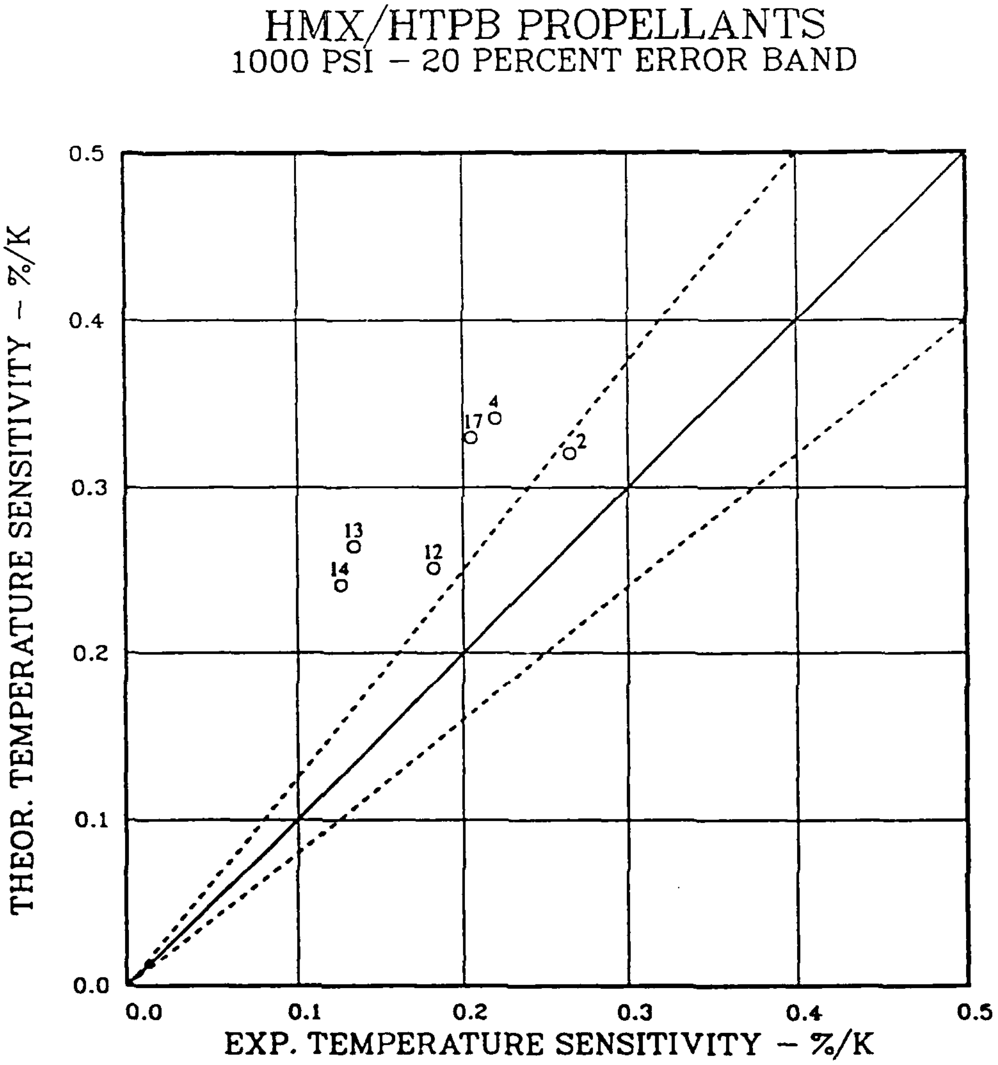

Figure 28
Theoretical Versus Experimental Temperature
Sensitivities for HMX/HTPB Propellants: Type I

4.2.2 AP Composite Propellants: Type II

The second class of propellants to be examined, Type II, contain only AP crystals dispersed in a HTPB binder medium. These propellants were also formulated by Hercules, Inc.[30] For the series of 21 propellants, the solids loading is constant at 87.37 percent and the particle size ranges from 0.7 to 450 microns.

Table 6 presents the formulation data for these AP/HTPB propellants. Table 7 presents the experimental data and the theoretical prediction for the burning rate at 500, 1000 and 2000 psi, the pressure exponent and an initial temperature of 298°K and the temperature sensitivity at 1000 psia. Figures 29, 30 and 31 plot the theoretical HYPEM values versus the experimental values for the burning rates at 1000 psi, the pressure exponents, and the temperature sensitivities, respectively, shown in Table 7. On each plot there is a number by each data point which corresponds to the propellant identification number in Table 6 and 7. As was previously seen, the burning rate and pressure exponent plots have 10 percent error bands while the temperature sensitivity plots have 20 percent error bands. The solid line represents perfect agreement between experiment and model prediction.

Table 6
AP/HTPB Propellant Formulations - 12.63% HTPB: Type II

		%AP							
		400μ	200μ	90μ	50μ	20μ	6μ	2μ	.7μ
	$\bar{D}$	448μ	195μ	71.2μ	44.2μ	22.6μ	5.23μ	1.89μ	0.69μ
No	σ	1.22	1.63	1.37	1.45	1.68	1.88	1.31	2.72
1		-	-	31.58	-	13.68	-	-	42.11
2		-	-	-	-	55.79	-	-	31.58
3		-	31.58	-	-	24.21	-	-	31.5
4		42.11	-	-	-	13.68	-	-	31.5
5		-	-	31.58	-	13.68	31.58	10.53	-
6		-	-	-	31.58	24.21	-	31.58	-
7		-	31.58	-	-	24.21	-	31.58	-
8		42.11	-	-	-	13.68	-	31.58	-
9		-	-	42.11	-	13.68	31.58	-	-
10		-	31.58	-	-	24.21	31.58	-	-
11		42.11	-	-	-	13.68	31.58	-	-
12		-	31.58	-	31.58	24.21	-	-	-
13		-	-	31.58	-	55.79	-	-	-
14		-	-	42.11	-	45.26	-	-	-
15		-	31.58	-	-	55.79	-	-	-
16		42.11	-	-	-	45.26	-	-	-
17		31.58	31.58	-	10.52	13.68	-	-	-
18		31.58	-	-	42.11	13.68	-	-	-
19		-	42.11	-	31.58	13.68	-	-	-
20		-	31.58	-	42.11	13.68	-	-	-
21		42.11	-	-	31.58	13.68	-	-	-

As can be seen in Figures 29 and 30 the HYPEM model predicts the burning rates and exponents for the majority of these propellants within ±10 percent. Figure 31 indicates that the HYPEM model's burning rate temperature sensitivity prediction within ±20 percent.

Table 7
Predicted and Experimental Burning Rates, Exponents and Temperature Sensitivities for AP/HTPB Propellants: Type II

	Burning Rate - in/sec						Exponent		Temperature Sensitivity %/°K	
	500psia		1000psia		2000psia					
No	r_{ex}	r_{th}	r_{ex}	r_{th}	r_{ex}	r_{th}	n_{ex}	n_{th}	$\sigma_{p,ex}$	$\sigma_{p,th}$
1	0.603	0.718	1.160	1.238	2.210	2.089	0.937	0.771	--	--
2	0.881	0.774	1.450	1.252	2.290	2.027	0.689	0.695	--	--
3	0.632	0.627	1.170	1.041	1.910	1.714	0.798	0.725	0.26	0.21
4	0.471	0.535	0.870	0.908	1.700	1.530	0.926	0.758	--	--
5	0.737	0.721	1.160	1.168	1.740	1.770	0.620	0.648	0.20	0.21
6	0.680	0.704	1.100	1.150	1.770	1.832	0.690	0.689	--	--
7	0.631	0.624	1.090	1.025	1.820	1.644	0.764	0.699	--	--
8	0.500	0.531	0.901	0.893	1.600	1.461	0.839	0.730	--	--
9	0.676	0.618	1.030	0.967	1.590	1.387	0.617	0.583	0.23	0.21
10	0.637	0.601	0.978	0.933	1.490	1.342	0.613	0.580	0.26	0.20
11	0.449	0.508	0.706	0.799	1.170	1.158	0.691	0.594	--	--
12	0.407	0.439	0.561	0.601	0.761	0.797	0.451	0.430	--	--
13	0.601	0.554	0.834	0.767	1.160	1.035	0.474	0.451	0.20	0.23
14	0.521	0.522	0.718	0.723	0.955	0.968	0.437	0.446	--	--
15	0.536	0.505	0.785	0.688	1.120	0.923	0.532	0.435	0.17	0.23
16	0.368	0.412	0.539	0.555	0.856	0.739	0.609	0.422	0.32	0.25
17	0.240	0.303	0.330	0.401	0.436	0.508	0.431	0.371	0.22	0.25
18	0.375	0.384	0.524	0.526	0.708	0.695	0.458	0.428	--	--
19	0.332	0.390	0.469	0.531	0.630	0.692	0.462	0.414	--	--
20	0.393	0.417	0.536	0.573	0.732	0.755	0.365	0.428	--	--
21	0.304	0.346	0.445	0.467	0.652	0.613	0.550	0.412	0.25	0.29

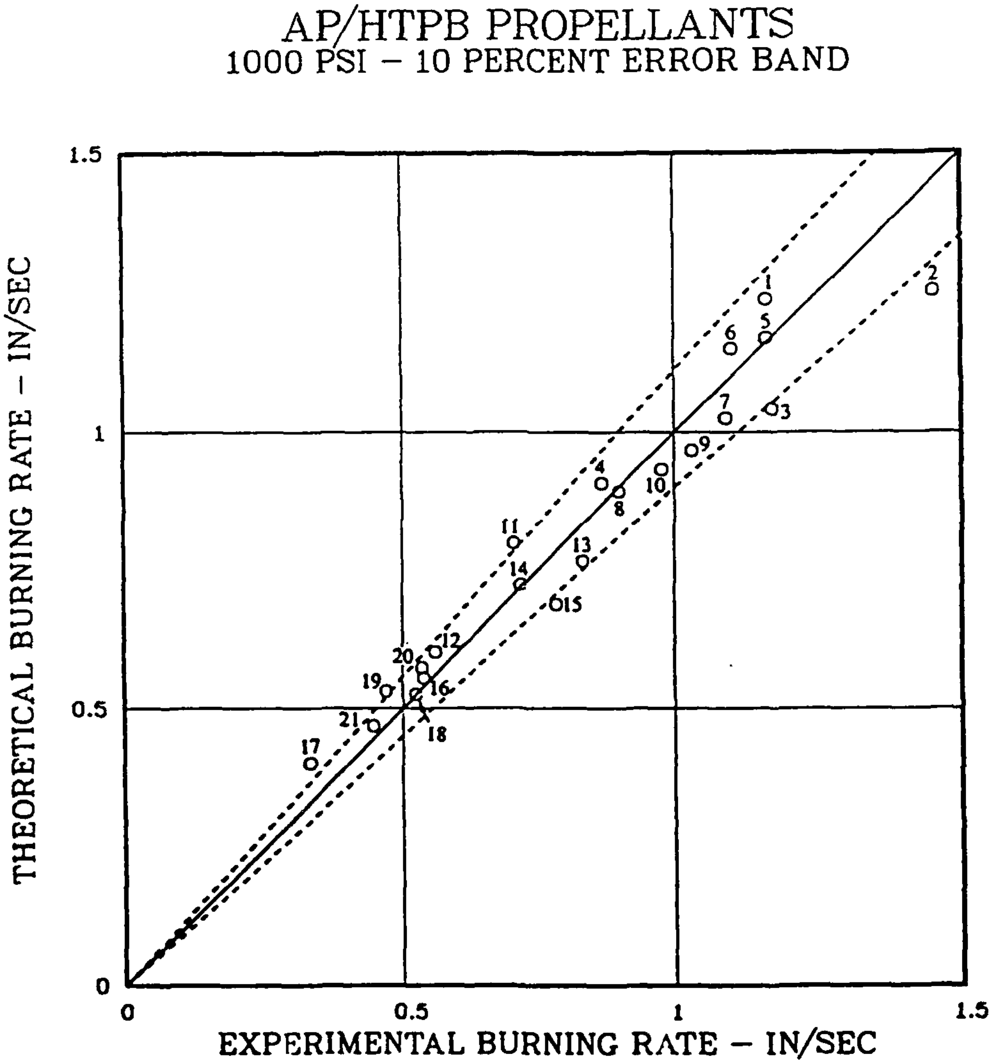

AP/HTPB PROPELLANTS
1000 PSI – 10 PERCENT ERROR BAND

Figure 29
Theoretical Versus Experimental Burning Rate
for AP/HTPB Propellants: Type II

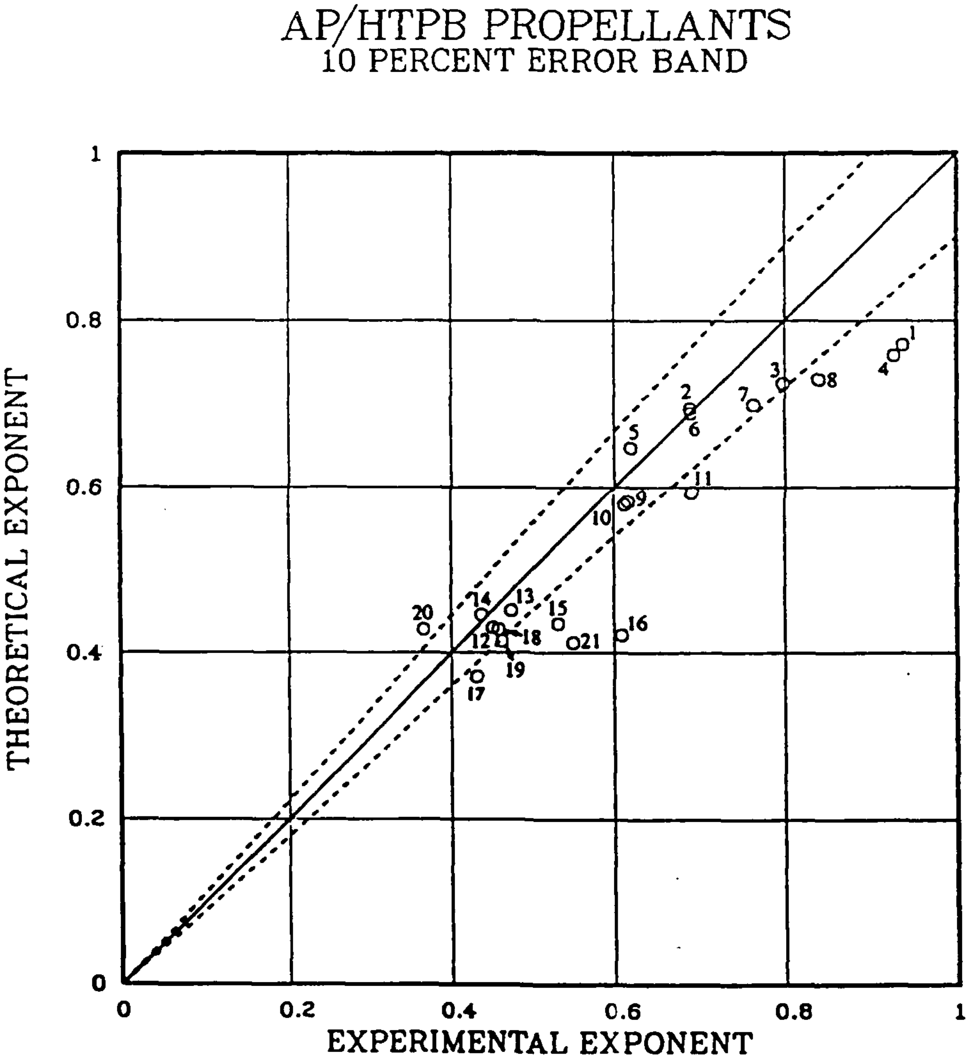

Figure 30
Theoretical Versus Experimental Exponent
for AP/HTPB Propellants: Type II

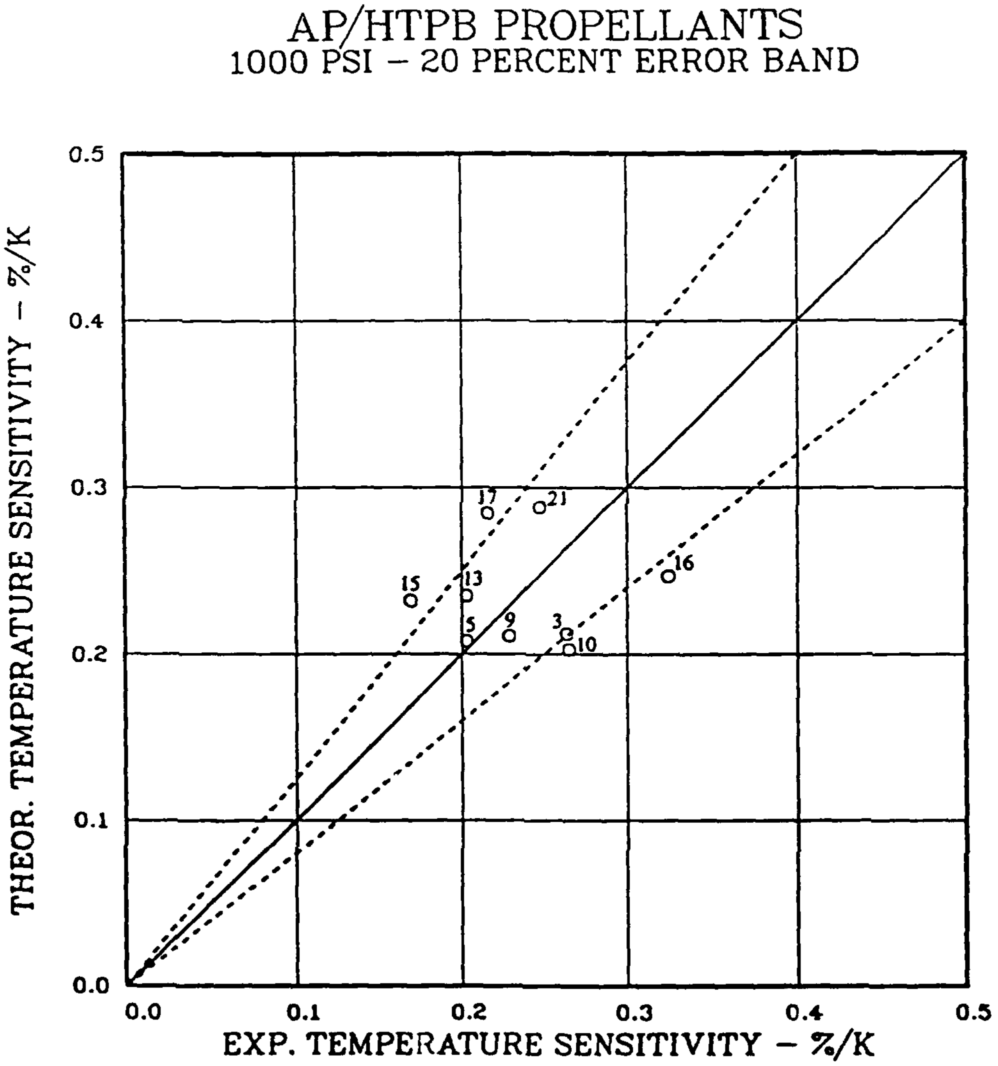

Figure 31
Theoretical Versus Experimental Temperature
Sensitivities for AP/HTPB Propellants: Type II

4.2.3 Composite Propellants Containing More HMX than AP: Type III

The third class of propellants to be examined, Type III, contain both HMX and AP crystals dispersed in a HTPB binder medium. In these propellants the percentage of HMX is between 60 and 78 percent and the percentage of AP is between 5 and 10 percent. These propellants were formulated by Hercules, Inc.[118] For the series of 13 propellants, the solids loading (amount of oxidizer) ranges from 70 percent to 78 percent. The particle size ranges from 4 to 200 microns for the HMX crystals and between 5 and 200 microns for the AP crystals.

Table 8 presents the formulation data for these HMX/AP/HTPB propellants. Table 9 presents the experimental data and the theoretical prediction for the burning rate at 400, 1000 and 1600 psia, the pressure exponent at an initial temperature of 298°K and the temperature sensitivity at 1000 psia. Figures 32, 33 and 34 plot the theoretical HYPEM values versus the experimental values for the burning rates at 1000 psi, the pressure exponents, and the temperature sensitivities, respectively, shown in Table 9. As shown previously, the data points numbered and error bands are included.

As can be seen in Figure 32, the HYPEM model predicts the burning rates for the majority of these propellants within ±10 percent. Figure 33 indicates that the model predicts the pressure exponent between +20 and -10 percent. Figure 34 indicates that the HYPEM model's burning rate temperature sensitivity prediction consistently over estimates the experimental prediction by more than 20 percent.

Table 8
HMX/AP/HTPB Propellant Formulations Containing More HMX than AP: Type III

		%HMX			%AP		
		200μ	58μ	4μ	200μ*	50μ	5μ
	$\bar{D}$	147μ	42.4μ	4.46μ	200μ	42.2μ	4.49μ
No	%HTPB σ	1.86	2.68	1.99	1.60	1.96	1.65
01	22.00	-	78.00	-	-	-	-
02	22.00	-	73.00	-	-	5.00	-
03	22.00	-	68.00	-	-	10.00	-
04	22.00	-	68.00	-	-	-	10.00
05	22.00	-	-	68.00		10.00	-
06	22.00	-	34.00	34.00	-	-	10.00
07	22.00	-	-	68.00	-	-	10.00
08	22.00	68.00	-	-	10.00	-	-
09	30.00	-	65.00	-	-	5.00	-
10	30.00	-	60.00	-	-	10.00	-
11	30.00	-	-	60.00	-	-	10.00
12	30.00	-	-	65.00	-	-	5.00
13	30.00	-	60.00	-	-	-	10.00

* **Data was not available to determine the distribution data of the 200μ particle size HMX crystals. The value shown is assumed.**

Table 9
Predicted and Experimental Burning Rates, Exponents and Temperature Sensitivities for HMX/AP/HTPB Propellants Containing More HMX than AP: Type III

	Burning Rate - in/sec						Exponent		Temperature Sensitivity %/°K	
	400psia		1000psia		1600psia					
No	r_{ex}	r_{th}	r_{ex}	r_{th}	r_{ex}	r_{th}	n_{ex}	n_{th}	$\sigma_{p,ex}$	$\sigma_{p,th}$
1	0.061	0.074	0.112	0.116	0.117	0.144	0.496	0.486	--	--
2	0.065	0.073	0.099	0.116	0.128	0.146	0.485	0.497	0.18	0.34
3	0.070	0.085	0.110	0.137	0.141	0.172	0.504	0.510	--	--
4	0.093	0.088	0.142	0.155	0.184	0.211	0.488	0.629	0.20	0.41
5	0.099	0.121	0.167	0.203	0.214	0.266	0.558	0.565	--	--
6	0.114	0.106	0.183	0.188	0.232	0.258	0.513	0.638	0.14	0.37
7	0.137	0.124	0.223	0.221	0.276	0.305	0.509	0.644	0.34	0.35
8	0.052	0.055	0.084	0.090	0.109	0.117	0.532	0.549	--	--
9	0.043	0.050	0.070	0.081	0.092	0.106	0.546	0.538	--	--
10	0.049	0.059	0.077	0.097	0.098	0.126	0.499	0.547	0.25	0.41
11	0.117	0.093	0.176	0.163	0.216	0.229	0.443	0.641	0.37	0.44
12	0.090	0.087	0.137	0.144	0.174	0.199	0.473	0.593	0.31	0.39
13	0.075	0.062	0.113	0.114	0.134	0.161	0.423	0.689	0.22	0.48

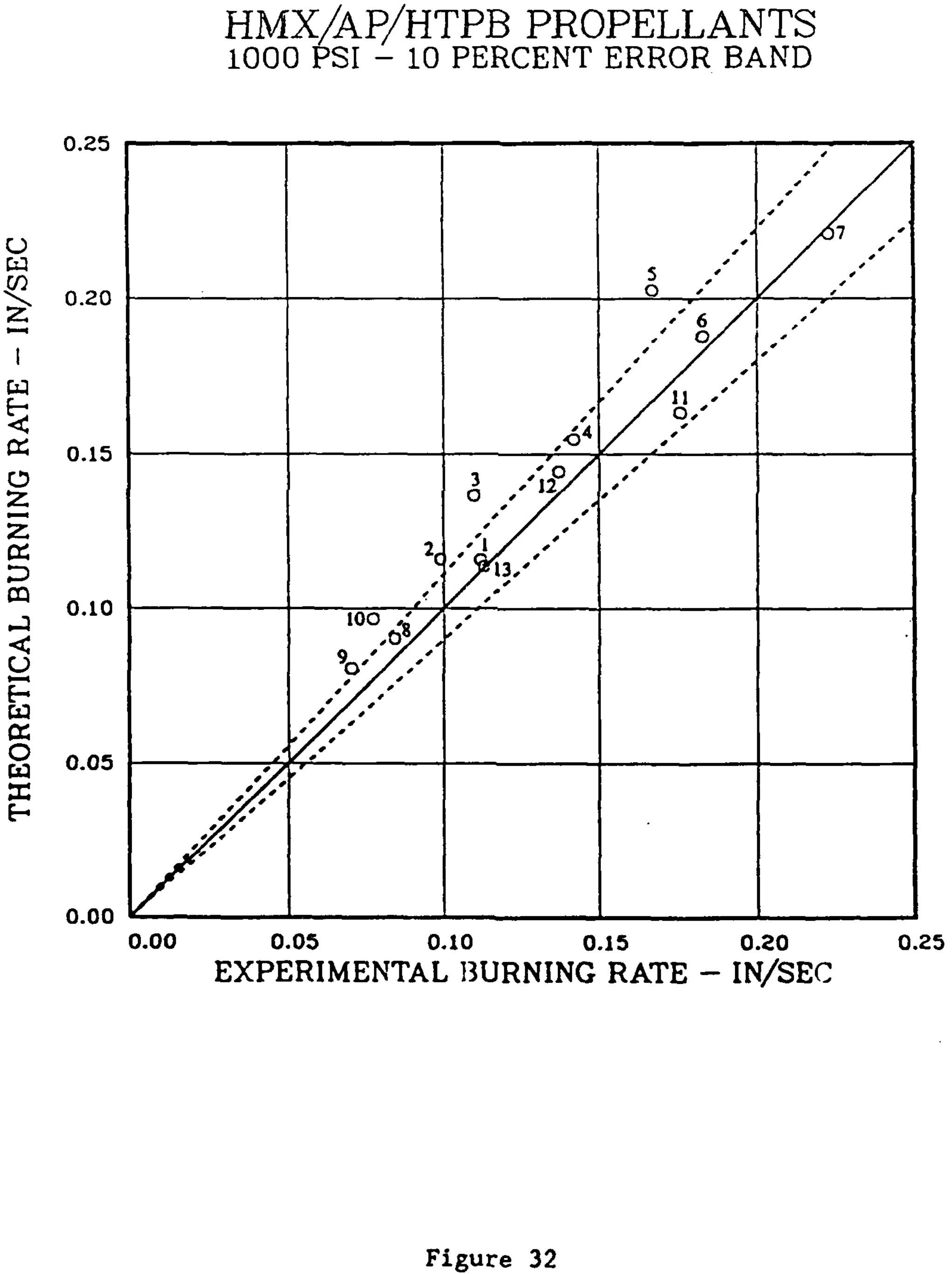

Figure 32
Theoretical Versus Experimental Burning Rate for HMX/AP/HTPB Propellants Containing More HMX than AP: Type III

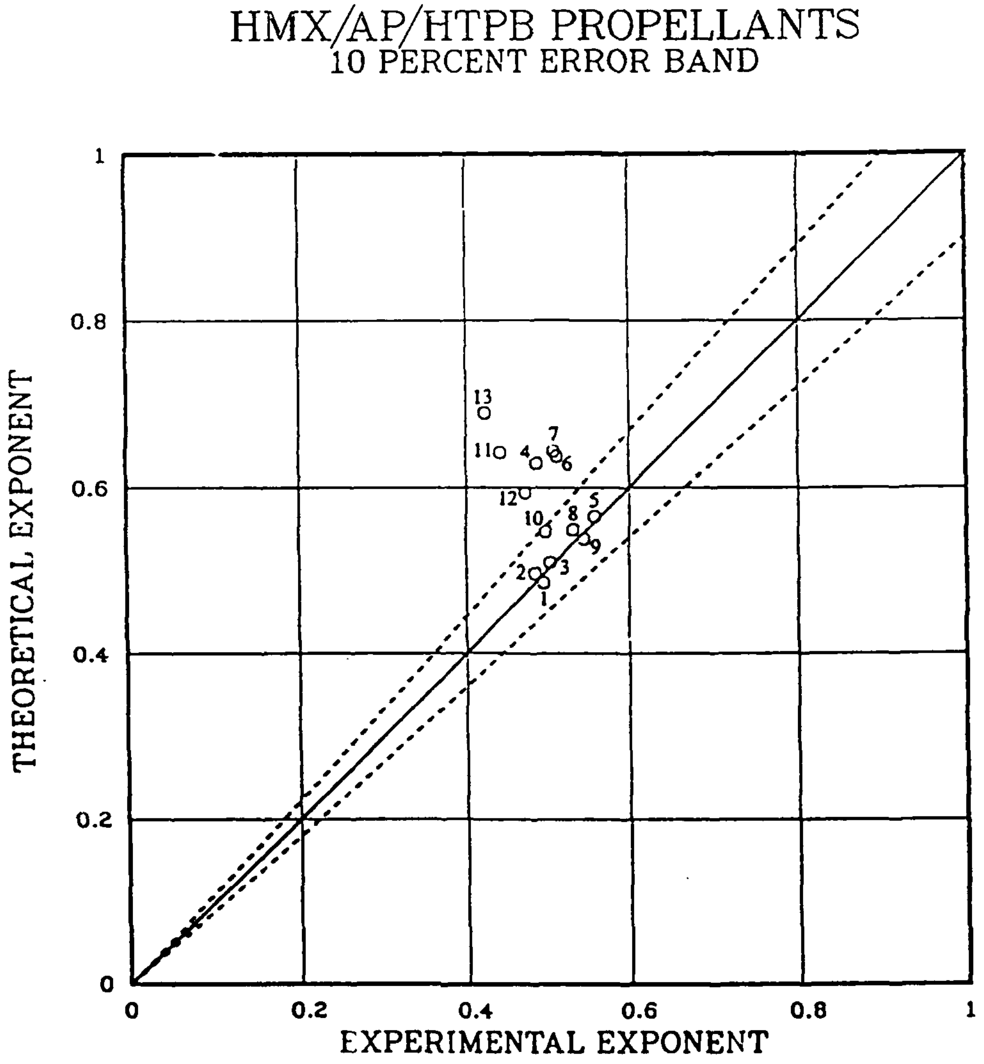

Figure 33
Theoretical Versus Experimental Exponent for HMX/AP/HTPB Propellants Containing More HMX than AP: Type III

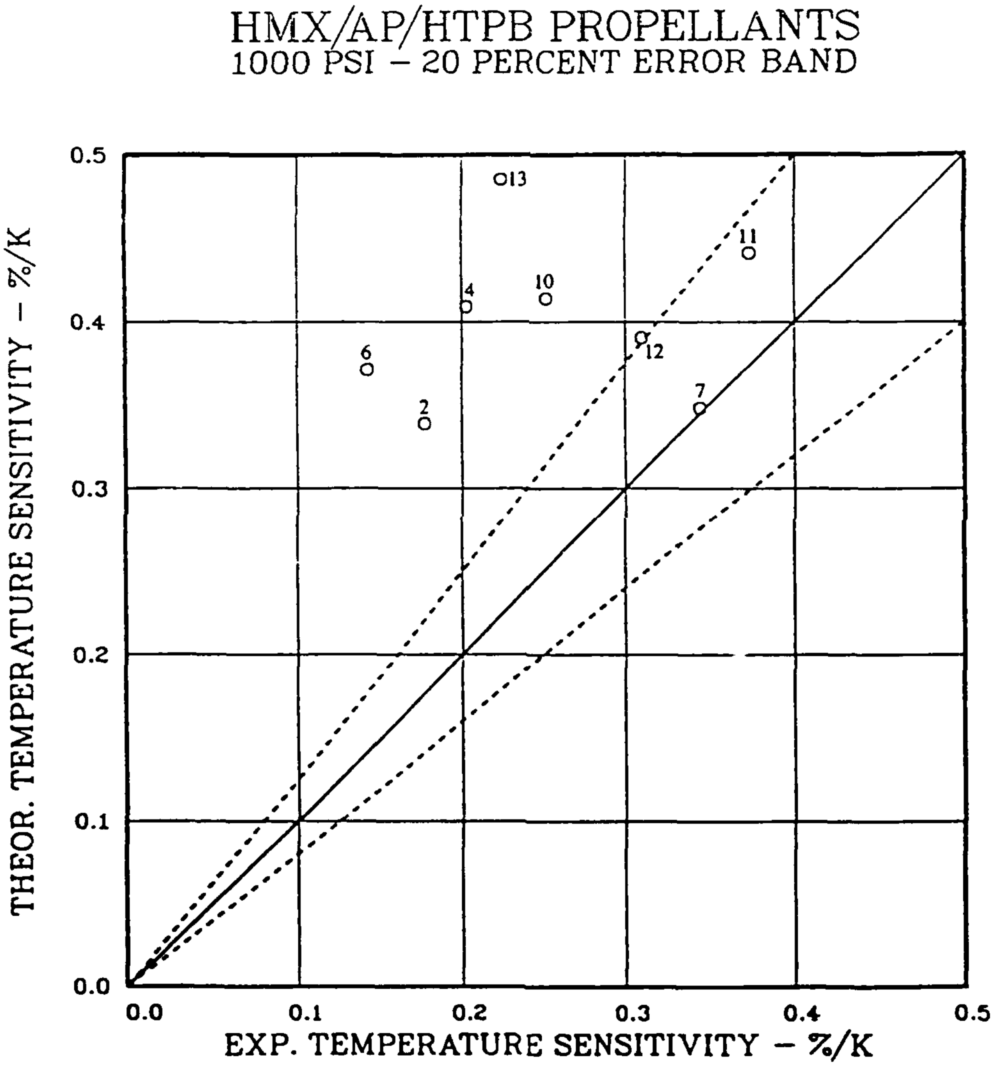

Figure 34
Theoretical Versus Experimental Temperature Sensitivities for HMX/AP/HTPB Propellants Containing More HMX than AP: Type III

4.2.4 Composite Propellants Containing More AP than HMX: Type IV

The fourth class of propellants, Type IV, to be examined contain both AP and HMX crystals dispersed in a HTPB binder medium. In these propellants the percentage of AP is between 72.37 and 77.37 percent and the percentage of HMX is between 10 and 15 percent. These propellants were formulated by Hercules, Inc.[29,30] For the series of 10 propellants, the solids loading was constant at 87.37 percent. The particle size ranges from 2 to 400 microns for the AP crystals and between 4 and 20 microns for the HMX crystals.

Table 10 presents the formulation data for these AP/HMX/HTPB propellants. Table 11 presents the experimental data and the theoretical prediction for the burning rate at 500, 1000 and 3000 psia, the pressure exponent at an initial temperature of 298°K and the temperature sensitivity at 1000 psia. Figures 35, 36 and 37 plot the theoretical HYPEM values versus the experimental values for the burning rates at 1000 psi, the pressure exponents, and the temperature sensitivities, respectively, shown in Table 11. As shown previously, the data points numbered and error bands are included.

As can be seen in Figure 35 the HYPEM model predicts the burning rates for the majority of these propellants within +15 to -10 percent. Figure 36 indicates that the model over predicts the pressure exponent by 20 percent. Figure 37 indicates that the HYPEM model's burning rate temperature sensitivity prediction is within ±20 percent.

Table 10
AP/HMX/HTPB Propellant Formulations Containing More
AP than HMX - 12.63% HTPB: Type IV

		%HMX		%AP			
		20μ	4μ	400μ	50μ	20μ	2μ
	$\bar{D}$	22.3μ	4.55μ	436μ	48.6μ	19.3μ	1.96μ
No	σ	2.89	2.02	1.16	1.43	1.80	1.38
1		-	10.00	42.11	-	13.68	21.58
2		-	10.00	42.11	21.58	13.68	-
3		10.00	-	42.11	-	13.68	-
4		10.00	-	42.11	21.58	13.68	-
5		10.00	-	-	42.11	13.68	21.58
6		-	15.00	42.11	-	13.68	16.58
7		-	15.00	42.11	16.58	13.68	-
8		15.00	-	42.11	-	13.68	16.58
9		15.00	-	42.11	16.58	13.68	-
10		-	15.00	-	42.11	13.68	16.58

Table 11
Predicted and Experimental Burning Rates, Exponents and Temperature Sensitivities for AP/HMX/HTPB Propellants Containing More AP than HMX: Type IV

	Burning Rate - in/sec						Exponent		Temperature Sensitivity %/°K	
	500psia		1000psia		3000psia					
No	r_{ex}	r_{th}	r_{ex}	r_{th}	r_{ex}	r_{th}	n_{ex}	n_{th}	$\sigma_{p,ex}$	$\sigma_{p,th}$
1	0.483	0.405	0.630	0.657	1.120	1.316	0.417	0.656	--	--
2	0.302	0.296	0.374	0.408	0.627	0.619	0.368	0.409	0.23	0.26
3	0.397	0.410	0.523	0.666	1.210	1.321	0.536	0.651	--	--
4	0.271	0.301	0.348	0.417	0.599	0.624	0.403	0.403	0.26	0.27
5	0.558	0.547	0.759	0.878	1.340	1.659	0.528	0.616	0.20	0.24
6	0.544	0.382	0.704	0.605	1.260	1.173	0.445	0.624	--	--
7	0.291	0.303	0.359	0.423	0.595	0.658	0.343	0.430	0.25	0.25
8	0.342	0.377	0.450	0.594	0.943	1.144	0.472	0.617	0.33	0.23
9	0.259	0.298	0.329	0.413	0.582	0.629	0.395	0.414	0.22	0.26
10	0.609	0.516	0.775	0.814	0.963*	1.238*	0.332	0.631	0.15	0.24

* The Pressure is 2000 psia for these burning rates

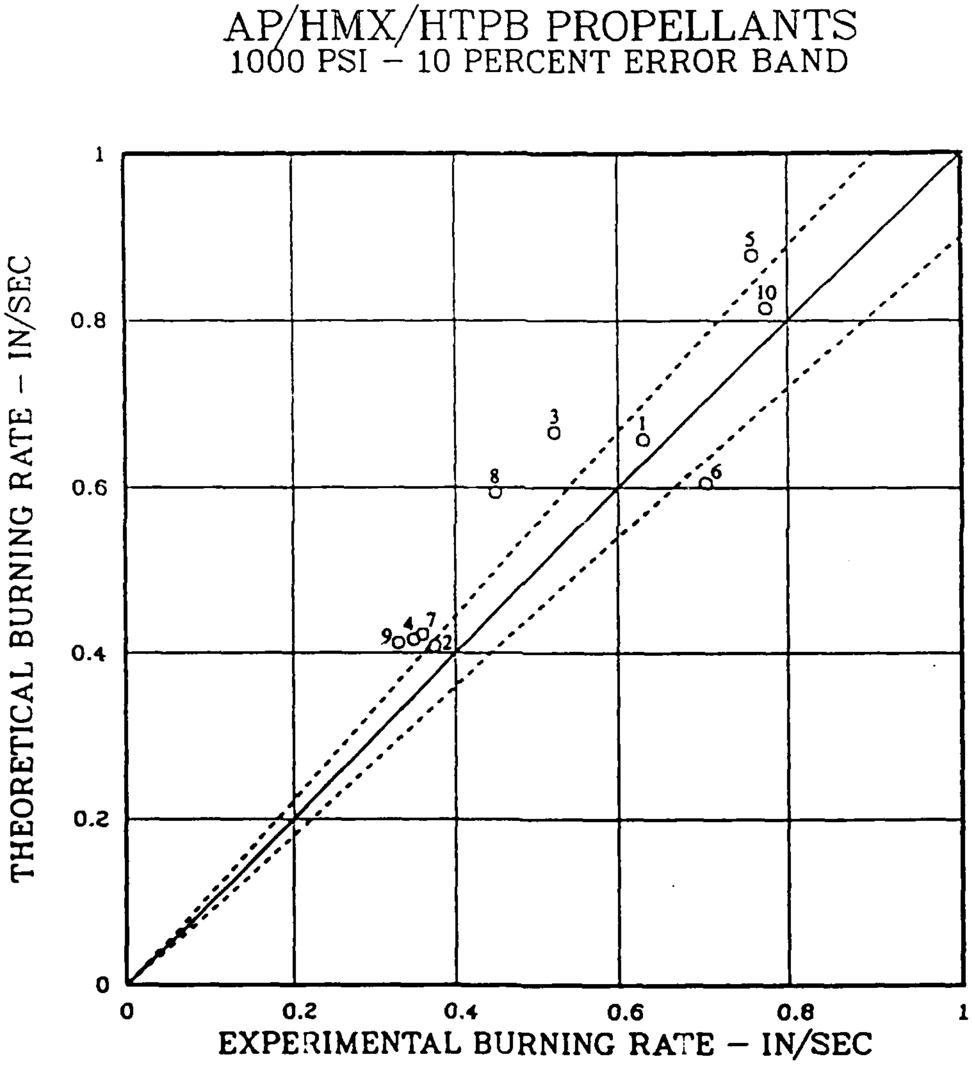

Figure 35
Theoretical Versus Experimental Burning Rate for AP/HMX/HTPB Propellants Containing More AP than HMX: Type IV

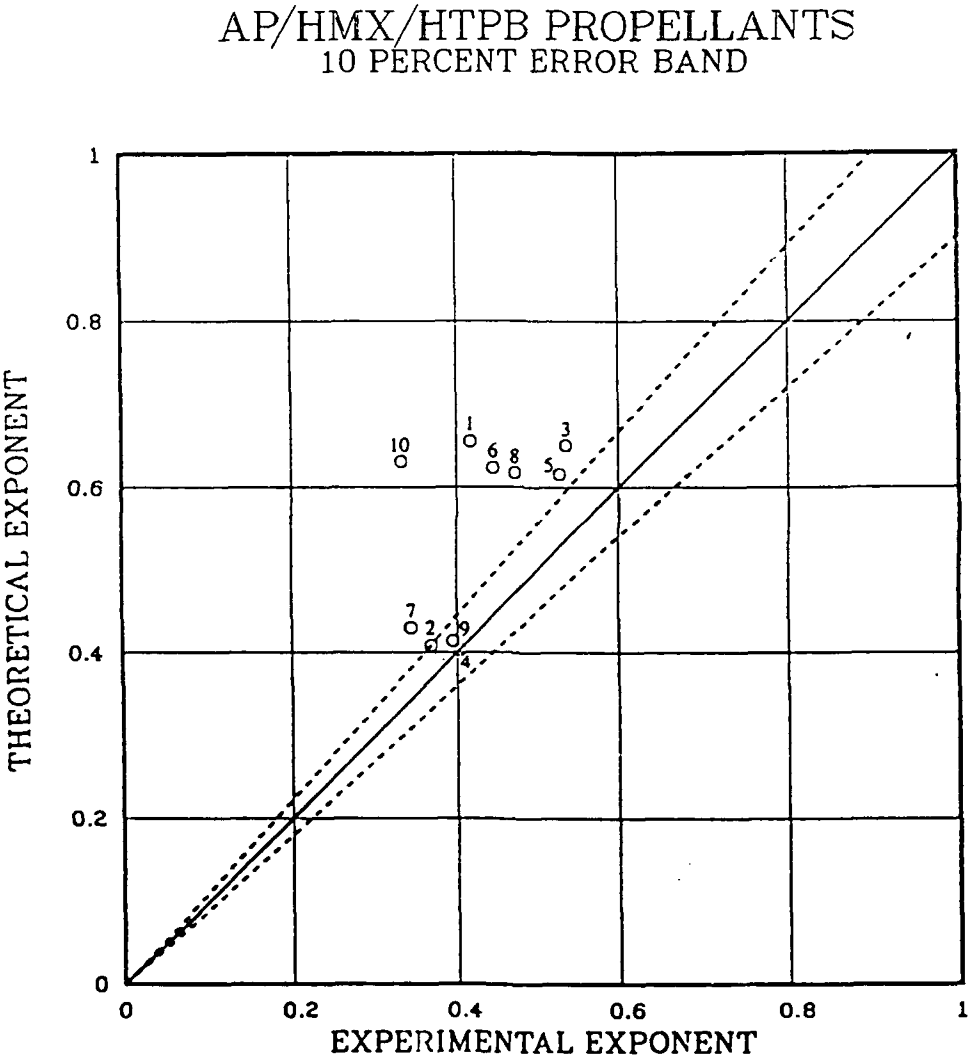

Figure 36
Theoretical Versus Experimental Exponent for AP/HMX/HTPB Propellants Containing More AP than HMX: Type IV

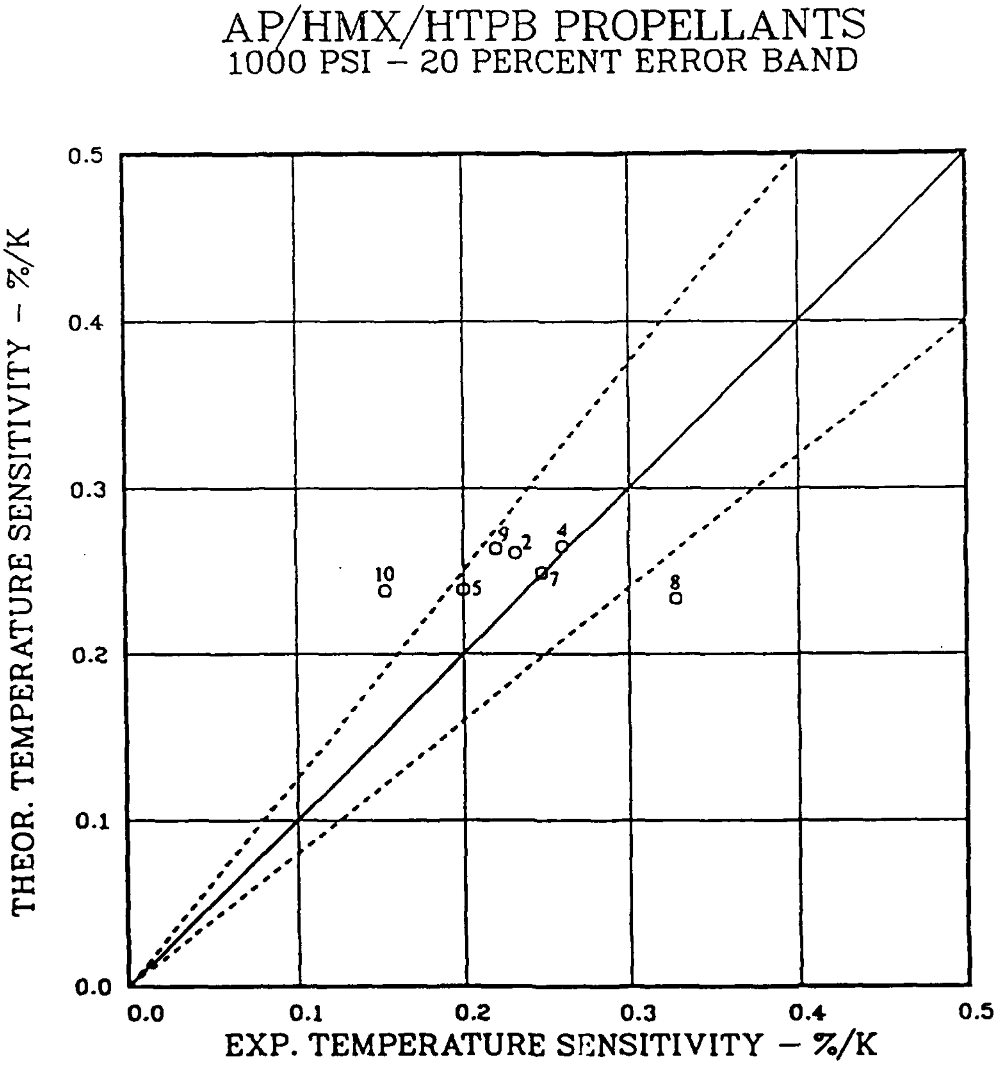

Figure 37
Theoretical Versus Experimental Temperature Sensitivities for HMX/AP/HTPB Propellants Containing More AP than HMX: Type IV

4.3 Summary of Combustion Model Results

The HYPEM composite combustion model computed the burning rate and pressure exponent for 61 different composite propellants. In addition, model computed burning rate temperature sensitivity for 30 individual propellants. These propellants contain HMX and/or AP oxidizer crystals of many different particle sizes and combinations in a HTPB inert binder.

Several important observations can be made about the behavior of the model when examining Figures 26 through 37. This can be accomplished by comparing the experimental data with the HYPEM model's prediction and examining the propellant formulations presented in Tables 4, 6, 8 and 10. The following observations are categorized by propellant type.

1. Type I propellants which contain only HMX particles (Tables 4 and 5, Figures 26, 27 and 28): Burning rate and pressure exponent prediction is quite good except for propellants containing only coarse or only fine HMX crystals. Some of the wide distribution propellant properties were also poorly predicted. Wide distribution propellants are those which contain very fine and very coarse particles. The predicted temperature sensitivity is consistently higher than the measured values for all propellants.

2. Type II propellants which contain only AP particles (Tables 6 and 7, Figures 29, 30 and 31): Burning rate, pressure exponent and temperature sensitivity prediction were all reasonably good. Some of the "wide distribution" propellants resulted in poor but acceptable model predictions that were usually better than 20 percent.

3. Type III propellants which contain more HMX crystals than AP crystals (Tables 8 and 9, Figures 32, 33 and 34): Burning rate prediction was acceptable but the pressure exponent prediction was higher than the experimental values for propellants with fine AP. In addition, the greater the difference between the HMX and fine AP particle size the greater the discrepancy. As with Type I propellants containing only HMX particles, the temperature sensitivity of Type III propellants is over predicted by the model.

4. Type IV propellants which contain more AP crystals than HMX crystals (Tables 10 and 11, Figures 35, 36 and 37): Burning rate prediction is usually within 20 percent and exhibits no noticeable trends. The pressure exponent is over predicted for those propellants with fine AP or "wide distributions" of AP. The HMX particle size does not appear to be a factor. Temperature sensitivity prediction is usually better than 20 percent.

In general the HYPEM model does a satisfactory job in predicting burning rates and pressure exponents. As with many other models of this type, it does have a difficult time with propellants containing a wide distribution of HMX and/or AP particle sizes. In addition, the HYPEM model over predicts the burning rate temperature sensitivity of propellants that contain all or mostly HMX.

The HYPEM model's difficulty in handling "wide distribution" propellants is due to the fundamental assumption that a propellant can be broken down into separate, monodisperse pseudo propellants. A consequence of this assumption is that different particle size pseudo propellants burn independently of each other. Unaccounted for interdependencies between large and small particles is one reason the HYPEM model poorly predicts combustion characteristics of "wide distribution" propellants. Possible interdependencies include flame, heat transfer, and mass interactions. Some of these effects have been minimized and the model's performance improved by the introduction of the mass interaction parameter and flame temperature corrections discussed previously in Section 3.1.6.1 and 3.1.6.2.

CHAPTER V

PARAMETRIC STUDIES

It has been shown that the HYPEM composite combustion model predicts the burning characteristics of a wide range of propellants containing HMX and/or AP crystals. The model will now be used to predict the effects of particle size, chamber pressure, oxidizer solids loading and propellant formulation changes on composite propellant burning characteristics. The HYPEM model's burning rate, pressure exponent, surface temperature and temperature sensitivity prediction is useful tailoring a propellant for a specific application. In addition, the systematic variation of propellant parameters provides insight to the controlling mechanisms of propellant combustion. Finally, these studies will address the limiting conditions of the combustion model.

5.1 Controlling Mechanisms

Understanding the controlling mechanisms in a combustion model is important in order to know the limitations of the model. Figure 38 plots the percent heat feedback of the HMX monopropellant flame and the primary flame to the propellant surface versus HMX particle size. The heat transfer from the primary flame is divided into that portion which acts on the HMX crystal (dashed line) and that portion which acts on the binder (dotted line). For all particle sizes the primary flame energy going to the binder is dominant. This is due to the large amount of energy required to heat up the binder because of its large surface decomposition energy, 500 cal/g. A large percentage of the binder acts as an ablative material that does not react with the HMX but does act as a very good heat sink. For small HMX crystals the HMX combustion is controlled purely by the primary flame. As the particle size is increased the HMX monopropellant flame becomes more dominant (solid line), eventually dominating the HMX crystal combustion.

A second way of examining the controlling mechanisms in the HMX portion of the HYPEM model is to examine the relative contribution of the four terms in the denominator of the time averaged burning rate expression for the HMX pseudo propellants. The equation is written below:

$$r = \frac{(D' + 2\Delta)}{\left[\dfrac{D'}{r_X} + t_{ign} + fr_b\dfrac{2\Delta}{r_b} + (1-fr_b)t_b\right]} \qquad (166)$$

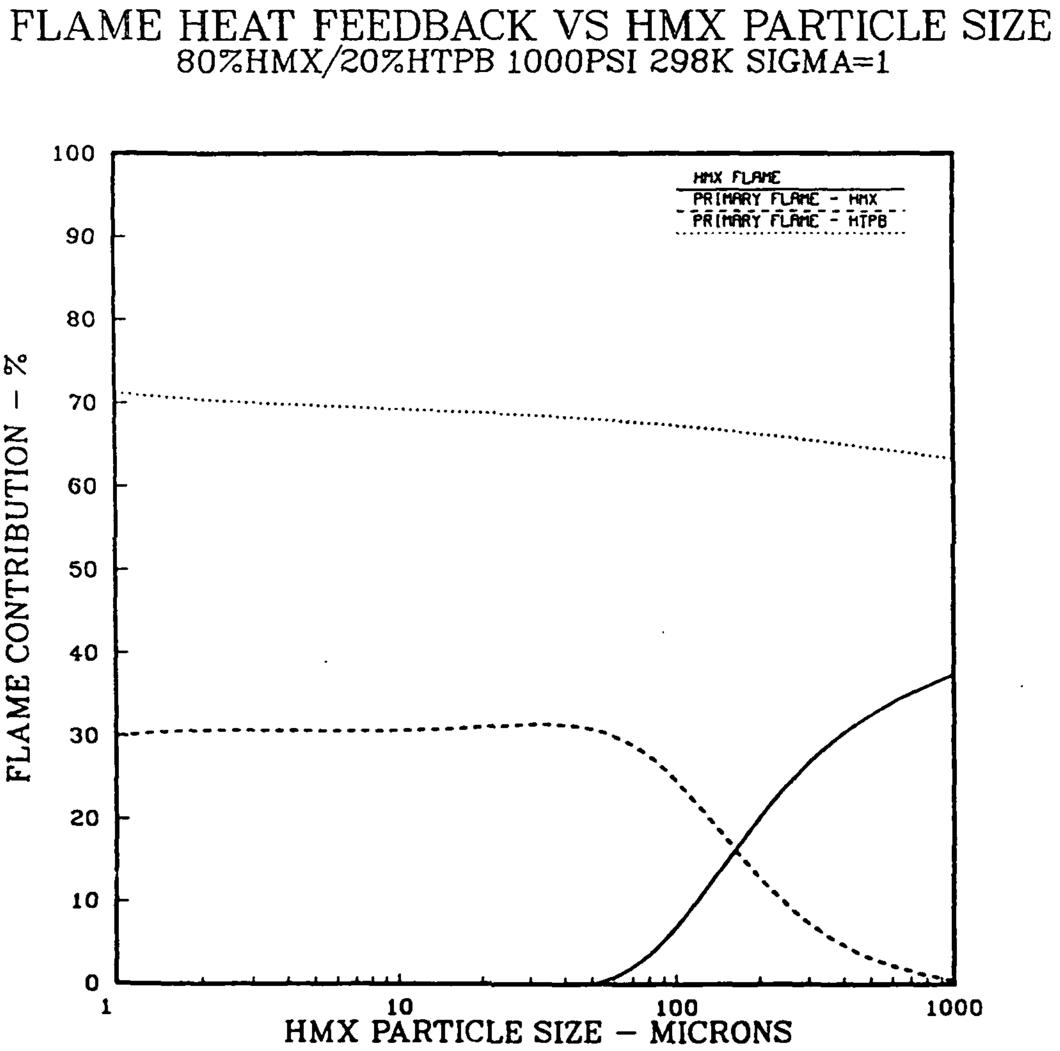

Figure 38
Flame Heat Feedback to the Propellant Surface Versus Oxidizer Particle Size for HMX Propellants

In Equation (166) D′ is the statistical intersection diameter of the HMX crystal and Δ is the distance from the HMX crystal edge to the edge of the assumed binder annulus. The terms in the denominator represent the oxidizer burning rate, r_X, oxidizer ignition delay time, t_{ign}, binder burn through time for a given HMX crystal, r_b, and the binder delay time, t_b. f_{rb} is the fraction of binder that reacts with the HMX.

The contributions in percent, of the four physical mechanisms that control the burning rate are illustrated in Figure 39. The contribution of each of the four mechanisms has been calculated on a percentage basis and plotted versus the HMX particle diameter. The HMX crystal burning rate term (solid line) is the greatest for fine particles but the other mechanisms contribute significantly. At 10 microns, the ignition delay time (dashed line) becomes the largest contributor and then increases until it is completely dominant for 100 micron and larger particles. For the larger particle sizes, the oxidizer rate drops to less than 10 percent contribution. The binder rate (dotted line) and the binder burn through time (dash-dotted line) contributions remain roughly constant at 10 and 15 percent respectively.

Figure 40 plots the percent heat feedback of the AP monopropellant flame, the primary flame, and the final flame to the propellant surface versus AP particle size. This plot shows a different behavior from the similar plot, Figure 38, for the HMX pseudo propellants. From Figure 40, it is evident that the primary flame (dashed line) dominates the combustion for small AP particles. The primary flame is the reaction between the pyrolysis products of the binder surface decomposition and the AP surface decomposition products. As the particle size increases the AP monopropellant flame (solid line) gains in importance. At the same time the final flame (dotted line), between AP monopropellant flame products and binder pyrolysis products, contributes to the surface energy. As the AP particles become very large, the AP monopropellant flame dominates the surface energy feedback. The obvious difference between Figures 38 and 40 is the way the primary flame is treated. This difference arises from the fact that in the HMX portion of the HYPEM model, all the binder does not react with the HMX. The two plots are similar in that the oxidizer monopropellant flame importance increases as particle size is increased.

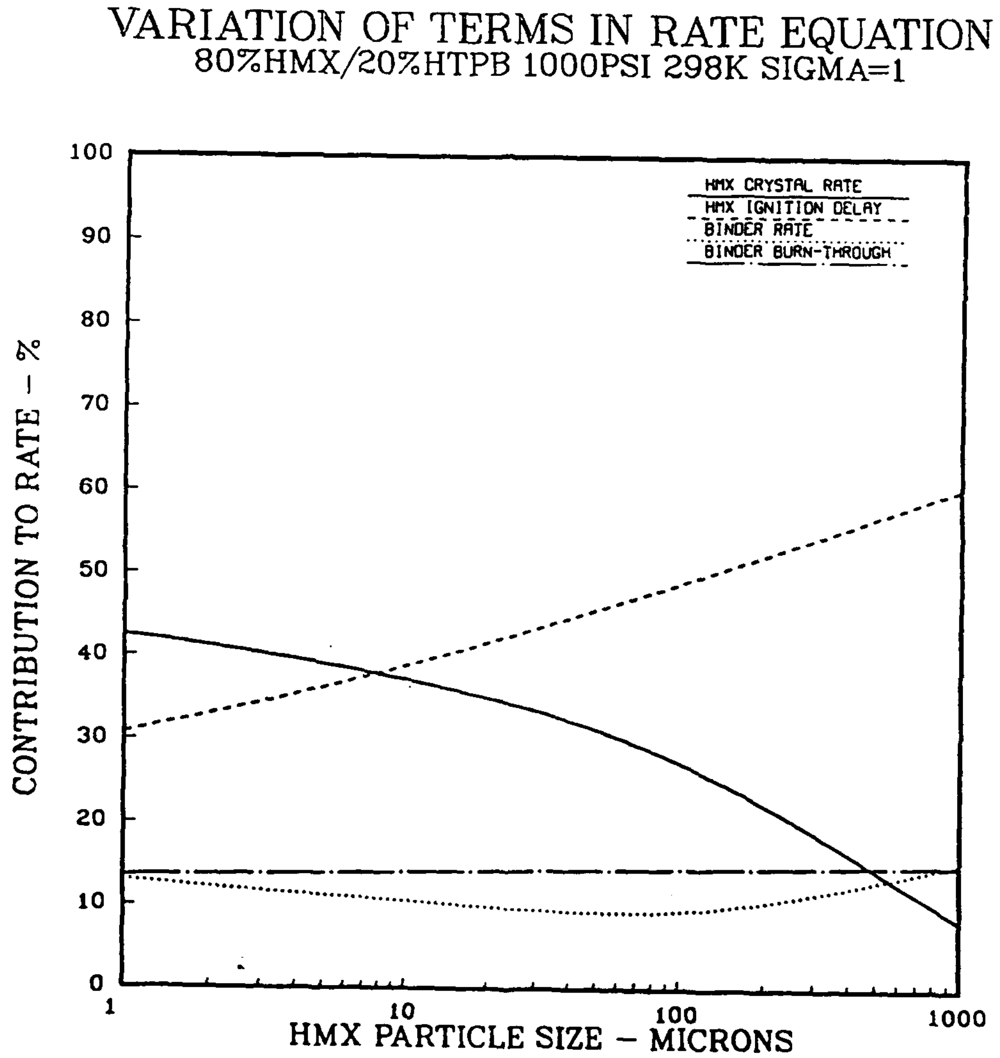

Figure 39
Percent Contribution of Terms in the Denominator of the HMX Rate Equation

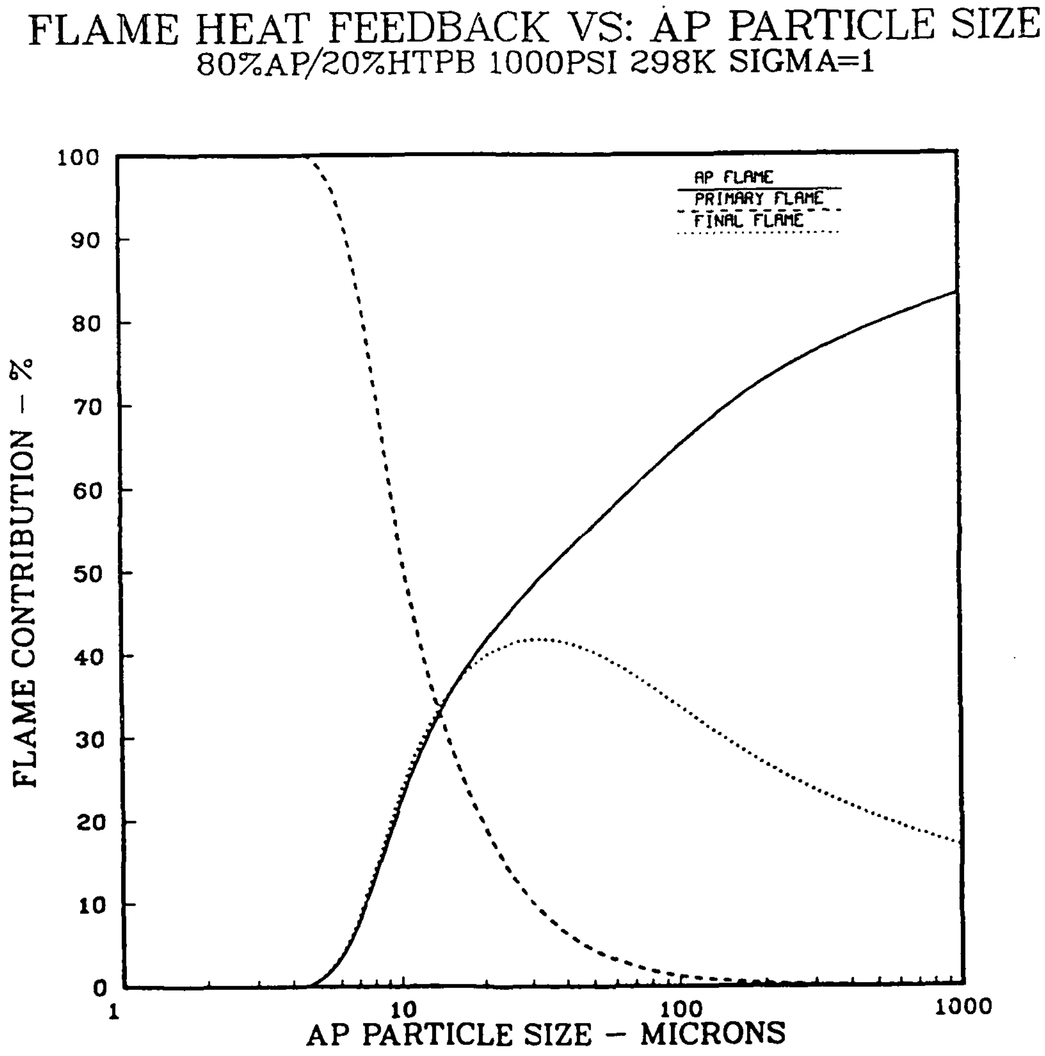

Figure 40
Flame Heat Feedback to the Propellant Surface Versus
Oxidizer Particle Size for AP Propellants

5.2 Particle Size

One of the primary factors that a propellant formulator can use to tailor a propellant's performance is the size of the oxidizer particles in the propellant. The following four graphs plot the burning rate, pressure exponent, propellant surface temperature and temperature sensitivity versus particle size for both HMX and AP/HTPB propellants. The solid line in each of these curves represents propellants that are 88 percent HMX and 12 percent HTPB. The dashed line represents propellants that are 88 percent AP and 12 percent HTPB. For these figures, and the ones that follow, the mode width parameter, σ_{OX}, for each propellant evaluated to create the curves was 2.0.

5.2.1 Burning Rate

Figure 41 plots the burning rate versus particle size. In Figure 41 the chamber pressure is 1000 psia and the propellant's initial temperature is 298°K. Figure 41 shows that the burning rate for HMX/HTPB propellants is not a strong function of particle size except for small HMX particles. Similar results have been shown experimentally.[30] Referring back to Figure 38 for small HMX crystals, the primary flame dominates the HMX combustion. For these smaller particle sizes the relatively cool primary flame between HMX and HTPB forces a relatively slow burning rate. Referring back to Figure 39 for large HMX crystals, the HMX crystal ignition delay time dominates the combustion and also forces a slow burning rate.

Figure 41 shows the characteristic "S" shaped burning rate curve that is experimentally observed for AP/HTPB propellants.[30] Referring back to Figure 40 for small AP crystals, the primary flame dominates the AP combustion. For these smaller particle sizes the very hot, close to the surface primary flame between AP and HTPB forces a relatively fast burning rate. Referring back to Figure 40 for large AP crystals, the AP monopropellant dominates the combustion and forces a slower burning rate. As is evident in Figure 41, a wide variation in burning rates can be achieved by varying the AP particle size.

5.2.2 Pressure Exponent

Figure 42 plots the pressure exponent versus particle size. The pressure exponent was determined by evaluating the burning rate at 500, 1000 and 2000 psi by using a least squares fit of the rate equation:

$$r = cP^n \tag{18}$$

where n is the pressure exponent. Figure 42 shows a gradual decrease in pressure exponent from 0.6 to 0.5 as HMX particle size is increased. The value of 0.6 for small HMX crystals is due the reaction order, 1.15, of the kinetically controlled primary flame (see Figure 38). The pressure exponent is approximately 1/2 the value of the reaction order for kinetically controlled flames. The decrease in pressure exponent as particle size increases is due to increased diffusional effects. The slight increase in exponent for very large HMX crystals is due to HMX monopropellant kinetic flame effects. This flame has a reaction order of 1.39. The reason the

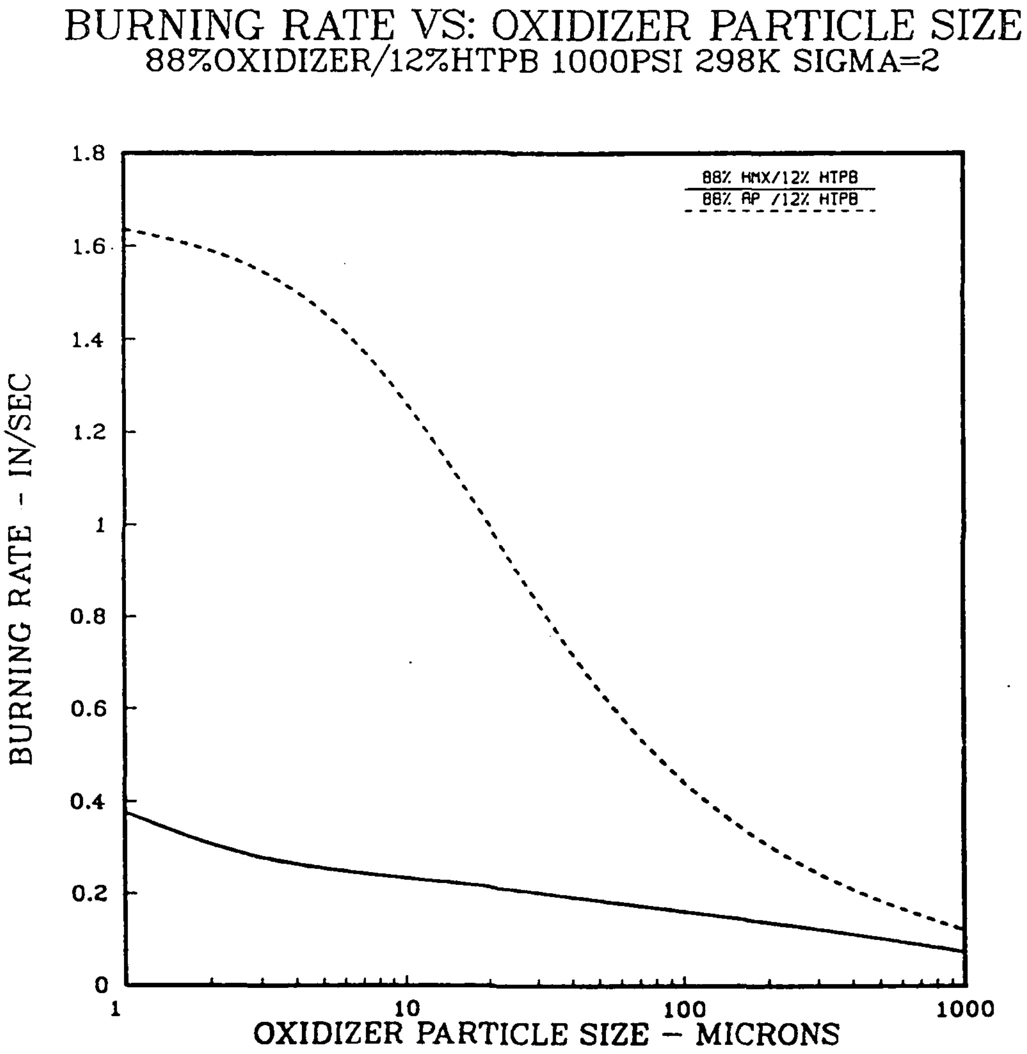

Figure 41
Burning Rate Versus Oxidizer Particle Size for both HMX/HTPB and AP/HTPB Propellants

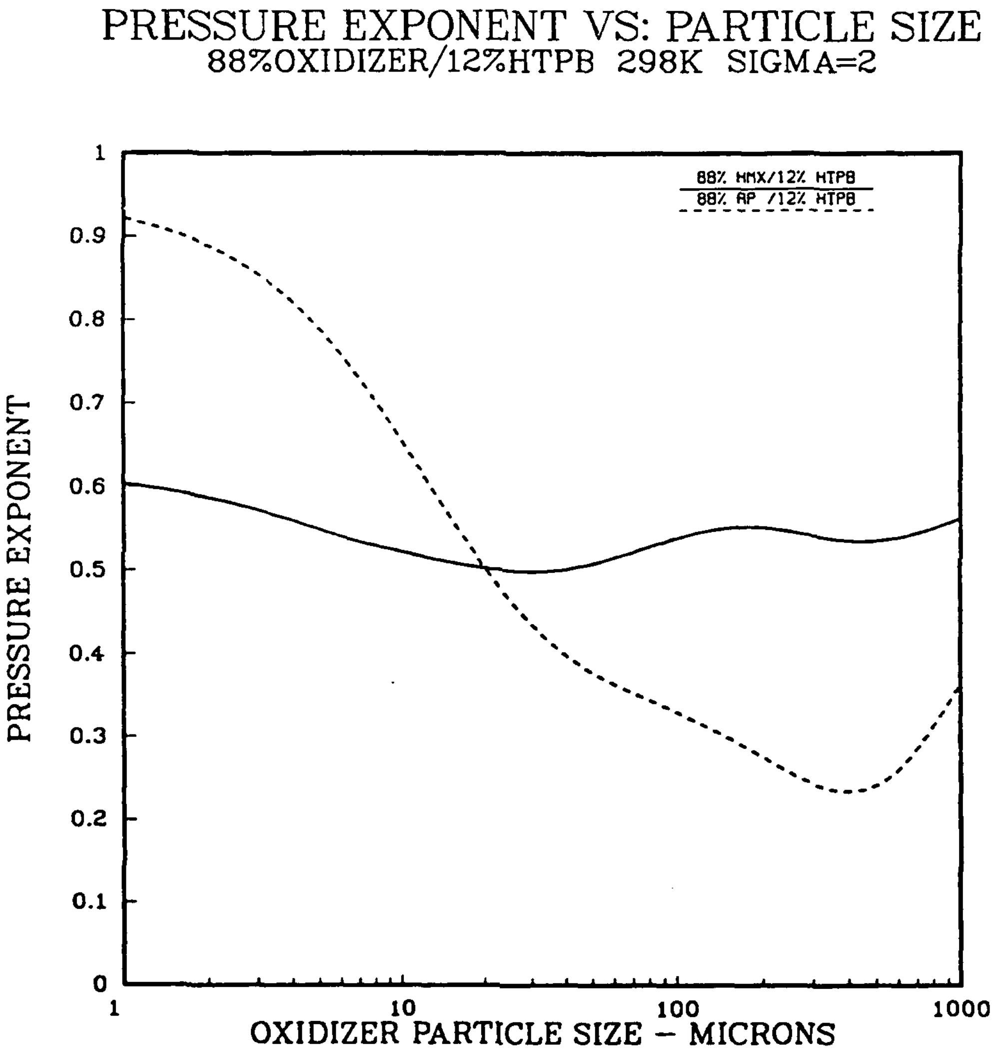

Figure 42
Pressure Exponent Versus Oxidizer Particle Size
for both HMX/HTPB and AP/HTPB Propellants

exponent only increases slightly is because of large HMX ignition delay times which control the combustion for very large particles (see Figure 39).

Examining Figure 42 for the AP pressure exponent shows that, for small AP crystals in which the primary flame is kinetically controlled, the exponent is high due the high reaction order associated with this flame, 2.0. As the AP particle size is increased the final diffusion flame and the diffusional effects of the primary flame cause a decrease in the pressure exponent (see Figure 40). The exponent begins to rise again for large AP particles as the kinetic AP monopropellant flame begins to dominate the combustion. This flame has a reaction order of 1.64.

5.2.3 Propellant Surface Temperature

The next particle size plot, Figure 43, shows surface temperature variations with differing particle sizes. In Figure 43 the chamber pressure is 1000 psia and the propellant's initial temperature is 298°K. The surface temperature plotted is a mass weighted average of the individual pseudo propellant surface temperatures computed by the combustion model. As expected, these trends follow the same pattern as the burning rate variations shown in Figure 41. The HMX propellants show little variation in their surface temperatures, while the surface temperature varies considerably for the AP propellants. In addition, the AP surface temperatures are 200 to 400°K higher than the HMX propellant surface temperature. These results are consistent with experimental observations.[63-65]

5.2.4 Temperature Sensitivity

Figure 44 is a plot of the temperature sensitivity versus oxidizer particle size. The temperature sensitivity was computed by computing the burning rate at initial propellant temperatures of 248, 298 and 348°K. The combustion pressure for these propellants is 1000 psia. Figure 44 indicates that HMX propellants will have a higher temperature sensitivity than will AP propellants and that both types will show an increased sensitivity as particle size is increased. For very large particles the AP propellant temperature sensitivity surpasses that of HMX. It has been shown experimentally that coarse AP particles can dramatically increase the temperature sensitivity, and coarse HMX particles cause a slight increase in temperature sensitivity.[155] In the section comparing experimental data with the HYPEM model's prediction (section 4.2), the HYPEM over predicted the temperature sensitivity when the propellant contained all or mostly HMX as a oxidizer. Based on those results, the temperature sensitivity values of the HMX propellants in Figure 44 are probably 20 to 40 percent high.

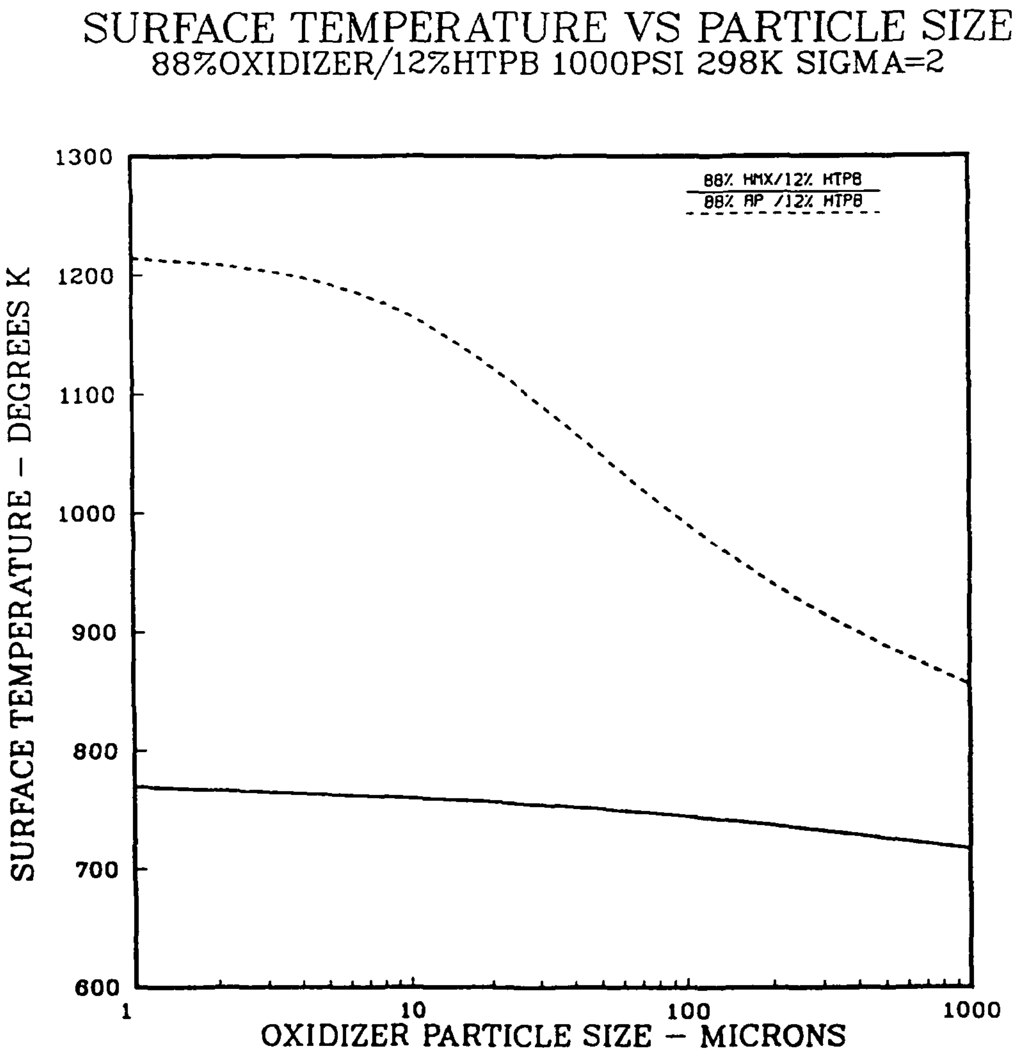

Figure 43
Propellant Surface Temperature Versus Oxidizer Particle Size for both HMX/HTPB and AP/HTPB Propellants

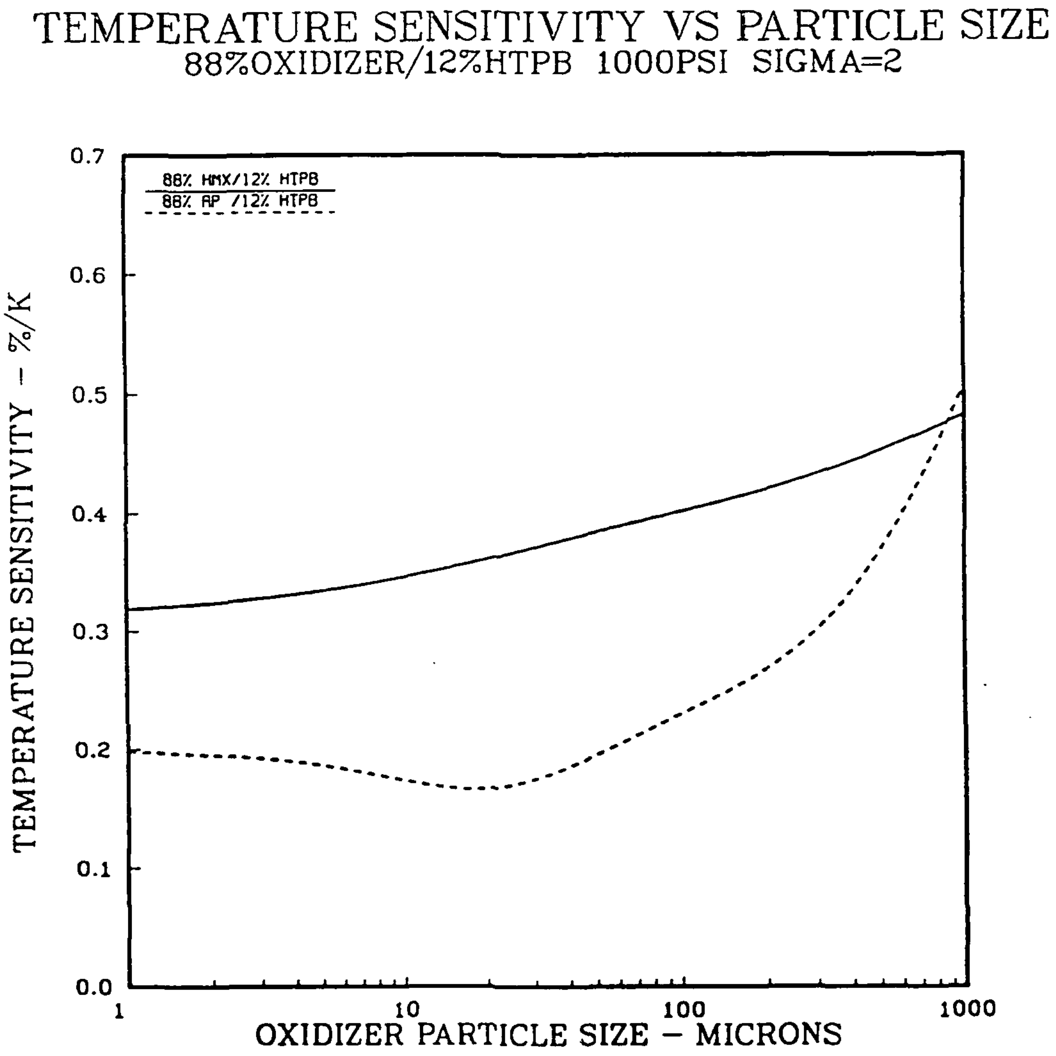

Figure 44
Temperature Sensitivity Versus Oxidizer Particle Size
for both HMX/HTPB and AP/HTPB Propellants

5.3 Pressure

To examine a propellant's behavior as particle size changes requires the use of monomodal particle size propellants, ie. propellants containing only one particle size distribution. In reality however, in order to meet the high solids loading of today's modern propellants, several distribution of particle sizes must be used. A realistic propellant might consist of fine 20μm particles and coarse 200μm particles. Figures 45 and 46 show the burning rate and surface temperature versus pressure for propellants that are 88 percent solids loaded containing a 50/50 mix of fine 20μm particle and coarse 200μm particles. In Figure 45 and 46 the initial propellant temperature is 298°K and the particle distributions have a sigma of 2.0. Four types of propellants are shown. The solid line represents propellants containing only HMX crystals, while the dashed line represents propellants containing just AP crystals. The remaining two lines depict propellants containing fine HMX mixed with coarse AP (dotted line) and fine AP with coarse HMX crystals (dotted-dash line). Since Figure 45 is plotted on a log-log scale the slope of the curve is the pressure exponent.

All propellants in Figures 45 and 46 show an increase in burning rate and surface temperature as pressure increases. Increasing the pressure causes an increase in the flame heat transfer to the surface since the various flames are closer to the surface. The propellants with only HMX have the lowest burning rates and surface temperatures. Conversely, the AP propellants have the highest burning rates and surface temperatures. The two combination propellants lie in between. The two propellants with fine HMX (bottom two lines) and the two propellants with fine AP (top two lines) both behave in a similar fashion.

Referring back to Figures 38 and 40 which plot the percent heat feedback from the various flames versus particle size, it was concluded that the primary flame controls the combustion for both HMX and AP fine particles. For the propellants in Figure 45 with fine HMX crystals, the cool primary flame suppresses the rate below that of the AP fine crystal propellants which have a hot primary flame. As the pressure increases the flame standoff distance of the primary flame becomes even smaller. Because of the very hot AP primary flame, propellants with fine AP will increase in burning rate faster than propellants containing fine HMX as is shown in Figure 45.

Figure 47 shows the effect of pressure on temperature sensitivity for the same bimodal propellants discussed in Figures 45 and 46. Each propellant contains a 50/50 mix of 200/20μm particles with 12 percent HTPB. The values in the Figure 47 at 1000 psi agree well with observed temperature sensitivity in the literature.[155-159] Figure 47 shows the least amount of temperature sensitivity fluctuations with the HMX/HTPB propellants (solid line). Propellants containing all or some AP show more temperature sensitivity variations as pressure is increased. These trends are partially supported by the literature. Experimental studies indicates the effect of pressure on temperature sensitivity has minimal effect on HMX/HTPB propellants and generally decreases or results in little change in the temperature sensitivity of AP/HTPB propellants.

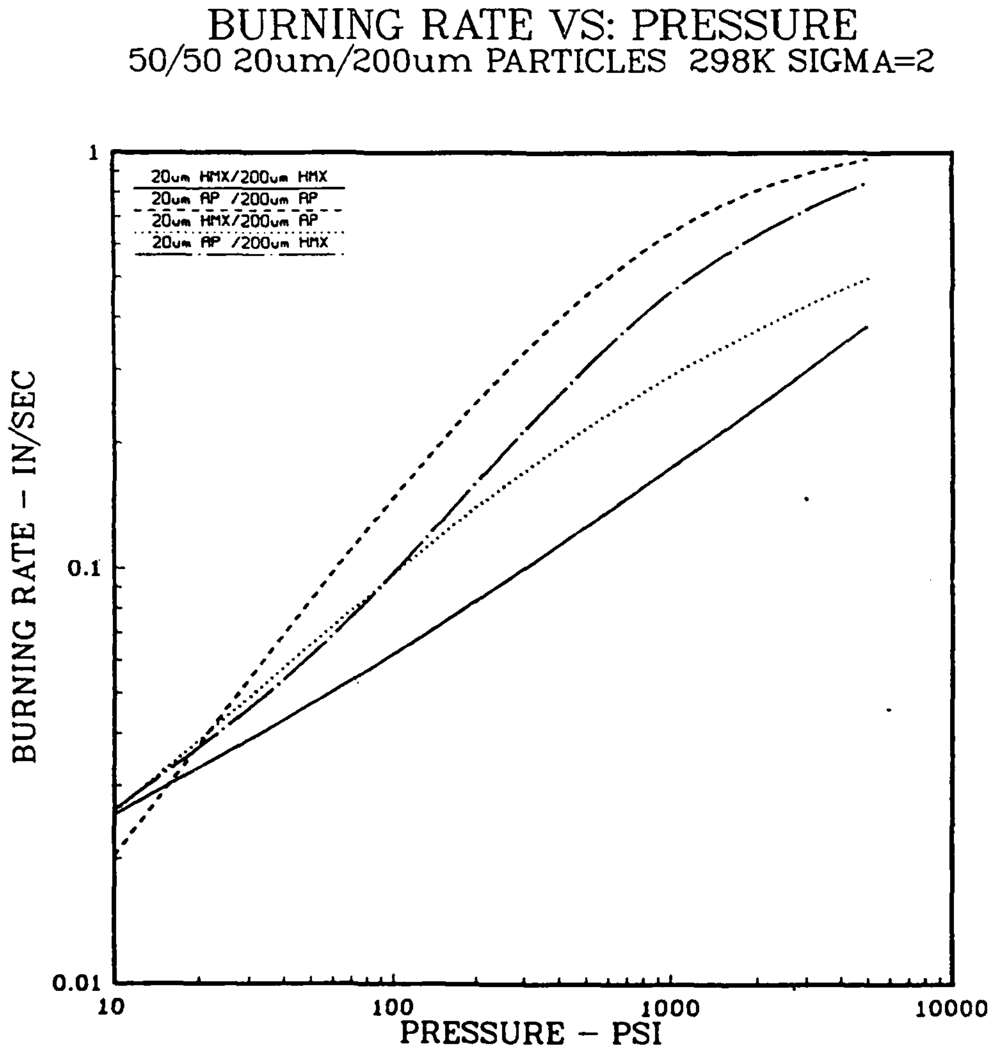

Figure 45
Burning Rate Versus Pressure for Bimodal Propellants Containing HMX and/or AP Particles (12% HTPB)

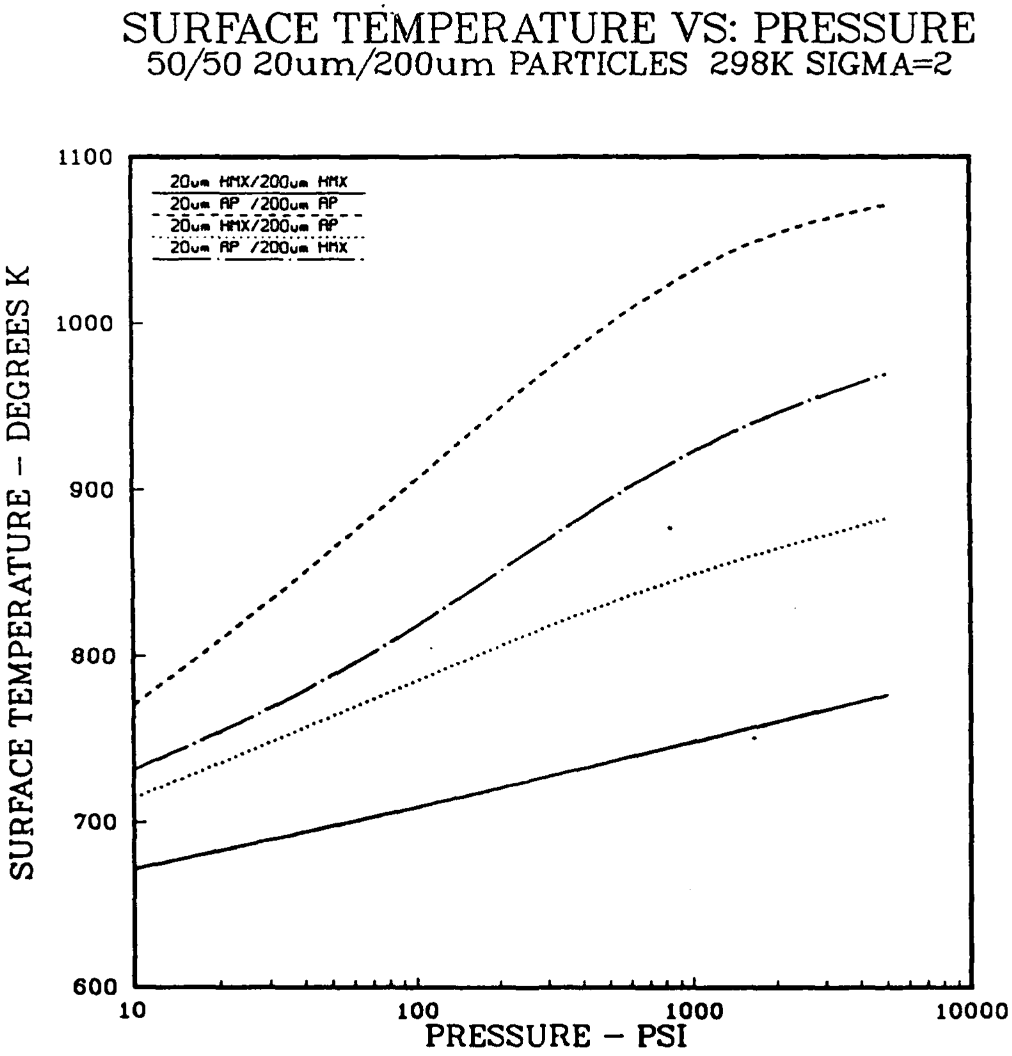

Figure 46
Surface Temperature Versus Pressure for Bimodal Propellants Containing HMX and/or AP Particles (12% HTPB)

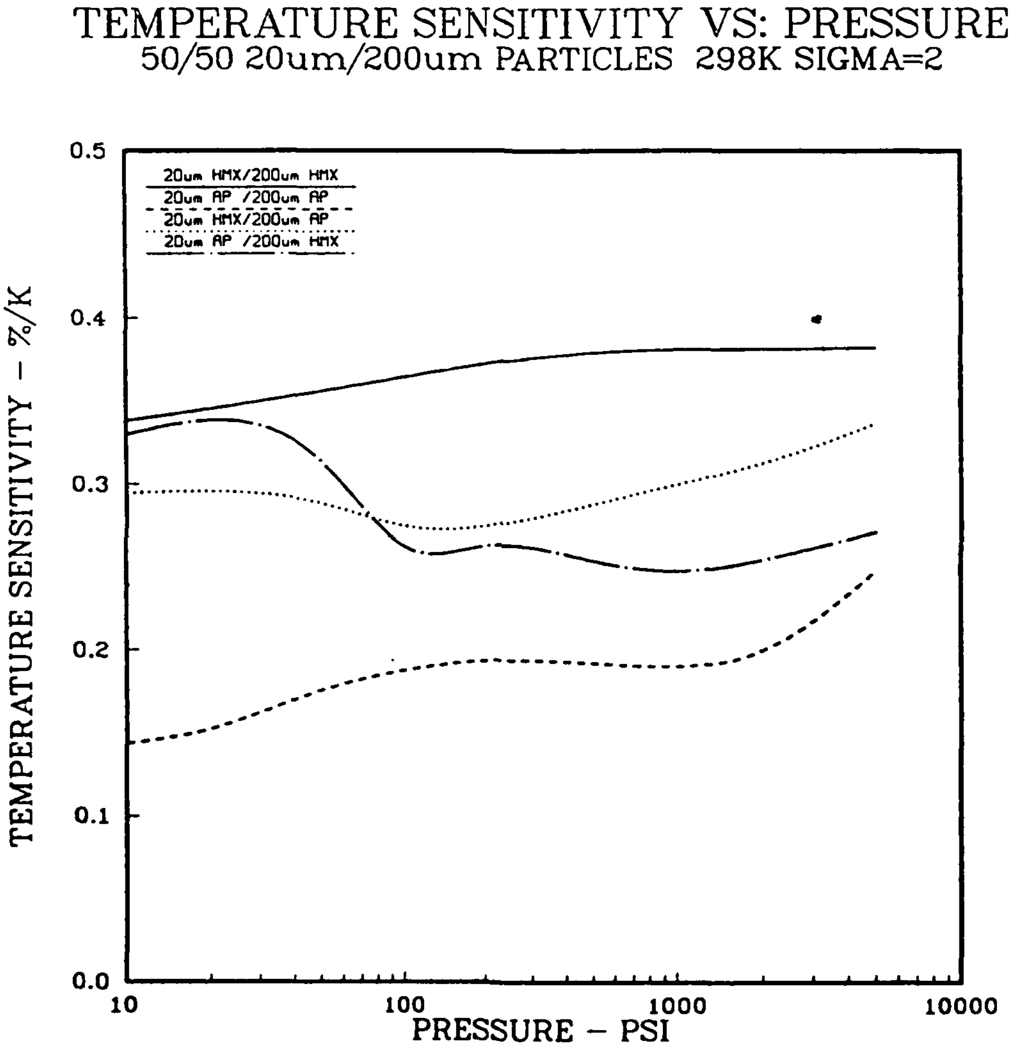

Figure 47
Temperature Sensitivity Versus Pressure for Bimodal Propellants Containing HMX and/or AP Particles (12% HTPB)

5.4 Oxidizer Solids Loading

The next series of graphs show the combustion characteristics of composite propellants as a function of oxidizer mass fraction or solids loading. The solids loading ranges from 60 percent (fuel rich) to 98 percent (fuel lean) in each figure. Each graph contains three lines which represent monomodal propellants containing fine 10μm, medium 100μm and coarse 400μm oxidizer particles. The particle distributions have a sigma of 2.0.

Figures 48 and 49 show burning rate versus solids loading for HMX/HTPB propellants and AP/HTPB propellants, respectively. In both graphs the pressure is 1000 psi and the initial propellant temperature is 298°K. Figure 48 for HMX/HTPB propellants indicates that the higher the solids loading the higher the burning rate or, conversely, the addition of any HTPB to the propellant will lower the burning rate. Behavior of this type is expected since HMX burns stoichiometrically as a monopropellant, and the addition of fuel will dilute and weaken the reaction.[30] As expected from previous theoretical and experimental results, the differing particle sizes have little influence on the burning rate.

The AP/HTPB curves in Figure 49 show a peak at approximately 90 percent solids loading for the 10μm AP particle curve and at 95 percent solids loading for the 100μm curve. A peak is expected since AP requires fuel to burn in stoichiometric proportions. The stoichiometric solids loading for an AP/HTPB mixture is close to 88 percent. The reason the burning rate peak is not seen for the coarser particles is that, for these larger particles, more of the energy is released in the final flame while the primary flame becomes less important. The final flame has a large flame standoff distance so less energy can be conducted to the surface of the propellant.

Figures 50 and 51 depict the pressure exponent variation with differing solids loading for HMX/HTPB and AP/HTPB propellants. The trends presented agree with the previous theoretical results. The pressure exponent of HMX/HTPB propellants is only affected slightly by changes in propellant characteristics. The AP/HTPB propellants in Figure 51 show much broader variation in the pressure exponent. All three particle size propellants at very high solids loading approach their monopropellant pressure exponents, since the combustion processes are dominated by the kinetic monopropellant oxidizer flames.

The final two graphs in this series, Figure 52 and 53, plot the temperature sensitivity variations with differing oxidizer solids loadings. In both figures the higher the solids loading the lower the temperature sensitivity. The figures indicate fuel rich propellants will have a high burning rate sensitivity to initial propellant temperature. When the conditions are closer to stoichiometric conditions, solids loading around 90 percent, the propellants containing the most coarse particles have the highest temperature sensitivity. This agrees with the results already presented showing temperature sensitivity variation with different particle sizes (Figure 42).

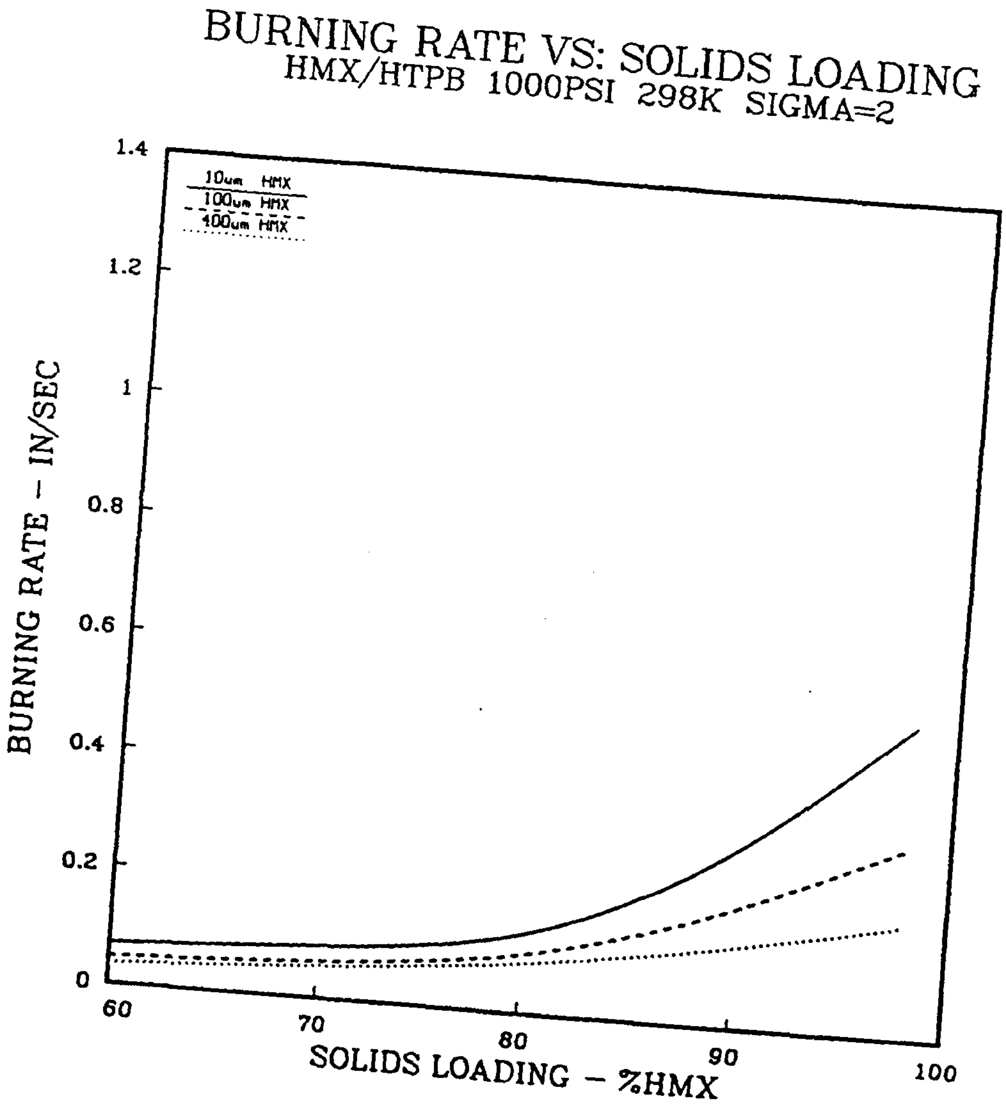

Figure 48
Burning Rate Versus Oxidizer Solids Loading for Monomodal HMX/HTPB Propellants

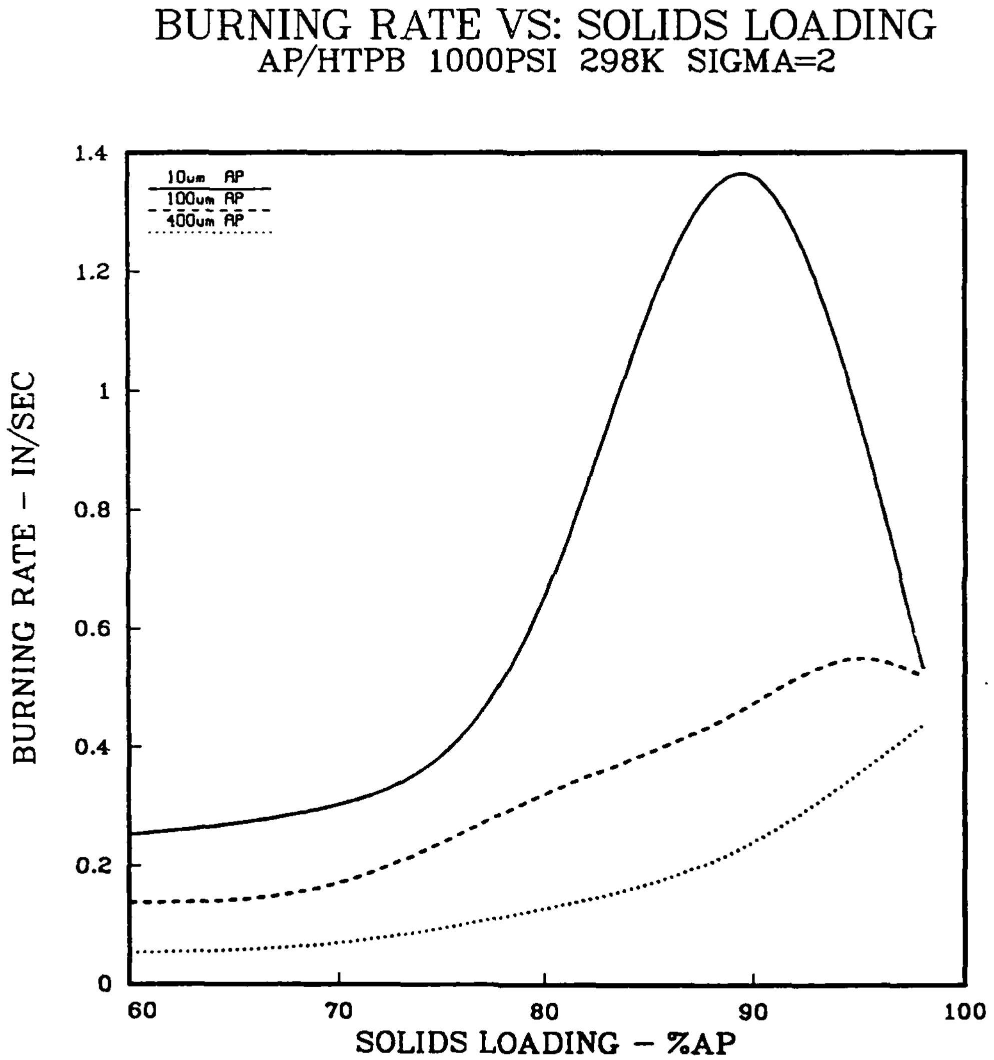

Figure 49
Burning Rate Versus Oxidizer Solids Loading for Monomodal AP/HTPB Propellants

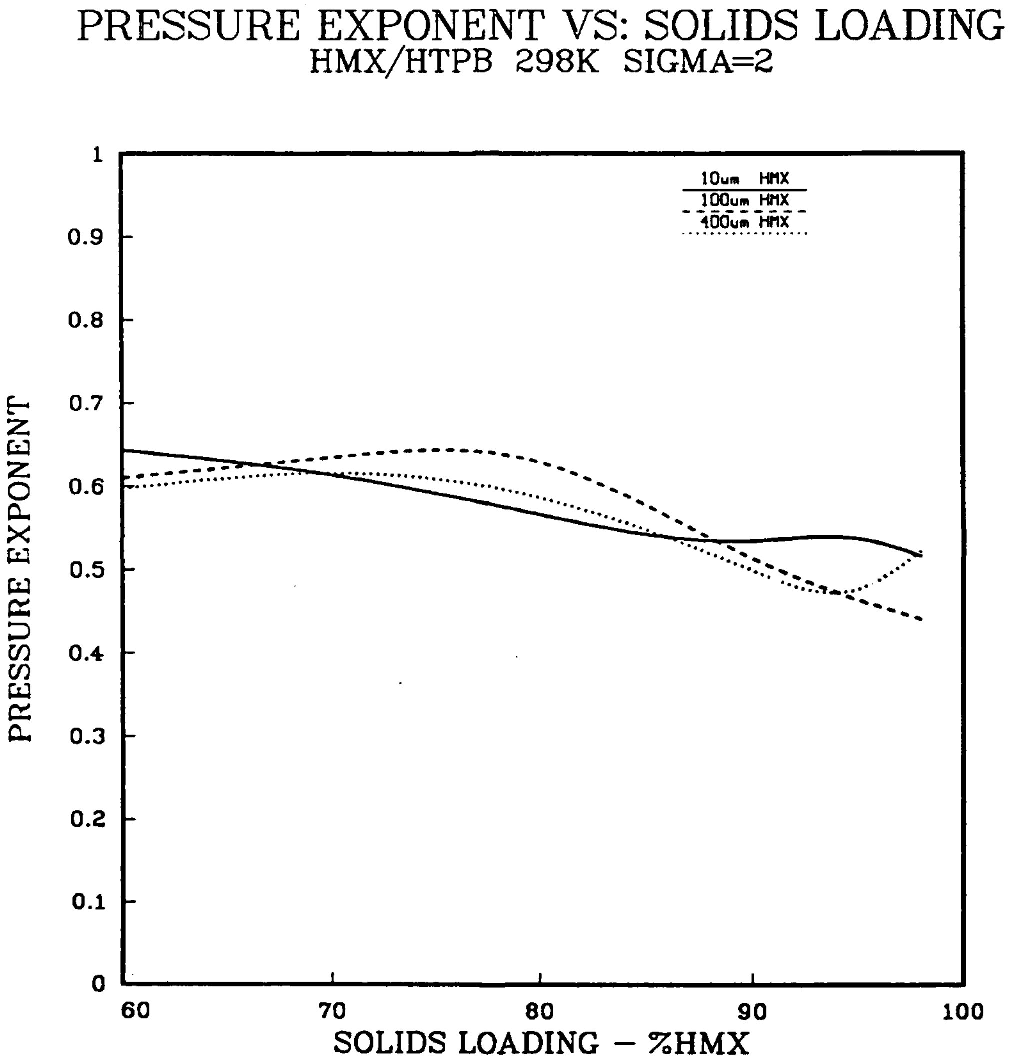

Figure 50
Pressure Exponent Versus Oxidizer Solids Loading for Monomodal HMX/HTPB Propellants

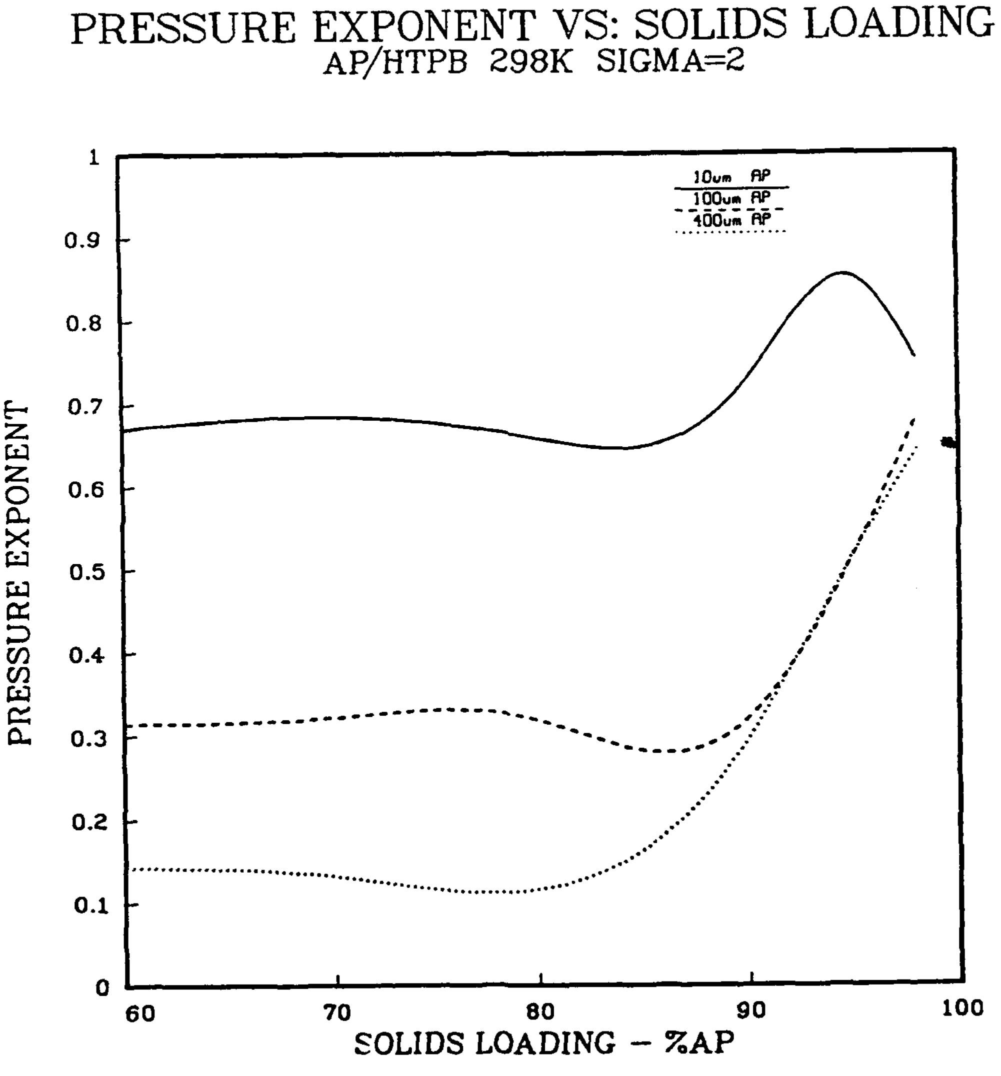

Figure 51
Pressure Exponent Versus Oxidizer Solids Loading for Monomodal AP/HTPB Propellants

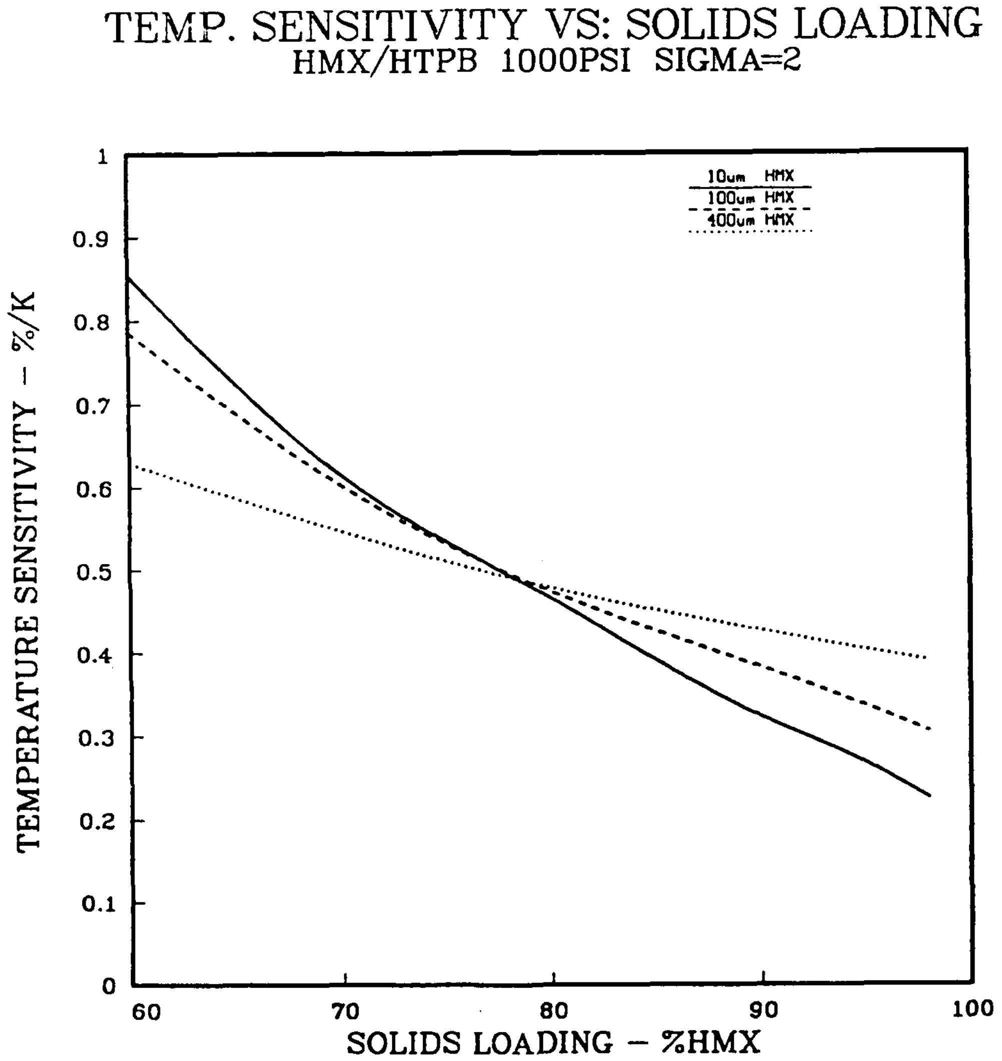

Figure 52
Temperature Sensitivity Versus Oxidizer Solids Loading for Monomodal HMX/HTPB Propellants

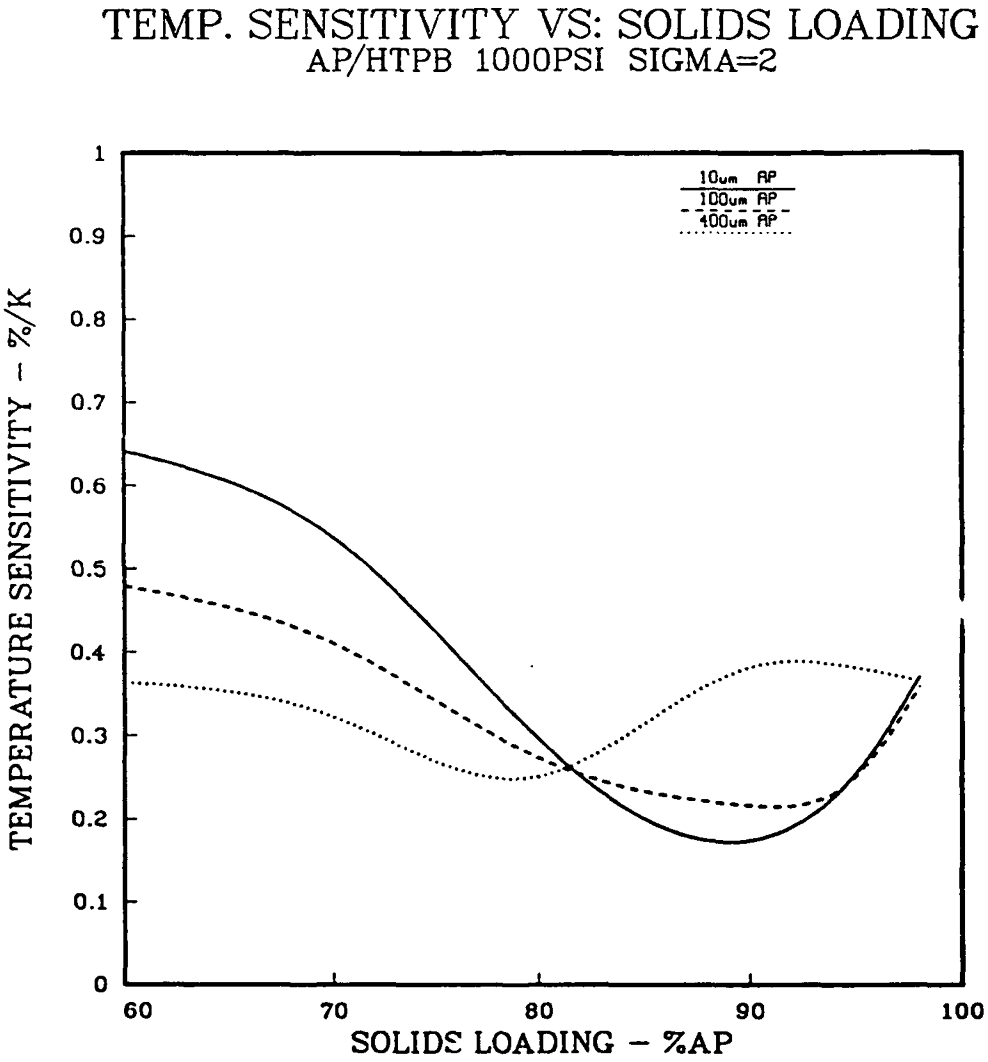

Figure 53
Temperature Sensitivity Versus Oxidizer Solids Loading for Monomodal AP/HTPB Propellants

5.5 Formulation Changes

The final series of plots presents the results of calculations in which the propellant formulation was changed. The following three figures show the effect of coarse to fine particle ratio on burning rate, pressure exponent and temperature sensitivity for bimodal propellants consisting of 200μm and 20μm oxidizer particles. In each plot the bimodal propellant property is plotted versus percent 200μm particles. The far left edge of the plot, 0% coarse, implies the propellant consists of all 20μm fine particles. The far right edge of the plot, 100% coarse, implies the propellant consists of all 200μm coarse particles. In addition, on each plot, four types of propellants are presented. The solid line represents propellants containing only HMX particles, the dashed line represents propellants containing only AP particles, the dotted line represents propellants containing coarse HMX and fine AP and the dash-dotted line represents propellants containing coarse AP and fine HMX. The mode width parameter, σ_{ox}, for each oxidizer distribution is 2.0.

Figure 54 shows the burning rate behavior versus the percent of coarse particles. The propellants containing fine AP show the greatest variation in burning rate with the fine AP/coarse HMX propellants yielding the greatest variation (dotted line). Conversely, propellants containing fine HMX crystals show the least variation in burning rate with the fine HMX/coarse HMX propellants yielding the least variation (solid line).

Figure 55 shows the pressure exponent variation for the same propellants. The propellants containing coarse HMX have the highest exponent while those with coarse AP have the lowest exponent. The amount of fine AP crystals combined with coarse HMX in a propellant causes the widest variation in burning rate. This type of propellant also yields the highest exponent as is seen in Figure 55. Unfortunately these two facts run counter to each other in the design of well behaved propellants, ie. fine AP/coarse HMX mixtures yield varied burning rates but also the highest pressure exponent.

Figure 56 plots the temperature sensitivity versus percent coarse oxidizer. In Figure 56, the temperature sensitivity is the highest for propellants with the most coarse HMX crystals. Propellants containing mostly fine AP particles will have the least burning rate sensitivity to initial propellant temperature. These observations indicate that the very hot primary flame associated with small AP crystals is relatively insensitive to initial propellant temperature. Furthermore, the monopropellant kinetic flame associated with larger particles is more sensitive to initial propellant temperature.

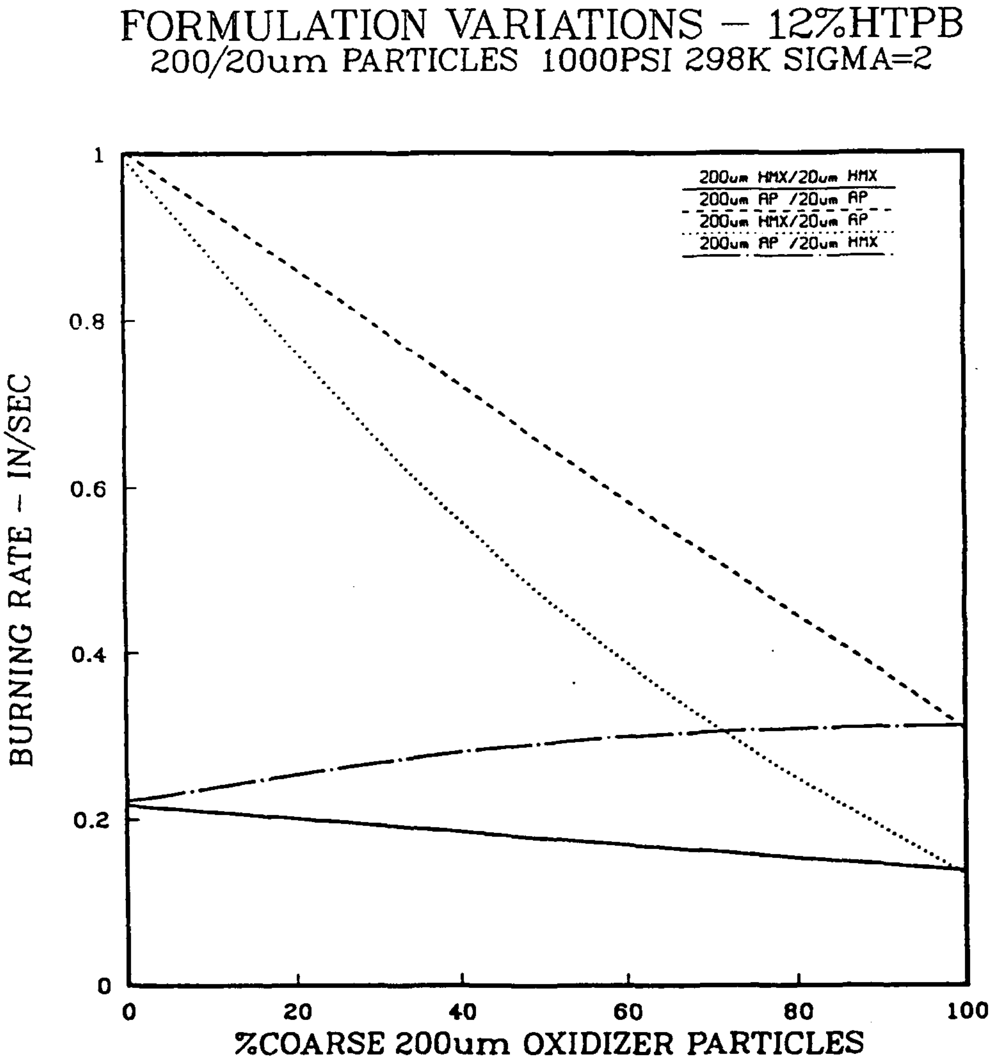

Figure 54
Burning Rate Versus Percent Coarse Oxidizer Crystals for
Bimodal Propellants Containing HMX and/or AP with HTPB

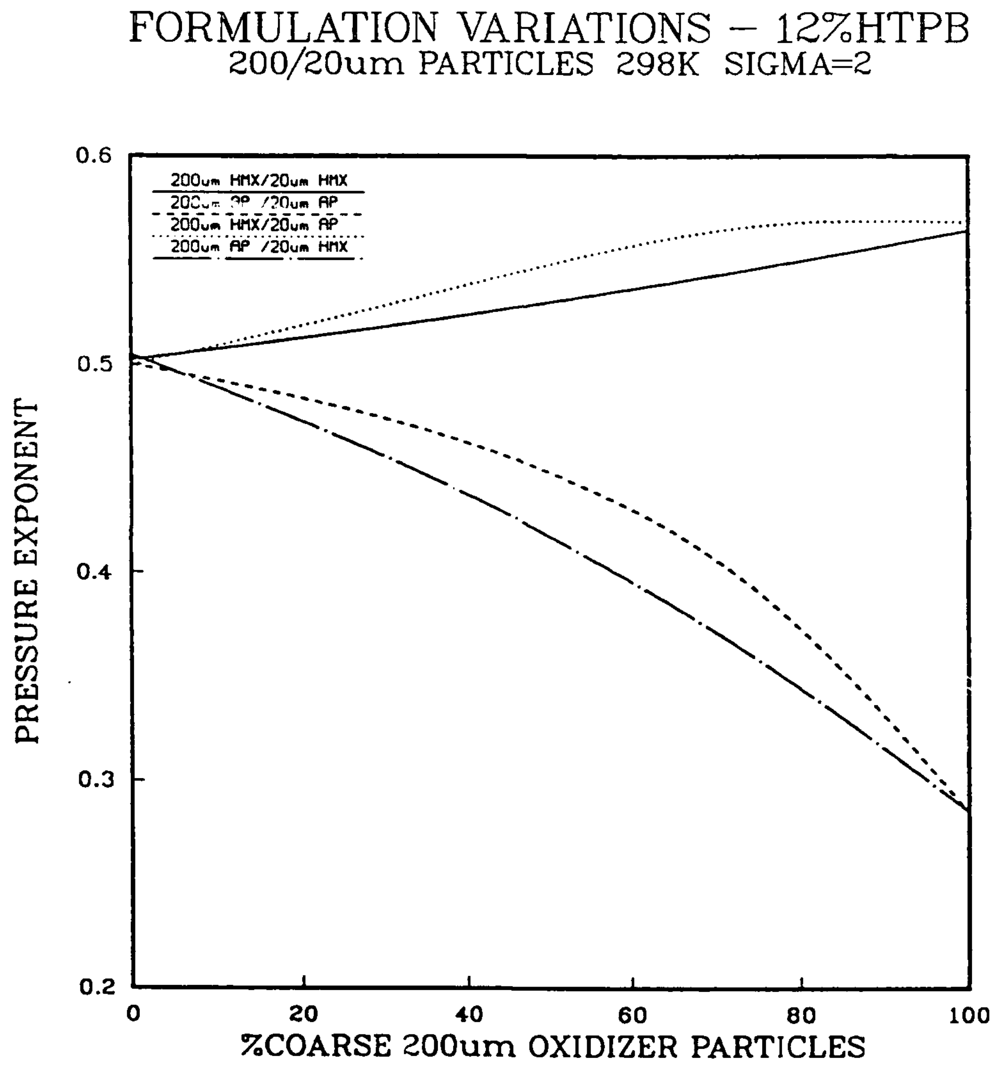

Figure 55
Pressure Exponent Versus Percent Coarse Oxidizer Crystals for Bimodal Propellants Containing HMX and/or AP with HTPB

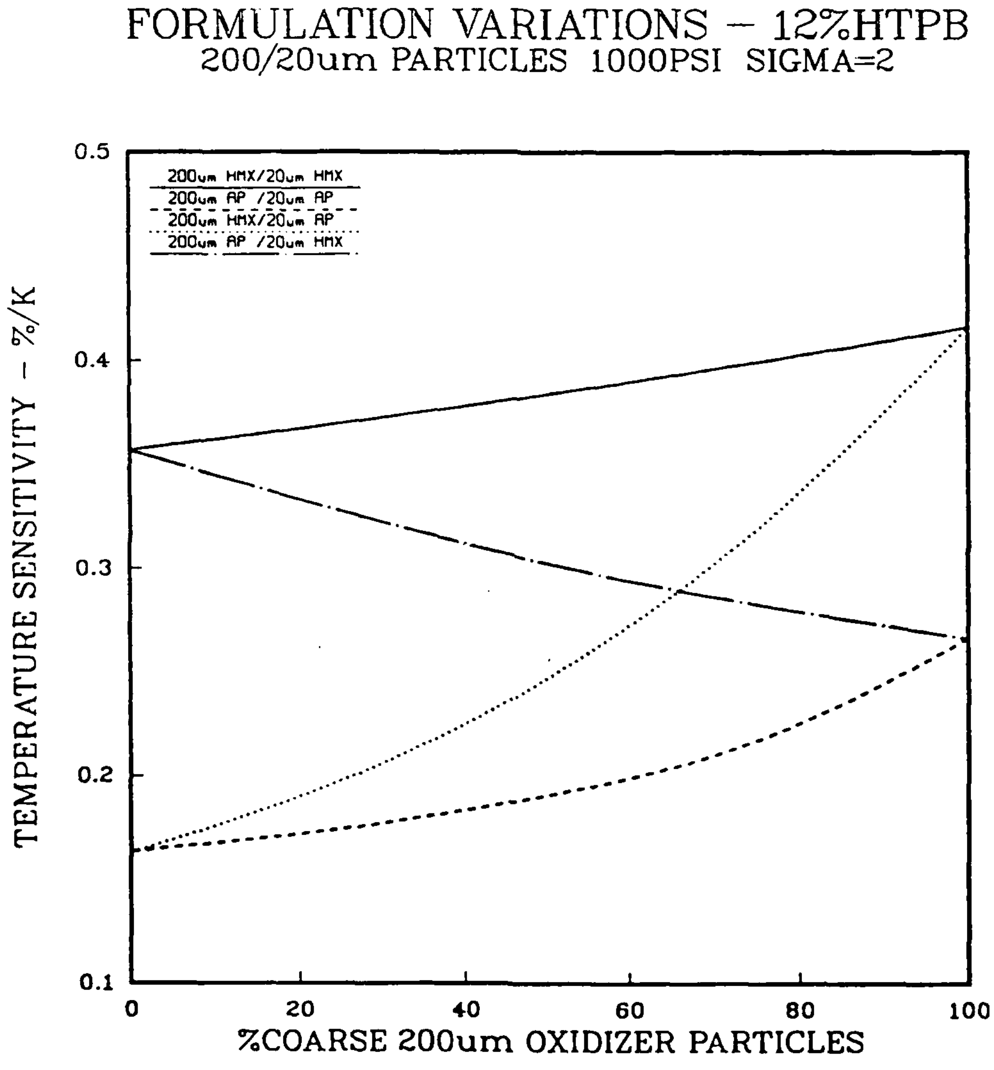

Figure 56
Temperature Sensitivity Versus Percent Coarse Oxidizer Crystals for Bimodal Propellants Containing HMX and/or AP with HTPB

CHAPTER VI

CONCLUSIONS

In this thesis the High Energy Petite Ensemble Model (HYPEM) has been presented. The model is a steady state, statistically based composite propellant combustion model which is able to predict the combustion characteristics of propellants consisting of HMX and/or AP mixed together in a HTPB fuel binder medium. The overall structure of the combustion model is based on the Petite Ensemble Model (PEM) which mathematically separates the propellant into unique pseudo propellants. These monodisperse pseudo propellants depend upon the statistical makeup of the individual oxidizer particle distributions in the propellant. The pseudo propellant burning rates are then statistically combined together to determine the total burning rate of the propellant.

The HYPEM combustion model treats the two oxidizer types, HMX and AP, in separate, unique fashions. The burning rate of the HMX pseudo propellants is computed by averaging the HMX combustion, HMX ignition delay, binder burn through and binder delay time as the propellant surface regresses. Time averaging is required due to the unsteady nature of HMX crystals burning in a composite propellants. The burning rate of the AP pseudo propellants is computed by space averaging over the entire burning surface of the pseudo propellant. Both the HMX and AP pseudo propellants use surface energy balances to compute the surface temperature of the individual oxidizer type and its surrounding binder.

The HYPEM composite propellant combustion model was used to predict the burning rate and the pressure exponent for 61 individual propellants containing one or both types of oxidizers. These propellants contained HMX particles from 4μm to 400μm and AP particles from 0.7μm to 450μm. The burning rate and pressure exponent results were most accurate for propellants containing only one type of oxidizer, however, the results for the combination propellants were usually within ±20 percent. The HYPEM model was also used to compute the temperature sensitivity of 30 individual propellants. Experimentally measured values of temperature sensitivity compared favorably with the predictions by the combustion model for propellants containing mostly or all AP. The HYPEM model consistently overpredicted the temperature sensitivity for propellants containing all or mostly HMX by 20 to 40 percent.

Various parametric studies were performed with the HYPEM combustion model. The experimentally observed small burning rate and pressure exponent dependence on HMX oxidizer particle size was correctly predicted by the model. In addition, the experimentally observed large burning rate dependence on AP particle size was shown by the model. The experimental observation that larger HMX and AP crystals will increase the temperature sensitivity was also verified by the model. Parametric studies showing the effect of pressure on burning rate, surface temperature and temperature sensitivity were also presented.

Parametric studies were performed examining the effect of propellant solids loading and the ratio of coarse to fine oxidizer crystals on bimodal propellant burning rate, pressure exponent and temperature sensitivity. The bimodal propellant results indicated a strong dependence on temperature sensitivity for fine AP/coarse HMX/HTPB propellants but little dependence with HMX/HTPB propellants. Considerable burning rate variations could be achieved by varying the ratio of coarse HMX with fine AP oxidizer crystals. However, these same propellants exhibited the highest pressure exponent. Studies like these, and similar studies where the formulation is systematically changed, can be used to understand propellant behavior and can aid in the development of new propellants.

REFERENCES

1. Summerfield, M., Sutherland, G. S., Webb, M. J., Taback, H. J., and Hall, K. P., "Burning Mechanism of Ammonium Perchlorate Propellants," *Solid Propellant Rocket Research*, Vol. 1, pp. 141-182, Academic Press, New York, 1960.

2. Ramohalli, K. N. R., "Steady-State Burning of Composite Propellants under Zero Cross-Flow Situation," *Fundamentals of Solid-Propellant Combustion*, American Institute of Aeronautics and Astronautics, Inc., New York, New York, pp. 409-477, 1984.

3. Steinz, J. A., Stang, P. L. and Summerfield, M., "The Burning Mechanism of Ammonium Perchlorate-Based Composite Solid Propellants," AIAA Paper No. 68-658, June, 1968.

4. Miller, R. R., Hartman, K. O. and Myers, R. B., "Prediction of Ammonium Perchlorate Particle Size Effect of Composite Propellant Burning Rate," CPIA Pub. 196, pp. 567-591, 1970.

5. Hermance, C. E., "A Model of Composite Propellant Combustion Including Surface Heterogeneity and Heat Generation," *AIAA Journal*, Vol. 4, pp. 1629-1637, September 1966.

6. Hermance, C. E., "A Detailed Model of the Combustion Composite Solid Propellants," *2nd Solid Propulsion Conference*, Anaheim, CA, June 1967.

7. Blum, E. H. and Wilhelm, R. H., "A Statistical Geometric Approach to Random-Packed Beds," *AICHE Industrial Chemical Engineering Symposium Series No. 4*, London Institute of Chemical Engineers, pp. 4:21-4:27, 1965.

8. Chaiken, R. F. and Anderson, W. H., "The Role of Binder in Composite Propellant Combustion," *ARS Progress in Astronautics and Rocketry, Vol. I: Solid Propellant rocket Research*, Academic Press, New York, 1960, pp. 227-249.

9. Nachbar, W., "A Theoretical Study of the Burning of a solid Propellant Sandwich," *ARS Progress in Astronautics and Rocketry, Vol. I: Solid Propellant rocket Research*, Academic Press, New York, 1960, pp. 207-226.

10. Heaston, R. J., "The Prediction of the Burning Rate Exponent of Solid Propellants," US Army Research and Development Group (Europe), European Research Office, Frankfurt, Germany, December 1966.

11. Fenn, J. B., "A Phalanx Flame Model for the Combustion of Composite Solid Propellants," Project Squid Technical Report PR-114-P, April 1967.

12. Culick, F. E. C. and Dehority, G. L., "An Elementary Calculation for the Burning Rate of Composite Solid Propellants," WSS/CI Paper 69-7, Spring Meeting, Western States Section, The Combustion Institute, April 28-30, 1969.

13. Beckstead, M. W., Derr, R. L., and Price, C. F., "A Model of Composite Solid Propellant Combustion Based on Multiple Flames," AIAA Journal, Vol. 8, pp. 2200-2207, December 1970.

14. Hamann, R. J., "Three Solid Propellant Combustion Models," Delft University of Technology, Memorandum M-215, Delft, The Netherlands, April 1974.

15. Cohen, N. S., Derr, R. L., and Price, C. F.,"Extended Model of Solid Propellant Combustion Based on Multiple Flames," 9th JANNAF Combustion Meeting, CPIA Pub. 231, Vol. II, pp. 25-42, December 1972.

16. Cohen, N. S., "Composite Propellant Burn Rate Modeling," Solid Rocket Motor Technology, AGARD-CP-259, pp. 11-1 - 11-21, July 1979.

17. Beckstead, M. W., "Combustion Calculations for Composite Solid Propellants," 13th JANNAF Combustion Meeting, CPIA Publication 281, Vol. II, pp. 299-312, December 1976.

18. Cohen, N. S. and Strand, L. D., "An Improved Model for the Combustion of AP Composite Propellants," AIAA Journal, Vol. 20, No. 12, pp. 1739-1746, December 1982.

19. King, M. K., "Model for Steady State Combustion of Unimodal Composite Solid Propellants," AIAA 16th Aerospace Sciences Meeting, Huntsville, AL, January 16-18, 1978.

20. Kishore, K., "Comprehensive View of the Combustion Models of Composite Solid Propellants," AIAA Journal, Vol. 17, No. 11, pp. 1216-1224, November 1979.

21. Burke, S. P. and Schumann, T. E. W., "Diffusion Flames," Industrial and Engineering Chemistry, Vol. 20, No. 10, pp. 998-1004, October 1928.

22. Williams, F. A., Combustion Theory, Addison-Wesley, pp. 37-45, 1965.

23. Glick, R. L., "On Statistical Analysis of Composite Solid Propellant Combustion," AIAA Journal, Vol. 12, pp. 384-385, March 1974.

24. Glick, R. L. and Condon, J. A., "Statistical Analysis of Polydisperse, Heterogeneous Propellant Combustion: Steady State," 13th JANNAF Combustion Meeting, CPIA Pub. 281, Vol. II, pp. 313-345, December 1976.

25. Condon, J. A. and Osborn, J. R., "The Effect of Oxidizer Particle Size Distribution on the Steady and Nonsteady Combustion of Composite Propellants," AFRPL-TR-78-17, June 1978.

26. Renie, J. P., Condon, J. A and Osborn, J. R., "Oxidizer Size Distribution Effects on Propellant Combustion," AIAA Journal, Vol. 17, pp. 877-883, August 1979.

27. Renie, J. P. and Osborn, J. R., "Combustion Response Calculations for Composite Solid Propellants," AFRPL-TR-81-25, Dec. 1981.

28. Renie, J. P. and Osborn, J. R., "Erosive Burning," AIAA Journal, Vol. 21, No. 12, pp. 1681-1689, December 1983.

29. Miller, R. R., Foster, R. L., Beckstead, M. W. and Jones, M. L., "Ballistic Control of Solid Propellants," AFRPL-TR-80-10, November 1980.

30. Miller, R. R., Jones, M. L., Foster, R. L. and Condon, J. A., "Ballistic Control of Solid Propellants," AFRPL-TR-81-058, Vol. I, April 1982.

31. Boggs, T. L., "The Thermal Behavior of Cyclotrimethylene-Trinitramine (RDX) and Cyclotetramethylenetetranitramine (HMX)," Fundamentals of Solid-Propellant Combustion, American Institute of Aeronautics and Astronautics, Inc., New York, New York, pp. 121-175, 1984.

32. Edward, J. T., "Wartime Research on RDX: A False Hypothesis Is Better Than No Hypothesis," Journal of Chemical Education, Vol. 64, No. 7., pp. 599-603, July 1987.

33. Goshgarian, B. B., "The Thermal Decomposition of RDX and HMX," AFRPL-TR-78-76, October 1978.

34. Axworthy, A. E., Flanigan, J. E., and Woolery, D. O., "High Temperature Pyrolysis Studies of HMX, RDX and TAGN," 15th JANNAF Combustion Meeting, CPIA Pub. 297, Vol. I, pp. 253-265, February 1979.

35. Axworthy, A. E., Flanigan, J. E., Woolery, D. O. and Gray, J. C., "Kinetic - Combustion Interactions of Nitramines," 16th JANNAF Combustion Meeting, CPIA Pub. 308, Vol. III, pp. 289-307, December 1979.

36. Fifer, R. A. and Holmes, H. E., "Kinetics of Nitramine Flame Reactions," 16th JANNAF Combustion Meeting, CPIA Pub. 308, Vol. II, pp. 35-50, December 1979.

37. Beyer, R. A. and Morgan, C. U., "Electron Spin Resonance Studies of HMX and RDX Thermal Decomposition." 16th JANNAF Combustion Meeting, CPIA Pub. 308, Vol. II, pp. 51-57, December 1979.

38. Flanigan, D. A. and Stokes, B. B., "HMX Deflagration and Flame Characterization," AFRPL-TR-79-94, Vol. I and II, October 1980.

39. Flanigan, J. E., Woolery, D. O. and Frankel, M. B., "HMX Combustion Modification Studies," 19th JANNAF Combustion Meeting, CPIA Pub. 366, Vol. II, pp. 147-156, October 1982.

40. Karpowicz, R. J., Gelfand, L. S. and Brill, T. B, Application of Solid-Phase Transition Kinetics to the Properties of HMX," AIAA Journal, Vol. 21, No. 2, pp. 310-312, February 1983.

41. Fifer, R. A., "Chemistry of Nitrate Ester and Nitramine Propellants," *Fundamentals of Solid-Propellant Combustion*, American Institute of Aeronautics and Astronautics, Inc., New York, New York, pp. 177-237, 1984.

42. Umstead, M. E., Lloyd, S. A. and Lin M. C., "Kinetic Modeling of Dimethylnitramine Thermal Decomposition--A Mechanistic Extrapolation to RDX Decomposition in the Gas Phase," *22nd JANNAF Combustion Meeting*, CPIA Pub. 432, Vol. I, pp. 515-521, October 1985.

43. Behrens Jr., R., "Simultaneous Thermogravimetric Modulated Beam Mass Spectrometry and Time-of-Flight Velocity Spectra Measurements of Thermal Decomposition Products from RDX and HMX," *23rd JANNAF Combustion Meeting*, CPIA Pub. 457, Vol. I, pp. 231-240, October 1986.

44. Morgan, C. U. and Beyer, R. A., "ESR and IR Spectroscopic Studies of HMX and RDX Thermal Decomposition," *15th JANNAF Combustion Meeting*, CPIA Pub. 297, Vol. I, pp. 359-366, February 1979.

45. Miller, P. J., Nauflett, G. W., Carlson, D. W. and Brasch, J. W., "The Thermal Decomposition of 1,3,5-Trinitrohexahydro-1,3,5-Triazine (RDX) and RDX_{d6} at High Pressures," *17th JANNAF Combustion Meeting*, CPIA Pub. 329, Vol. II, pp. 479-491, November 1980.

46. Beyer, R. A. and DeWilde, M. A., "Convective Heating of Energetic Materials," BRL-TR-2701, December, 1985.

47. Klein, N. and Keller, G. E., "Gun Propellant Combustion at Elevated Pressure," *15th JANNAF Combustion Meeting*, CPIA Pub. 297, Vol. I, pp. 525-536, February 1979.

48. Harris, L. E. and McIlwain, M. E., "Coherent Anti-Stokes Raman (CARS) Temperature Measurements in a Propellant Flame," *Combustion and Flame*, No. 48, pp. 97-100, 1982

49. Aron K. and Harris, L. E., "CARS Probe of RDX Decomposition," *Chemical Physics Letters*, Vol. 103, No. 5, pp. 413-417, January 1983.

50. Parr, T. P. and Hanson-Parr, D. M., "The Application of Imaging Laser Induced Fluorescence to the Measurement of HMX and Aluminized Propellant Ignition and Deflagration Flame Structure," Presented at the 23rd JANNAF Combustion Meeting, Hampton, VA, October 1986.

51. Parr, T. P. and Hanson-Parr, D. M., "Species and Temperature Profiles in Ignition and Deflagration of HMX," Presented at the Spring Meeting of the Western States Section of The Combustion Institute, Provo, Utah, April 6-7, 1987.

52. Pfau, J. P., Rocchio, J. J. and Wires R. A., "New Aspects of HMX Thermal Decomposition as Studied by Pyrolysis/Mass Spectroscopy," *15th JANNAF Combustion Meeting*, CPIA Pub. 297, Vol. I, pp. 267-293, February 1979.

53. Schroeder, M. A., "Critical Analysis of Nitramine Decomposition Results: Some Comments on Chemical Mechanisms," 16th JANNAF Combustion Meeting, CPIA Pub. 308, Vol. II, pp. 17-34, December 1979.

54. Schroeder, M. A., "Critical Analysis of Nitramine Decomposition Data: Product Distributions From HMX and RDX Decomposition," 18th JANNAF Combustion Meeting, CPIA Pub. 346, Vol. II, pp. 395-413, October 1981.

55. Schroeder, M. A., "Critical Analysis of Nitramine Decomposition Data: Some Suggestions for Needed Research Work," ARBRL-MR-3181, June 1982.

56. Schroeder, M. A., "Critical Analysis of Nitramine Decomposition Data: Some Preliminary Comments on Autoacceleration and Autoinhibition in HMX and RDX," 19th JANNAF Combustion Meeting, CPIA Pub. 366, Vol. I, pp. 321-329, October 1982.

57. Price, E. W., "Comment on Thermal Decomposition Kinetics of Polybutadiene Binders," AIAA Journal of Spacecraft and Rockets, Vol. 20, No. 3, p. 320, June 1983.

58. Branch, M. C., "Chemical Kinetics of Gas Phase Decomposition Products of Nitramine Propellants," 21st JANNAF Combustion Meeting, CPIA Pub. 412, Vol. I, pp. 409-415, October 1984.

59. Fifer, R. A., Liebman, S. A., Duff, P. J., Fickie, K. D. and Schroeder, M. A., "Thermal Degradation Mechanisms of Nitramine Propellants," 22nd JANNAF Combustion Meeting, CPIA Pub. 432, Vol. II, pp. 537-546, October 1985.

60. Melius, C. F. and Binkley, J. S., "Quantum Chemical Calculations of the Decomposition of Nitramines: Thermochemistry and Reaction Pathways," 23rd JANNAF Combustion Meeting, CPIA Pub. 457, Vol. I, pp. 241-248, October 1986.

61. BenReuven, M. and Caveny, L. H., "Nitramine Flame Chemistry and Deflagration Interpreted in Terms of a Flame Model," AIAA Journal, Vol. 19, No. 10, pp. 1276-1285, October 1981.

62. Cohen, N. S., "Report of Workshop on HMX Propellant Combustion Modeling," 16th JANNAF Combustion Meeting, CPIA Pub. No. 308, Vol. II, pp. 219-240, December 1979.

63. Hanson-Parr, D. M. and Parr, T. P., "Condensed Phase Temperature Profiles in Deflagrating HMX," 20th JANNAF Combustion Meeting, CPIA Pub. 383, Vol. I, pp. 281-291, October 1983.

64. Flanigan, D. A., "Nitramine Combustion," Morton Thiokol, Inc., Huntsville, AL, AFRPL-TR-84-004, January 1984.

65. Lengelle, G. and Duterque, J., "Combustion Des Propergols a Base D'Octogene," AGARD/PEP Specialists Meeting on Smokeless Propellants, Florence, 9-10 September, 1985.

66. Rocchio, J. J. and Juhasz, A. A., "HMX Thermal Decomposition Chemistry and its Relation to HMX-Composite Propellant Combustion," 11th JANNAF Combustion Meeting, CPIA Pub. 261, Vol. I, pp. 247-265, September 1974.

67. Schroeder, M. A., "Critical Analysis of Nitramine Decomposition Data: Activation Energies and Frequency Factors for HMX and RDX Decomposition," BRL-TR-2673, September 1985.

68. Schroeder, M. S., "Critical Analysis of Nitramine Decomposition Data: Activation Energies and Frequency Factors For HMX and RDX Decomposition," 17th JANNAF Combustion Meeting, CPIA Pub. 329, Vol. II, pp. 493-508, November 1980.

69. Farber, M. and Srivastava, R. D., "Thermal Decomposition of HMX," 16th JANNAF Combustion Meeting, CPIA Pub. 308, Vol. II, pp. 59-71, December 1979.

70. Fifer, R. A., "Cage Effects in the Thermal Decomposition of Nitramines and other Energetic Materials," 19th JANNAF Combustion Meeting, CPIA Pub. 366, Vol. I, pp. 311-319, October 1982.

71. Kraeutle, K. J., "A Contribution to the Knowledge of HMX Decomposition and Application of Results," 17th JANNAF Combustion Meeting, CPIA Pub. 329, Vol. II, pp. 509-525, November 1980.

72. Kraeutle, K. J., "The Thermal Decomposition of HMX: Effect of Experimental Conditions and of Additives," 18th JANNAF Combustion Meeting, CPIA Pub. 347, Vol. II, pp. 383-394, October 1981.

73. Kraeutle, K. J., "The Differential Thermal Analysis of HMX at Atmospheric and Superatmospheric Pressures," 19th JANNAF Combustion Meeting, CPIA Pub. 366, Vol. I, pp. 331-341, October 1982.

74. Taylor, R. E., Stark, R. L., Shoemaker, R. L. and Koshigoe, L. G., "Specific Heat of Octahydro-1,3,5,7-Tetranitro-1,3,5,7-Tetrazocine (HMX)," TPRL-314, Thermophysical Properties Research Laboratory, Purdue University, West Lafayette, IN, January 1983.

75. Koshigoe, L. G., Shoemaker, R. L. and Taylor, R. E., "Specific Heat of HMX," AIAA Journal, Vol. 22, No. 19, November 1984.

76. Stark, J. A. and Taylor, R. E., "Determination of Thermal Transport Properties in Ammonium Perchlorate," AIAA Journal of Propulsion and Power, Vol. 1, No. 5, pp. 409-411, October 1985.

77. Taylor, R. E., Stark, J. A., Shoemaker, R. L. and Koshigoe, L. G., "Thermophysical Properties of Propellants," Thermophysical Properties Research Laboratory, Purdue University, West Lafayette, IN, 1985.

78. Price, C. F., Boggs, T. L., Eisel, J. L., Atwood, A. I., Zurn, D. E., "Gas Phase Kinetics During Normal Combustion," 17th JANNAF Combustion Meeting, CPIA Pub. 329, Vol. II, pp. 401-411, November 1980.

79. Boggs, T. L., Price, C. F., Atwood, A. I., Zurn, D. E. and Derr, R. L., "The Role of Gas Phase Reactions in Deflagration-to-Detonation Transition," *7th Symposium on Detonation*, Vol. 1, pp. 85-93, June 1981.

80. Jones, M. L., Elrick, D. E., Herriott, G. E., Mihlfeith, C. M. and McCarty, K. P., "Nitramine Combustion Studies," AFRPL-TR-82-079, Hercules Incorporated, Cumberland, Maryland, April 1983.

81. Bradley, H. H., "Unified Theory of Solid Propellant Ignition," Naval Weapons Center, China Lake, California, Report NWC-TP-5618, August 1974.

82. Beckstead, M. W., Derr, R. L. and Price, C. F., "The Combustion of Solid Monopropellants and Composite Propellants," *13th Symposium (International) on Combustion*, The Combustion Institute, Pittsburgh, Pa., pp. 1047-1058, 1971.

83. Kuznetsov, V. T. and Skorik, A. I., "Ignition of Octogen by a Light Flux," *Fizika Goreniya i Vzryvia*, Vol. 13, pp. 271-274, March-April 1977.

84. Hermance, C. E., "Solid-Propellant Ignition Theories and Experiments," *Fundamentals of Solid-Propellant Combustion*, American Institute of Aeronautics and Astronautics, Inc., New York, New York, pp. 239-304, 1984.

85. Cohen, A. and Decker, L. J., "Shock Tube Propellant Reactions: Ignition of M-9 and Catalysis of RDX," *17th JANNAF Combustion Meeting*, CPIA Pub. 329, Vol. II, pp. 469-478, November 1980.

86. Derr, R. L., Boggs, T. L., Zurn, D. E. and Dibble, E. J., "The Combustion Characteristics of HMX," *11th JANNAF Combustion Meeting*, CPIA Pub. 261, Vol. I, pp. 231-241, September 1974.

87. Isom, K. B., "A Window Bomb Study of HMX Combustion," *11th JANNAF Combustion Meeting*, CPIA Pub. 261, Vol. I, pp. 243-246, September 1974.

88. Juhasz, A. A. and Rocchio, J. J., "High Pressure Burning Rates of Nitramine Propellants," *14th JANNAF Combustion Meeting*, CPIA Pub. 292, Vol. II, pp. 81-99, August 1977

89. Cole, J. E. and Fifer, R. A., "Burn Rate Behavior of High Density Binderless HMX," *16th JANNAF Combustion Meeting*, CPIA Pub. 308, Vol. II, pp. 1-15, December 1979.

90. Fifer, R. A., and Cole, J. E., "Burning Rate for Steel-Cased, Pressed Binderless HMX," *17th JANNAF Combustion Meeting*, CPIA Pub. 329, Vol. II, pp. 413-429, November 1980.

91. Fifer, R. A. and Cole, J. E., "Burning Rate Transitions for HMX Burned as a Binderless Propellant," AD-A090389, June 1980.

92. Lenchitz, C., "The Role of Thermochemistry in HMX Propellant Burning," *12th JANNAF Combustion Meeting*, CPIA Pub. 273, Vol. II, pp. 301-321, August 1975.

93. Nauflett, G. W., Carlson, D., Austin, T. D. and Brasch, J. W., "Effects of Pressure and Melting Behavior on the Combustion of Propellants Containing RDX and Some RDX Admixtures," 16th JANNAF Combustion Meeting, CPIA Pub. 308, Vol. II, pp. 95-111, December 1979.

94. Lenchitz, C., Bottei, L. A., Hayes, E., Haywood, B. and Fifer, R. A., "Anomalies in Nitramine Propellant Combustion," 16th JANNAF Combustion Meeting, CPIA Pub. 308, Vol. III, pp. 309-329, December 1979.

95. Yee, R. Y., Adicoff, A. and Dibble, E. J., "Surface Properties of HMX Crystal," 17th JANNAF Combustion Meeting, CPIA Pub. 329, Vol. II, pp. 461-468, November 1980.

96. Boggs, T. L., Price, D. E., Zurn, D. E., Derr, R. L. and Dibble, E. J., "The Self-Deflagration of Cyclotetramethylene-tetranitramine (HMX)," AIAA Paper Number 77-859, AIAA/SAE 13th Propulsion Conference, Orlando, Florida, July 1977.

97. Boggs, T. L., Eisel, J. L., Price, C. F. and Zurn, D. E., "High Pressure Burning Rates of Cyclotetramethylenetetranitramine (HMX)," 15th JANNAF Combustion Meeting, CPIA Pub. 297, Vol. I, pp. 241-251, February 1979.

98. Boggs, T. L., Price, C. F., Atwood, A. I., Zurn, D. E. and Eisel, J. L., "The Combustion of HMX," 17th JANNAF Combustion Meeting, CPIA Pub. 329, Vol. II, pp. 431-439, November 1980.

99. Yu, S., Hsieh, W. H. and Kuo, K. K., "Ignition of Nitramine Propellants Under Rapid Pressurization," AIAA/SAE/ASME 19th Joint Propulsion Conference, Seattle, Washington, June 1983.

100. Kim, J. U., Torikai, T. and Kuo, K. K., "Thermal Decomposition and Ignition of a Series of New Nitramine LOVA Propellants by CO_2 Laser," 23rd JANNAF Combustion Meeting, CPIA Pub. 457, Vol. I, pp. 269-279, October 1986.

101. Simmons, R. L., "High Pressure Ballistics of Nitramine Gun Propellants," 9th JANNAF Combustion Meeting, CPIA Pub. 231, Vol. III, pp. 41-58, December 1972.

102. Stiefel, L., "Review of Workshop on the Combustion of Nitramine Propellants for Guns," 10th JANNAF Combustion Meeting, CPIA Pub. 243, Vol. I, pp. 199-213, August 1973.

103. Cohen, N. S., "Combustion of Nitramine Propellants," 11th JANNAF Combustion Meeting, CPIA Pub. 261, Vol. I, pp. 267-283, September 1974.

104. Cohen, N. S. and Price, C. F., "Combustion of Nitramine Propellants," AIAA Journal of Spacecraft Rockets," Vol. 12, No. 10, October 1975.

105. Moy, B. K., "Burning Rate Studies of HMX Propellants at High Pressures," AFATL-TR-75-53, March 1975.

106. Geene, R. W., Rocchio J. J., May, I. W. and Deas, R. W., "Results of Recent Theoretical and Experimental Studies of Nitramine Gun Propellant Performance," 13th JANNAF Combustion Meeting, CPIA Pub. 281, pp. 9-19, December 1976.

107. Flanigan, J. E., "Relationship of Nitramine Combustion Phenomena and Chemical Structure," 13th JANNAF Combustion Meeting, CPIA Pub. 281, pp. 69-73, December 1976.

108. Simmons, R. L., "Workshop Report on Nitramine Gun Propellant Combustion," 13th JANNAF Combustion Meeting, CPIA Pub. 281, pp. 1-8, December 1976.

109. Lehman, B. D., "Advanced Nitramine Gun Propellant Formulations," 14th JANNAF Combustion Meeting, CPIA Pub. 292, Vol. II, pp. 67-80, August 1977.

110. Fifer, R. A., "Workshop Report: Fundamental Reactions In Solid Propellant Combustion," ARBRL-TR-02166, May 1979.

111. Mitchell, S. E. Irish, C. G. and Chang, M. S., "Synthesis and Characterization of a Linear Nitramine," 18th JANNAF Combustion Meeting, CPIA Pub. 347, Vol. I, pp. 195-206, October 1981.

112. Cohen, N. S. and Strand, L. D., "Nitramine Propellant Research," 13th JANNAF Combustion Meeting, CPIA Pub. 281, pp. 75-87, December 1976.

113. Kubota, N., "Physiochemical Processes of HMX Propellant Combustion," Nineteenth Symposium (International) on Combustion, The Combustion Institute, pp. 777-785, 1982.

114. McCarty, K. P., "Mechanism of Combustion of HMX Propellants," 14th JANNAF Combustion Meeting, CPIA Pub. 292, Vol. I, pp. 243-258, December 1977.

115. Kubota, N., "Combustion Mechanisms of Nitramine Composite Propellants," Eighteenth Symposium (international) on Combustion, The Combustion Institute, pp. 187-194, 1981.

116. Kubota, N., "Survey of Rocket Propellants and Their Combustion Characteristics," Fundamentals of Solid-Propellant Combustion, American Institute of Aeronautics and Astronautics, Inc., New York, New York, pp. 1-52, 1984.

117. Kuwahara, T. and Kubota, N., "Combustion of RDX/AP Composite Propellants at Low Pressures," AIAA Journal of Spacecraft and Rockets, Vol. 21, No. 5, pp. 502-507, 1984.

118. McCarty, K. P., "HMX Propellant Combustion Studies," AFRPL-TR-79-61, November 1979.

119. Stiefel, L., "The Effect of Composition on the Burning Rate of HMX Containing Propellants - A Review," 9th JANNAF Combustion Meeting, CPIA Pub. 231, Vol. III, pp. 25-40, December 1972.

120. Fifer, R. A. and McBratney, W. F., "Catalysis of Nitramine Propellants by Metal Borohydrides," ARBRL-MR-03300, July 1983.

121. BenReuven, M., Caveny, L. H., Vichnevetsky, R. J., and Summerfield, M., "Flame Zone and Sub-Surface Reaction Model for Deflagrating RDX," Proceedings of 16th Symposium (International) on Combustion, The Combustion Institute, Pittsburgh, PA, pp. 1223-1233, 1976.

122. BenReuven, M. and Caveny, L. H., "HMX Deflagration and Flame Characterization," AFRPL-TR-79-94, October 1980.

123. BenReuven, M. and Summerfield, M., "Analysis of Solid Propellant Combustion in a Closed Vessel Including Secondary Reaction," 17th JANNAF Combustion Meeting, CPIA Pub. 329, Vol. II, pp. 441-459, November 1980.

124. Ben BenReuven, M. and Summerfield, M., "Combustion of Nitramine Propellants," ARBRL-CR-00507, 1983.

125. Cohen, N. S., Lo, G. A. and Crowley, J. C., "Simplifications and Variations of the Ben BenReuven-Caveny Model of HMX Combustion," 18th JANNAF Combustion Meeting, CPIA Pub. 347, Vol. II, pp. 361-371, October 1981.

126. Cohen, N. S., Lo, G. A. and Crowley, J. C., "Model and Chemistry of HMX Combustion," AIAA JOURNAL, Vol. 23, No. 2, pp. 276-282, January 1985.

127. Beckstead, M. W. and McCarty, K. P., "Calculated Combustion Characteristics of Nitramine Mono-Propellants," 13th JANNAF Combustion Meeting, CPIA Pub. 281, pp. 57-68, December 1976.

128. Price, C. F., Boggs, T. L. and Bradley, H. H., "Modeling the Combustion of Monopropellants," 14th JANNAF Combustion Meeting, CPIA Pub. 292, Vol. I, pp. 307-324, October 1977.

129. Price, C. F., Boggs, T. L. and Derr, R. L., "The Steady State Combustion Behavior of Ammonium and HMX," Presented at the 17th Aerospace Sciences Meeting, New Orleans, LA, January 15-17, 1979.

130. Beckstead, M. W., "Combustion Mechanisms of Composite Solid Propellants," 19th JANNAF Combustion Meeting, CPIA Pub. 366, Vol. II, pp. 93-100, October 1982.

131. Parr, T. P., Hanson-Parr, D. L, Boggs, T. L. and Price, C. F., "Modeling of the Temperature Sensitivity of HMX Burning Rates using the Simple BDP Model," 19th JANNAF Combustion Meeting, CPIA Pub. 366, pp. 289-297, Vol. II, October 1982.

132. Price, C. F., Boggs, T. L., Parr, T. P, and Hanson-Parr, D. P., "A Modified BDP Model Applied to the Self-Deflagration of HMX," 19th JANNAF Combustion Meeting, CPIA Pub. 366, Vol. II, pp. 299-310, October 1982.

133. Price, C. F. and Boggs, T. L., "Modeling the Self-Deflagration of HMX," 20th JANNAF Combustion Meeting, CPIA Pub. 383, October 1983.

134. Price, C. F. and Boggs, T. L., "A Simultaneous Mathematical Treatment of Deflagration and Ignition Phenomena," 22nd JANNAF Combustion Meeting, CPIA Pub. 432, Vol. I, pp. 505-513, October 1985.

135. Cohen, N. S., Price, C. F., Strand, L. D. and Moy, B. K., "Combustion of Nitramine Propellants," 12th JANNAF Combustion Meeting, CPIA Pub. 273, Vol. I, pp. 49-58, August 1975.

136. Cohen, N. S., Price, C. F. and Strand, L. D., Analytical Model of the Combustion of Multicomponent Solid Propellants," AIAA Paper Number 77-927, AIAA/SAE Joint Propulsion Conference, July 1977.

137. Beckstead, M. W., "A Model for Solid Propellant Combustion," 14th JANNAF Combustion Meeting, CPIA Pub. 292, Vol. I, pp. 281-306, December 1977.

138. Cohen, N. S., "Review of Composite Propellant Burn Rate Modeling," AIAA Journal, Vol. 18, No. 3, March 1980.

139. Beckstead, M. W., "Modeling Calculations for HMX Composite Propellants," 16th JANNAF Combustion Meeting, CPIA Pub. 308, Vol. III, pp. 241-268, December 1979.

140. Beckstead, M. W. and McCarty, K. P., "Modeling Calculations for HMX Composite Propellants," AIAA Journal, Vol. 20, No. 1, pp. 106-115, January 1982.

141. Beckstead, M. W., "Ballistic Control of Solid Propellants," AFRPL-TR-81-058, Vol. III, April 1982.

142. Beckstead, M. W., Gordon, D. L. and Pack, E. S., "Ballistic Control of Solid Propellants," AFRPL-TR-81-058, Vol. IV, April 1982.

143. McCarty, K. P., Isom, K. B. and Jacox, J. L., "Effect of Formulation Variables on HMX Propellant Combustion," 15th JANNAF Combustion Meeting, PIA Pub. 297, Vol. II, pp. 11-42, February 1979.

144. McCarty, K. P., Beckstead, M. W., Isom, K. B. and Jacox, J. L., "RDX Propellant Combustion," 16th JANNAF Combustion Meeting, Vol. III, CPIA Pub. 308, pp. 269-288, December 1979.

145. Renie, J. P. and Osborn, J. R., "The Implicit Flame Interaction Model," 15th JANNAF Combustion Meeting, CPIA Pub. No. 297, Vol. II, pp. 217-240, February 1979.

146. Strahle, W. C., "Some Statistical Considerations in the Burning of Composite Solid Propellants," AIAA Journal, Vol. 16, pp. 843-847, August 1978.

147. Shannon, L. J. and Peterson, E. E., "Deflagration Characteristics of Ammonium Perchlorate Strands," AIAA Journal, Vol. 2, pp. 168-169, January 1964.

148. Carslaw, H. S. and Jaeger, J. C., Conduction of Heat in Solids, 2nd Ed., Oxford University Press, London, 1959.

149. Blomshield, F. S. and Osborn, J. R., "Effect of Variable Solid Phase Thermal Properties on Propellant Combustion," Acta Astronautica, Vol. 12, No. 12, pp. 1017-1025, 1985.

150. Blomshield, F. S., "AP/HMX Composite Propellant Modeling," 23rd JANNAF Combustion Meeting, CPIA Pub. 457, Vol. I, pp. 197-202, October 1986.

151. Cruise, D. R., "Theoretical Computations of Equilibrium Compositions, Thermodynamic Properties, and Performance Characteristics of Propellants Systems," NWC-TP-6037, April 1979.

152. Juhasz, A. A., "Round Robin Results of the Closed Bomb and Strand Burner," CPIA Pub. 361, July 1982.

153. Cohen, N. S., and Flanigan, D. A., "Mechanisms and Models of Solid-Propellant Burn Rate Temperature Sensitivity: A Review," AIAA Journal, Vol. 23, No. 10, October 1985.

154. Renie, J. P., Osborn, J. R. and Murphy, J. M., "Effect of Erosive Burning on Pressure and Temperature Sensitivity," Acta Astronautica, Vol. II, No. 7-8, pp. 459-467, 1984.

155. Cohen, N. S. and Flanigan, D. A., "A Literature Review of Solid Propellant Burn Rate Temperature Sensitivity," AFRPL-TR-83-042, October 1983.

156. Boggs, T. L., Price, D. E., Zurn, D. E., Derr, R. L. and Dibble, E. J., "Temperature Sensitivity of Deflagration Rates of Cyclotetramethylenetetranitramine (HMX)," 13th JANNAF Combustion Meeting, CPIA Pub. 281, pp. 45-56, December 1976.

157. Parr, T. P., Boggs, T. L., Price, C. F. and Hanson-Parr, D. P., "Measurement of the Temperature Sensitivities of ANAP-A and HMX Burning Rates," 19th JANNAF Combustion Meeting, CPIA Pub. 366, Vol. II, pp. 281-288, October 1982.

158. Stokes, B. B., Booth, D. W., Glick, R. L. and Cohen, N., "Temperature Sensitivity Technology," AFRPL-TR-86-023, June 1986.

159. Kubota, N. and Okuhara, H., "Burning Rate Temperature Sensitivity of HMX Propellants," AIAA 22nd Joint Propulsion Conference, Paper No. AIAA-86-1593, 1986.

APPENDIX

Sample Computer Printout

A sample computer printout is presented which represents a test run of the HYPEM computer code. In this test case the computer propellant consists of 44 percent HMX, 44 percent AP and 12 percent HTPB. The HMX crystals consist of a single distribution of particles with a mean particle size of 200μm with a sigma of 2.2. The AP crystals consist of a single distribution of particles with a mean particle size of 50μm with a sigma of 1.8. The propellant burning rate is evaluated at 500, 1000 and 2000 psia and at initial propellant temperatures of 248.15, 298.15 and 348.15°K. The first page of the output lists all HYPEM model inputs and initial conditions. After calculations are completed for a particular initial propellant temperature at all three pressures, a summary is printed which lists the burning rate at the three pressures along with the computed pressure exponent. After calculations are completed for all three initial propellant temperatures, each at all three pressures, a summary is printed which lists the burning rates, pressure exponents at all three initial propellant temperatures and the temperature sensitivity at each of the three pressures. Other important output includes the various surface temperatures and flame heights. For the HMX pseudo propellants the percent contribution from the various terms in the time averaged burn rate equation are output and for the AP pseudo propellants the percent heat transfer to the surface from the AP flame, primary flame and final flame are output.

```
******************************************* HIGH ENERGY PETITE ENSEMBLE MODEL -- HYPEM *******************************************

**********[FRED.HYPEM.HYFOR]TEST.DAT                       is the OUTPUT FILE and was CREATED at 22:16:28 on  7-NOV-88:

 RHOAP-AP CRYSTAL DENSITY                     1.950  g/cm^3        MODES-NUMBER OF OXIDIZER CRYSTAL MODES           2
  RHOX-HMX CRYSTAL DENSITY                    1.900  g/cm^3           XN-EXPONENT IN VF=CD**N EXPRESSION      3.00000
   RHOB-BINDER CRYSTAL DENSITY                0.920  g/cm^3           C1-AP CONSTANT FOR VF=CD**N EQ.         0.00000
   RHOT-TOTAL PROPELLANT DENSITY              1.702  g/cm^3           C2-HMX CONSTANT FOR VF=CD**N EQ.        0.00000
   ALAP-AP TOTAL MASS FRACTION              0.44000                  VAP-TOTAL AP VOLUMETRIC FRACTION         0.38397
    ALX-HMX TOTAL MASS FRACTION             0.44000                   VX-TOTAL HMX VOLUMETRIC FRACTION        0.39407
    ALB-BINDER TOTAL MASS FRACTION          0.12000                   VB-TOTAL BINDER VOLUMETRIC FRACTION     0.22196
    AAP-AP DECOMPOSITION FREQUENCY FACTOR 173859.00  g/cm^2-sec    EAP-AP DECOMPOSITION ACTIVATION ENERGY   22000.00  cal/mole
     AX-HMX DECOMPOSITION FREQUENCY FACTOR 0.117E+18  g/cm^2-sec     EX-HMX DECOMPOSITION ACTIVATION ENERGY  50000.00  cal/mole
     AB-BINDER PYROLYSIS FREQUENCY FACTOR     300.00  g/cm^2-sec     EB-BINDER PYROLYSIS ACTIVATION ENERGY   16900.00  cal/mole
   CSAP-AP SOLID PHASE SPECIFIC HEAT        0.26150  cal/g-K      DCSAP-CHANGE IN CSAP WITH TEMPERATURE    .000519400  cal/g-K^2
    CSX-HMX SOLID PHASE SPECIFIC HEAT       0.24600  cal/g-K       DCSX-CHANGE IN CSX WITH TEMPERATURE     .000652000  cal/g-K^2
    CSB-BINDER SOLID PHASE SPECIFIC HEAT    0.45490  cal/g-K       DCSB-CHANGE IN CSB WITH TEMPERATURE     .000593000  cal/g-K^2
   CPAP-AP GAS PHASE SPECIFIC HEAT          0.23218  cal/g-K     XLAMAP-AP GAS PHASE THERMAL CONDUCTIVITY  .000399000  cal/cm-s-K
    CPX-HMX GAS PHASE SPECIFIC HEAT         0.25333  cal/g-K      XLAMX-HMX GAS PHASE THERMAL CONDUCTIVITY .003611200  cal/cm-s-K
 FACTAP-AP FLAME TEMPERATURE PARAMETER      2.44008              DIFFAP-AP GAS PHASE THERMAL DIFFUSIVITY   .162440002  cm^2-A/s-K
  FACTX-HMX FLAME TEMPERATURE PARAMETER     2.29026               DIFFX-HMX GAS PHASE THERMAL DIFFUSIVITY  .162440002  cm^2-A/s-K
   AAPF-AP FLAME FREQUENCY FACTOR   (s-sec)   278.5  g/cm^3-s-A     APF-PRIMARY FLAME FREQUENCY FACTOR         179.0  g/cm^3-s-A
   EAPF-AP FLAME ACTIVATION ENERGY  (A-atm) 10450.0  cal/mole       EPF-PRIMARY FLAME ACTIVATION ENERGY      20594.0  cal/mole
  DELAP-AP FLAME REACTION ORDER                1.64              DELPF-PRIMARY FLAME REACTION ORDER           2.00
    AXF-HMX FLAME FREQUENCY FACTOR             13.8  g/cm^3-s-A   AXPF-HMX PRIMARY FLAME FREQUENCY FACTOR       77.3  g/cm^3-s-A
    EXF-HMX FLAME ACTIVATION ENERGY         22021.0  cal/mole      EXPF-HMX PRIMARY FLAME ACTIVATION ENERGY  16746.0  cal/mole
  DELXF-HMX FLAME REACTION ORDER               1.39              DELXPF-HMX PRIMARY FLAME REACTION ORDER      1.15
   HLAP-AP LATENT HEAT                       39.000  cal/g        PHIPF-AP PF STOICH. OXIDIZER/FUEL RATIO     5.211
    HLX-HMX LATENT HEAT                       5.000  cal/g        PHIFF-FF STOICH. OXIDIZER/FUEL RATIO       12.129
    QDB-BINDER HEAT OF DECOMPOSITION        500.000  cal/g       PHIXPF-HMX PF STOICH. OXIDIZER/FUEL RATIO   10.143
 CIAPRF-AP REF. IGNITION DELAY CONSTANT      4.3210                CIXRF-HMX REF. IGNITION DELAY CONSTANT     0.7800
 EXIGAP-AP IGNITION DELAY DIAMETER EXPONENT  1.7000                EXIGX-HMX IGNITION DELAY DIAMETER EXPONENT 1.1000
   TMAP-AP MELTING POINT                     865.00  K               TMX-HMX MELTING POINT                    553.00  K
 TREFAP-AP REF. TEMP. FOR IGNITION DELAY     480.00  K             TREFX-HMX REF. TEMP. FOR IGNITION DELAY    675.00  K

 ETASTA-INITIAL NON-DIM. DIFFUSITON HEIGHT  0.10000              ETALIM-B-S FLAME CONVERGENCE LIMIT       .000100000
 NUMBST-MAX NUMBER OF B-S TERMS CONSIDERED      100              BSTLIM-MINIMUM TERM IS B-S FLAME SERIES  .000010000
 ITLIM1-MAX ITERATIONS FOR B-S ANALYSIS         100                TSLIM-CONVERGENCE LIMIT ON SURFACE TEMP.  0.10000  K
 ITLIM2-MAX ITERATIONS FOR SURFACE TEMP.        100                  RBA-BINDER BURN RATE COEFFICIENT          4.54
 TSAPIN-INITIAL AP SURFACE TEMPERATURE       900.00  K           TSMAXA-MAXIMUM AP SURFACE TEMPERATURE     2000.00  K
  TSXIN-INITIAL HMX SURFACE TEMPERATURE      600.00  K           TSMAXX-MAXIMUM HMX SURFACE TEMPERATURE     800.00  K
  TSBIN-INITIAL BINDER SURFACE TEMPERATURE  1200.00  K           TSMAXB-MAX. BINDER SURFACE TEMPERATURE    2500.00  K
  BPMAX-MAX. FRACTION OF XPF HEAT TO HMX     0.8000                  BPA-BP CONSTANT                        0.9344
  BFMIN-MINIMUM FRACTION OF HMX IN XPF       0.2000                  FRA-FRACTION BINDER REACTING CONSTANT  0.8749
  FOALD-INTEGRAL OF F/ALD OVER ALL D       0.999796                  TBA-BINDER DELAY TIME CONSTANT         1.8991
   ALDF-AP MASS FRACTION AUGMENTATION      0.985000              ALDFMN-MINIMUM VALUE FOR ALDF            0.900000
  ALDFX-HMX MASS FRACTION AUGMENTATION     1.015464              ALDFMX-MAXIMUM VALUE FOR ALDF            1.125000

  IFLAG-OPTION FLAGS (1-10)              0000000000              IDEBUG-DEBUG OPTION FLAGS (1-10)         0000000000

 COMBUSTION PRESSURE (psia) =  500.00   1000.00   2000.00
 INITIAL TEMPERATURE (K)    =  248.15    298.15    348.15

 MODE OXI.   MEAN   MODE WIDTH   MASS     NUMBER    LOG.   STARTING    ENDING
  NO. TYPE DIAMETER PARAMETER FRACTION OF PART.   DIF.   PART. SIZE PART. SIZE
             (DBAR)   (SIGMA)    (ALM)    (IDIV)  (DLND)  (DSTART)    (DSTOP)

  1    AP   50.00    1.800     0.4400      23    0.1986      5.63      444.42
  2   HMX  200.00    2.200     0.4400      23    0.2664     10.67     3747.90
```

```
*****PSEUDO PROPELLANT INPUT PARAMETERS for all 2 MODE(S) for all PRESSURES and TEMPERATURES

              *****MODE 1*****                               *****MODE 2*****

        D         F        AL     VOL     RHO              D         F        AL     VOL     RHO

 1     5.63 0.000299 0.8668 0.7543 1.6969        24    10.67 0.000223 0.8936 0.8026 1.7066
 2     6.86 0.000990 0.8668 0.7543 1.6969        25    13.93 0.000738 0.8936 0.8026 1.7066
 3     8.37 0.002930 0.8668 0.7543 1.6969        26    18.18 0.002184 0.8936 0.8026 1.7066
 4    10.21 0.007733 0.8668 0.7543 1.6969        27    23.73 0.005765 0.8936 0.8026 1.7066
 5    12.45 0.018208 0.8668 0.7543 1.6969        28    30.98 0.013574 0.8936 0.8026 1.7066
 6    15.19 0.038246 0.8668 0.7543 1.6969        29    40.44 0.028512 0.8936 0.8026 1.7066
 7    18.52 0.071665 0.8668 0.7543 1.6969        30    52.78 0.053426 0.8936 0.8026 1.7066
 8    22.59 0.119798 0.8668 0.7543 1.6969        31    68.90 0.089308 0.8936 0.8026 1.7066
 9    27.55 0.178650 0.8668 0.7543 1.6969        32    89.93 0.133182 0.8936 0.8026 1.7066
10    33.61 0.237667 0.8668 0.7543 1.6969        33   117.39 0.177179 0.8936 0.8026 1.7066
11    40.99 0.282065 0.8668 0.7543 1.6969        34   153.22 0.210277 0.8936 0.8026 1.7066
12    50.00 0.298637 0.8668 0.7543 1.6969        35   200.00 0.222630 0.8936 0.8026 1.7066
13    60.99 0.282065 0.8668 0.7543 1.6969        36   261.06 0.210277 0.8936 0.8026 1.7066
14    74.38 0.237667 0.8668 0.7543 1.6969        37   340.75 0.177178 0.8936 0.8026 1.7066
15    90.73 0.178650 0.8668 0.7543 1.6969        38   444.78 0.133181 0.8936 0.8026 1.7066
16   110.66 0.119798 0.8668 0.7543 1.6969        39   580.57 0.089308 0.8936 0.8026 1.7066
17   134.98 0.071665 0.8668 0.7543 1.6969        40   757.80 0.053426 0.8936 0.8026 1.7066
18   164.63 0.038246 0.8668 0.7543 1.6969        41   989.15 0.028512 0.8936 0.8026 1.7066
19   200.80 0.018208 0.8668 0.7543 1.6969        42  1291.12 0.013574 0.8936 0.8026 1.7066
20   244.92 0.007733 0.8668 0.7543 1.6969        43  1685.28 0.005765 0.8936 0.8026 1.7066
21   298.73 0.002930 0.8668 0.7543 1.6969        44  2199.77 0.002184 0.8936 0.8026 1.7066
22   364.37 0.000990 0.8668 0.7543 1.6969        45  2871.33 0.000738 0.8936 0.8026 1.7066
23   444.42 0.000299 0.8668 0.7543 1.6969        46  3747.91 0.000223 0.8936 0.8026 1.7066
```

```
***** MODE 1 AP*** 23 PARTICLES, the PRESSURE IS   500.00 psia and the INITIAL PROPELLANT TEMPERATURE is   248.15 DEGREES KELVIN

       D      R     TSOX   TSB     TS     BF      XAPK       XPFK       XPFD      XFFD     HTAP   HTPF   HTFF  TF   TSQDAP  TSQDB ITER
   MICRONS cm/s      K      K      K              . . . . . . MICRONS . . . . . .           % HEAT TRANSFER   K      K       K

 1    5.63  1.271  993.2 1535.2 1065.4 1.000    16.130     6.784      1.442     0.000    0.00 100.00   0.00 2485.  -540.  -174.  6
 2    6.86  1.257  992.1 1532.0 1064.0 1.000    15.948     6.708      1.795     0.000    0.00 100.00   0.00 2485.  -540.  -174.  4
 3    8.37  1.240  990.8 1528.2 1062.4 1.000    15.721     6.614      2.244     0.000    0.00 100.00   0.00 2485.  -541.  -174.  4
 4   10.21  1.218  989.1 1523.3 1060.2 1.000    15.439     6.496      2.816     0.000    0.00 100.00   0.00 2485.  -541.  -174.  4
 5   12.45  1.191  986.9 1517.2 1057.5 1.000    15.087     6.349      3.551     0.000    0.00 100.00   0.00 2485.  -542.  -174.  4
 6   15.19  1.157  984.0 1509.5 1054.0 1.000    14.649     6.167      4.500     0.000    0.00 100.00   0.00 2485.  -543.  -175.  4
 7   18.52  1.116  980.4 1499.7 1049.6 1.000    14.111     5.943      5.729     0.000    0.00 100.00   0.00 2485.  -544.  -175.  4
 8   22.59  1.065  975.8 1487.5 1043.9 1.000    13.456     5.669      7.323     0.000    0.00 100.00   0.00 2486.  -546.  -176.  5
 9   27.55  0.963  966.3 1461.8 1032.3 0.759    12.143     5.122      9.245     9.944    9.82  81.58   8.60 2486.  -549.  -177.  5
10   33.61  0.887  957.9 1441.5 1022.3 0.547    11.160     4.711     11.793    12.038   20.66  62.18  17.16 2487.  -551.  -177.  5
11   40.99  0.830  949.9 1425.5 1013.2 0.396    10.431     4.406     15.227    15.001   29.75  46.85  23.40 2488.  -554.  -178.  5
12   50.00  0.783  939.2 1411.9 1002.2 0.285     9.824     4.154     19.877    19.117   37.38  34.94  27.68 2488.  -558.  -180.  5
13   60.99  0.744  918.2 1399.8  982.4 0.204     9.295     3.937     26.270    24.841   43.84  25.84  30.32 2489.  -565.  -182.  6
14   74.38  0.703  898.8 1386.9  963.8 0.144     8.754     3.713     34.922    32.640   49.59  18.89  31.52 2490.  -572.  -184.  6
15   90.73  0.657  887.8 1371.8  952.2 0.101     8.164     3.466     46.425    43.070   54.88  13.65  31.47 2491.  -576.  -185.  5
16  110.66  0.609  876.3 1355.3  940.1 0.070     7.556     3.211     61.802    57.030   59.75   9.77  30.48 2492.  -580.  -187.  5
17  134.98  0.560  864.4 1337.6  927.5 0.048     6.936     2.951     82.239    75.578   64.25   6.93  28.82 2492.  -584.  -188.  6
18  164.63  0.512  852.2 1318.7  914.4 0.033     6.315     2.690    109.240   100.045   68.39   4.88  26.73 2493.  -589.  -190.  5
19  200.80  0.463  839.7 1298.9  900.9 0.023     5.708     2.434    144.775   132.175   72.17   3.41  24.42 2494.  -594.  -191.  5
20  244.92  0.417  828.9 1278.1  888.3 0.015     5.121     2.186    191.146   174.047   75.56   2.37  22.06 2495.  -598.  -192.  5
21  298.73  0.372  821.9 1256.5  879.8 0.010     4.560     1.948    250.981   228.083   78.55   1.64  19.81 2495.  -600.  -193.  5
22  364.37  0.330  814.7 1234.7  870.6 0.007     4.039     1.727    328.629   298.076   81.15   1.13  17.72 2496.  -603.  -194.  5
23  444.42  0.291  807.4 1212.9  861.4 0.005     3.563     1.524    429.266   388.611   83.42   0.77  15.81 2496.  -606.  -195.  5

********** THE BURN RATE for this MODE is 0.8032 cm/sec or 0.3162 in/sec and the AVERAGE SURFACE TEMPERATURE is  994.07 K

***** MODE 2 HMX** 23 PARTICLES, the PRESSURE IS   500.00 psia and the INITIAL PROPELLANT TEMPERATURE is   248.15 DEGREES KELVIN

       D      ROX     RB      R     TSOX    TSB     TS     BF   BP   FRB  DNOM1 DNOM2 DNOM3 DNOM4    XXK   XXPFK  XXPFD    TX     TFX   ITER
   MICRONS .......cm/sec......      K       K       K                   ........PERCENT........    .....MICRONS......    K      K     #

24   10.67  1.229  0.995  0.546  655.1 1470.1  741.8 1.00 0.40 0.30 39.84 45.51  7.70  6.95    21.3  115.0     9.7 3148.2 2601.4 11
25   13.93  1.221  0.989  0.529  655.0 1468.6  741.6 1.00 0.40 0.30 38.84 46.72  7.50  6.95    27.9  114.3    12.7 3148.2 2601.4  3
26   18.18  1.212  0.982  0.511  654.9 1466.7  741.3 1.00 0.40 0.30 37.79 47.98  7.29  6.95    36.4  113.4    16.6 3148.3 2601.5  3
27   23.73  1.200  0.972  0.492  654.7 1464.3  740.9 1.00 0.40 0.30 36.71 49.27  7.07  6.95    47.5  112.3    21.6 3148.3 2601.5  3
28   30.98  1.184  0.960  0.470  654.5 1461.1  740.3 1.00 0.40 0.30 35.61 50.59  6.85  6.96    62.0  110.8    28.2 3148.3 2601.5  3
29   40.44  1.164  0.945  0.448  654.2 1457.1  739.6 1.00 0.40 0.30 34.48 51.95  6.62  6.96    80.9  109.0    36.9 3148.4 2601.6  3
30   52.78  1.290  0.842  0.466  656.0 1428.8  738.2 0.78 0.30 0.27 32.34 53.42  7.00  7.25   105.6  114.3    48.1 3148.4 2601.6  4
31   68.90  1.106  0.901  0.396  653.4 1445.2  737.6 1.00 0.40 0.29 32.05 54.85  6.11  6.99   137.8  103.7    62.8 3148.5 2601.7  4
32   89.93  1.067  0.870  0.368  652.7 1436.8  736.2 1.00 0.40 0.29 30.93 56.21  5.88  6.98   179.9  100.0    82.0 3148.6 2601.8  3
33  117.39  1.018  0.833  0.338  652.0 1426.2  734.3 1.00 0.40 0.29 29.70 57.69  5.61  7.00   234.8   95.5   107.0 3148.7 2601.9  3
34  153.22  0.960  0.788  0.305  651.0 1413.1  732.0 1.00 0.40 0.29 28.45 59.20  5.34  7.01   306.4   90.1   139.6 3148.8 2602.0  3
35  200.00  0.892  0.734  0.271  649.7 1396.9  729.2 1.00 0.40 0.29 27.18 60.74  5.06  7.03   309.1   83.8   182.3 3149.0 2602.2  3
36  261.06  0.815  0.674  0.235  648.2 1377.4  725.8 1.00 0.41 0.29 25.88 62.31  4.77  7.04   282.2   76.5   237.9 3149.2 2602.4  3
37  340.75  0.758  0.618  0.208  647.0 1358.5  722.7 0.83 0.37 0.28 24.53 63.91  4.40  7.16   262.5   71.0   310.6 3149.4 2602.6  3
38  444.78  0.742  0.523  0.188  646.6 1323.4  718.6 0.66 0.29 0.26 22.75 65.52  4.36  7.36   256.7   67.0   405.4 3149.6 2602.8  3
39  580.57  0.748  0.401  0.167  646.8 1270.7  713.2 0.53 0.21 0.24 19.99 67.76  4.64  7.62   258.9   62.4   529.1 3149.9 2603.1  4
40  757.80  0.769  0.288  0.149  647.2 1210.8  707.2 0.43 0.14 0.22 17.35 69.52  5.35  7.77   265.9   56.5   690.6 3150.3 2603.5  4
41  989.15  0.794  0.204  0.129  647.8 1154.1  701.6 0.35 0.09 0.21 14.60 71.31  6.22  7.87   274.6   49.3   901.5 3150.6 2603.8  4
42 1291.12  0.818  0.146  0.109  648.3 1103.9  696.8 0.28 0.06 0.20 11.93 73.11  7.02  7.94   282.9   41.8  1176.7 3150.9 2604.1  4
43 1685.28  0.839  0.106  0.089  648.7 1059.9  692.5 0.22 0.04 0.19  9.48 74.91  7.63  7.98   290.1   34.6  1535.9 3151.2 2604.4  4
44 2199.77  0.847  0.078  0.070  648.9 1021.2  688.5 0.20 0.03 0.19  7.39 76.68  7.92  8.00   292.7   28.0  2004.8 3151.4 2604.6  4
45 2871.33  0.847  0.058  0.053  648.9  986.4  684.8 0.20 0.03 0.18  5.64 78.43  7.92  8.01   292.5   22.4  2616.8 3151.6 2604.8  4
46 3747.91  0.846  0.044  0.040  648.8  954.7  681.4 0.20 0.02 0.18  4.19 80.14  7.67  8.01   292.3   17.8  3415.7 3151.8 2605.0  4

********** THE BURN RATE for this MODE is 0.2763 cm/sec or 0.1088 in/sec and the AVERAGE SURFACE TEMPERATURE is  727.11 K
```

```
***** MODE 1 AP*** 23 PARTICLES, the PRESSURE IS  1000.00 psia and the INITIAL PROPELLANT TEMPERATURE is   248.15 DEGREES KELVIN

       D      R    TSOX    TSB     TS      BF        XAPK       XPFK       XPFD        XFFD      HTAP    HTPF   HTFF   TF   TSQDAP  TSQDB ITER
   MICRONS cm/s     K       K       K                . . . . . . .  MICRONS  . . . . . . .       % HEAT TRANSFER      K      K       K

 1     5.63 2.279 1048.0 1715.6 1136.9 1.000      9.226      2.968      1.554      0.000     0.00 100.00    0.00 2499.  -571.  -168.  9
 2     6.86 2.220 1045.3 1706.6 1133.4 1.000      8.981      2.890      1.959      0.000     0.00 100.00    0.00 2499.  -572.  -169.  4
 3     8.37 2.148 1041.9 1695.3 1129.0 1.000      8.680      2.794      2.480      0.000     0.00 100.00    0.00 2499.  -573.  -169.  4
 4    10.21 2.059 1037.7 1681.2 1123.4 1.000        313      2.678      3.153      0.000     0.00 100.00    0.00 2500.  -574.  -169.  4
 5    12.45 1.953 1032.3 1663.8 1116.4 1.000      7.874      2.537      4.021      0.000     0.00 100.00    0.00 2500.  -576.  -170.  5
 6    15.19 1.813 1024.9 1640.0 1106.8 0.965      7.297      2.353      5.122      5.803     1.27  97.63    1.10 2501.  -578.  -171.  4
 7    18.52 1.597 1012.6 1601.0 1090.9 0.675      6.411      2.071      6.427      6.806    14.08  74.42   11.50 2502.  -583.  -172.  5
 8    22.59 1.462 1003.8 1574.8 1079.9 0.483      5.857      1.893      8.209      8.308    24.86  55.92   19.23 2502.  -586.  -173.  5
 9    27.55 1.360  996.3 1553.9 1070.6 0.347      5.439      1.760     10.611     10.419    33.76  41.61   24.62 2503.  -588.  -174.  5
10    33.61 1.272  988.7 1535.4 1061.5 0.248      5.079      1.645     13.843     13.324    41.22  30.67   28.11 2503.  -591.  -174.  5
11    40.99 1.190  980.1 1517.0 1051.6 0.176      4.742      1.537     18.186     17.279    47.60  22.39   30.01 2504.  -594.  -175.  5
12    50.00 1.110  968.0 1498.4 1038.6 0.124      4.412      1.431     24.029     22.632    53.16  16.19   30.65 2505.  -598.  -176.  5
13    60.99 1.034  944.0 1480.0 1015.4 0.086      4.095      1.331     31.991     29.913    58.07  11.62   30.31 2506.  -607.  -179.  6
14    74.38 0.955  921.7 1459.7  993.4 0.060      3.765      1.226     42.573     39.584    62.57   8.26   29.16 2507.  -615.  -181.  6
15    90.73 0.870  908.2 1436.8  978.6 0.041      3.421      1.115     56.318     52.170    66.71   5.82   27.48 2508.  -620.  -183.  6
16   110.66 0.786  894.3 1412.6  963.4 0.028      3.084      1.007     74.313     68.616    70.44   4.07   25.49 2509.  -626.  -185.  6
17   134.98 0.705  880.2 1387.6  947.8 0.019      2.759      0.902     97.762     89.992    73.78   2.83   23.39 2510.  -631.  -186.  5
18   164.63 0.629  866.0 1362.2  932.1 0.013      2.453      0.803    128.232    117.689    76.75   1.96   21.29 2511.  -637.  -188.  5
19   200.80 0.558  851.7 1336.5  916.2 0.009      2.169      0.711    167.741    153.489    79.38   1.35   19.27 2512.  -643.  -190.  5
20   244.92 0.492  839.3 1310.6  902.1 0.006      1.907      0.626    218.567    199.456    81.68   0.92   17.40 2513.  -648.  -191.  5
21   298.73 0.430  831.0 1284.3  891.3 0.004      1.667      0.547    283.162    257.869    83.64   0.63   15.73 2513.  -651.  -192.  5
22   364.37 0.376  822.5 1258.5  880.6 0.003      1.452      0.477    366.122    332.722    85.34   0.43   14.22 2514.  -655.  -193.  5
23   444.42 0.327  814.2 1233.2  870.0 0.002      1.261      0.415    472.561    428.543    86.84   0.29   12.87 2514.  -658.  -194.  5

********** THE BURN RATE for this MODE is 1.1243 cm/sec or 0.4426 in/sec and the AVERAGE SURFACE TEMPERATURE is 1028.10 K

***** MODE 2 HMX** 23 PARTICLES, the PRESSURE IS  1000.00 psia and the INITIAL PROPELLANT TEMPERATURE is   248.15 DEGREES KELVIN

       D      ROX     RB      R     TSOX    TSB     TS     BF   BP   FRB  DNOM1 DNOM2 DNOM3 DNOM4    XXK   XXPFK  XXPFD     TX     TFX  ITER
   MICRONS .......cm/sec......       K       K      K                    ........PERCENT........    .....MICRONS......     K      K     #

24    10.67  1.826  1.442  0.807  662.0 1570.8  758.6 1.00 0.39 0.30 39.59 45.51  8.00  6.89   21.3   74.4     9.7 3196.2 2625.1 12
25    13.93  1.809  1.430  0.779  661.8 1568.3  758.2 1.00 0.39 0.30 38.59 46.72  7.79  6.90   27.9   73.7    12.7 3196.2 2625.1  3
26    18.18  1.788  1.414  0.749  661.6 1565.1  757.7 1.00 0.39 0.30 37.55 47.98  7.57  6.90   36.4   72.8    16.6 3196.3 2625.1  3
27    23.73  1.761  1.394  0.717  661.3 1560.9  757.0 1.00 0.39 0.30 36.48 49.27  7.34  6.91   47.5   71.7    21.6 3196.3 2625.2  3
28    30.98  1.726  1.368  0.682  661.0 1555.5  756.2 1.00 0.39 0.30 35.39 50.59  7.10  6.92   62.0   70.3    28.2 3196.4 2625.2  3
29    40.44  1.682  1.335  0.643  660.5 1548.7  755.0 1.00 0.39 0.30 34.27 51.95  6.86  6.93   80.9   68.6    36.9 3196.4 2625.3  3
30    52.78  1.628  1.294  0.602  660.0 1540.0  753.6 1.00 0.39 0.30 33.12 53.33  6.60  6.94  105.6   66.4    48.1 3196.5 2625.4  3
31    68.90  1.561  1.244  0.557  659.2 1529.0  751.8 1.00 0.39 0.30 31.95 54.75  6.33  6.96  137.8   63.7    62.8 3196.6 2625.5  3
32    89.93  1.480  1.183  0.508  658.3 1515.3  749.5 1.00 0.39 0.30 30.76 56.21  6.06  6.98  179.9   60.4    82.0 3196.8 2625.6  3
33   117.39  1.384  1.110  0.456  657.2 1498.4  746.7 1.00 0.40 0.30 29.54 57.69  5.77  7.01  173.5   56.5   107.0 3196.9 2625.8  3
34   153.22  1.273  1.026  0.402  655.7 1477.8  743.2 1.00 0.40 0.30 28.29 59.20  5.47  7.04  159.5   52.0   139.6 3197.1 2626.0  3
35   200.00  1.224  0.935  0.367  655.1 1454.6  740.1 0.80 0.34 0.28 26.86 60.75  5.18  7.21  153.4   49.4   182.3 3197.3 2626.2  3
36   261.06  1.216  0.783  0.339  655.0 1411.8  735.5 0.65 0.27 0.26 24.96 62.32  5.30  7.42  152.4   46.9   237.9 3197.6 2626.5  3
37   340.75  1.238  0.603  0.307  655.3 1353.0  729.5 0.53 0.19 0.24 22.25 64.32  5.78  7.65  155.0   43.8   310.6 3198.0 2626.8  4
38   444.78  1.277  0.441  0.278  655.8 1289.0  723.2 0.43 0.13 0.22 19.50 66.03  6.68  7.80  159.8   39.7   405.4 3198.3 2627.2  4
39   580.57  1.321  0.319  0.245  656.4 1228.7  717.3 0.35 0.09 0.21 16.61 67.77  7.72  7.90  165.3   34.8   529.1 3198.7 2627.5  4
40   757.80  1.363  0.232  0.210  656.9 1175.0  712.0 0.29 0.06 0.20 13.78 69.53  8.72  7.97  170.5   29.7   690.6 3199.0 2627.8  4
41   989.15  1.398  0.171  0.174  657.3 1127.2  707.3 0.23 0.04 0.20 11.15 71.32  9.51  8.02  174.9   24.7   901.5 3199.2 2628.1  4
42  1291.12  1.414  0.127  0.140  657.5 1084.7  703.0 0.20 0.03 0.19  8.84 73.11  9.99  8.05  176.9   20.1  1176.7 3199.5 2628.4  4
43  1685.28  1.414  0.095  0.109  657.5 1046.4  698.9 0.20 0.03 0.19  6.89 74.91 10.13  8.08  176.7   16.2  1535.9 3199.7 2628.6  4
44  2199.77  1.413  0.072  0.083  657.5 1011.3  695.2 0.20 0.02 0.18  5.23 76.69  9.99  8.09  176.6   12.9  2004.8 3199.9 2628.8  4
45  2871.33  1.413  0.054  0.061  657.5  979.1  691.7 0.20 0.02 0.18  3.89 78.44  9.59  8.09  176.5   10.2  2616.8 3200.1 2629.0  4
46  3747.91  1.413  0.042  0.044  657.5  949.4  688.6 0.20 0.02 0.18  2.82 80.13  8.96  8.08  176.5    8.0  3415.7 3200.3 2629.2  4

********** THE BURN RATE for this MODE is 0.3840 cm/sec or 0.1512 in/sec and the AVERAGE SURFACE TEMPERATURE is  737.04 K
```

```
***** MODE 1 AP*** 23 PARTICLES, the PRESSURE IS  2000.00 psia and the INITIAL PROPELLANT TEMPERATURE is   248.15 DEGREES KELVIN

        D      R    TSOX    TSB      TS      BF        XAPK       XPFK       XPFD         XFFD      HTAP   HTPF    HTFF   TF  TSQDAP  TSQDB ITER
    MICRONS cm/s     K       K       K                 . . . . . . MICRONS . . . . . . .          % HEAT TRANSFER       K     K       K

 1     5.63 3.737 1099.4 1905.5 1206.8 1.000        4.795      1.194      1.727      0.000    0.00 100.00   0.00 2511.  -595.  -164.  9
 2     6.86 3.522 1092.9 1880.5 1197.8 1.000        4.511      1.124      2.196      0.000    0.00 100.00   0.00 2511.  -597.  -164.  4
 3     8.37 3.274 1084.9 1850.6 1186.9 1.000        4.185      1.043      2.796      0.000    0.00 100.00   0.00 2512.  -600.  -165.  4
 4    10.21 2.859 1070.6 1797.7 1167.4 0.782        3.641      0.910      3.495      3.816    9.06  83.57   7.37 2513.  -605.  -166.  5
 5    12.45 2.557 1058.9 1756.3 1151.8 0.551        3.247      0.812      4.417      4.567   21.18  62.51  16.31 2514.  -609.  -167.  5
 6    15.19 2.351 1050.1 1726.5 1140.2 0.394        2.980      0.746      5.665      5.653   30.99  46.41  22.59 2514.  -612.  -168.  5
 7    18.52 2.185 1042.4 1701.2 1130.2 0.282        2.764      0.693      7.341      7.157   39.05  34.19  26.76 2515.  -615.  -169.  5
 8    22.59 2.035 1034.8 1677.3 1120.4 0.201        2.570      0.644      9.583      9.205   45.81  24.95  29.24 2516.  -617.  -170.  5
 9    27.55 1.889 1026.6 1653.0 1110.1 0.142        2.381      0.598     12.572     11.961   51.61  18.04  30.35 2516.  -620.  -170.  5
10    33.61 1.744 1017.3 1627.9 1098.7 0.099        2.193      0.551     16.535     15.637   56.67  12.92  30.41 2517.  -623.  -171.  5
11    40.99 1.598 1006.3 1601.0 1085.5 0.069        2.005      0.504     21.764     20.496   61.16   9.17  29.67 2518.  -627.  -172.  5
12    50.00 1.453  991.3 1573.0 1068.8 0.047        1.818      0.458     28.653     26.889   65.15   6.46  28.38 2519.  -633.  -174.  5
13    60.99 1.319  964.0 1545.4 1041.4 0.032        1.643      0.415     37.874     35.381   68.73   4.53  26.74 2520.  -643.  -177.  6
14    74.38 1.187  938.7 1516.3 1015.7 0.022        1.471      0.372     49.875     46.394   71.98   3.16  24.87 2522.  -653.  -180.  6
15    90.73 1.055  922.8 1485.1  997.6 0.015        1.303      0.330     65.109     60.385   74.85   2.18  22.97 2523.  -660.  -181.  5
16   110.66 0.931  906.7 1453.5  979.5 0.010        1.147      0.291     84.726     78.341   77.39   1.50  21.11 2524.  -666.  -183.  5
17   134.98 0.818  890.7 1422.0  961.5 0.007        1.004      0.255    109.932    101.334   79.63   1.03  19.34 2525.  -673.  -185.  5
18   164.63 0.716  874.8 1391.0  943.6 0.005        0.876      0.223    142.303    130.760   81.61   0.71  17.68 2526.  -680.  -187.  9
19   200.80 0.624  859.1 1360.6  925.9 0.003        0.762      0.194    183.879    168.423   83.38   0.48  16.14 2527.  -686.  -189.  6
20   244.92 0.542  845.6 1330.7  910.2 0.002        0.660      0.168    236.932    216.383   84.94   0.33  14.73 2528.  -692.  -190.  5
21   298.73 0.469  836.3 1301.0  898.2 0.001        0.569      0.145    303.679    276.710   86.27   0.22  13.51 2528.  -696.  -191.  5
22   364.37 0.404  827.1 1272.4  886.4 0.001        0.490      0.125    388.948    353.598   87.47   0.15  12.38 2529.  -701.  -193.  5
23   444.42 0.349  818.0 1244.8  874.9 0.001        0.422      0.108    498.048    451.752   88.56   0.10  11.34 2530.  -705.  -194.  5

********** THE BURN RATE for this MODE is 1.4746 cm/sec or 0.5806 in/sec and the AVERAGE SURFACE TEMPERATURE is 1057.11 K

***** MODE 2 HMX** 23 PARTICLES, the PRESSURE IS  2000.00 psia and the INITIAL PROPELLANT TEMPERATURE is   248.15 DEGREES KELVIN

        D      ROX     RB      R     TSOX    TSB      TS    BF   BP   FRB  DNOM1 DNOM2 DNOM3 DNOM4    XXK   XXPFK  XXPFD    TX     TFX  ITER
    MICRONS .......cm/sec......     K       K       K                    .........PERCENT........    .....MICRONS......    K      K     #

24    10.67 2.689  2.070  1.180  668.8 1682.9  776.7 1.00 0.38 0.31 39.30 45.52  8.34  6.84    21.3   47.8     9.7 3237.1 2645.9  9
25    13.93 2.652  2.043  1.134  668.5 1678.6  776.0 1.00 0.38 0.31 38.31 46.72  8.12  6.85    27.9   47.2    12.7 3237.2 2646.0  3
26    18.18 2.605  2.009  1.084  668.2 1673.1  775.1 1.00 0.38 0.31 37.28 47.98  7.88  6.87    36.4   46.3    16.6 3237.2 2646.0  3
27    23.73 2.545  1.966  1.029  667.8 1666.0  774.0 1.00 0.38 0.31 36.22 49.27  7.63  6.88    47.5   45.3    21.6 3237.3 2646.1  3
28    30.98 2.471  1.912  0.969  667.3 1656.9  772.6 1.00 0.38 0.31 35.13 50.59  7.37  6.90    62.0   44.0    28.2 3237.4 2646.2  3
29    40.44 2.379  1.845  0.903  666.6 1645.5  770.7 1.00 0.38 0.31 34.02 51.95  7.10  6.93    80.9   42.4    36.9 3237.5 2646.3  3
30    52.78 2.266  1.763  0.832  665.7 1631.2  768.4 1.00 0.38 0.31 32.88 53.33  6.82  6.96   103.8   40.4    48.1 3237.6 2646.4  3
31    68.90 2.132  1.664  0.755  664.7 1613.4  765.6 1.00 0.39 0.30 31.72 54.75  6.53  7.00    97.6   38.0    62.8 3237.8 2646.6  3
32    89.93 2.004  1.554  0.682  663.6 1592.7  762.4 0.94 0.37 0.30 30.49 56.22  6.21  7.09    91.7   35.7    82.0 3238.0 2646.8  3
33   117.39 1.972  1.393  0.637  663.3 1560.8  758.8 0.77 0.32 0.28 28.93 57.69  6.09  7.29    90.3   34.3   107.0 3238.2 2647.0  3
34   153.22 1.986  1.158  0.596  663.4 1509.7  753.5 0.64 0.24 0.26 26.90 59.21  6.38  7.50    90.9   32.7   139.6 3238.5 2647.3  3
35   200.00 2.036  0.899  0.550  663.9 1444.9  746.9 0.53 0.17 0.24 24.20 61.02  7.06  7.72    93.1   30.6   182.3 3238.9 2647.7  4
36   261.06 2.107  0.672  0.502  664.5 1376.7  740.2 0.44 0.12 0.23 21.36 62.65  8.13  7.86    96.3   27.8   237.9 3239.3 2648.1  4
37   340.75 2.184  0.497  0.448  665.1 1312.7  734.0 0.36 0.08 0.22 18.38 64.33  9.34  7.96    99.8   24.5   310.6 3239.6 2648.4  4
38   444.78 2.254  0.368  0.388  665.6 1254.9  728.3 0.29 0.06 0.21 15.43 66.04 10.50  8.03   103.0   21.0   405.4 3240.0 2648.8  4
39   580.57 2.314  0.275  0.327  666.1 1202.8  723.2 0.23 0.04 0.20 12.66 67.78 11.48  8.09   105.7   17.6   529.1 3240.3 2649.1  4
40   757.80 2.348  0.206  0.267  666.4 1156.1  718.5 0.20 0.03 0.20 10.19 69.54 12.14  8.13   107.2   14.4   690.6 3240.5 2649.3  4
41   989.15 2.346  0.156  0.211  666.3 1113.7  713.9 0.20 0.03 0.19  8.08 71.32 12.44  8.17   107.1   11.7   901.5 3240.8 2649.6  4
42  1291.12 2.345  0.118  0.164  666.3 1074.7  709.8 0.20 0.02 0.19  6.26 73.12 12.43  8.19   107.0    9.3  1176.7 3241.0 2649.9  4
43  1685.28 2.345  0.090  0.124  666.3 1038.8  706.0 0.20 0.02 0.19  4.75 74.91 12.14  8.21   107.0    7.4  1535.9 3241.3 2650.1  4
44  2199.77 2.344  0.069  0.092  666.3 1005.7  702.4 0.20 0.02 0.18  3.52 76.68 11.57  8.22   106.9    5.8  2004.8 3241.5 2650.3  4
45  2871.33 2.344  0.053  0.067  666.3  975.1  699.2 0.20 0.02 0.18  2.57 78.43 10.79  8.22   106.9    4.6  2616.8 3241.7 2650.5  4
46  3747.91 2.344  0.040  0.048  666.3  946.5  696.1 0.20 0.01 0.18  1.83 80.11  9.85  8.21   106.9    3.6  3415.7 3241.8 2650.6  4

********** THE BURN RATE for this MODE is 0.5455 cm/sec or 0.2148 in/sec and the AVERAGE SURFACE TEMPERATURE is  745.56 K
```

```
********** FINAL RESULTS FOR AN INITIAL PROPELLANT TEMPERATURE OF  248.15 K

  PRESSURE       RATE         RATE        TS
    psia        cm/sec       in/sec       K

   500.000      0.5397       0.2125     860.593
  1000.000      0.7542       0.2969     882.571
  2000.000      1.0101       0.3977     901.334

THE CONSTANTS C AND N IN ST. ROBERTS BURNING RATE LAW, RATE = C*P**N ARE:

C = 0.01289300 (RATE IN in/sec)
N = 0.45204964
THE COEFFICIENT OF DETERMINATION IS 0.99848300
```

```
***** MODE 1 AP*** 23 PARTICLES, the PRESSURE IS   500.00 psia and the INITIAL PROPELLANT TEMPERATURE is   298.15 DEGREES KELVIN

        D       R    TSOX    TSB     TS      BF       XAPK       XPFK       XPFD       XFFD     HTAP   HTPF    HTFF   TF   TSQDAP  TSQDB ITER
    MICRONS  cm/s     K       K       K               . . . . . . MICRONS . . . . . .            % HEAT TRANSFER      K      K       K

  1    5.63  1.440 1004.3 1570.4 1079.7 1.000      13.411      6.476      1.457      0.000    0.00 100.00   0.00 2591.  -536.  -173.  6
  2    6.86  1.423 1003.1 1566.9 1078.2 1.000      13.252      6.400      1.818      0.000    0.00 100.00   0.00 2591.  -537.  -173.  4
  3    8.37  1.402 1001.6 1562.6 1076.3 1.000      13.055      6.304      2.277      0.000    0.00 100.00   0.00 2591.  -537.  -173.  4
  4   10.21  1.375  999.6 1557.1 1073.9 1.000      12.808      6.185      2.866      0.000    0.00 100.00   0.00 2591.  -538.  -173.  4
  5   12.45  1.342  997.1 1550.3 1070.8 1.000      12.500      6.036      3.624      0.000    0.00 100.00   0.00 2591.  -539.  -173.  4
  6   15.19  1.301  993.9 1541.5 1066.8 1.000      12.117      5.852      4.607      0.000    0.00 100.00   0.00 2591.  -540.  -174.  4
  7   18.52  1.251  989.7 1530.7 1061.7 1.000      11.647      5.625      5.884      0.000    0.00 100.00   0.00 2591.  -541.  -174.  4
  8   22.59  1.142  980.7 1505.8 1050.6 0.739      10.632      5.134      7.438      7.925   10.86  79.58   9.56 2591.  -544.  -175.  5
  9   27.55  1.063  972.8 1487.2 1041.4 0.538       9.900      4.781      9.508      9.625   21.16  61.10  17.74 2591.  -547.  -176.  5
 10   33.61  1.003  964.9 1472.0 1032.5 0.393       9.336      4.509     12.290     12.009   29.86  46.37  23.77 2591.  -549.  -177.  5
 11   40.99  0.952  953.6 1459.0 1020.9 0.285       8.862      4.280     16.059     15.317   37.22  34.84  27.94 2591.  -553.  -178.  5
 12   50.00  0.908  930.9 1447.3  999.6 0.206       8.456      4.083     21.248     19.919   43.44  26.00  30.55 2591.  -561.  -180.  6
 13   60.99  0.861  912.9 1434.4  982.4 0.147       8.016      3.871     28.262     26.183   49.09  19.16  31.75 2591.  -567.  -182.  6
 14   74.38  0.808  901.9 1419.3  970.8 0.103       7.528      3.635     37.652     34.612   54.36  13.94  31.70 2591.  -571.  -184.  5
 15   90.73  0.754  890.4 1402.8  958.7 0.072       7.018      3.389     50.270     45.953   59.27  10.04  30.69 2591.  -575.  -185.  5
 16  110.66  0.697  878.5 1385.0  946.0 0.050       6.491      3.135     67.137     61.105   63.87   7.17  28.96 2591.  -579.  -186.  5
 17  134.98  0.640  866.3 1366.0  932.8 0.034       5.958      2.877     89.579     81.235   68.16   5.09  26.75 2591.  -584.  -188.  5
 18  164.63  0.583  853.8 1346.1  919.3 0.024       5.432      2.623    119.336    107.870   72.14   3.58  24.28 2591.  -588.  -189.  5
 19  200.80  0.528  843.9 1325.1  908.0 0.016       4.916      2.374    158.439    142.841   75.76   2.50  21.74 2591.  -592.  -191.  5
 20  244.92  0.475  837.1 1303.5  899.2 0.011       4.419      2.134    209.526    188.523   78.98   1.74  19.28 2591.  -595.  -191.  5
 21  298.73  0.425  830.1 1281.8  890.3 0.007       3.956      1.910    276.620    248.413   81.82   1.20  16.98 2591.  -597.  -192.  5
 22  364.37  0.379  823.1 1260.2  881.4 0.005       3.531      1.705    364.772    326.958   84.31   0.83  14.87 2591.  -600.  -193.  5
 23  444.42  0.338  816.1 1239.0  872.5 0.003       3.145      1.519    480.712    430.076   86.47   0.57  12.96 2591.  -603.  -194.  5

********** THE BURN RATE for this MODE is 0.9122 cm/sec or 0.3591 in/sec and the AVERAGE SURFACE TEMPERATURE is  999.51 K

***** MODE 2 HMX** 23 PARTICLES, the PRESSURE IS   500.00 psia and the INITIAL PROPELLANT TEMPERATURE is   298.15 DEGREES KELVIN

        D      ROX     RB      R      TSOX    TSB      TS    BF   BP   FRB  DNOM1 DNOM2 DNOM3 DNOM4    XXK   XXPFK  XXPFD     TX     TFX  ITER
    MICRONS .......cm/sec......        K       K       K                    ........PERCENT........    .....MICRONS......    K      K     #

 24   10.67  1.323  1.275  0.629  656.4 1535.9  750.0 1.00 0.40 0.33 42.63 43.09  7.64  6.64    21.3  116.6     9.7 3229.0 2682.2 12
 25   13.93  1.315  1.268  0.611  656.3 1534.3  749.7 1.00 0.40 0.33 41.66 44.24  7.46  6.64    27.9  115.9    12.7 3229.0 2682.2  3
 26   18.18  1.305  1.259  0.592  656.2 1532.3  749.4 1.00 0.40 0.33 40.65 45.44  7.27  6.65    36.4  115.1    16.6 3229.0 2682.2  3
 27   23.73  1.292  1.247  0.571  656.0 1529.7  748.9 1.00 0.40 0.33 39.61 46.66  7.08  6.65    47.5  113.9    21.6 3229.0 2682.2  3
 28   30.98  1.275  1.231  0.549  655.8 1526.3  748.4 1.00 0.40 0.33 38.55 47.92  6.87  6.66    62.0  112.5    28.2 3229.0 2682.2  3
 29   40.44  1.253  1.212  0.524  655.5 1521.9  747.7 1.00 0.40 0.33 37.46 49.21  6.67  6.66    80.9  110.6    36.9 3229.0 2682.2  3
 30   52.78  1.401  1.035  0.549  657.4 1480.2  744.9 0.78 0.28 0.29 35.11 50.58  7.30  7.02   105.6  116.3    48.1 3229.0 2682.2  4
 31   68.90  1.197  1.155  0.469  654.7 1508.9  745.6 0.99 0.39 0.32 35.14 51.94  6.22  6.70   137.8  105.5    62.8 3229.0 2682.2  4
 32   89.93  1.151  1.118  0.437  654.0 1500.3  744.1 1.00 0.40 0.32 34.04 53.27  5.99  6.69   179.9  101.6    82.0 3229.0 2682.2  3
 33  117.39  1.099  1.071  0.403  653.2 1489.0  742.2 1.00 0.40 0.32 32.85 54.69  5.75  6.71   234.8   97.1   107.0 3229.0 2682.2  3
 34  153.22  1.038  1.014  0.366  652.3 1474.9  739.8 1.00 0.40 0.32 31.63 56.14  5.50  6.73   306.4   91.8   139.6 3229.0 2682.2  3
 35  200.00  0.966  0.947  0.328  651.1 1457.7  736.9 1.00 0.40 0.32 30.39 57.62  5.24  6.75   306.6   85.5   182.3 3229.0 2682.2  3
 36  261.06  0.883  0.871  0.297  649.6 1437.0  733.3 1.00 0.40 0.32 29.12 59.13  4.96  6.78   280.5   78.2   237.9 3229.0 2682.2  3
 37  340.75  0.824  0.796  0.255  648.4 1415.6  730.0 0.82 0.36 0.30 27.77 60.69  4.62  6.92   261.6   72.7   310.6 3229.0 2682.2  3
 38  444.78  0.807  0.662  0.233  648.0 1373.3  725.2 0.65 0.28 0.28 25.91 62.25  4.68  7.16   256.1   68.7   405.4 3229.0 2682.2  3
 39  580.57  0.814  0.493  0.210  648.2 1311.0  718.7 0.53 0.20 0.26 23.15 64.24  5.18  7.44   258.5   64.1   529.1 3229.0 2682.2  4
 40  757.80  0.837  0.345  0.189  648.7 1242.6  711.8 0.43 0.13 0.24 20.27 65.95  6.17  7.61   265.6   58.0   690.6 3229.0 2682.2  4
 41  989.15  0.864  0.240  0.166  649.2 1180.2  705.7 0.35 0.08 0.22 17.23 67.69  7.35  7.73   274.2   50.7   901.5 3229.0 2682.2  4
 42 1291.12  0.889  0.170  0.142  649.7 1126.4  700.4 0.28 0.05 0.21 14.26 69.47  8.46  7.81   282.3   43.0  1176.7 3229.0 2682.2  4
 43 1685.28  0.911  0.123  0.117  650.1 1079.9  695.8 0.22 0.04 0.21 11.51 71.26  9.36  7.87   289.1   35.7  1535.9 3229.0 2682.2  4
 44 2199.77  0.918  0.090  0.094  650.2 1039.4  691.6 0.20 0.03 0.20  9.13 73.05  9.91  7.91   291.5   29.0  2004.8 3229.0 2682.2  4
 45 2871.33  0.918  0.067  0.073  650.2 1003.1  687.7 0.20 0.02 0.20  7.10 74.85 10.11  7.94   291.4   23.3  2616.8 3229.0 2682.2  4
 46 3747.91  0.917  0.050  0.055  650.2  970.1  684.2 0.20 0.02 0.19  5.39 76.64 10.01  7.95   291.2   18.5  3415.7 3229.0 2682.2  4

********** THE BURN RATE fr this MODE is 0.3335 cm/sec or 0.1313 in/sec and the AVERAGE SURFACE TEMPERATURE is  734.37 K
```

```
***** MODE 1 AP*** 23 PARTICLES, the PRESSURE IS  1000.00 psia and the INITIAL PROPELLANT TEMPERATURE is   298.15 DEGREES KELVIN

        D      R    TSOX   TSB     TS      BF      XAPK       XPFK      XPFD       XFFD     HTAP   HTPF   HTFF   TF  TSQDAP  TSQDB ITER
     MICRONS cm/s    K      K      K               . . . . . . MICRONS . . . . . .          % HEAT TRANSFER      K     K      K

 1     5.63  2.578 1060.3 1759.3 1153.4 1.000     7.580      2.816      1.582      0.000     0.00 100.00   0.00 2609.  -567.  -167.  8
 2     6.86  2.506 1057.3 1749.0 1149.4 1.000     7.368      2.738      2.000      0.000     0.00 100.00   0.00 2609.  -568.  -168.  4
 3     8.37  2.417 1053.5 1736.2 1144.4 1.000     7.107      2.641      2.540      0.000     0.00 100.00   0.00 2609.  -569.  -168.  4
 4    10.21  2.310 1048.7 1720.3 1138.1 1.000     6.791      2.523      3.237      0.000     0.00 100.00   0.00 2609.  -571.  -168.  4
 5    12.45  2.166 1042.0 1698.2 1129.4 0.969     6.369      2.367      4.129      4.668     1.13  97.89   0.98 2609.  -573.  -169.  4
 6    15.19  1.933 1030.4 1660.4 1114.3 0.687     5.682      2.111      5.199      5.490    13.52  75.32  11.16 2609.  -577.  -170.  5
 7    18.52  1.780 1021.9 1634.3 1103.4 0.495     5.233      1.945      6.648      6.701    24.11  57.05  18.84 2609.  -579.  -171.  5
 8    22.59  1.663 1014.4 1613.2 1094.2 0.357     4.889      1.817      8.600      8.399    32.95  42.75  24.30 2609.  -582.  -172.  5
 9    27.55  1.562 1006.9 1594.2 1085.1 0.257     4.591      1.706     11.227     10.737    40.41  31.71  27.88 2609.  -584.  -172.  5
10    33.61  1.467  998.0 1575.6 1074.9 0.183     4.312      1.602     14.769     13.928    46.82  23.29  29.89 2609.  -588.  -173.  5
11    40.99  1.374  984.7 1556.9 1060.9 0.130     4.039      1.501     19.556     18.266    52.44  16.96  30.61 2609.  -592.  -175.  5
12    50.00  1.286  958.9 1538.2 1036.0 0.091     3.780      1.405     26.104     24.190    57.41  12.28  30.32 2609.  -601.  -177.  6
13    60.99  1.191  938.0 1517.2 1015.2 0.063     3.501      1.301     34.808     32.068    62.05   8.79  29.16 2609.  -609.  -180.  6
14    74.38  1.090  924.4 1493.8 1000.2 0.044     3.206      1.191     46.224     42.414    66.36   6.23  27.41 2609.  -614.  -181.  5
15    90.73  0.991  910.4 1469.1  984.8 0.030     2.914      1.083     61.276     56.030    70.30   4.38  25.31 2609.  -619.  -183.  5
16   110.66  0.895  896.2 1443.6  969.1 0.020     2.630      0.977     81.048     73.874    73.88   3.07  23.05 2609.  -625.  -184.  5
17   134.98  0.803  881.9 1417.6  953.3 0.014     2.361      0.877    106.963     97.196    77.09   2.13  20.77 2609.  -630.  -186.  5
18   164.63  0.717  867.6 1391.6  937.4 0.009     2.109      0.784    140.898    127.647    79.96   1.48  18.57 2609.  -636.  -188.  5
19   200.80  0.637  856.2 1365.2  924.0 0.006     1.874      0.696    184.941    167.119    82.46   1.02  16.52 2609.  -641.  -189.  5
20   244.92  0.563  848.1 1338.7  913.4 0.004     1.656      0.615    241.759    218.018    84.63   0.70  14.67 2609.  -644.  -190.  5
21   298.73  0.497  840.0 1312.7  903.0 0.003     1.461      0.543    315.738    284.157    86.52   0.48  13.00 2609.  -647.  -191.  5
22   364.37  0.438  832.0 1287.5  892.7 0.002     1.286      0.478    412.094    370.126    88.17   0.33  11.50 2609.  -651.  -192.  5
23   444.42  0.385  824.1 1263.1  882.5 0.001     1.132      0.421    537.916    482.163    89.63   0.22  10.15 2609.  -654.  -193.  5

********** THE BURN RATE for this MODE is 1.2860 cm/sec or 0.5063 in/sec and the AVERAGE SURFACE TEMPERATURE is 1034.82 K

***** MODE 2 HMX** 23 PARTICLES, the PRESSURE IS  1000.00 psia and the INITIAL PROPELLANT TEMPERATURE is   298.15 DEGREES KELVIN

        D      ROX     RB      R     TSOX    TSB     TS     BF   BP   FRB  DNOM1 DNOM2 DNOM3 DNOM4    XXK   XXPFK  XXPFD    TX     TFX   ITER
     MICRONS .......cm/sec......      K       K      K                     ........PERCENT........   .....MICRONS......    K      K     #

24    10.67  1.966  1.847  0.930  663.2 1645.8  767.8 1.00 0.39 0.33 42.36 43.09  7.97  6.58    21.3   75.5     9.7 3278.0 2706.9 10
25    13.93  1.948  1.831  0.900  663.1 1643.1  767.4 1.00 0.39 0.33 41.40 44.24  7.78  6.58    27.9   74.8    12.7 3278.0 2706.9  3
26    18.18  1.925  1.811  0.868  662.9 1639.6  766.8 1.00 0.39 0.33 40.40 45.44  7.58  6.59    36.4   74.0    16.6 3278.0 2706.9  3
27    23.73  1.896  1.785  0.833  662.6 1635.1  766.1 1.00 0.39 0.33 39.37 46.66  7.37  6.60    47.5   72.9    21.6 3278.0 2706.9  3
28    30.98  1.859  1.753  0.795  662.3 1629.4  765.2 1.00 0.39 0.33 38.32 47.92  7.15  6.61    62.0   71.5    28.2 3278.0 2706.9  3
29    40.44  1.813  1.711  0.754  661.8 1622.0  764.0 1.00 0.39 0.33 37.24 49.21  6.93  6.62    80.9   69.7    36.9 3278.0 2706.9  3
30    52.78  1.755  1.660  0.708  661.3 1612.6  762.5 1.00 0.39 0.33 36.14 50.53  6.69  6.64   105.6   67.5    48.1 3278.0 2706.9  3
31    68.90  1.684  1.597  0.658  660.6 1600.9  760.6 1.00 0.39 0.33 35.01 51.88  6.45  6.66   137.8   64.8    62.8 3278.0 2706.9  3
32    89.93  1.598  1.520  0.604  659.6 1586.2  758.2 1.00 0.39 0.33 33.85 53.27  6.19  6.69   179.9   61.5    82.0 3278.0 2706.9  3
33   117.39  1.497  1.429  0.546  658.5 1568.1  755.3 1.00 0.39 0.33 32.66 54.69  5.93  6.72   172.2   57.7   107.0 3278.0 2706.9  3
34   153.22  1.380  1.324  0.483  657.1 1546.3  751.7 0.99 0.39 0.33 31.33 56.27  5.62  6.78   158.8   53.2   139.6 3278.0 2706.9  4
35   200.00  1.329  1.195  0.445  656.5 1518.1  748.2 0.79 0.34 0.31 29.99 57.63  5.41  6.97   153.0   50.6   182.3 3278.0 2706.9  3
36   261.06  1.322  0.979  0.413  656.4 1466.1  742.5 0.64 0.26 0.28 27.99 59.14  5.65  7.22   152.1   48.1   237.9 3278.0 2706.9  3
37   340.75  1.346  0.733  0.379  656.7 1396.5  735.4 0.53 0.18 0.26 25.22 60.94  6.37  7.47   154.9   44.9   310.6 3278.0 2706.9  4
38   444.78  1.388  0.524  0.344  657.2 1323.7  728.1 0.43 0.12 0.24 22.23 62.58  7.56  7.63   159.8   40.7   405.4 3278.0 2706.9  4
39   580.57  1.435  0.374  0.306  657.8 1257.6  721.6 0.35 0.08 0.23 19.08 64.25  8.92  7.74   165.2   35.8   529.1 3278.0 2706.9  4
40   757.80  1.479  0.270  0.264  658.3 1200.0  715.9 0.28 0.05 0.22 15.98 65.96 10.23  7.83   170.2   30.5   690.6 3278.0 2706.9  4
41   989.15  1.515  0.198  0.221  658.7 1149.5  710.9 0.23 0.04 0.21 13.08 67.71 11.33  7.89   174.3   25.5   901.5 3278.0 2706.9  4
42  1291.12  1.531  0.147  0.180  658.9 1105.0  706.4 0.20 0.03 0.21 10.52 69.48 12.07  7.94   176.2   20.8  1176.7 3278.0 2706.9  4
43  1685.28  1.530  0.110  0.142  658.9 1065.0  702.1 0.20 0.02 0.20  8.32 71.26 12.44  7.97   176.1   16.8  1535.9 3278.0 2706.9  4
44  2199.77  1.530  0.083  0.110  658.9 1028.5  698.2 0.20 0.02 0.20  6.44 73.06 12.49  8.00   176.0   13.4  2004.8 3278.0 2706.9  4
45  2871.33  1.529  0.063  0.083  658.9  995.1  694.7 0.20 0.02 0.19  4.88 74.86 12.23  8.03   176.0   10.6  2616.8 3278.0 2706.9  4
46  3747.91  1.529  0.048  0.062  658.9  964.3  691.4 0.20 0.02 0.19  3.62 76.64 11.69  8.04   175.9    8.3  3415.7 3278.0 2706.9  4

********** THE BURN RATE for this MODE is 0.4635 cm/sec or 0.1825 in/sec and the AVERAGE SURFACE TEMPERATURE is  744.27 K
```

```
***** MODE 1 AP*** 23 PARTICLES, the PRESSURE IS  2000.00 psia and the INITIAL PROPELLANT TEMPERATURE is   298.15 DEGREES KELVIN

        D      R    TSOX    TSB     TS      BF      XAPK      XPFK       XPFD       XFFD     HTAP   HTPF    HTFF   TF  TSQDAP  TSQDB ITER
    MICRONS cm/s     K       K      K               . . . . . .  MICRONS  . . . . . .      % HEAT TRANSFER       K      K       K

 1     5.63  4.195 1112.1 1956.1 1224.5 1.000     3.874     1.119      1.772      0.000     0.00 100.00    0.00 2625.   -591.  -162.  8
 2     6.86  3.935 1104.8 1927.7 1214.4 1.000     3.634     1.050      2.259      0.000     0.00 100.00    0.00 2625.   -593.  -163.  4
 3     8.37  3.495 1091.7 1877.3 1196.3 0.809     3.227     0.932      2.838      3.101     7.80  85.76    6.43 2625.   -598.  -164.  5
 4    10.21  3.138 1080.0 1833.7 1180.4 0.574     2.898     0.837      3.589      3.708    19.81  64.75   15.44 2625.   -602.  -165.  5
 5    12.45  2.893 1071.1 1802.2 1168.5 0.413     2.671     0.772      4.605      4.581    29.69  48.41   21.90 2625.   -605.  -166.  5
 6    15.19  2.695 1063.3 1775.6 1158.2 0.297     2.489     0.719      5.969      5.792    37.86  35.88   26.26 2625.   -607.  -167.  5
 7    18.52  2.517 1055.6 1750.7 1148.2 0.212     2.325     0.671      7.798      7.444    44.76  26.34   28.90 2625.   -610.  -168.  5
 8    22.59  2.345 1047.4 1725.5 1137.7 0.150     2.166     0.625     10.245      9.676    50.70  19.15   30.15 2625.   -613.  -168.  5
 9    27.55  2.173 1038.0 1699.3 1126.1 0.106     2.007     0.580     13.503     12.665    55.93  13.79   30.28 2625.   -616.  -169.  5
10    33.61  2.000 1026.6 1671.5 1112.5 0.074     1.847     0.533     17.824     16.638    60.59   9.85   29.56 2625.   -620.  -170.  5
11    40.99  1.878 1010.4 1642.7 1094.6 0.051     1.688     0.488     23.556     21.899    64.77   6.98   28.25 2625.   -626.  -172.  5
12    50.00  1.668  981.0 1614.1 1065.3 0.035     1.540     0.445     31.273     28.930    68.53   4.94   26.53 2625.   -637.  -175.  6
13    60.99  1.506  957.1 1583.5 1040.5 0.024     1.391     0.402     41.320     38.065    71.98   3.46   24.55 2625.   -646.  -178.  6
14    74.38  1.346  940.9 1551.1 1022.2 0.016     1.243     0.359     54.226     49.800    75.09   2.41   22.50 2625.   -652.  -179.  5
15    90.73  1.196  924.7 1518.4 1003.8 0.011     1.105     0.319     70.980     64.987    77.86   1.67   20.47 2625.   -659.  -181.  5
16   110.66  1.058  908.6 1485.9  985.5 0.007     0.977     0.282     92.707     84.616    80.32   1.15   18.53 2625.   -665.  -183.  6
17   134.98  0.933  892.6 1453.9  967.3 0.005     0.861     0.249    120.869    109.977    82.51   0.79   16.70 2625.   -672.  -185.  7
18   164.63  0.820  876.8 1422.7  949.5 0.003     0.757     0.219    157.418    142.780    84.45   0.54   15.00 2625.   -679.  -187.  6
19   200.80  0.719  864.2 1391.9  934.4 0.002     0.664     0.192    204.403    184.893    86.16   0.37   13.47 2625.   -684.  -188.  6
20   244.92  0.627  855.0 1361.5  922.5 0.002     0.579     0.167    264.489    238.718    87.63   0.25   12.11 2625.   -688.  -189.  5
21   298.73  0.546  846.1 1332.2  910.8 0.001     0.505     0.146    342.102    308.091    88.95   0.17   10.88 2625.   -692.  -190.  6
22   364.37  0.476  837.3 1304.2  899.5 0.001     0.440     0.127    442.824    397.934    90.14   0.12    9.74 2625.   -696.  -191.  6
23   444.42  0.416  828.8 1277.6  888.6 0.000     0.384     0.111    573.894    514.612    91.22   0.08    8.70 2625.   -700.  -192.  6

********** THE BURN RATE for this MODE is 1.6871 cm/sec or 0.6642 in/sec and the AVERAGE SURACE TEMPERATURE is 1064.32 K

***** MODE 2 HMX** 23 PARTICLES, the PRESSURE IS  2000.00 psia and the INITIAL PROPELLANT TEMPERATURE is   298.15 DEGREES KELVIN

        D      ROX      RB      R      TSOX    TSB     TS    BF   BP   FRB  DNOM1 DNOM2 DNOM3 DNOM4    XXK   XXPFK  XXPFD    TX      TFX  ITER
    MICRONS .......cm/sec......       K       K      K                      .........PERCENT........    .....MICRONS......   K       K     #

24    10.67 70.580  1.670  0.598   606.3 1317.5  826.1 1.00 0.02 0.00  0.76 80.71  0.07 18.46   21.3  132.0     9.7 3320.0 2728.7100**
25    13.93  2.857  2.614  1.309   669.8 1764.3  786.3 1.00 0.38 0.34 41.06 44.29  8.11  6.54   27.9   48.0    12.7 3320.0 2728.7100**
26    18.18  2.807  2.571  1.257   669.5 1758.3  785.4 1.00 0.38 0.34 40.11 45.44  7.91  6.55   36.4   47.1    16.6 3320.0 2728.7   3
27    23.73  2.744  2.517  1.197   669.1 1750.6  784.2 1.00 0.38 0.34 39.09 46.66  7.68  6.57   47.5   46.1    21.6 3320.0 2728.7   3
28    30.98  2.665  2.449  1.132   668.6 1740.9  782.7 1.00 0.38 0.34 38.04 47.92  7.44  6.59   62.0   44.8    28.2 3320.0 2728.7   3
29    40.44  2.567  2.365  1.059   667.9 1728.5  780.8 1.00 0.38 0.34 36.97 49.21  7.19  6.63   80.9   43.2    36.9 3320.0 2728.7   3
30    52.78  2.448  2.262  0.980   667.1 1713.0  778.4 1.00 0.38 0.34 35.87 50.53  6.93  6.67  103.0   41.2    48.1 3320.0 2728.7   3
31    68.90  2.305  2.139  0.894   666.0 1693.9  775.4 1.00 0.38 0.34 34.75 51.88  6.66  6.71   97.0   38.8    62.8 3320.0 2728.7   3
32    89.93  2.175  1.995  0.814   665.0 1670.7  772.0 0.93 0.37 0.33 33.54 53.27  6.37  6.82   91.5   36.5    82.0 3320.0 2728.7   3
33   117.39  2.141  1.762  0.763   664.7 1631.1  767.5 0.77 0.31 0.31 31.91 54.69  6.34  7.06   90.1   35.1   107.0 3320.0 2728.7   3
34   153.22  2.157  1.432  0.717   664.9 1568.7  761.0 0.63 0.23 0.29 29.76 56.14  6.79  7.31   90.7   33.5   139.6 3320.0 2728.7   3
35   200.00  2.213  1.084  0.665   665.3 1492.2  753.3 0.53 0.16 0.27 26.95 57.79  7.73  7.53   93.1   31.4   182.3 3320.0 2728.7   4
36   261.06  2.290  0.794  0.610   665.9 1415.0  745.6 0.44 0.11 0.25 23.87 59.35  9.09  7.69   96.3   28.5   237.9 3320.0 2728.7   4
37   340.75  2.371  0.580  0.546   666.5 1344.9  738.7 0.36 0.07 0.24 20.65 60.95 10.60  7.80   99.7   25.2   310.6 3320.0 2728.7   4
38   444.78  2.444  0.427  0.476   667.1 1282.9  732.6 0.29 0.05 0.23 17.46 62.59 12.07  7.88  102.8   21.6   405.4 3320.0 2728.7   4
39   580.57  2.506  0.317  0.404   667.5 1227.9  727.1 0.23 0.04 0.22 14.45 64.27 13.33  7.95  105.4   18.1   529.1 3320.0 2728.7   4
40   757.80  2.539  0.238  0.333   667.7 1178.9  722.1 0.20 0.03 0.22 11.76 65.97 14.27  8.00  106.8   14.9   690.6 3320.0 2728.7   4
41   989.15  2.537  0.179  0.267   667.7 1134.6  717.4 0.20 0.02 0.21  9.44 67.72 14.80  8.05  106.7   12.1   901.5 3320.0 2728.7   4
42  1291.12  2.536  0.136  0.210   667.7 1093.9  713.1 0.20 0.02 0.21  7.42 69.48 15.01  8.09  106.7    9.7  1176.7 3320.0 2728.7   4
43  1685.28  2.535  0.103  0.162   667.7 1056.7  709.1 0.20 0.02 0.20  5.72 71.27 14.89  8.12  106.7    7.7  1535.9 3320.0 2728.7   4
44  2199.77  2.535  0.079  0.122   667.7 1022.3  705.4 0.20 0.02 0.20  4.32 73.07 14.46  8.15  106.6    6.1  2004.8 3320.0 2728.7   4
45  2871.33  2.534  0.060  0.091   667.7  990.6  702.1 0.20 0.01 0.19  3.21 74.86 13.76  8.17  106.6    4.8  2616.8 3320.0 2728.7   4
46  3747.91  2.534  0.046  0.066   667.7  961.1  698.9 0.20 0.01 0.19  2.35 76.64 12.84  8.18  106.6    3.7  3415.7 3320.0 2728.7   4

********** THE BURN RATE for this MODE is 0.6571 cm/sec or 0.2587 in/sec and the AVERAGE SURFACE TEMPERATURE is  752.22 K
```

```
********** FINAL RESULTS FOR AN INITIAL PROPELLANT TEMPERATURE OF  298.15 K

 PRESSURE        RATE        RATE        TS
   psia         cm/sec      in/sec       K

  500.000       0.6228      0.2452     866.937
 1000.000       0.8748      0.3444     889.546
 2000.000       1.1721      0.4614     908.271

THE CONSTANTS C AND N IN ST. ROBERTS BURNING RATE LAW, RATE = C*P**N ARE:

C = 0.01452064 (RATE IN in/sec)
N = 0.45608306
THE COEFFICIENT OF DETERMINATION IS 0.99814898
```

```
***** MODE 1 AP*** 23 PARTICLES, the PRESSURE IS   500.00 psia and the INITIAL PROPELLANT TEMPERATURE is   348.15 DEGREES KELVIN

       D      R    TSOX    TSB     TS      BF      XAPK      XPFK       XPFD         XFFD     HTAP   HTPF    HTFF   TF   TSQDAP  TSQDB ITER
   MICRONS cm/s     K      K       K                . . . . . . . MICRONS  . . . . . . .      % HEAT TRANSFER      K       K      K

 1     5.63 1.621 1015.0 1605.3 1093.6 1.000     11.526     6.211      1.473        0.000    0.00 100.00   0.00 2698.   -533.   -172.  6
 2     6.86 1.600 1013.6 1601.5 1091.9 1.000     11.384     6.134      1.841        0.000    0.00 100.00   0.00 2698.   -534.   -172.  4
 3     8.37 1.575 1011.8 1596.7 1089.7 1.000     11.206     6.037      2.312        0.000    0.00 100.00   0.00 2698.   -534.   -172.  4
 4    10.21 1.543 1009.5 1590.6 1086.9 1.000     10.984     5.917      2.918        0.000    0.00 100.00   0.00 2698.   -535.   -172.  4
 5    12.45 1.503 1006.5 1582.9 1083.3 1.000     10.707     5.766      3.702        0.000    0.00 100.00   0.00 2698.   -536.   -172.  4
 6    15.19 1.454 1002.6 1573.2 1078.6 1.000     10.364     5.580      4.720        0.000    0.00 100.00   0.00 2698.   -537.   -173.  4
 7    18.52 1.342  993.9 1550.2 1068.0 0.741      9.576     5.153      5.973        6.344   10.85  79.48   9.67 2697.   -540.   -174.  5
 8    22.59 1.260  985.9 1532.5 1058.7 0.545      9.002     4.842      7.639        7.701   20.81  61.49  17.70 2696.   -542.   -175.  5
 9    27.55 1.196  976.2 1518.3 1048.4 0.401      8.558     4.600      9.877        9.601   29.25  47.04  23.71 2696.   -545.   -176.  5
10    33.61 1.144  957.0 1506.5 1030.2 0.294      8.209     4.409     12.931       12.252   36.29  35.75  27.96 2695.   -552.   -178.  5
11    40.99 1.096  934.9 1495.0 1009.5 0.214      7.880     4.228     17.101       15.912   42.41  26.90  30.69 2694.   -559.   -180.  5
12    50.00 1.041  923.1 1481.7  997.5 0.153      7.497     4.020     22.711       20.876   48.10  19.92  31.98 2693.   -563.   -181.  5
13    60.99 0.982  912.1 1466.9  986.0 0.109      7.089     3.798     30.308       27.625   53.37  14.59  32.04 2692.   -567.   -183.  5
14    74.38 0.921  900.7 1450.8  974.0 0.076      6.656     3.564     40.568       36.751   58.33  10.59  31.09 2692.   -571.   -184.  5
15    91.73 0.857  888.8 1433.2  961.3 0.053      6.203     3.319     54.366       49.019   63.04   7.62  29.35 2691.   -575.   -185.  5
16   110.66 0.791  876.6 1414.2  948.2 0.037      5.739     3.069     72.851       65.430   67.50   5.44  27.06 2690.   -580.   -187.  5
17   134.98 0.726  864.8 1394.2  935.4 0.025      5.273     2.818     97.513       87.286   71.70   3.85  24.45 2689.   -584.   -188.  5
18   164.63 0.661  858.5 1373.0  927.1 0.017      4.805     2.567    129.997      116.097   75.55   2.70  21.74 2689.   -586.   -189.  5
19   200.80 0.599  852.0 1351.5  918.6 0.012      4.358     2.327    173.109      154.277   79.04   1.89  19.08 2688.   -589.   -190.  5
20   244.92 0.541  845.4 1330.0  910.0 0.008      3.941     2.103    230.394      204.926   82.13   1.31  16.56 2688.   -591.   -190.  5
21   298.73 0.487  838.8 1308.9  901.4 0.005      3.558     1.898    306.694      272.278   84.85   0.91  14.24 2687.   -594.   -191.  5
22   364.37 0.439  832.2 1288.3  893.0 0.004      3.210     1.712    408.660      362.140   87.22   0.62  12.15 2687.   -596.   -192.  5
23   444.42 0.396  825.8 1268.5  884.8 0.002      2.899     1.545    545.654      482.687   89.29   0.43  10.29 2686.   -599.   -193.  4

********** THE BURN RATE for this MODE is 1.0348 cm/sec or 0.4074 in/sec and the AVERAGE SURFACE TEMPERATURE is 1000.78 K

***** MODE 2 HMX** 23 PARTICLES, the PRESSURE IS   500.00 psia and the INITIAL PROPELLANT TEMPERATURE is   348.15 DEGREES KELVIN

       D     ROX     RB      R     TSOX    TSB     TS    BF   BP   FRB  DNOM1 DNOM2 DNOM3 DNOM4    XXK   XXPFK  XXPFD     TX     TFX  ITER
   MICRONS .......cm/sec......     K       K       K                    ........PERCENT........    .....MICRONS......    K       K     #

24    10.67 1.425  1.567  0.730  657.7 1595.1  757.4 1.00 0.39 0.35 45.90 39.93  7.79  6.39    21.3  117.5     9.7 3310.7 2763.9 25
25    13.93 1.417  1.558  0.711  657.6 1593.4  757.1 1.00 0.39 0.35 44.98 41.00  7.63  6.39    27.9  116.8    12.7 3310.7 2763.9  3
26    18.18 1.406  1.547  0.691  657.4 1591.3  756.8 1.00 0.39 0.35 44.04 42.11  7.46  6.39    36.4  115.9    16.6 3310.7 2763.9  3
27    23.73 1.392  1.532  0.669  657.3 1588.5  756.3 1.00 0.39 0.35 43.07 43.25  7.28  6.40    47.5  114.7    21.6 3310.6 2763.8  3
28    30.98 1.374  1.513  0.645  657.0 1584.9  755.8 1.00 0.39 0.35 42.08 44.42  7.10  6.40    62.0  113.3    28.2 3310.6 2763.8  3
29    40.44 1.351  1.490  0.619  656.8 1580.2  755.0 1.00 0.39 0.35 41.06 45.61  6.92  6.41    80.9  111.4    36.9 3310.6 2763.8  3
30    52.78 1.520  1.217  0.652  658.8 1523.0  750.7 0.77 0.26 0.31 38.45 46.86  7.86  6.83   105.6  117.3    48.1 3310.3 2763.5  4
31    68.90 1.293  1.417  0.561  656.0 1565.7  752.8 0.98 0.38 0.35 38.88 48.13  6.53  6.46   137.8  106.5    62.8 3310.4 2763.6  4
32    89.93 1.241  1.375  0.524  655.3 1557.1  751.3 1.00 0.39 0.35 37.85 49.40  6.31  6.45   179.9  102.5    82.0 3310.3 2763.5  3
33   117.39 1.187  1.318  0.486  654.5 1545.1  749.3 1.00 0.39 0.35 36.72 50.72  6.08  6.47   234.8   98.0   107.0 3310.2 2763.4  3
34   153.22 1.121  1.249  0.445  653.6 1530.3  746.9 1.00 0.39 0.35 35.58 52.08  5.85  6.49   306.4   92.7   139.6 3310.1 2763.3  3
35   200.00 1.044  1.169  0.401  652.4 1512.1  743.8 1.00 0.39 0.35 34.40 53.48  5.60  6.52   304.8   86.4   182.3 3309.9 2763.1  3
36   261.06 0.957  1.076  0.354  650.9 1490.2  740.2 1.00 0.39 0.34 33.20 54.90  5.35  6.55   279.3   79.3   237.9 3309.7 2762.9  3
37   340.75 0.894  0.978  0.318  649.8 1465.8  736.6 0.82 0.35 0.33 31.87 56.36  5.04  6.72   261.1   73.7   310.6 3309.4 2762.6  3
38   444.78 0.876  0.797  0.291  649.4 1416.0  731.0 0.65 0.27 0.30 29.78 58.01  5.19  7.02   255.9   69.7   405.4 3309.1 2762.3  4
39   580.57 0.885  0.579  0.268  649.6 1344.3  723.5 0.53 0.18 0.27 27.15 59.58  6.00  7.28   258.6   65.0   529.1 3308.7 2761.9  4
40   757.80 0.910  0.397  0.244  650.1 1268.7  715.9 0.43 0.12 0.25 23.99 61.18  7.35  7.47   265.9   58.8   690.6 3308.2 2761.4  4
41   989.15 0.938  0.273  0.216  650.6 1202.0  709.2 0.35 0.07 0.24 20.63 62.83  8.93  7.60   274.4   51.5   901.5 3307.8 2761.0  4
42  1291.12 0.964  0.193  0.186  651.0 1145.6  703.7 0.28 0.05 0.23 17.32 64.52 10.46  7.70   282.2   43.8  1176.7 3307.5 2760.7  4
43  1685.28 0.986  0.139  0.157  651.4 1097.2  698.8 0.22 0.04 0.22 14.22 66.24 11.78  7.77   288.7   36.4  1535.9 3307.2 2760.4  4
44  2199.77 0.994  0.102  0.128  651.5 1055.3  694.5 0.20 0.03 0.21 11.50 67.98 12.70  7.82   291.0   29.6  2004.8 3307.0 2760.2  4
45  2871.33 0.993  0.076  0.101  651.5 1017.8  690.5 0.20 0.02 0.21  9.14 69.76 13.23  7.87   290.9   23.8  2616.8 3306.7 2759.9  4
46  3747.91 0.993  0.057  0.079  651.5  983.9  686.9 0.20 0.02 0.20  7.12 71.56 13.42  7.90   290.8   19.0  3415.7 3306.5 2759.7  4

********** THE BURN RATE for this MODE is 0.4069 cm/sec or 0.1602 in/sec and the AVERAGE SURFACE TEMPERATURE is  740.91 K
```

```
***** MODE 1 AP*** 23 PARTICLES, the PRESSURE IS  1000.00 psia and the INITIAL PROPELLANT TEMPERATURE is   348.15 DEGREES KELVIN

       D      R    TSOX    TSB     TS      BF        XAPK        XPFK        XPFD       XFFD     HTAP   HTPF   HTFF   TF  TSQDAP  TSQDB ITER
   MICRONS cm/s     K      K       K                 . . . . . . . MICRONS . . . . . .          % HEAT TRANSFER      K     K      K

 1     5.63  2.896 1071.9 1802.6 1169.2 1.000       6.451       2.685       1.611       0.000    0.00 100.00   0.00 2721.  -563.  -166.  8
 2     6.86  2.809 1068.5 1791.1 1164.8 1.000       6.261       2.606       2.043       0.000    0.00 100.00   0.00 2721.  -564.  -166.  4
 3     8.37  2.702 1064.2 1776.6 1159.1 1.000       6.028       2.508       2.601       0.000    0.00 100.00   0.00 2721.  -566.  -167.  4
 4    10.21  2.573 1058.8 1758.6 1152.0 1.000       5.746       2.390       3.325       0.000    0.00 100.00   0.00 2720.  -567.  -167.  4
 5    12.45  2.315 1047.6 1721.0 1137.3 0.722       5.180       2.152       4.193       4.445   11.80  78.33   9.88 2720.  -571.  -168.  5
 6    15.19  2.140 1038.9 1694.1 1126.1 0.523       4.795       1.992       5.360       5.406   22.39  59.83  17.78 2719.  -574.  -169.  5
 7    18.52  2.006 1031.0 1672.6 1116.5 0.380       4.500       1.868       6.930       6.755   31.32  45.17  23.52 2718.  -576.  -170.  5
 8    22.59  1.891 1022.8 1653.3 1106.8 0.275       4.248       1.762       9.048       8.617   38.88  33.74  27.37 2718.  -579.  -171.  5
 9    27.55  1.784 1011.8 1634.9 1094.8 0.197       4.014       1.664      11.915      11.170   45.39  24.97  29.64 2717.  -583.  -172.  5
10    33.61  1.684  990.0 1617.0 1073.5 0.140       3.799       1.574      15.843      14.681   51.02  18.37  30.60 2716.  -590.  -174.  6
11    40.99  1.581  964.8 1598.0 1049.1 0.099       3.580       1.481      21.177      19.453   56.14  13.40  30.45 2715.  -599.  -177.  6
12    50.00  1.468  950.4 1576.0 1033.7 0.069       3.330       1.376      28.243      25.792   61.01   9.64  29.35 2714.  -604.  -178.  5
13    60.99  1.352  936.7 1552.3 1018.7 0.048       3.072       1.269      37.650      34.228   65.54   6.88  27.58 2713.  -609.  -180.  5
14    74.38  1.236  922.8 1527.3 1003.3 0.033       2.815       1.162      50.142      45.411   69.73   4.87  25.40 2712.  -615.  -181.  5
15    90.73  1.123  908.6 1501.6  987.5 0.023       2.563       1.057      66.682      60.184   73.57   3.43  23.00 2711.  -620.  -183.  5
16   110.66  1.015  894.3 1475.3  971.7 0.015       2.322       0.957      88.557      79.673   77.06   2.40  20.54 2710.  -626.  -185.  5
17   134.98  0.914  880.7 1448.9  956.4 0.010       2.095       0.862     117.448     105.349   80.19   1.67  18.14 2709.  -631.  -186.  5
18   164.63  0.818  873.0 1421.9  946.1 0.007       1.877       0.772     155.066     138.803   82.93   1.15  15.92 2709.  -634.  -187.  5
19   200.80  0.730  865.2 1395.5  935.9 0.005       1.678       0.690     204.629     182.800   85.32   0.79  13.89 2708.  -637.  -188.  5
20   244.92  0.651  857.6 1369.9  925.8 0.003       1.499       0.616     270.149     240.856   87.41   0.55  12.04 2707.  -640.  -189.  5
21   298.73  0.581  850.0 1345.1  916.0 0.002       1.338       0.550     356.959     317.638   89.23   0.37  10.39 2707.  -643.  -190.  5
22   364.37  0.518  842.7 1321.4  906.5 0.001       1.196       0.491     472.489     419.648   90.82   0.26   8.92 2706.  -646.  -191.  5
23   444.42  0.464  835.6 1298.8  897.3 0.001       1.071       0.440     626.821     555.695   92.22   0.17   7.61 2706.  -649.  -192.  6

********** THE BURN RATE for this MODE is 1.4641 cm/sec or 0.5764 in/sec and the AVERAGE SURFACE TEMPERATURE is 1036.80 K

***** MODE 2 HMX** 23 PARTICLES, the PRESSURE IS  1000.00 psia and the INITIAL PROPELLANT TEMPERATURE is   348.15 DEGREES KELVIN

       D      ROX      RB       R      TSOX    TSB      TS    BF   BP   FRB  DNOM1 DNOM2 DNOM3 DNOM4    XXK   XXPFK  XXPFD     TX     TFX  ITER
   MICRONS .......cm/sec......       K       K       K                     ........PERCENT........    .....MICRONS......    K      K     #

24    10.67  2.118  2.266  1.078  664.5 1713.6  776.2 1.00 0.38 0.36 45.61 39.93  8.15  6.31   21.3   76.1     9.7 3360.8 2789.7 17
25    13.93  2.09   2.247  1.047  664.4 1710.7  775.7 1.00 0.38 0.36 44.70 41.01  7.97  6.32   27.9   75.4    12.7 3360.8 2789.7  3
26    18.18  2.075  2.223  1.014  664.2 1706.9  775.1 1.00 0.38 0.36 43.77 42.11  7.79  6.32   36.4   74.6    16.6 3360.8 2789.6  3
27    23.73  2.044  2.191  0.977  663.9 1702.1  774.4 1.00 0.38 0.36 42.81 43.25  7.61  6.33   47.5   73.5    21.6 3360.7 2789.6  3
28    30.98  2.004  2.152  0.936  663.6 1695.9  773.4 1.00 0.38 0.36 41.82 44.42  7.41  6.35   62.0   72.1    28.2 3360.7 2789.5  3
29    40.44  1.955  2.102  0.891  663.1 1688.1  772.2 1.00 0.38 0.36 40.81 45.61  7.21  6.36   80.9   70.3    36.9 3360.6 2789.5  3
30    52.78  1.893  2.040  0.841  662.6 1678.1  770.6 1.00 0.38 0.36 39.78 46.84  6.99  6.39  105.6   68.1    48.1 3360.5 2789.4  3
31    68.90  1.817  1.963  0.785  661.9 1665.5  768.6 1.00 0.38 0.36 38.72 48.11  6.77  6.41  137.8   65.4    62.8 3360.4 2789.2  3
32    89.93  1.726  1.870  0.725  661.0 1649.8  766.2 1.00 0.38 0.36 37.63 49.40  6.53  6.44  179.9   62.2    82.0 3360.2 2789.1  3
33   117.39  1.617  1.760  0.659  659.9 1630.6  763.1 1.00 0.38 0.35 36.51 50.72  6.28  6.48  171.3   58.3   107.0 3360.0 2788.9  3
34   153.22  1.495  1.633  0.589  658.5 1607.6  759.5 0.99 0.38 0.35 35.31 52.15  6.00  6.54  158.4   54.0   139.6 3359.8 2788.7  4
35   200.00  1.441  1.457  0.545  657.9 1573.7  755.3 0.79 0.32 0.33 33.90 53.48  5.85  6.77  152.8   51.3   182.3 3359.6 2788.4  3
36   261.06  1.434  1.168  0.507  657.8 1512.0  748.7 0.64 0.24 0.30 31.70 55.00  6.23  7.06  152.1   48.8   237.9 3359.2 2788.1  4
37   340.75  1.462  0.854  0.472  658.1 1432.2  740.5 0.53 0.17 0.28 28.92 56.49  7.28  7.31  155.0   45.5   310.6 3358.7 2787.6  4
38   444.78  1.508  0.600  0.432  658.6 1352.2  732.4 0.43 0.11 0.26 25.66 58.02  8.84  7.48  160.0   41.3   405.4 3358.2 2787.1  4
39   580.57  1.557  0.425  0.386  659.2 1281.7  725.4 0.35 0.07 0.25 22.21 59.59 10.59  7.61  165.4   36.3   529.1 3357.8 2786.7  4
40   757.80  1.602  0.306  0.336  659.7 1221.3  719.4 0.28 0.05 0.24 18.81 61.20 12.30  7.70  170.2   31.0   690.6 3357.5 2786.4  4
41   989.15  1.639  0.223  0.285  660.1 1168.8  714.2 0.23 0.03 0.23 15.59 62.85 13.79  7.77  174.2   25.9   901.5 3357.2 2786.0  4
42  1291.12  1.655  0.166  0.235  660.3 1122.7  709.5 0.20 0.03 0.22 12.74 64.53 14.91  7.83  175.9   21.2  1176.7 3356.9 2785.8  4
43  1685.28  1.654  0.124  0.189  660.2 1081.4  705.0 0.20 0.02 0.22 10.25 66.25 15.62  7.88  175.8   17.2  1535.9 3356.6 2785.5  4
44  2199.77  1.653  0.093  0.149  660.2 1043.7  701.0 0.20 0.02 0.21  8.09 68.00 15.99  7.92  175.8   13.7  2004.8 3356.4 2785.3  4
45  2871.33  1.653  0.071  0.116  660.2 1009.3  697.4 0.20 0.02 0.21  6.27 69.77 15.99  7.96  175.8   10.9  2616.8 3356.2 2785.1  4
46  3747.91  1.652  0.054  0.088  660.2  977.6  694.0 0.20 0.02 0.20  4.78 71.57 15.66  7.99  175.7    8.6  3415.7 3356.0 2784.9  4

********** THE BURN RATE for this MODE is 0.5656 cm/sec or 0.2227 in/sec and the AVERAGE SURFACE TEMPERATURE is  750.75 K
```

```
***** MODE 1 AP*** 23 PARTICLES, the PRESSURE IS  2000.00 psia and the INITIAL PROPELLANT TEMPERATURE is   348.15 DEGREES KELVIN

       D      R    TSOX    TSB     TS     BF       XAPK       XPFK      XPFD        XFFD     HTAP   HTPF   HTFF   TF  TSQDAP  TSQDB ITER
   MICRONS cm/s      K      K      K                . . . . . .  MICRONS . . . . . .       % HEAT TRANSFER     K     K       K

 1    5.63  4.676 1124.0 2006.0 1241.5 1.000     3.250      1.054      1.819       0.000    0.00 100.00   0.00 2741.  -587.  -161.  9
 2    6.86  4.246 1112.9 1961.5 1225.9 0.869     2.958      0.959      2.300       2.538    5.15  90.53   4.32 2740.  -591.  -162.  4
 3    8.37  3.809 1100.5 1913.7 1208.8 0.619     2.660      0.861      2.905       3.016   17.26  69.05  13.69 2739.  -595.  -164.  5
 4   10.21  3.514 1091.3 1879.6 1196.3 0.446     2.458      0.795      3.723       3.709   27.40  52.02  20.58 2739.  -598.  -164.  4
 5   12.45  3.280 1083.2 1851.3 1185.5 0.322     2.297      0.743      4.823       4.671   35.86  38.81  25.34 2738.  -601.  -165.  5
 6   15.19  3.072 1075.3 1825.2 1175.2 0.231     2.154      0.696      6.302       5.990   43.00  28.67  28.33 2738.  -603.  -166.  5
 7   18.52  2.872 1066.6 1799.5 1164.3 0.165     2.017      0.652      8.285       7.779   49.17  20.97  29.85 2737.  -606.  -167.  5
 8   22.59  2.674 1056.6 1772.5 1151.9 0.116     1.881      0.607     10.942      10.189   54.62  15.20  30.18 2736.  -610.  -168.  5
 9   27.55  2.474 1043.0 1744.5 1136.4 0.082     1.744      0.563     14.493      13.416   59.48  10.93  29.59 2735.  -614.  -169.  5
10   33.61  2.282 1017.7 1716.1 1110.7 0.057     1.614      0.520     19.289      17.757   63.84   7.83  28.33 2734.  -623.  -171.  6
11   40.99  2.091  988.8 1686.4 1081.7 0.039     1.485      0.478     25.695      23.529   67.85   5.58  26.57 2732.  -634.  -174.  6
12   50.00  1.894  971.6 1654.0 1062.5 0.027     1.348      0.433     33.999      31.020   71.59   3.93  24.49 2731.  -640.  -176.  6
13   60.99  1.703  955.4 1620.5 1044.0 0.018     1.215      0.390     44.867      40.801   74.97   2.75  22.29 2730.  -647.  -178.  5
14   74.38  1.524  939.1 1587.0 1025.4 0.013     1.090      0.350     59.098      53.573   78.01   1.91  20.08 2729.  -653.  -180.  5
15   90.73  1.359  922.9 1553.7 1007.0 0.009     0.974      0.312     77.728      70.240   80.72   1.33  17.95 2728.  -660.  -181.  5
16  110.66  1.208  907.0 1521.1  988.8 0.006     0.868      0.278    102.197      92.065   83.16   0.92  15.92 2727.  -666.  -183.  4
17  134.98  1.071  891.9 1489.1  971.5 0.004     0.772      0.247    134.171     120.505   85.30   0.63  14.07 2726.  -672.  -185.  6
18  164.63  0.946  883.1 1457.3  959.6 0.003     0.682      0.218    175.421     157.218   87.15   0.43  12.42 2725.  -676.  -186.  5
19  200.80  0.834  874.3 1426.6  947.9 0.002     0.603      0.193    229.383     205.145   88.77   0.30  10.93 2724.  -680.  -187.  6
20  244.92  0.736  865.8 1397.4  936.6 0.001     0.533      0.170    300.317     268.024   90.22   0.20   9.58 2724.  -683.  -188.  6
21  298.73  0.650  857.5 1369.6  925.7 0.001     0.471      0.150    393.915     350.839   91.51   0.14   8.36 2723.  -687.  -189.  6
22  364.37  0.576  849.5 1343.3  915.3 0.001     0.418      0.133    518.038     460.469   92.66   0.09   7.24 2722.  -691.  -190.  6
23  444.42  0.512  841.9 1318.8  905.4 0.000     0.372      0.119    683.796     606.639   93.71   0.06   6.23 2722.  -694.  -191.  7

*******.*** THE BURN RATE for this MODE is 1.9198 cm/sec or 0.7558 in/sec and the AVERAGE SURFACE TEMPERATURE is 1066.61 K

***** MODE 2 HMX** 23 PARTICLES, the PRESSURE IS  2000.00 psia and the INITIAL PROPELLANT TEMPERATURE is   348.15 DEGREES KELVIN

       D     ROX     RB      R      TSOX    TSB      TS    BF   BP   FRB  DNOM1 DNOM2 DNOM3 DNOM4     XXK   XXPFK  XXPFD     TX     TFX  ITER
   MICRONS .......cm/sec......       K       K       K                    ........PERCENT........     .....MICRONS......      K      K     #

24   10.67  3.122  3.245  1.578   671.4 1847.1   796.5 1.00 0.37 0.37 45.28 39.94  8.54  6.24    21.3    49.0     9.7 3404.1 2812.8 28
25   13.93  3.080  3.205  1.526   671.2 1842.1   795.8 1.00 0.37 0.37 44.38 41.01  8.35  6.25    27.9    48.4    12.7 3404.0 2812.8  3
26   18.19  3.026  3.153  1.468   670.9 1835.6   794.8 1.00 0.37 0.37 43.45 42.12  8.16  6.27    36.4    47.5    16.6 3404.0 2812.7  3
27   23.73  2.958  3.087  1.403   670.5 1827.3   793.5 1.00 0.37 0.37 42.50 43.25  7.95  6.30    47.5    46.5    21.6 3403.9 2812.6  3
28   30.98  2.874  3.005  1.332   669.9 1816.8   792.0 1.00 0.37 0.37 41.52 44.42  7.73  6.33    62.0    45.2    28.2 3403.8 2812.5  3
29   40.44  2.769  2.903  1.252   669.3 1803.6   790.0 1.00 0.37 0.37 40.52 45.62  7.50  6.36    85.2    43.6    36.9 3403.7 2812.4  3
30   52.78  2.642  2.779  1.165   668.4 1787.0   787.5 1.00 0.37 0.37 39.48 46.85  7.26  6.41   102.4    41.6    48.1 3403.5 2812.3  3
31   68.90  2.491  2.630  1.068   667.4 1766.5   784.3 1.00 0.37 0.36 38.42 48.11  7.01  6.46    96.5    39.3    62.8 3403.3 2812.1  3
32   89.93  2.355  2.446  0.979   666.4 1740.4   780.7 0.93 0.36 0.36 37.26 49.40  6.75  6.59    91.3    37.0    82.0 3403.1 2811.8  3
33  117.39  2.320  2.128  0.922   666.1 1692.3   775.3 0.76 0.29 0.33 35.59 50.73  6.82  6.86    90.0    35.6   107.0 3402.8 2811.5  3
34  153.22  2.340  1.691  0.868   666.3 1618.4   767.6 0.63 0.22 0.31 33.24 52.15  7.46  7.15    90.8    34.0   139.6 3402.3 2811.1  4
35  200.00  2.402  1.253  0.813   666.8 1531.0   758.7 0.53 0.15 0.28 30.32 53.56  8.74  7.37    93.2    31.8   182.3 3401.8 2810.6  4
36  261.06  2.486  0.905  0.749   667.4 1446.4   750.2 0.44 0.10 0.27 26.99 55.01 10.47  7.54    96.5    28.9   237.9 3401.3 2810.1  4
37  340.75  2.571  0.657  0.674   668.0 1371.7   742.8 0.36 0.07 0.25 23.49 56.50 12.36  7.65    99.9    25.5   310.6 3400.9 2809.6  4
38  444.78  2.647  0.482  0.592   668.5 1306.8   736.4 0.29 0.05 0.24 20.03 58.03 14.19  7.75   102.9    22.0   405.4 3400.5 2809.3  4
39  580.57  2.710  0.358  0.506   668.9 1249.5   730.7 0.23 0.03 0.24 16.75 59.60 15.83  7.82   105.3    18.5   529.1 3400.2 2808.9  4
40  757.80  2.742  0.268  0.422   669.1 1198.6   725.4 0.20 0.03 0.23 13.79 61.21 17.12  7.88   106.7    15.2   690.6 3399.9 2808.6  4
41  989.15  2.740  0.202  0.343   669.1 1152.8   720.6 0.20 0.02 0.22 11.22 62.86 17.99  7.94   106.6    12.3   901.5 3399.6 2808.3  4
42 1291.12  2.739  0.153  0.274   669.1 1110.9   716.1 0.20 0.02 0.22  8.96 64.54 18.51  7.99   106.6     9.9  1176.7 3399.3 2808.1  4
43 1685.28  2.738  0.116  0.215   669.1 1072.5   712.0 0.20 0.02 0.21  7.03 66.26 18.68  8.03   106.6     7.9  1535.9 3399.1 2807.8  4
44 2199.77  2.737  0.089  0.166   669.1 1037.1   708.2 0.20 0.02 0.21  5.43 68.01 18.49  8.08   106.5     6.2  2004.8 3398.9 2807.6  4
45 2871.33  2.736  0.068  0.126   669.1 1004.5   704.7 0.20 0.01 0.20  4.13 69.78 17.98  8.11   106.5     4.9  2616.8 3398.7 2807.4  4
46 3747.91  2.735  0.052  0.094   669.1  974.2   701.5 0.20 0.01 0.20  3.09 71.57 17.19  8.15   106.5     3.8  3415.7 3398.5 2807.2  4

********** THE BURN RATE for this MODE is 0.7994 cm/sec or 0.3147 in/sec and the AVERAGE SURFACE TEMPERATURE is  758.11 K
```

```
********** FINAL RESULTS FOR AN INITIAL PROPELLANT TEMPERATURE OF  348.15 K

 PRESSURE          RATE        RATE         TS
   psia           cm/sec      in/sec         K

  500.000         0.7208      0.2838      870.842
 1000.000         1.0149      0.3996      893.772
 2000.000         1.3596      0.5353      912.363

THE CONSTANTS C AND N IN ST. ROBERTS BURNING RATE LAW, RATE = C*P**N ARE:

C = 0.01664221 (RATE IN in/sec)
N = 0.45772263
THE COEFFICIENT OF DETERMINATION IS 0.99795628

********** TEMPERATURE SENSITIVITY RESULTS

PRESSURE   SIGMA      BURN RATES IN in/sec AT THESE INITIAL PROPELLANT TEMPERATURE (DEGREES K)
  psia      %/K
                      248.15      298.15      348.15

  500.00  0.289286    0.2125      0.2452      0.2838
 1000.00  0.296897    0.2969      0.3444      0.3996
 2000.00  0.297152    0.3977      0.4614      0.5353

 "C" IN R=CP^N -----0.012893    0.014521    0.016642
 "N" IN R=CP^N -----0.452050    0.456083    0.457723

 ***** CPU TIME for this CASE =   358.090 SECONDS, TOTAL =  0.099 HOURS
```

INITIAL DISTRIBUTION

- 7 Naval Air Systems Command
  - AIR-5004 (2)
  - AIR-536 (1)
  - AIR-930 (2)
  - AIR-933 (1)
  - AIR-93D (1)
- 2 Chief of Naval Operations
- 6 Chief of Naval Research
  - OCNR-10 (1)
  - OCNR-10P (1)
  - OCNR-11 (1)
  - OCNR-111 (1)
  - OCNR-1132P
    - R. Miller (1)
    - J. R. Patton, Jr. (1)
- 5 Naval Sea Systems Command
  - SEA-62D3
    - Adicoff (1)
    - Kilroy (1)
  - SEA-62D31, Cassel (1)
  - Technical Library (2)
- 1 Space and Naval Warfare Systems Command (SPAWAR-005)
- 1 Commander in Chief, U. S. Pacific Fleet (Code 325)
- 1 Commander, Third Fleet, San Francisco
- 1 Commander, Seventh Fleet, San Francisco
- 2 Naval Academy, Annapolis (Director of Research)
- 2 Naval Ordnance Station, Indian Head
  - Code 525, P. Stang (1)
  - Technical Library (1)
- 3 Naval Postgraduate School, Monterey
  - Code 57, Fuhs (1)
  - Code 57NT, Netzer (1)
  - Technical Library (1)
- 3 Naval Research Laboratory
  - Code 2021 (1)
  - Code 6130, Chemistry Division (1)
  - Technical Library (1)
- 2 Naval Surface Warfare Center, White Oak Laboratory, Silver Spring
  - Code R10, S. Jacobs (1)
  - Code R16, Dr. G. B. Wilmot (1)
- 1 Naval Underwater Systems Center, Newport (Code 5B331, R. S. Lazar)
- 1 Naval War College, Newport
- 1 Naval Weapons Evaluation Facility, Kirtland Air Force Base (Code 401)
- 2 Navy Strategic Systems Projects Office
  - SP-2741, R. Kinert (1)
  - NSP-2731, Throckmorton (1)
- 1 Army Missile Command, Redstone Arsenal (AMSMI-RD-PR-T, J. G. Carver)
- 1 Army Ballistic Research Laboratory, Aberdeen Proving Ground (AMXAR-TSB-S (STINFO))
- 1 Rock Island Arsenal (E. Haug)
- 1 Air Force Munitions Systems Division, Eglin Air Force Base (AFATL/DLDL, O. K. Heiney)
- 1 Air Force Intelligence Agency, Bolling Air Force Base (AFIA/INTAW, Maj. R. Esaw)
- 2 Air Force of Scientific Research
  - L. Caveny (1)
  - B. T. Wolfson (1)

3 Air Force Astronautics Laboratory, Edwards Air Force Base
  AFAL/CA, Dr. R. Weiss (1)
  AFAL/MKP, R. Geisler (1)
  AFAL/PAC, W. C. Andrepont (1)
12 Defense Technical Information Center, Alexandria
2 George C. Marshall Space Flight Center (NASA), Huntsville, AL
  EP-25, J. Q. Miller (1)
  R. J. Richmond (1)
1 Lewis Research Center (NASA), Cleveland, OH (R. J. Priem)
1 Lyndon B. Johnson Space Center (NASA), Houston, TX (Code EP, J. G. Thibodaux)
1 National Aeronautics and Space Administration, Washington, DC (Code RP, F. W. Stephenson, Jr.)
1 Aerojet Tactical Systems, Sacramento, CA, via AFPRO (Deptartment 4350, M. Ditore)
1 Aeronautical Research Associates of Princeton Incorporated, Princeton, NJ (R. A. Beddini)
1 Arvin Calspan, Advanced Technology Center, Buffalo, NY (E. B. Fisher)
1 Atlantic Research Corporation, Alexandria, VA (M. K. King)
1 Atlantic Research Corporation, Gainesville, VA (Dr. R. H. Woodward Waesche)
1 Battelle Memorial Institute, Columbus, OH (A. A. Putman)
1 Brigham Young University, Provo, UT (673/WldB, M. Beckstead)
2 California Institute of Technology, Jet Propulsion Laboratory, Pasadena, CA
  F. E. C. Culick (1)
  L. D. Strand (1)
1 California State University Sacramento, Sacramento, CA (School of Engineering, F. H. Reardon)
1 General Applied Sciences Laboratory, Inc., Westbury, Long Island, NY (J. Erdos)
1 General Dynamics Corporation, Pomona, CA, via NAVPRO (P. L. Boettcher)
3 Georgia Institute of Technology, Atlanta, GA
  E. W. Price (1)
  W. C. Strahle (1)
  B. T. Zinn (1)
1 Hercules Incorporated, Allegany Ballistics Laboratory, Rocket Center, MD (R. R. Miller)
3 Hercules Incorporated, Magna, UT
  G. Butcher (1)
  Raun (1)
  R. L. Simmons (1)
1 Hercules Incorporated, McGregor, TX (W. G. Haymes)
1 Hudson Institute Incorporated, Center for Naval Analyses, Alexandria, VA (Tehnical Library)
1 Institute for Defense Analyses, Alexandria, VA (R. C. Oliver)
4 Lockheed Missiles and Space Company, Sunnyvale, CA, via NAVPRO
  R. Byrd (1)
  J. Linsk (1)
  G. Lo (1)
  H. Marshall (1)
1 Morton Thiokol Corporation, Wasatch Division, Brigham City, UT, via AFPRO
2 Morton Thiokol Corporation, Huntsville, AL
  J. Deur (1)
  D. A. Flanigan)
1 Pennsylvania State University, State College, PA (Applied Research Laboratory, G. M. Faeth)
2 Princeton Combustion Research Laboratories, Princeton, NJ
  M. Micci (1)
  M. Summerfield)
1 Purdue University, West Lafayett, IN (School of Mechanical Engineering, J. R. Osborn)
1 Rockwell International Corporation, Canoga Park, CA (BA08, J. E. Flanagan)
1 Science Applications Incorporated, Canoga Park, CA (R. B. Edelman)
1 Southwest Research Institute, San Antonio, TX (Fire Research Section, W. H. McLain)
2 Stone Engineering Company, Huntsville, AL
  H. C. Allen (1)
  W. C. Stone (1)
1 TRW Systems Incorporated, Redondo Beach, CA (A. C. Ellings)
1 The Aerospace Corporation, Los Angeles, CA (E. M. Landsbaum)

1 The Johns Hopkins University, Applied Physics Laboratory, Laurel, MD (CPIA, T. W. Christian)
1 United Technologies Corporation, Chemical ystems Division, Sunnyvale, CA (R. S. Brown)
1 United Technologies Research Center, East Hartford, CT (Document Control Section)
1 Universal Propulsion Company Incorporated, Phoenix, AZ
1 University of California, San Diego, Scripps Institute of Oceanography, La Jolla, CA (Ames Department, F. A. Williams)
1 University of Illinois, Champaign, IL (AAE Department, H. Krier)
1 University of Southern California, Los Angeles, CA (Mechanical Engineering Department OHE200, M. Gerstein)
2 University of Utah, Salt Lake City, UT
  Department of Chemical Engineering, A. D. Baer (1)
  G. A. Flandro (1)
1 University of Waterloo, Ontario, Canada (Department of Mechanical Engineering, C. E. Hermance) via Naval Air Systems Command (Air-960)
2 Whittaker Corporation, Bermite Division, Saugus, CA
  L. Bloom (1)
  L. LoFiego (1)